Reservoir Quality Evolution in Upper Devonian Strata of the North Sea

TANG, LONGXUN

Reservoir Quality Evolution in Upper Devonian Strata of the North Sea

This thesis is submitted for the degree of

Doctor of Philosophy at Durham University

Longxun Tang

Department of Earth Sciences, Durham University

January 2018

`

Abstract

In the UK North Sea, the Devonian has been perceived little potential to be hydrocarbon reservoir for a long time. Since 1970s, a number of discoveries, though their initial targets were not Devonian, have proved that the Upper Devonian Buchan Formation is porous, permeable and productive with considerable reservoir quality heterogeneity. The Alma Field (Block 30/24, UK Central North Sea) possessed relatively complete oil-bearing Buchan Formation sandstones with anomalously high reservoir quality, which provides a good opportunity to study this poorly understood Palaeozoic reservoir. The study has employed various methods from macro to micro scale by integrating analogue outcrops, drilled cores, thin section observations, SEM analysis and several geochemistry methods (EDX, XRD, cathodoluminescence, stable isotopic analysis and fluid inclusion thermometry). It has been recognized that the braided-fluvial channel and aeolian dune sandstones form the main types of reservoir with good horizontal connectivity in the Buchan Formation of the Alma Field. The Buchan Formation sandstones have experienced, due to consistently shallow burial depth until Paleogene and then rapidly buried into today's maximum depth (2.7 km – 3.2 km), less significant compaction and highly variable cementation in fluvial and aeolian sandstones. Dolomite cement occurred prevalently in both sandstones and the overlying Permian Zechstein dolomite is the most possible carbon source. The quartz overgrowth is extensive in fluvial sandstones but absent in aeolian sandstones; this difference is due to the presence of early-formed grain coating illite/smectite (I/S), which is only occurred in aeolian sandstones, originated from fluvial distal sector and formed by the mechanical infiltration. This grain coating I/S have effectively inhibited quartz overgrowth which maintained anomalously high reservoir quality in aeolian sandstones. Including but not limited to Alma Field, the outcomes of this study should have broad applications to the future hydrocarbon explorations targeting Devonian in the Central and Northern North Sea.

Declaration

I declare that this thesis, which I submit for the degree of Doctor of Philosophy at Durham University, is my own work, except where acknowledgement is made in the text, and not substantially the same as any work which has previously been submitted at this or any other university for any degree, diploma or other qualification.

November 2017

Acknowledgment

I would like to express my deepest thanks to all the people who have supported me throughout my PhD and especially to my amazing supervisory team: Jon Gluyas and Stuart Jones, who have offered me this PhD project and helped me through the whole time.

Firstly, I would like to thank **Professor Jon Gluyas** and **Dr Stuart Jones** for being such professional, kind and helpful throughout my whole PhD career. I can still recall our first meeting, first discussion, first time field trip and many other first things. For me, an oversea student, their doors were always open to me and their supports helped me not just to improve me as a geologist, it helped me growing as a more mature person. Their supports are highly appreciated and became invaluable during my four-year time in Durham.

I would also like to thank everyone from the Department of Earth Sciences for being great and making this a very enjoyable time. Thanks to Nwachukwu Chimaobi, Meiyan Fu, Mingjie Liu, Chen Xiong, Yueren Xu, Ang Li, Junjie Liu, Zeyang Liu, Nadia Narayan and many other people for providing great discussions and being very helpful. Furthermore, I would like to thank Dr Bernard Besley for providing data and helpful discussions; Mr Russel Ball for providing helpful skills on facies modelling in Petrel; Mr Ian Chaplin for the preparation of hundreds of thin sections; Mr Leon Bowen for his support and time at the scanning electron microscope, and Dr Geoff Nowell for the assistance on preparing isotopic samples. Thanks are also given to Mr Yinben Zhang in the Geological Exploration and Development Research Institute of Sichuan Petroleum Administration (Petro China) for constructive opinions; Miss Binqi Wei in the University of Leeds for useful discussions.

Finally, I would like to thank my beloved parents, my dear wife Xintong Li and all my friends for all the love and supports they have given me throughout this time – I couldn't have done it without you.

So thank you all.

Contents

List of figures

List of tables

RESERVOIR QUALITY EVOLUTION IN UPPER DEVONIAN STRATA OF THE NORTH SEA

CHAPTER 1: INTRODUCTION

Chapter outline

1.1 Research context

1.2 Aim of this research

1.3 Techniques and methods used in this research

1.4 Research database

1.5 Thesis structure

1.1 Research context

Accurate prediction of reservoir quality is crucial throughout the 'entire life' of a field exploitation (Sneider, 1990). An appropriate reservoir quality prediction with good accuracy is, and will continue to be the main challenge in petroleum exploration (Bukar, 2013). The importance of accurate pre-drill reservoir quality evaluation is growing as hydrocarbon exploration in the North Sea is increasingly focusing on the deeper and stratigraphically older targets. Since the access to the deeper reservoirs is usually limited in form of cores, conventional well logs and low-resolution seismic survey, a better understanding of reservoir quality is often model-driven. Currently, many models of reservoir quality are empirical and may only be applicable in the specific fields or basins, therefore, careful integration of available data are usually used to predict, prior to drilling, the potential impact of facies and diagenesis on porosity and permeability.

Devonian rocks are widely distributed in the North Sea and adjacent onshore areas (**Figure 1.1**) but commonly perceived to have little hydrocarbon reservoir potential, and the penetration of Devonian strata has often been taken as termination of the exploration wells (Downie, 2009). Despite this, a number of discoveries both in UK and Norwegian sectors (**Table 1.1**) have proved that the Devonian strata, especially the Upper Devonian Group, are effective reservoirs when the Jurassic Kimmeridge Clay-sourced hydrocarbons are trapped in adjacent and structurally elevated Devonian structural highs (e.g. Richards, 1985b; Edwards, 1991; Robson, 1991; Knight et al., 1993; Gambaro and Currie, 2003). The unusual discoveries in these very ancient rocks may have raised the hope that the Devonian Formation in North Sea could be economically valuable. Comparing with those Mesozoic and Cainozoic reservoir targets, these older and usually deeper strata now need to claim more attentions as the North Sea becomes a mature exploration area.

So far, the current discoveries suggest that the Devonian reservoirs have commonly low to, at best, moderate-good reservoir quality and were locally improved by fault-induced fractures if they still remain open (Downie, 2009). This dual-poro/perm system has resulted in the difficulties in evaluating reservoir quality and increased uncertainties in calculation of recoverable hydrocarbons; additionally, the Devonian penetrations are limited due to the fact that Devonian strata were never considered to be the main exploration targets. Therefore, the current understanding of these reservoir sandstones is very poor.

Table 1.1 Hydrocarbon accumulations in Devonian-associated reservoirs of the UK Continental Shelf (UKCS) and Norwegian North Sea. Data are collected and summarized from Bifani and Smith (1985), Robson (1991), Gluyas et al. (2005), Trewin and Bramwell (1991), Knight et al. (1993), Edwards (1991), Gambaro and Currie (2003) and Johnston et al. (1995).

Field	Location	Reservoirs	Hydrocarbons
Ardmore	UK 30/24	Permian Rotliegend; Permian Zechstein; Devonian Buchan	15.2 million m3 oil from Devonian and Permian reservoirs, 5500 barrels oil/day from Devonian interval
Auk	UK 30/16	Permian Rotliegend; Permian Zechstein; Devonian Buchan	529 million barrels recoverable oil
Buchan	UK 21/1	Upper Devonian-Carboniferous sandstones	120 million barrels recoverable oil
Clair	UK 208/6	Late Devonian to Early Carboniferous sandstones	Approximately greater than 300 million barrels oil, may be up to 1.5 billion barrels
Embla	Norwegian 2/7	Early Permian; Carboniferous and/or Late Devonian age	At least 215 million barrels, may be up to 1.03 billion barrels oil to be explored
Stirling	UK 16/21	Middle to Late Devonian sandstones	Peak oil flow rate at 4334 barrels oil/day

The Ardmore Field (previous name ‘Argyll’, now part of ‘Alma/Galia Project’ owned by EnQuest PLC) is situated in UK Blocks 30/24 and 30/25 in the south-west of the Central Graben. It is one of the Devonian-productive oil fields (Bifani and Smith, 1985; Robson, 1991) in the North Sea and has a relatively complete Upper Devonian reservoir with good core coverage although the original targets of the field were the shallower, younger Permian

Rotliegend and Zechstein reservoirs. This provides a good opportunity to understand how the Devonian reservoir performed and what controls the reservoir quality. Gluyas et al. (2005) reported that the Upper Devonian reservoir is a predominantly fluvial sequence with minor presence of aeolian deposits, and the reservoir quality has a very large variation from completely cemented sandstones to loosely compacted and poorly cemented sandstones, which implies a great reservoir quality heterogeneity. Therefore, we choose Ardmore Field as the main research target in this project and try to understand how the Upper Devonian sandstone reservoirs evolved and the main controls on the reservoir quality. This research delivers a comprehensive understanding of the sedimentology, petrography, diagenesis, reservoir quality evolution and basin evolution of the Upper Devonian sandstones in the area of the selected field. In this research, several types of data and techniques are employed in order to assess the facies architecture, controls on reservoir quality, and reconstruct the diagenetic and burial histories. Beyond the studied areas and this project, the outcomes are expected to be useful references for the pre-drilling prediction for the future Devonian explorations in the North Sea.

1.2 Aim of this research

The main aim of this research is to have a better understanding on the controls of reservoir quality in these ‘unusually-productive’ Upper Devonian sandstone reservoirs, why the reservoir quality varies significantly in the vertical direction within meter scale, how the potential reservoir distributes and use geochemical methods to reconstruct and quantitatively describe the diagenetic and burial histories. To achieve these, efforts have been made by employing several techniques and methods to investigate the sedimentary facies, facies architectures, lithology, petrography, diagenesis and burial history. The results provide insights into poorly-understood Upper Devonian strata, and can be useful tools and references for those wishing

to target Devonian age reservoirs with exploration wells in the North Sea. The outcomes also have broad applications in other areas with similar provenance.

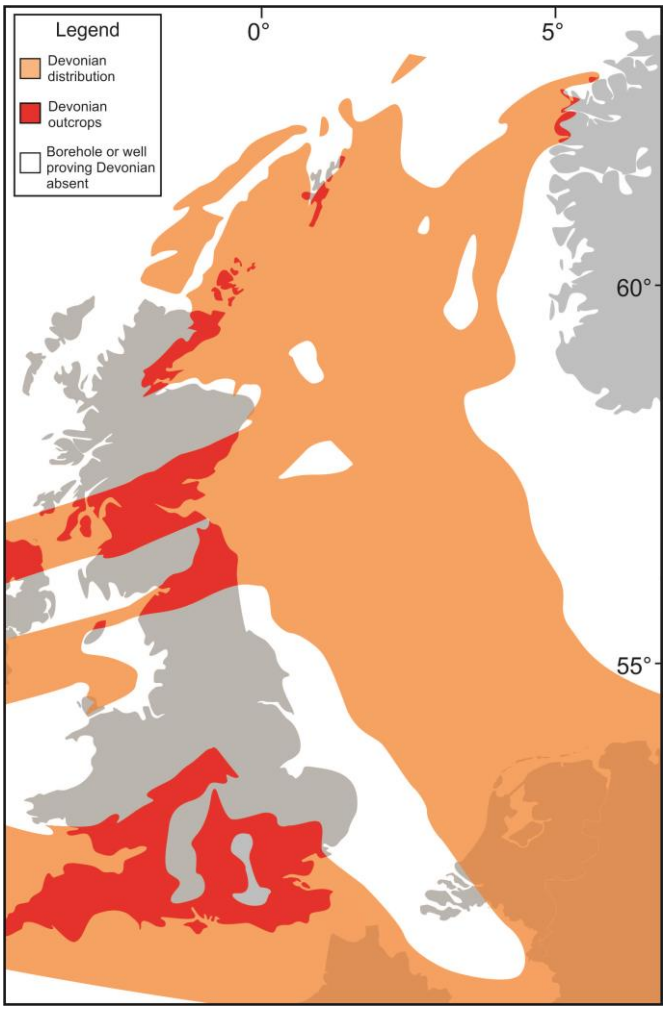

Figure 1.1 General distributions of Devonian strata in the North Sea and associated onshore/offshore areas. Original version from Downie (2009), modified by Longxun Tang.

Generally, the objectives of this research include:

- To describe the cores and define the sedimentary lithology and facies in details;
- To investigate the vertical and lateral architectures and connectivity of potential reservoir sand bodies on a field-wide scale by using outcrop analogue measurements, core study, well logging data and numerical facies modelling;

- To determine the main controls on reservoir quality from macro (facies) to micro (effect of clay minerals) scales, with the special attentions paid to the positive effect and mechanism of grain coating illite/smectite (I/S) in aeolian sandstones;
- To quantitatively research the diagenetic events using geochemical methods and locate them in the burial history;
- To develop an integrated burial-thermal-diagenetic histories for the local basin;
- To improve the understanding of the Upper Devonian strata in the UK North Sea.

1.3 Techniques and methods used in this research

1.3.1 Investigation and measurement on analogue outcrops

Due to the sparse and very limited offshore Devonian penetrations, we have investigated analogue Devonian outcrops in Dunnet Head and Orkney, which were deposited under similar provenance with the selected field (Trewin and Hurst, 2009). The aim is to recognize and have a general view of the Devonian fluvial depositions, and measure the geometry of Devonian fluvial channel sand body as the references for determining geometry parameters when doing numerical simulation for subsurface fluvial sand body.

1.3.2 Core logging and sampling

Core samples in this study are from the Upper Devonian Buchan members encountered in the Ardmore Field, Central North Sea. The sampling and logging of cores were undertaken at BGS core store in Keyworth and EnQuest core centre in Aberdeen. The depth intervals have been chosen according to the internal well reports provided by EnQuest. Although the sampling points have covered all the lithology types, the main focus is on those sandstones with different sedimentary structures and variable reservoir quality. The very coarse and extremely

fine depositions, such as conglomeratic basal lag and muddy flood plain deposits, are not the main focus of this research.

1.3.3 Wireline log analysis

The Argyll Field (to be called 'Ardmore' and 'Alma' in the following chapters) was firstly developed in the late 1970s and then abandoned in 1992. The well logging was operated during 1969 to 1992 by Hamilton Brothers Oil Company. The initial targets were the Permian Zechstein and Rotliegend intervals, therefore the drilled cores are not completed for presenting whole Upper Devonian sequence. The lithology and vertical facies structure in the uncored wells are mainly achieved by well log data interpretation, and the net/gross ratio can also be roughly calculated. The lateral correlations between adjacent wells were attempted by comparing well log responses (Besly, 2011) in same stratigraphic units in adjacent wells with references from analogue outcrop measurements mentioned above.

1.3.4 Facies modelling by numerical simulation software

By integrating the parameters and outcomes from analogue outcrop measurements and well log interpretation, the architectures of favourable facies can be achieved by numerical simulations. In this study, we have chosen Schlumberger's software Petrel (V. 2014) for the modelling of facies architectures. The object modelling module in the Petrel allows users to populate a facies model with different bodies by defining various geometry parameters, facies types and fraction for each component. The basic principle of modelling is upscaling high-resolution well log data and point attribute data into the geo-cellular grids by using stochastic modelling algorithms. Therefore, the correct facies identification (well log explanation) and suitable geometry parameters (referred from outcrop measurement and lateral well log correlation) are critical for an appropriate modelling result. The outcomes provide realistic representation of the scales, distributions and evolution of the depositional facies.

1.3.5 Thin section petrography

Core samples are manufactured into thin sections for microscopy observations. Visible porosity is highlighted by the impregnated blue epoxy. The general mineral composition is accomplished using 300 counts per thin section on a standard petrographic microscope (Leica DM2500P) and point counting stage (Petrog – Conwy Valley Systems Limited). These basic observations (e.g. grain size, sorting and roundness, QFR composition, visible porosity, grain contact relationship, cement types, fraction of clay coated and non-coated grains, etc.) are used to select samples for additional petrographic analysis, including intergranular volume (IGV), total cement and the extended parameters such as porosity-loss by mechanical compaction (COPL) and porosity-loss by cementation (CEPL). The helium porosity and permeability data used in this study was provided by EnQuest.

1.3.6 Scanning Electron Microscopy (SEM) equipped with Energy-Dispersive X-ray (EDX)

Selected polished thin sections and tiny rock chips (approx. 1 cm * 1 cm * 0.5 cm) are coated by 40 nm carbon and 35 nm gold prior to analysis by a Hitachi SU-70 scanning electron microscope (SEM) equipped with an energy-dispersive X-ray detector (EDX). The SEM analysis on the thin sections and bulk rock chips were conducted at 5 kV to 20 kV acceleration voltages with beam currents of 1.0 nA and 0.6 nA, respectively. The SEM can provide high magnitude enlargement for clay morphology and pore space geometry. The SEM-EDX was used for rapid identification of chemical species (i.e., K ratio in I/S mixed minerals).

1.3.7 X-ray diffraction (XRD) analysis

X-ray diffraction (XRD) analysis was conducted by X-ray Mineral Services Ltd. Quantification for clay fraction (the < 2 micron clay fraction phases) have been analysed for a full interpretation particularly with respect to silica minerals, feldspar, mica, clay minerals, carbonate compositions, evaporates (anhydrite/gypsum) and heavy minerals.

1.3.8 QEMSCAN technique

A very fine-grained fluvial sample (siltstone) was selected for QEMSCAN (quantitative evaluation of minerals by scanning electron microscopy) analysis with the aim to provide a quantitative petrographic characterisation. The sample was cut to give a flat surface and impregnated with Struers Epofix resin within a 30 mm diameter mould. The sample was polished, carbon coated and measured using automated mineral analysis at the Rocktype QEMSCAN facility. The FEI QEMSCAN technique combines SEM and X-ray (EDX) technology to provide automated petrographic description of geological samples in the form of high resolution images and spatially resolved compositional and textural data.

1.3.9 Cathoduluminescence (CL)

The cathodoluminescence (CL) analysis has been undertaken on selected thin sections with visible macro-quartz overgrowths by using Gata MonoCL system. The purpose is to distinguish whether the quartz overgrowth was formed by a single precipitation or multiple generations.

1.3.10 Fluid inclusion thermometry

Eleven double-polished detached wafers are chosen to determine the conditions of quartz cementation and formation water salinity. Fluid inclusion analysis was undertaken by Linkam THMS600 Cooling-Heating Stage in State Key Laboratory of Oil and Gas Reservoir Geology and Exploitation, Chengdu University of Technology (CDUT). The temperature range of the instrument is from −196°C to 600°C with a precision of < 0.1°C. The rate of temperature increase can be controlled to within 1°C/min when approaching the critical point. The purpose is to measure the precipitation temperature (the homogenization temperature, T_h) of quartz overgrowth in the samples and the composition of the trapped fluid. The results can increase

the accuracy of diagenetic and burial history reconstruction, and also provide useful compositional information of the formation fluid.

1.3.11 Stable isotope analysis

The stable isotope analysis involves carbon and oxygen elements and is mainly applied on authigenic carbonate cements (in this study, dolomite is predominant). The analysis is measured by the Scottish Universities Environmental Research Centre (SUERC) in the University of Glasgow. Seventeen sandstone samples with variable percentage of dolomite cements were gently disaggregated with a hammer and then crushed into powder in a mortar and at least 1 mg of dolomite powder are obtained for each sample. The value of $\delta^{13}C$ and $\delta^{18}O$ were determined on CO_2 liberating from dolomite cements dissolved by 100% H_3PO_4 at 50°C. The isotopic composition of CO_2 is reported in units of ‰ relative to Pee Dee belemnite (PDB). The purpose is to determine the possible source and formation temperature of these carbonate cements.

1.3.12 One-dimensional burial history

The Schlumberger's PetroMod (V. 2012.2) software is employed for modelling the basin evolution in one dimension. The one-dimensional modelling provides a good insight into geothermal isogram in the subsurface and is based on a forward modelling algorithm to generate the burial history. However, the stratigraphic units between Devonian and Palaeocene contain many unconformities due to multiple episodes of tectonic uplift and erosion; therefore the true thicknesses of missing and incomplete stratigraphic units are mainly inferred from nearby wells and fields containing the missing units. The lithology types for those missing strata are determined according to the BGS project 'Lexicon of Named Rock Units' and the standard litho-stratigraphic nomenclature of the UK North Sea (Deegan and Scull, 1977). The key parameters for the modelling, including palaeo-heat flow, paleo water depth (PWD)

and sediment water interface temperature (SWIT) are mainly collected from previous studies (Cornford, 1994; Graham et al., 2003).

1.4 Research database

The database for this research comprises core data sampled at different depths, on which the various techniques were applied. Other data types include the wireline logs, well reports and other supporting documents (**Table 1.2**).

Table 1.2 Types and quantities of the data employed in this research

Item	Quantity
Field	1
Wells with Devonian cores	7
Composite well logging curves	20
Thin sections	126
SEM rock chips	18
XRD Samples	7
Fluid inclusion samples	11
QEMSCAN sample	1
Cathodoluminescence samples	4
Carbonate samples for isotopic analysis	17

1.5 Thesis structure

Chapter 1 gives a brief introduction of the topic and the rationale behind the project. It also gives a brief overview of the aims and objectives of the thesis and how they will be addressed. The techniques used and database involved in this project are also briefly introduced.

Chapter 2 summarizes the geological background of the North Sea and British Isles in the Devonian age, and has reviewed the hydrocarbon exploration history in the North Sea and the main controls of sandstone reservoir quality.

Chapter 3 is a facies and petrography investigation of Upper Devonian Buchan Formation outcrops in Dunnet Head and Orkney, and discusses the potential of these outcrops to be the analogues of offshore Upper Devonian reservoirs in the North Sea. The chapter is in a paper format titled 'Facies and petrography assessment of the Buchan Formation (Upper Devonian) outcrops, Dunnet Head and Orkney, Northern Scotland'. This chapter has been submitted to the ***Scottish Journal of Geology*** and is now under review.

Chapter 4 presents and discusses the reservoir architecture and reservoir quality heterogeneity in a paper format titled 'Fluvial and aeolian facies architecture and reservoir heterogeneity of the Upper Devonian Buchan Formation, Central North Sea, UK'. This chapter has been published in the ***International Journal of Geosciences***.

Chapter 5 presents and discusses the general petrographic and diagenetic features as it affects the reservoir rock from Ardmore Field, special attentions are given to the effect of grain coating illite/smectite (I/S). The chapter is in a paper format titled 'Porosity preservation due to grain coating illite/smectite: evidence from Buchan Formation (Upper Devonian) of the Ardmore Field, UK North Sea'. This chapter has been accepted by the ***Proceedings of Geologists' Association*** and is now in press.

Chapter 6 presents the quantitative analysis on diagenesis by using a couple of geochemical methods and reconstructs the diagenesis and burial history in a paper format titled 'Diagenetic and geochemical studies of the Buchan Formation (Upper Devonian) in the Central North Sea'. This chapter has been accepted by the ***Petroleum Science*** and is now in press.

Chapter 7 is a review of the studied field in a paper format titled 'The Alma/Ardmore/Argyll Field, Blocks 30/24 and 30/25a, UK North Sea'. This chapter has been accepted by the ***Geo-***

logical Society of London and will be published in the ***GSL Memoir Book 'United Kingdom Oil and Gas Fields 50 Years Commemorative Atlas'***.

Chapter 8 is a general summary and conclusion for the whole work, a brief analysis on the uncertainties involved during the research, and some suggestions for the further work.

For the chapters written in paper formats, it involves some degrees of repetition of material from one chapter to another, especially the geological background of the studied field, methodology sections, and some basic petrographic information.

CHAPTER 2: LITERATURE REVIEW OF THE RELEVANT RESEARCH

Chapter outline

2.1 Geological background of the North Sea and the British Isles in the Devonian age

- 2.1.1 Tectonic setting
- 2.1.2 Paleoclimate
- 2.1.3 Stratigraphy and depositional environment

2.2 Hydrocarbon exploration in the UK North Sea

2.3 Reservoir quality of sandstones: a review

- 2.3.1 Reservoir quality controlling factors in siliciclastic rocks
- 2.3.2 The grain coating minerals
- 2.3.3 Other reservoir quality controlling factors

2.1 Geological background of the North Sea and the British Isles in the Devonian age

2.1.1 Tectonic setting

The component parts of the British Isles were separated by the Iapetus Ocean – the north of Scotland was part of Laurentia, and the rest part of Avalonia before the Silurian (Van Staal et al., 1998). The Caledonian Orogeny led to the gradual closure of Iapetus Ocean due to the collision of these continents and this ancient ocean was finally closed around the Middle to Late Silurian (Soper et al., 1992) (**Figure 2.1**). The closure was oblique with movement along a series of sinistral strike-slip faults, such as Great Glen, Walls Boundary, Highland Boundary and Southern Upland Faults (Graham et al., 2003) (**Figure 2.2**).

The closure of Iapetus Ocean created a new giant continent called 'Laurussia'. Paleomagnetic data suggests this new continent was located in a low-latitude position between 15° to 30° S during the Devonian (Tarling, 1985; Witzke and Heckel, 1988).

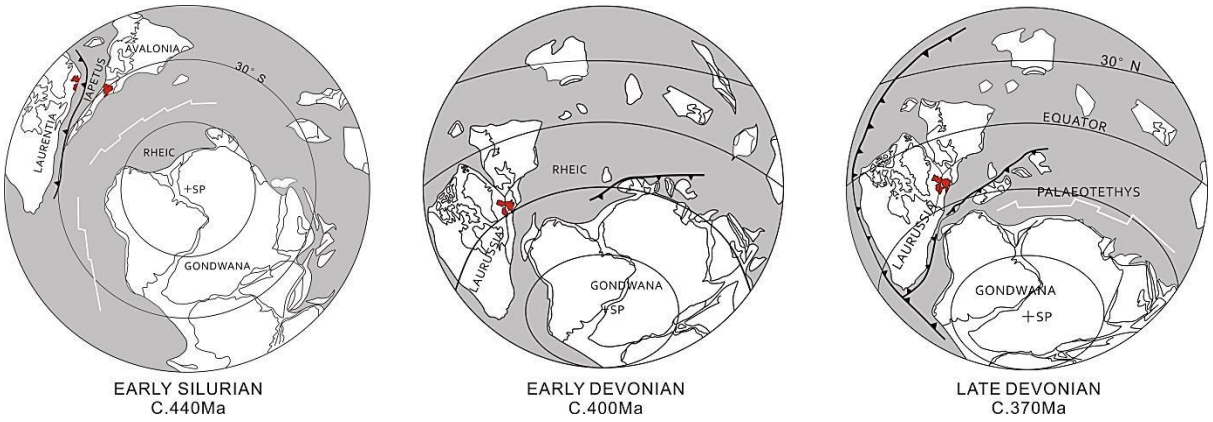

Figure 2.1 The global palaeogeography maps from Early Silurian to Late Devonian; note the red parts display the location of British Isles. After Woodcock and Strachan (2009), modified by Longxun Tang.

The suture of Iapetus Ocean in Britain is located south of Southern Upland and extends south-westwards and north-eastwards. After the closure, the tectonic regime in Midland Valley altered from compression to continuous extension after the closure of Iapetus Ocean and

thus provided accommodation space for local deposition (e.g. Strathmore Basin in Midland Valley, **Figure 2.3A**). It was in these small depo-centres where the first terrestrial Devonian sediments occurred (Marshall, 1991).

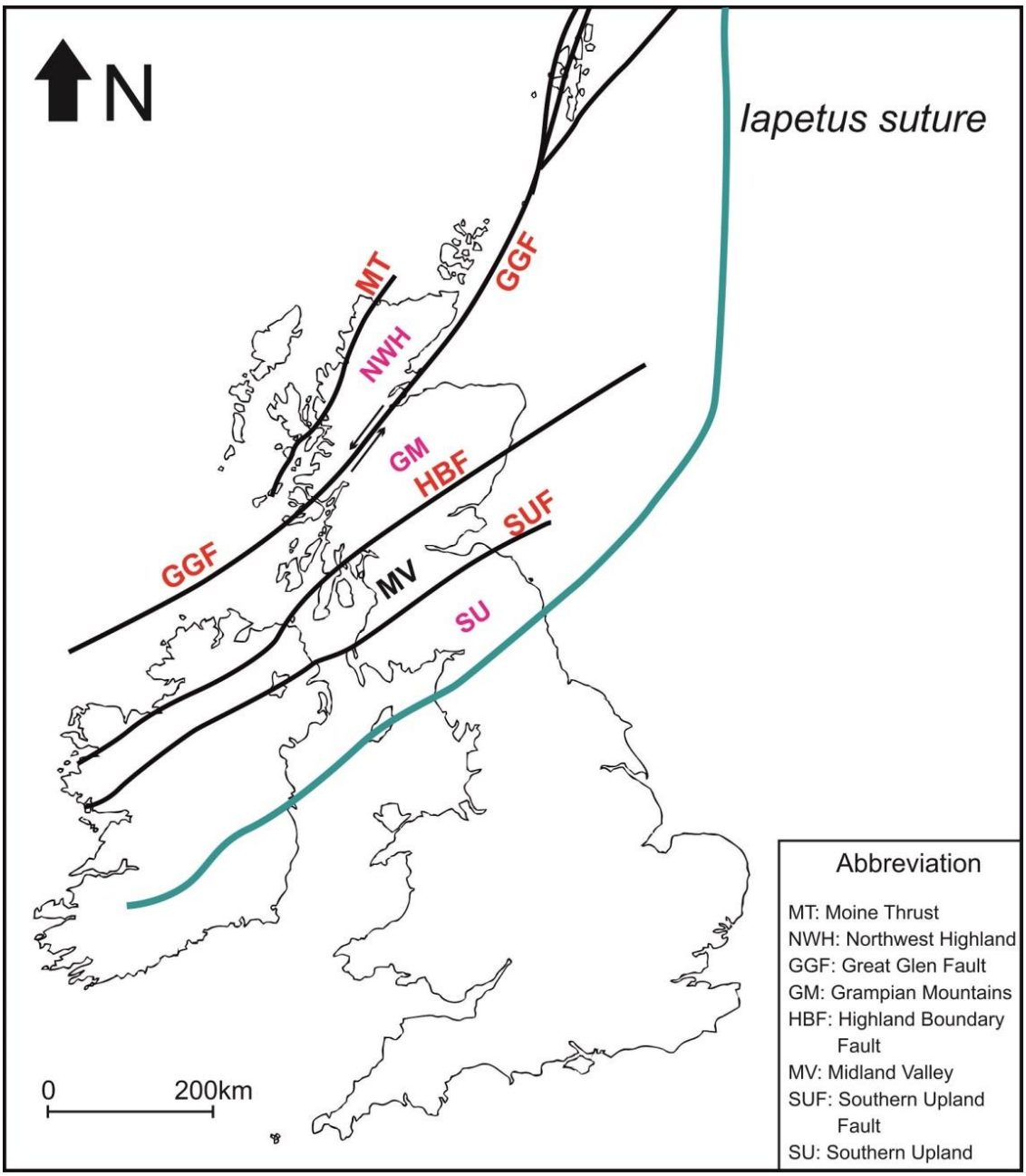

Figure 2.2 The Iapetus suture and its induced faults.

The similar extensional movement also occurred along Great Glen, Walls Boundary, Highland Boundary and Southern Upland Faults and formed a series of half-graben sub-basins (Norton et al., 1986; Seguret et al., 1989; Dewey and Strachan, 2003). Initially, these half-

graben sub-basins were separated and dominated by internal drainage on small-scale alluvial fan with local lakes (Graham et al., 2003). In the Mid-Devonian, these small basins were coalesced into a single system which is known as the lacustrine-dominated Orcadian Basin (Astin, 1990). This basin contained several depo-centres and extended from western Norway, east Greenland, Shetland, Orkney and across to its southernmost margin, the southern shore of Moray Firth (**Figure 2.3B**). In the Middle and Southern North Sea, the presence of a narrow trough of marine transgression (**Figure 2.3B**) was suggested by Glennie (2009) and proved by the Middle Devonian Kyle Limestone penetrated in the Auk (Trewin and Bramwell, 1991) and Argyll (renamed to 'Ardmore', now part of 'Alma/Galia' project) Fields (Robson, 1991; Gluyas et al., 2005).

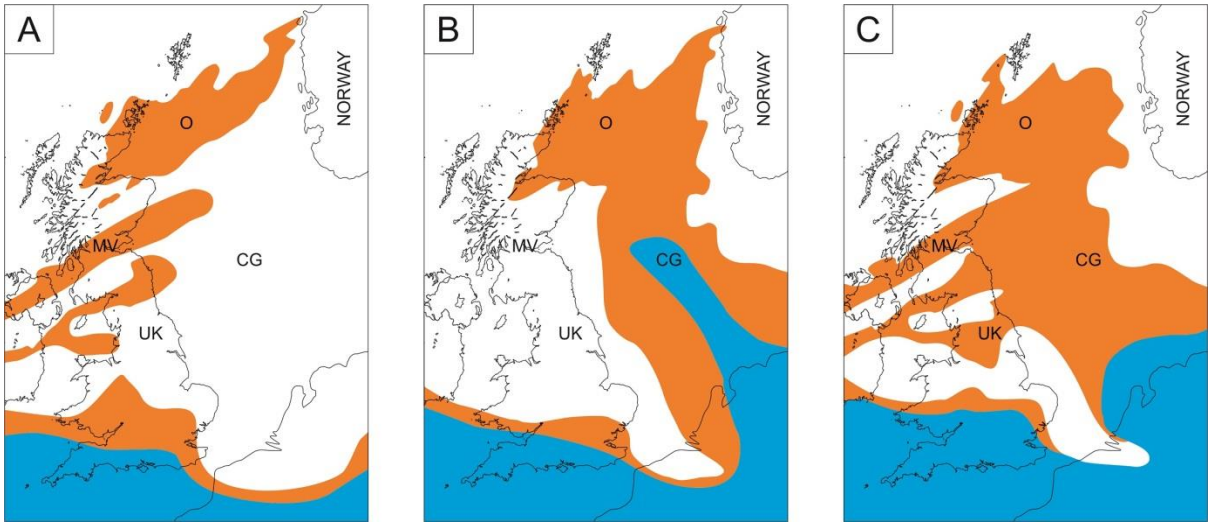

Figure 2.3 Simplified maps for distribution of Lower (A), Middle (B) and Upper (C) Devonian strata in the British Isles and North Sea. Orange: terrestrial deposition; blue: marine deposition. O-Orcadian Basin, CG-Central Graben, MV-Midland Valley. After Glennie (2009), slightly modified by Longxun Tang.

In the late Middle Devonian and early Late Devonian age, the extensional movements were reactivated and the whole North Sea area are now dominated by a more opened drainage system (**Figure 2.3C**), which was originated from several sediment source areas, such as Northwest Highlands, Grampian Mountains and Southern Uplands. From this time on, the domi-

nant sedimentary process in North Sea area changed from lacustrine to fluvial. The Upper Devonian mainly presented in Orcadian Basin and Central/Northern North Sea with predominantly fluvial-braided deposition (Robson, 1991; Trewin and Bramwell, 1991). Aeolian deposition is also reported but not as popular as fluvial facies (Hall and Chisholm, 1987). Beyond the Orcadian Basin and Central/Northern North Sea, there are no Devonian penetrations in the Southern North Sea possibly due to that the Devonian might be too deep to form any part of the local hydrocarbon system (Glennie, 2009).

2.1.2 Paleoclimate

The global climate of the whole Devonian age has been suggested to be a warm period and the temperatures have slight variations (**Figure 2.4**). Joachimski et al. (2009) used oxygen isotopes in conodont apatite to reconstruct the paleo-temperature history for the Devonian, their calculations show that the surface seawater temperature was 30°C – 32°C in the Early and Late Devonian, and about 22°C – 28°C between the end of Early Devonian and the beginning of Late Devonian. Kiessling (2002) showed that the distribution of tropical reef zone stretched from 46° S to 40° N and 38° S to 45° N in the early and late Devonian age, respectively. Another evidence of global-scale warm climate is the few presence of glaciation, only one Devonian-related glacial example was reported by Caputo et al. (2008).

For the studied areas in this project, Witzke and Heckel (1988) claimed that the North Sea Basin and British Isles were approximately located around 30° S in the Early Devonian, and then successively moved northwards to about 15° S to 10° S in the Late Devonian. The characteristic redbed sections (the Old Red Sandstone) have been reported in over 150 wells and thus proved the local climate was generally hot and arid (Graham et al., 2003).

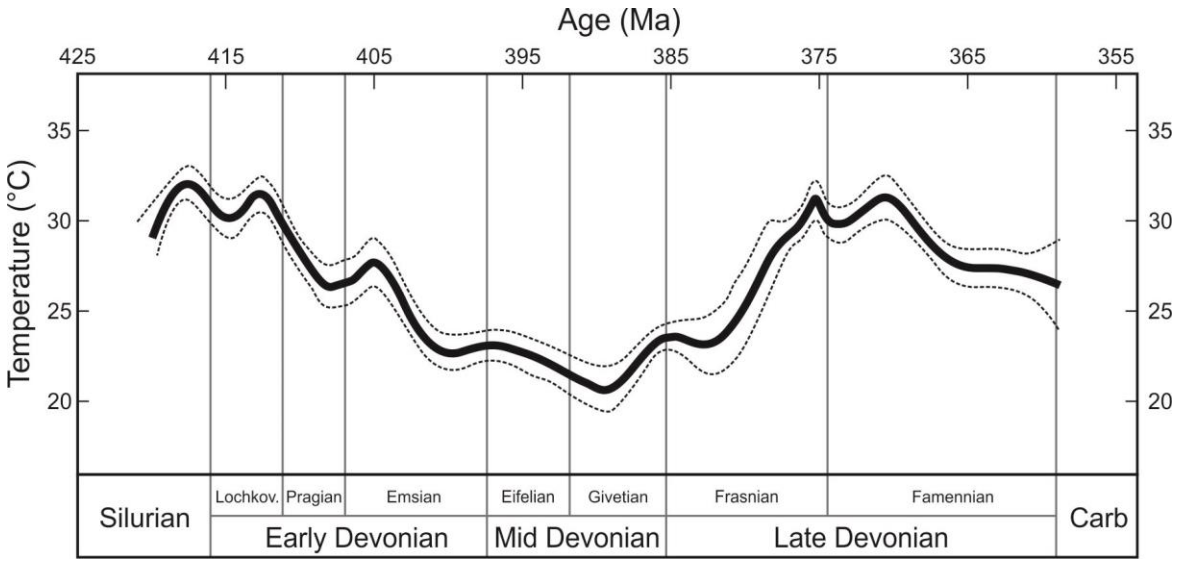

Figure 2.4 Palaeo-temperature of the late Silurian and Devonian calculated from $\delta^{18}O$ of conodont apatite, assuming a $\delta^{18}O$ value for Devonian sea water of −1‰ V_{SMOW}. After Joachimski et al. (2009) , slightly modified by Longxun Tang.

2.1.3 Stratigraphy and depositional environment

The Devonian strata in the British Isles and North Sea area can be divided into Lower, Middle and Upper Devonian Groups, which correspond to the Early, Middle and Late Devonian ages (Graham et al., 2003; Glennie, 2009). Unfortunately, there is no well penetration or outcrop containing a complete Devonian sequence, thus the stratigraphic subdivision is mainly based on regional-scale unconformities (Cameron, 1993a).

2.1.3.1 Lower Devonian Group

The Lower Devonian Group was largely deposited on the eroded Caledonian basement, so that the base of the Lower Devonian Group is a clear angular unconformity (Graham et al., 2003). The deposition is distributed in limited areas, mainly in the Orcadian Basin, Scotland Midland Valley and its contiguous offshore areas, and southern England (**Figure 2.3A**).

Figure 2.5 The Lower Devonian conglomerate in Sarclet, Northern Scotland, notes the quartz pebbles and pink-coloured matrix which contains abundant potassium feldspars. Photo was taken by Longxun Tang.

The distribution of Lower Devonian Group in the Orcadian Basin is around the basin margins, the alluvial-fan conglomerates and sandstones are the main lithofacies (**Figure 2.5**), and the depositional environment varied to confined local lakes in the Strathpeffer area (Mykura, 2002), and this allowed the preservation of organic algal materials. The similar lacustrine examples are proved by the wells 12/27-1, 12/27-2, 12/28-2 and 13/19-1 in the Moray Firth

(Andrews et al., 1990), where the grey to reddish brown, laminated siltstones and claystones, and silty calcareous sandstones are predominant. Apart from alluvial and lacustrine environments, in the Orkney Mainland, the Lower Devonian Yesnaby Sandstone Formation is suggested to be of aeolian origin (Mykura, 2002). The distribution of Lower Devonian Group in the offshore Orcadian Basin is difficult to measure due to the poor seismic data and few well penetrations, and the thickness of Lower Devonian is believed to be highly variable, a proposed lacustrine shale with maximum 976 m thickness is reported from well 12/27-1 (Richards, 1985a; Marshall, 1998).

In the Scotland Midland Valley and its contiguous offshore areas, the Lower Devonian Group accumulated in a number of separated but superimposed basins between the Highland Boundary Fault and Southern Upland Fault (Armstrong and Paterson, 1970; Cameron and Stephenson, 1985; Haughton and Bluck, 1988). The main depositional environments were alluvial fan, fluvial and lacustrine deposits, the locally thick volcaniclastic sediments and lavas are also presented (Graham et al., 2003).

The Lower Devonian Group in southern Wales and southern-southwestern England has been studied by several researches. Shallow marine deposits were reported in the Southeast Devon by the presence of structures made by burrowing animals, tracks or trails, relatively rich fauna of brachiopods, corals, bryozoa, gastropods and trilobites (Dieter, 1967). The marine deposition decreased northwards and became alluvial-fluvial dominated, Marriott and Wright (1993) investigated the fossil soils in the Early Devonian Moor Cliffs Formation and Rat Island Mudstone (Freshwater West Formation) of south Dyfed, South Wales and proposed that depositions occurred on a flood plain under a seasonal, semi-arid climate. Allen (1983) studied the Lower Devonian Brownstones in the Ross-on-Wye in the southern Welsh Borders, he concluded that the main depositional facies are the low-sinuosity braided streams.

In the other areas of British Isles and Central and Southern North Sea, the Lower Devonian Group is rarely found.

2.1.3.2 Middle Devonian Group

Comparing with Lower Devonian Group, the Middle Devonian Group has a wider distribution in the North Sea but less occurrence in the onshore British Isles (**Figure 2.3B**).

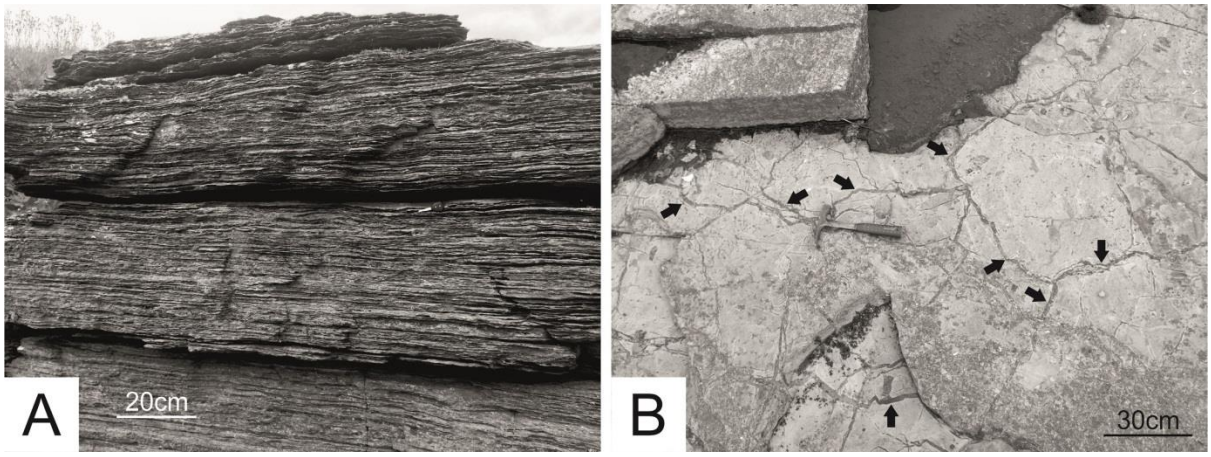

Figure 2.6 (A) Typical lacustrine flagstone depositions, the Middle Devonian Flagstone Group, Caithness, Northern Scotland; (B) The polygonal sand-filled desiccation cracks (black arrows) were probably formed during subaerial exposure observed in a typical Middle Devonian lacustrine flagstones, Pennyland Shore, Thurso, Northern Scotland. Photos were taken by Longxun Tang.

In the onshore areas, the Middle Devonian Group is mainly distributed in the Caithness and southern England but absent in the Midland Valley and Southern Upland (Gatliff, 1994). Trewin and Hurst (2009) has investigated several localities in the Caithness, they confirmed that the widely distributed Middle Devonian flagstones (**Figures 2.6A and 2.6B**), which contain abundant fish fossils, were deposited in lacustrine condition, and this was interpreted as the margin of Orcadian Lake in the Middle Devonian age. In the southern England, Tunbridge (1984) studied the Middle Devonian Hangman Sandstone Group in the North Devon and proposed that the main depositional facies were sandy ephemeral stream and clay playa on an extensive alluvial plain. Scrutton (1977) described the limestone deposition in the

South Devon and suggested it was deposited in a shallow shelf setting. Orchard (1978) studied the carbonate complex on the outer shelf ridge around Plymouth and proposed that the back-reef facies were developed. Burton and Tanner (1986) investigated the shallow water argillaceous facies in the eastern Cornwall, the presence of rich Eifelian trilobite faunas suggested a shallow marine setting.

The Middle Devonian Group is more extensive in the North Sea area, there was a narrow marine trough extended from Southern North Sea to Central Graben, where was thought to be the northernmost of this trough. This could be proved by the Middle Devonian penetration in the Auk and Ardmore Fields (Robson, 1991; Trewin and Bramwell, 1991; Gluyas et al., 2005). In the well 30/16-5 of Auk Field, the Middle Devonian limestones directly overlie the schistose basement, which is possibly the base of Devonian sequence. The fossiliferous limestones containing corals, bryozoans, brachiopods and crinoids were reported in the well 38/03-1.

Apart from this marine trough, other areas of North Sea are considered to be mainly terrestrial depositions in the Middle Devonian age, mainly alluvial-fluvial systems and lacustrine depositions. The 'Orcadian Lake' was believed existing in the centre of Orcadian Basin during the Middle Devonian (Trewin, 1989), and the occasional (c. 10%) deeper-water deposits of laminated, organic-rich calcareous siltstones and major ephemeral lake deposits of shrinkage-cracked, thin laminations of mud, coarse silt and fine sands were reported by Rogers and Astin (1991). Depositions around the 'Orcadian Lake' are the sequences of alluvial-fluvial systems which originated from the Northern and Grampian Highlands (Mykura, 2002). The 'Orcadian Lake' was featured as periodic expansions and regressions, the Achanarras and Sandwick fish beds in the Caithness were thought to be its maximum level (Glennie, 2009). To the northern margin of the 'Orcadian Lake', Allen and Mange-Rajetzky (1992) described

an alluvial fan and alluvial plain depositions with occasionally aeolian sediments in the Clair area.

2.1.3.3 Upper Devonian Group

The Upper Devonian Group in the British Isles and North Sea is mainly composed by alluvial-origin fluvial monotonous sandstones and minor aeolian sediments were also reported in the Orcadian Basin.

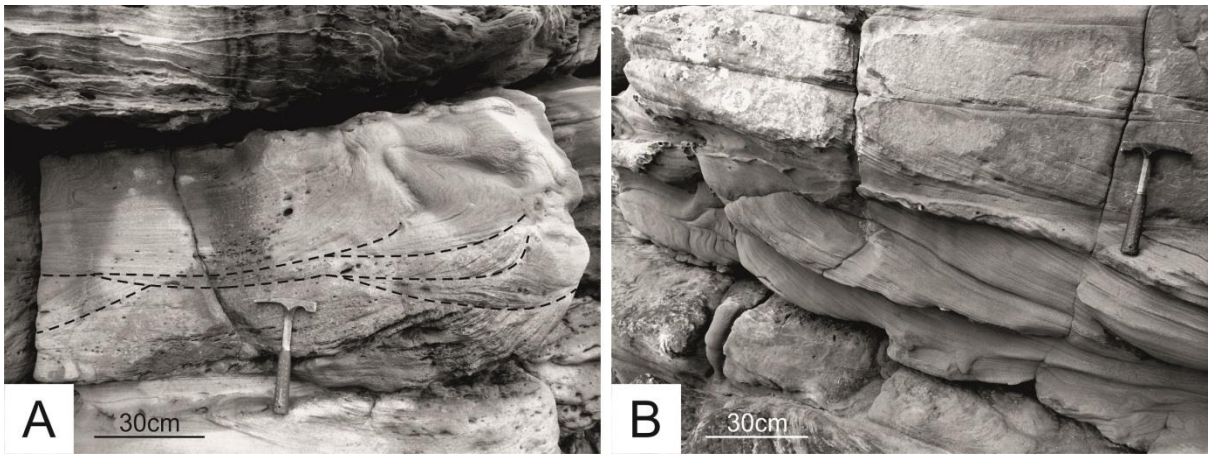

Figure 2.7 (A) Typical fluvial trough cross bedding sandstones, Upper Devonian Sandstone Group, Dunnet Head, Northern Scotland; (B) Typical fluvial planar cross bedding sandstones with soft sediment deformation, Upper Devonian Sandstone Group, Dunnet Head, Northern Scotland. Note the handle of hammer is 35 cm in length. Photos were taken by Longxun Tang.

The Upper Devonian Group is marked by the extension of alluvial-plain and fluvial braided system comparing with its underlying Middle Devonian lacustrine deposition (Graham et al., 2003) (**Figure 2.3C**). This change indicates the drainage system now could cover a basin-scale area rather than being limited within the mountain front areas in Early and Middle Devonian age. Trewin and Hurst (2009) investigated an outcrop mainly composed by Upper Devonian trough cross bedded, red to buff coloured sandstones in Dunnet Head and summarized the depositional facies was braided fluvial channels on a low-angle alluvial fan (**Figure 2.7**). In the Scottish Border, mainly the Midland Valley areas, the Upper Devonian Group

was suggested to be a fluviatile succession and has an unconformable contact with its underlying Silurian strata, a combination of high sinuosity stream systems and low sinuosity braided stream channels were proposed by their research, and the paleo-current direction is suggested from southwest to northeast (Leeder, 1973). Aeolian sediments were also reported by Hall and Chisholm (1987), they described the mixture of grain fall laminae and climbing ripple laminae, and that cross-bedded downward-wedging units of grain flow origin are interbedded with the finely laminated sandstones. They also examined the dip angle: the rose diagrams show that the dominance of winds was from easterly direction. To the south, in South Wales and Welsh Borderland, a maximum thickness of 1200 ft. Upper Devonian Group sandstones were reported by Allen (1965), he proposed that the deposit is composed by two sedimentary cycles, and each cycle contains alluvial deposits at base and gradually changed to marginal-marine deposits upward.

In the North Sea areas, there is no report of marine deposition during the Late Devonian. Many wells have encountered the Upper Devonian Group. The main depocentres include East Shetland Platform, Orcadian Basin (mainly in Outer Moray Firth Basin) and Central North Sea. There are no Devonian-reservoir oil fields in the East Shetland Platform, but Holloway et al. (1991) has used gravity and seismic data and interpreted the presence of Upper Devonian sediments.

In the Outer Moray Firth Basin, the Buchan Field (Blocks 20/5a and 21/1a) and Stirling Field (Block 16/21) contain typical Upper Devonian Buchan sandstones, which are interpreted as sandstones deposited in alluvial-fluvial facies with interbedded sheet flood or overbank mudstones (Edwards, 1991; Gambaro and Currie, 2003).

The Upper Devonian Group occurred in similar facies throughout the Central North Sea. Sandstones are mainly fine to medium grained with interbedded silts and shales, indicating

that the Central North Sea area was covered by a basinal-scale fluvial system (Gatliff, 1994). This could also be proved by a couple of oil fields all have penetrated into the similar Upper Devonian sequence. Gluyas et al. (2005), Bifani and Smith (1985) and Robson (1991) investigated the Ardmore Field in the Block 30/24, UKCS and proposed that the main depositional facies of Upper Devonian Group was mainly composed by fluvial and variable quantity of aeolian deposits. A 3000 ft. thick of porous sandstones with interbedded shales in the Auk Field, Block 30/16 UKCS, were reported by Trewin and Bramwell (1991), which was interpreted as fluvial system and flood plain deposits. The Embla Field is located in Norwegian sector (Block 2/7) and contains brown to red, very fine to fine-grained, moderately to well-sorted micaceous sandstones and silty mudstones, deposited in a flood plain/lacustrine environment (Knight et al., 1993).

2.2 Hydrocarbon exploration in the UK North Sea

The North Sea area is one of the most prolific hydrocarbon provinces in the world (**Figure 2.8**), the total recoverable reserves including adjacent onshore areas are about 100 billion barrels, of which nearly 50% was discovered within UK sectors (Spencer et al., 1996). The general stratigraphy and oil/gas-bearing formation of Northern, Central and Southern North Sea are summarized in **Figure 2.9**.

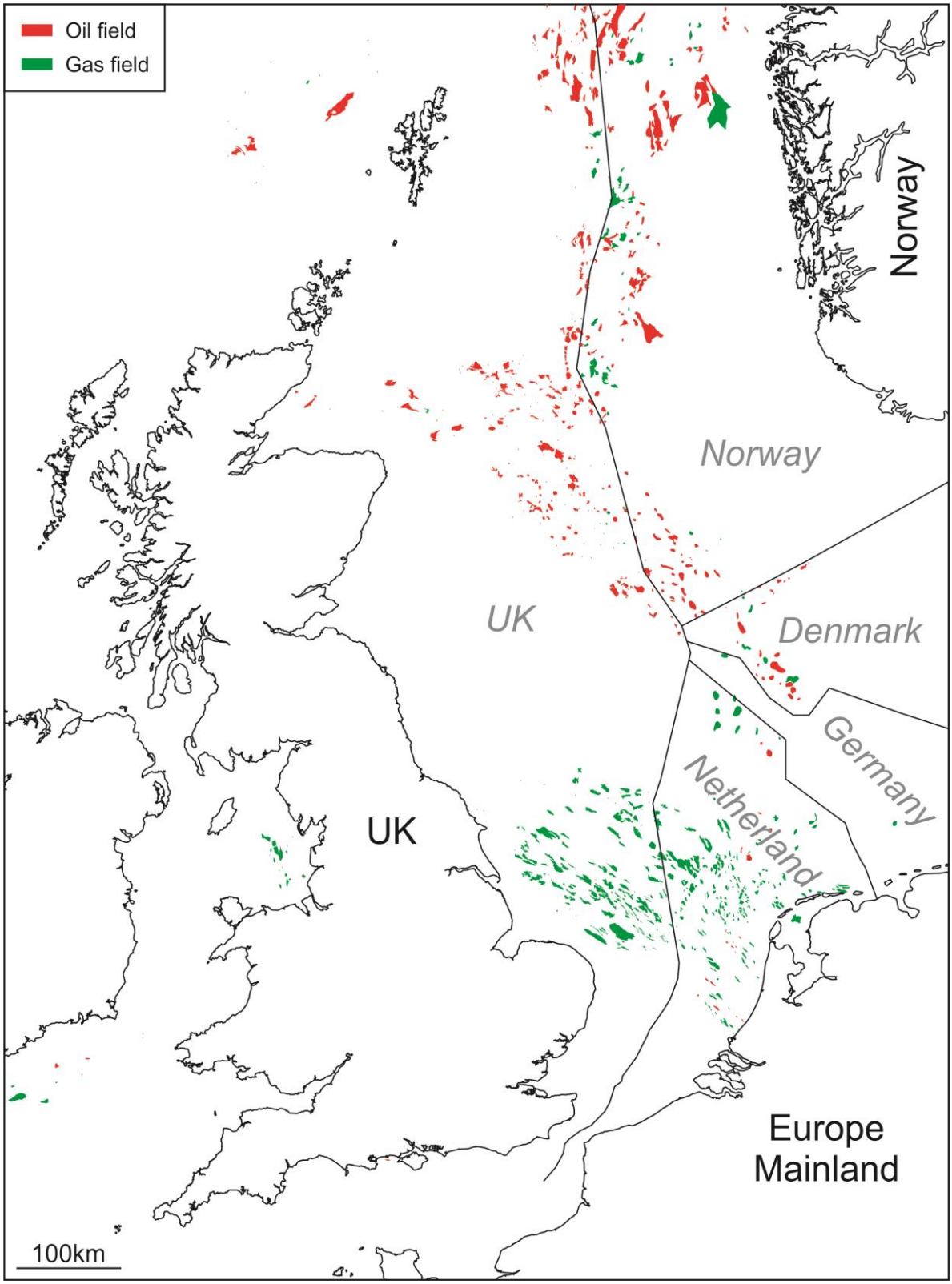

Figure 2.8 The up-to-date discoveries of offshore oil and gas fields in the North Sea. Origin data and figure from Oil & Gas Authority, simplified and modified by Longxun Tang.

Before 1964

Oil exploration began onshore UK (Derbyshire) in 1918 (Craig et al., 2013), but only a few small fields were discovered over the next forty years. The picture in western Europe changed dramatically in the late 1950s with discovery of the giant Groningen Gasfield and Annerveen Field in the Netherlands by Shell/Esso in 1959 and 1962 (Veenhof, 1996; Roels, 2001). The stratigraphic correlation of gas-bearing Permian sandstones provided the possibility that this sandstone reservoir, and thus the potential to find gas fields, could extend from Netherland to the North Sea (Glennie, 2009). From 1962 to 1964, several companies undertook marine seismic and aeromagnetic surveys, and provided an initial view of North Sea geological configuration.

1964-1970

BP commenced the offshore exploration in 1964 in the Southern North Sea Permian Basin and the first commercial discovery, the giant West Sole Gasfield in UK Block 48/6, was found in 1965, and initial reserves were 1.873 trillion cubic feet (TCF) within the Permian Lower Leman Sandstone Formation (Winter and King, 1991). After that, in the November of 1969, the first offshore oil field in UK sector, the Arbroath and Montrose Fields in Blocks 22/17 and 22/18, was found in the Palaeocene Forties Sandstone interval and oil is trapped by mudstones of the Sele Formation, and the reservoir sandstones were deposited in a prograde submarine fan. During the 1970, three important discoveries were made: the Forties Field located in Block 21/10, produced commercial oil from thick Late Palaeocene sandstones deposited in two major sand-rich submarine fan sequences (Wills, 1991). The Auk Field located in Block 30/16, produced light and low-sulphur crude oil at a rate of 940 m^3 per day from a thin collapse-brecciated and vugular dolomite, and underlying Permian Rotliegend Sandstones are also productive (Trewin and Bramwell, 1991). The Josephine Discovery from well 30/13-1,

has a flow rate of 128 m^3 per day from Jurassic sands at the depth of 3600 m (Erratt et al., 2005).

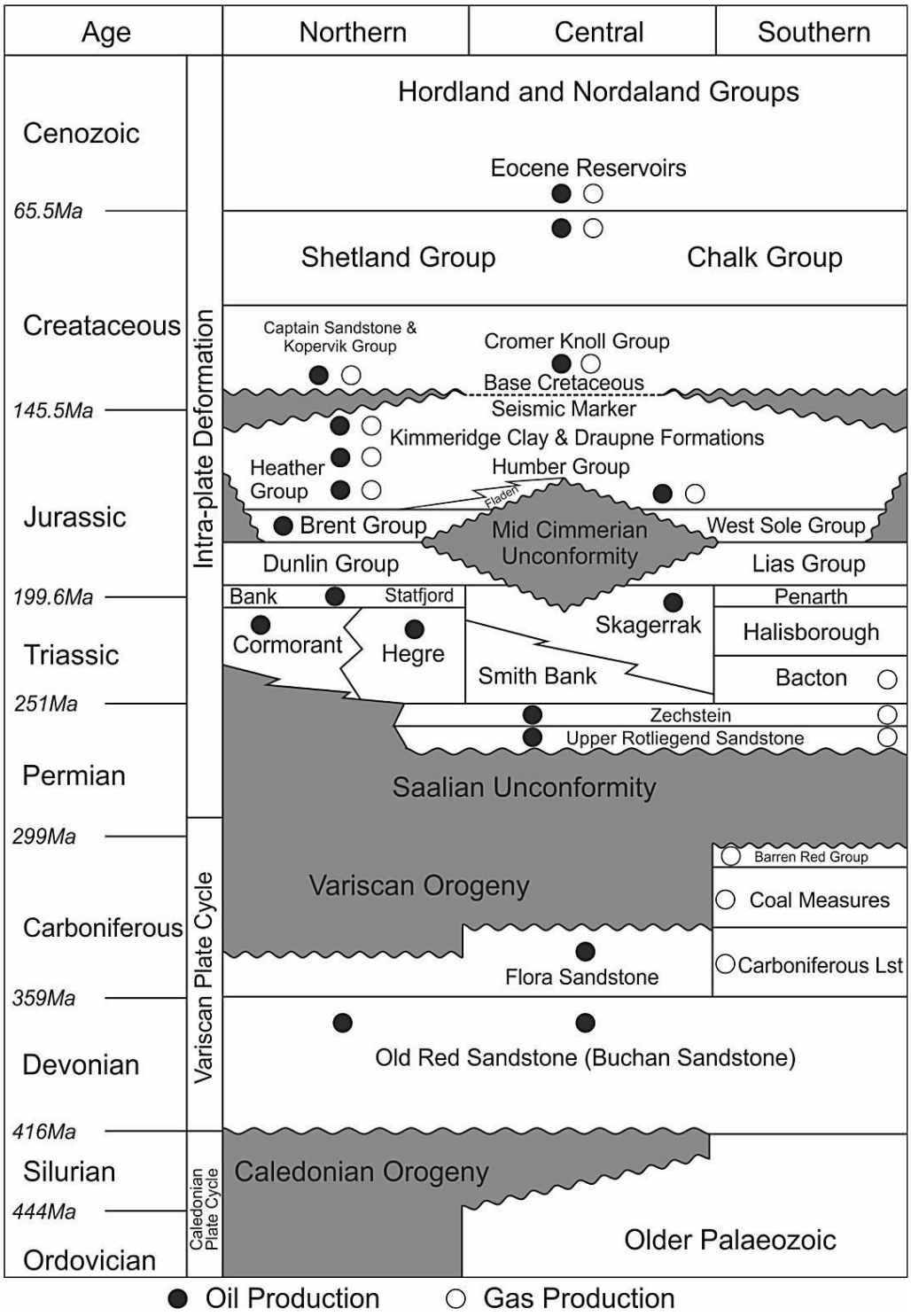

Figure 2.9 A simplified stratigraphic table of Northern, Central and Southern North Sea with notes of main oil/gas-bearing reservoirs. After Glennie (2009), slightly modified by Longxun Tang.

1971-1976

In 1971, the discovery of Brent Field was usually thought to be the milestone of the North Sea hydrocarbon exploration, the field is located in the Block 211/29 and produced 6500 barrels oil per day from oil-bearing Jurassic sands of deltaic and shallow marine origin, the recoverable hydrocarbon was 286 million m^3 for oil and 108 million m^3 for gas (Bowen, 1975; Struijk and Green, 1991; Taylor et al., 2003).

The success in Brent Field provided the information that the Brent style 'buried high' structure is an ideal trap for hydrocarbon deposition. Based on this theory, several similar fields were successfully discovered, they include: the Statfjord Field, located in Blocks 211/24 and 211/25, which has produced 5 billion barrels of oil and gas until 2016 (Nyland, 2016). The Piper Field, located in Block 15/17, containing approximately 172 million barrels of oil and 14 billion cubic feet of gas (OGJ, 2017). The Claymore Field, located in Block 14/19, containing approximately 1.45 billion barrels oil, until today 0.41 billion barrels oil has been produced (Compernolle et al., 2016).

Apart from Brent-style discovery, another Auk-type field was also found by Hamilton in 1971. The Argyll Field (renamed to 'Ardmore' and now part of 'Alma/Galia' development) in Block 30/24 produced commercial oil from Permian Zechstein dolomites and Rotliegend sandstones, and the later production proved that the underlying Devonian sandstones are also productive (Robson, 1991; Gluyas et al., 2005), although when first discovered what we now know to be Devonian sandstones were thought to belong to the Permian Rotliegend. During this period, the Jurassic Kimmeridge Clay has been recognized for its important source-rock characteristics. Additionally, the potential of Devonian sandstones was also illustrated by the discoveries of Buchan Field (Blocks 20/5a and 21/1a) in 1974, about 30,000 barrels/day of oil

were produced from Devonian sandstones with low porosity and permeability enhanced by intense fracturing (Edwards, 1991).

1977-1985

Considerable interests were still focused on the Jurassic targets; furthermore, Lower Cretaceous, Palaeocene and Eocene reservoirs became more prominent in this period (Glennie, 2009).

In the Central North Sea, a number of discoveries were found within the Upper Jurassic shallow marine sandstones (Saigal et al., 1992). These included Clyde, Duncan, East Duncan and Innes Fields (Robson, 1991). The hydrocarbon-bearing and productive Lower Cretaceous, which is mainly composed of turbidite sandstones, is distributed in the limited areas within Witch Ground Graben and Fisher Bank Basin in the Quadrants 14 and 16 of Northern North Sea (O'driscoll et al., 1990; Jeremiah, 2000). Beyond these areas, the Lower Cretaceous has poor potential. There are several large accumulations (200 million to 400 million barrels) in the Tertiary, and the hydrocarbon types range from gas/condensate to heavy oil (Glennie, 2009).

A small number of gas fields were discovered and started producing gas in the middle of 1980s, these include Esmond (Block 43/13a), Forbes (Block 43/8) and Gordon (Blocks 43/15 and 43/20), which were all operated by Hamilton Brothers (Glennie, 2009), the main reservoirs are Triassic Bunter Sandstone Group.

1985-1993

Several political and economic events (world-wide glut of oil, global stock-market collapse and Gulf War) had made the oil-price volatile during this period, the North Sea hydrocarbon exploration also suffered with few wells drilled. Despite this, there were also some discover-

ies in the Northern North Sea from Tertiary deep-water sand fans, the heavy oil and gas were found from the well 3/30a-3 in the Frigg Field (Brewster, 1991). BP found medium-gravity oil from Gryphon and Forth Fields in the Quadrant 9 (Newman et al., 1993). In the Central North Sea, Shell/Esso made a number of discoveries in the Eocene sands in the Gannet area along the western margin of the Central Graben. In the Southern North Sea, Arco, Conoco and BP have discovered several gas fields which had been described in details by Abbotts (1991).

Recent times and future trend

Until the end of 2014, about 42 billion barrels oil equivalent (BOE) have been produced from the UKCS **(Figure 2.10**). 210 oil fields (including oil fields and condensate fields) and 115 gas fields were in production (OGA, 2017). Most of the largest oil fields are within Mesozoic and Cenozoic strata and were discovered during the half-century since 1960s (**Figure 2.11**). The UK North Sea is now considered to be a mature petroleum province (Glennie, 2009).

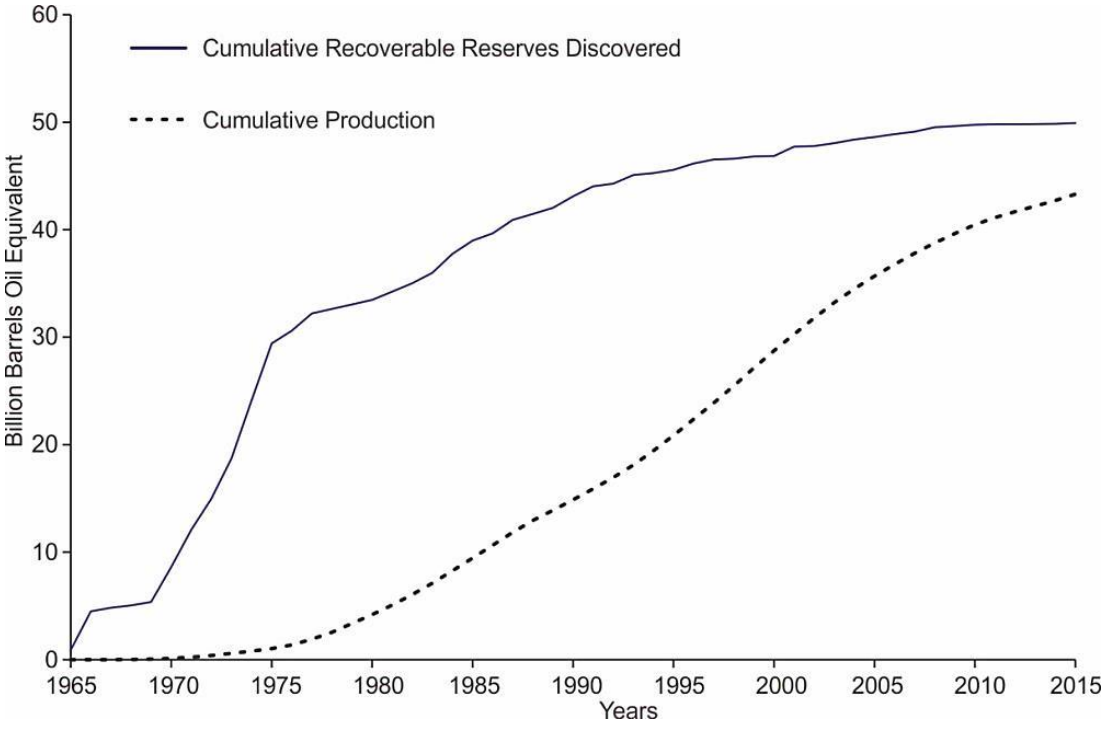

Figure 2.10 Rate of Discovery versus Rate of Production (Wood, 2014).

However, the Palaeozoic strata, especially the older objectives in the Carboniferous and Devonian strata are relatively unexplored and less well understood. The Carboniferous-Permian petroleum system in the Southern North Sea and onshore Europe is estimated to contain 22 to 184 million barrels of oil, and 3.6 to 14.9 trillion cubic feet of natural gas, approximately 62 million barrels of oil and 13 trillion cubic feet of gas are in offshore areas, and 26 million barrels of oil and 1.9 trillion cubic feet of gas are in onshore areas.

The older and commonly deeper Devonian strata have been generally assumed to have little hydrocarbon potential and regarded as only suitable for the termination depth for exploration wells (Glennie, 2009). However, there are several discoveries both in UK and Norwegian sections proved the considerable hydrocarbon potential in Devonian strata. Four oil fields in UK North Sea (Argyll, Buchan, Stirling and West Brae) and one field in Norwegian North Sea (Embla) have produced oil either solely from Devonian or Devonian-Carboniferous formations. The total recoverable hydrocarbon within Devonian is not totally clear but has increased more attentions for the future exploration.

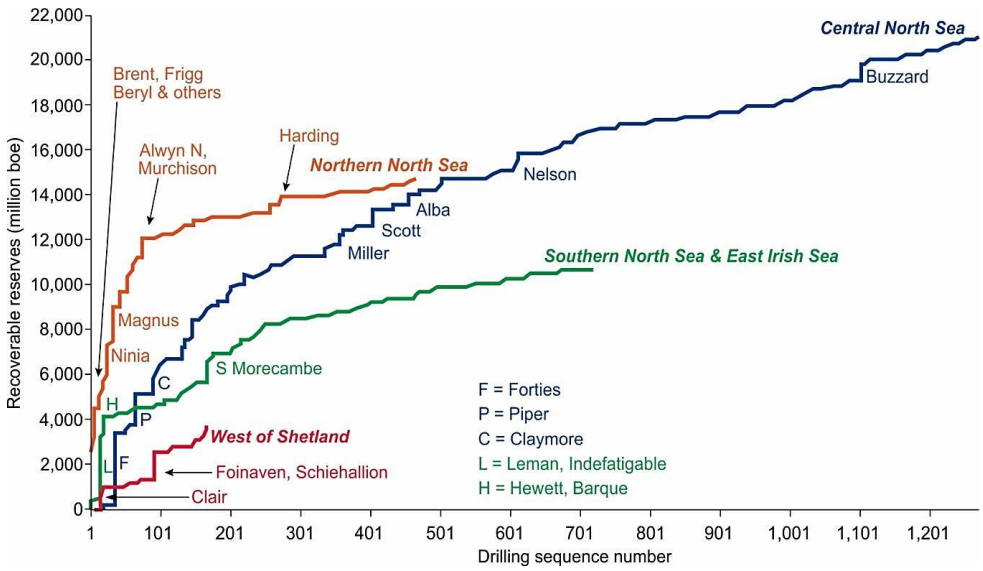

Figure 2.11 "Creaming" curves for areas of UKCS (Oil & Gas, 2012).

2.3 Reservoir quality of sandstones: a review

2.3.1 Reservoir quality controlling factors in siliciclastic rocks

The reservoir quality is defined by the hydrocarbon storage capacity and deliverability. The hydrocarbon storage capacity is characterized by the effective porosity and the size of the reservoir, whereas the deliverability is closely related to the permeability. At least within siliciclastic rocks, there is generally a positive correlation between porosity and $\log_{10}$ permeability. The exact relationship varies by various factors; however, increased porosity is commonly accompanied by increased permeability (Grier and Marschall, 1992). Generally there are three main controls on reservoir quality:

2.3.1.1 Depositional facies

Depositional facies can exert a considerable influence on the reservoir quality in relatively shallow depth. Each depositional facies would produce sand bodies with certain size and shape, by determining: a). Types and amounts of detrital grains; b). Detrital grain compositions; and c). Rate and distribution of depositions (Bloch and McGowen, 1994). In the shallow-buried rocks, lithofacies is the main control on reservoir quality, itself a product of the depositional facies (Weber, 1980).

Even in deeply-buried sandstones, reservoir quality of each facies does not change significantly if reservoirs were not affected by extremely heavy diagenetic process. Weber (1980) described as ‘one often finds the same general contrasts in permeability of the reservoir that existed in the original sandstone body but with an enhancement of the ratio between maximum and minimum permeability’.

In the diagenetically-simple rocks, reservoir quality is related to the facies-controlled parameters, such as framework composition and texture (Bloch and McGowen, 1994). These parameters can be expressed quantitatively and used to predict reservoir quality when the calibration data set is available. In this study, however, quantitative reservoir quality prediction is

much less accurate due to the diagenetic processes was extensive and complex. However, even in these diagenetically-complex rocks, the original composition generally controls the diagenetic history. Consequently, understanding the relationship between depositional facies and diagenesis can make qualitative evaluation of reservoir quality possible.

2.3.1.2 Diagenesis

Diagenesis will modify the original pore space during and following burial. Typically the reservoir quality is affected by four diagenetic mechanisms: compaction, cementation, dissolution and recrystallization. These mechanisms are mainly controlled by the detrital composition, burial process (time, depth and temperature), formation fluid and pressure.

a. Compaction

Compaction reduces porosity by grain rotation and rearrangement into a denser packing configuration (Hantschel and Kauerauf, 2009a; Brzesowsky et al., 2014), plastic deformation of ductile grains and breakage of brittle grains (Pettijohn et al., 2012). Physically, mechanical compaction is the result of effective overburden stress (Hantschel and Kauerauf, 2009b) and the main porosity reducer in shallow to medium burial depth (< 2.5 km) (Paxton et al., 2002). Rocks containing high ductile grains, such as mica, detrital clay clasts, and some volcanic clasts are more vulnerable to experience porosity reductions by mechanical compaction compared to those which are mainly made of rigid grains (i.e. quartz).

Since the porosity commonly has a negative relationship with burial depth, Gluyas and Cade (1997) have investigated numerous data both from actual fields and laboratory tests, and proposed an empirical equation for predicting porosity (± 2.5%) of clean, normally pressured and uncemented sands at 95% confidence level (**Figure 2.12**). Although the uncemented sands are uncommon in the natural circumstances, however, this compaction-only trend pro-

vides the theoretical maximum porosity (P_{max}) for a given depth, and the deviation of actual porosity to P_{max} may be roughly estimated as authigenic mineral volumes.

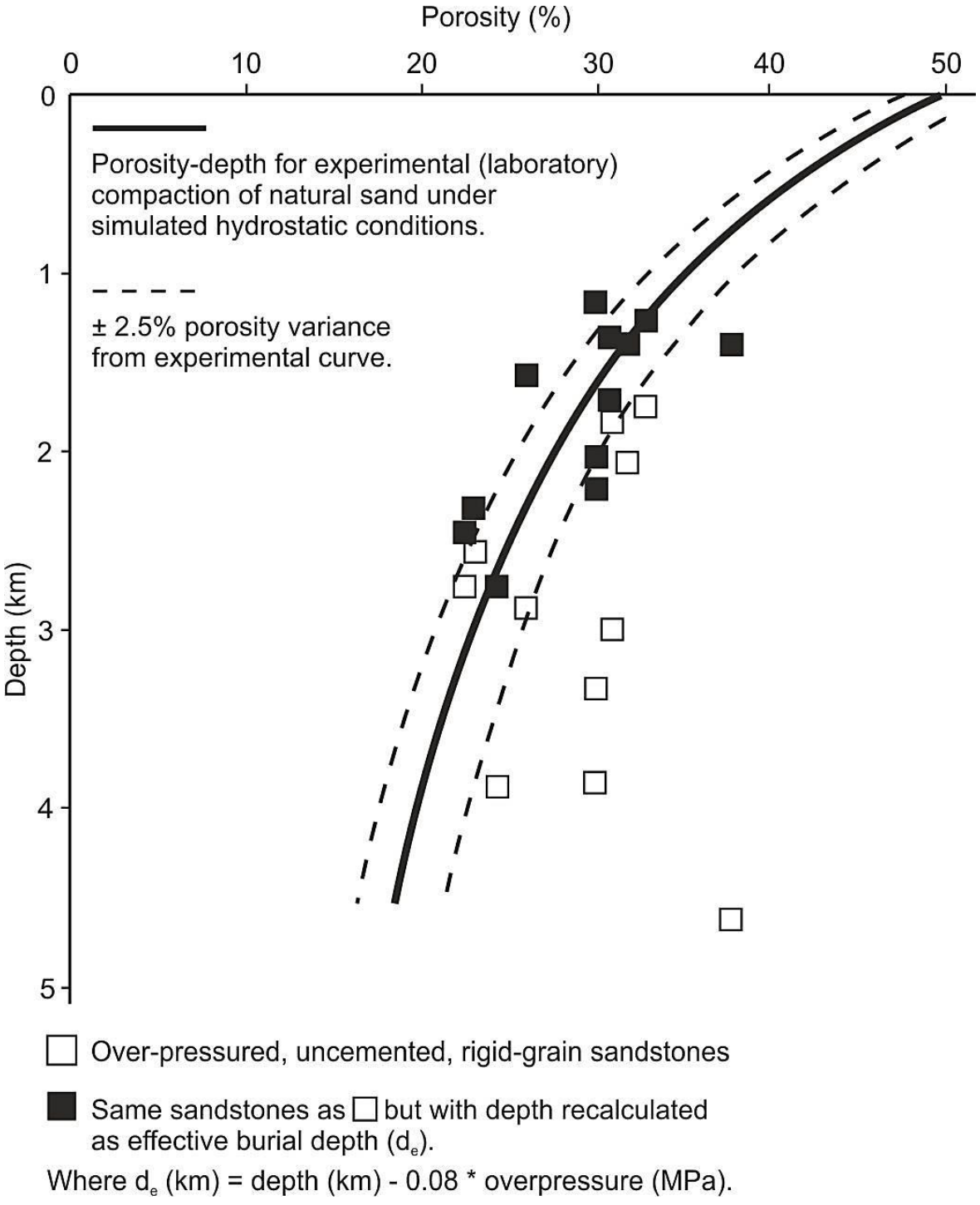

Figure 2.12 Porosity-depth relationship for uncemented, rigid-grain sandstones under hydrostatically pressured (calculated as the effective burial depth) and overpressure samples. After Gluyas and Cade (1997), slightly modified by Longxun Tang.

b. Cementation

Cementation is the most significant but not the only process consolidating loose sands into sandstones (Bridge and Demicco, 2008). It consists of mineral materials precipitated chemically from pore fluids and could occur at either early, middle or late stages in the diagenetic history (Hayes, 1979). Precipitation of authigenic minerals usually reduces reservoir quality by occupying intergranular pore space; however, cementation can also protect porosity if it supports the framework before the grains undergo further compaction. In this case, porosity would be limitedly decreased by compaction and it is possible to maintain good porosity at considerable depth (Ali et al., 2010).

Table 2.1 Common cement types and their usual crystal shapes (Welton, 1984).

Cement type	**Subtype**	**Common Crystal Form**
Authigenic clay	Chlorite	Rosette pattern platy
	Dickite	Thicker platy
	Illite	Fibrous, hairy
	Kaolinite	Platy
	Smectite	Crenulated, honeycomb
Carbonate	Calcite	Fibrous, bladed, granular, blocky, poikilotopic, syn-axial rim
	Dolomite	Rhombohedral, blocky, granular
	Siderite	Granular, blocky, bladed
Feldspar	Orthoclase	Syn-axial overgrowth, prismatic
	Plagioclase	Syn-axial overgrowth, prismatic
Iron oxide	Hematite	Disc-shaped
Silica	Quartz	Syn-axial overgrowth, prismatic
Sulphate	Anhydrite	Blocky, bladed
	Barite	-
	Gypsum	Blocky, bladed, prismatic
Zeolite	-	Platy, bladed, fibrous, prismatic, blocky

Cementation is closely related to many parameters, such as composition of the pore fluids, temperature, pH, available time for cementation and so on. Therefore, cementation can be promoted when those parameters are suitable thereby decreases porosity. Many mineral types can form cements; **Table 2.1** lists some common cement types and their usual crystal shape.

Calcite, dolomite, ankerite and siderite are the most common carbonate cement types in clastic rocks (Boggs Jr, 2006). The precipitations of carbonate cement require several physical and chemical conditions such as the concentration of carbonate in the formation water, pH value of the solution, temperature, partial pressure of CO_2 and the presence of the seed crystal as initial site for further growth, etc. (Harris et al., 1985). The effect of carbonate cement on reservoir quality is still on debate. The deterioration of reservoir quality occurs when sandstones are heavily cemented by carbonates. The massive carbonate-cemented horizons would compartmentalize reservoirs by acting as flow barriers between source rocks and reservoirs (Kantorowicz et al., 1987; Carvalho et al., 1995). The pore throats would also be blocked by the by-products (such as ferroan dolomite and iron oxide/oxyhydroxide) of carbonate cement once reacting with injected acid (Morad, 2009). On the other hand, an early-formed, lightly cemented carbonate may help decreasing porosity loss from compaction and provide secondary porosity when encountered acid formation water in the medium to deep burial depth (Schmidt and McDonald, 1979).

Quartz overgrowth is responsible for porosity and permeability reduction in moderately to deeply buried quartz-rich sandstones in various basins (Bjorlykke and Egeberg, 1993; Walderhaug, 1996). It typically forms syntaxial cements on framework host quartz grains during burial diagenesis at temperature above 70°C (Worden and Burley, 2003). The main sources of silica have been suggested to be from: 1). Dissolution of quartz grains by pressure dissolution; 2). Silica dissolved in circulating pore fluids by flow over quartz grains; 3). Silica (including amorphous phases) from shales; and 4). Liberation of silica during mineral reac-

tions (Leder and Park, 1986). The development of quartz overgrowth are closely related to many petrographic, mineralogical, physical and chemical factors, such as grain size, mineralogy, clay coatings, temperature history, pH condition and so on (Walderhaug, 1996).

Authigenic clay cements are common in all kinds' facies sandstones, the most common authigenic clay cement types are kaolinite/dickite, illite and chlorite. The types, occurrences, and distributions of authigenic clays are closely related to the reservoir quality, particularly permeability and water saturation (Wilson and Pittman, 1977). Clay minerals can modify pore size and shape by pore filling, pore lining (often regarded as grain coatings, details in chapter 2.3.2) or complex combination of these.

Authigenic feldspar commonly occurs but less abundant than carbonate, quartz overgrowth and clay cements. It usually presents as overgrowths around detrital feldspar host grains but occasionally as cement or newly formed crystal without a feldspar host grain (Ali et al., 2010).

c. Dissolution and secondary porosity

The post-depositional dissolution of detrital grains or cements usually results in the creation of secondary porosity (Taylor et al., 2010). Leaching of feldspars, lithic fragments and carbonates is very common (**Table 2.2**) and the importance of dissolution on improving reservoir quality has been reported in numerous studies (e.g. Loucks et al., 1979; Schmidt and McDonald, 1979; Mathisen, 1984; Taylor, 1990b; Ehrenberg and Jakobsen, 2001). The contribution of secondary porosity in deeply buried sandstones produced a big debate, opposing opinions mainly focused on the lack of convincing geochemical mechanisms that the dissolution and mass transfer could occur in the deep subsurface (Bjørlykke, 1984; Giles, 1987; Giles and De Boer, 1990).

Table 2.2 Common dissolvable matters and their portion of secondary porosity (Schmidt and McDonald, 1979).

Dissolvable matters	Portion of secondary porosity
Calcite	Major
Dolomite	Major
Siderite	Major
Feldspar	Major
Sulphate	Minor*
Other evaporates	Minor*
Silicate	Very minor
*: Maybe of major portion under specific conditions	

To evaluate the effect of dissolution, Taylor et al. (2010) has investigated the Permian to Eocene sandstones from the Gulf of Mexico, West Africa and North Sea. The results show that the volume of secondary porosity is probably overestimated in some publications. They suggested that no apparent relationship between temperature and secondary porosity created by framework grain dissolution is shown among their samples. The greatest value of secondary porosity is about 5% and the average value of secondary porosity is just 2%. They also concluded that the secondary porosity could be important in some specific situations but overall it only possesses a minor fraction of total porosity. The true effect of dissolution in sandstone is still in debate. In this study, dissolution of feldspar is commonly sighted, but the contribution of secondary porosity is generally minor, with the greatest value of 4% and an average value about 2.5% of total porosity.

d. Recrystallization

Recrystallization mainly occurs in carbonate and clay minerals and has variable effects on reservoir quality. Dolomitization of a limestone precursor may increase porosity by forming a space-supporting framework (Weyl, 1960) and the mole-for-mole shrinkage (Mg^{2+} replaced Ca^{2+}) which could create at most 13% secondary porosity (Dominguez, 1992). For the clay

recrystallization, illitization is the most common process which could occur on kaolinite and smectite precursors and usually reduced reservoir quality, the fibrous/hairy crystal shape usually complicates the fluid pathway therefore decreases permeability.

2.3.1.3 Structural deformation

The structural deformations, such as folds, faults and diapirs, will create fracturing and brecciation thus modifies the reservoir quality. The fracturing induced porosity is low (approx. 1%) but permeability could be significantly increased if the fractures keep open and are not filled by mineralization. For the brecciation process, except where the extensive cementations occurred in the breccia, it can increase reservoir quality due to shearing or collapse (Mitra, 1988). However, in this study, structural deformation did not play an important role on modifying reservoir quality.

2.3.2 The grain coating minerals

The effect of grain coating minerals on reservoir quality in siliciclastic reservoirs has been reported by numerous studies and is also a key finding in this project. The grain coating minerals are well known for the positive effect in preventing quartz cementation (e.g. Heald and Larese, 1974; Pittman, 1992; Ehrenberg, 1993; Bloch et al., 2002; Berger et al., 2009; Ajdukiewicz and Lander, 2010; Taylor et al., 2010). The negative effect of grain coating minerals are also reported for filling the intergranular pore space (e.g. Dewers and Ortoleva, 1991; Worden and Morad, 2003; Morad et al., 2010; Taylor et al., 2010; Wilson et al., 2014). Good reservoir quality is not strictly related to the absence of quartz overgrowth (Heald and Larese, 1974), but the presence of continuous and thick developed grain coating minerals are frequently associated with good porosity (Pittman, 1992).

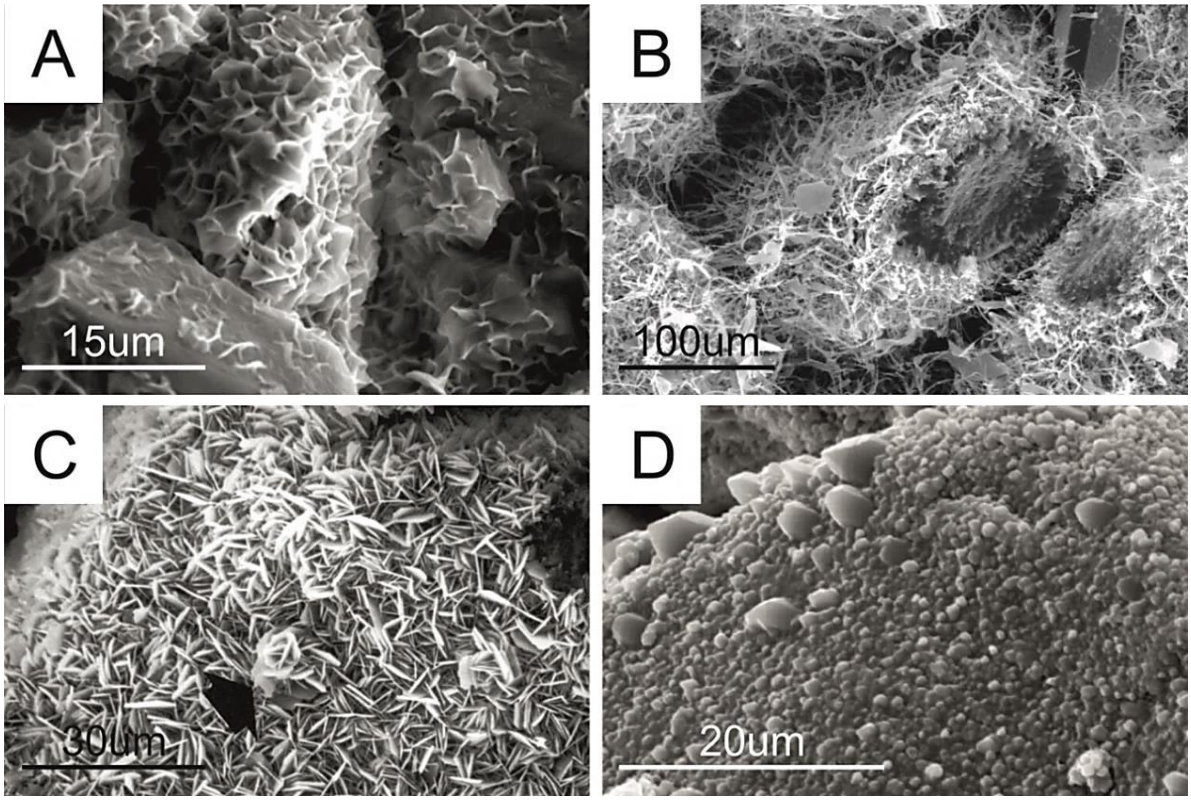

Figure 2.13 SEM microscopy photos for: (A) Grain coating smectite (Fesharaki et al., 2007); (B) Grain coating illite (Wilson et al., 2014); (C) Grain coating chlorite (Welton, 1984); (D) Grain coating micro-crystallized quartz (Taylor et al., 2010).

The occurrence of grain coats has been reported in a large variety of depositional environments, such as alluvial fan, delta, fluvial channel, shallow marine and aeolian facies (e.g. Carrigy and Mellon, 1964; Pittman and Lumsden, 1968; Heald and Larese, 1974; Dixon et al., 1989; Pittman, 1992). Although there is no generally preferred facies type for grain coats to develop, however, the necessary cations (e.g. Fe^{3+}, Mg^{2+}, and K^{+}) for authigenic grain coats were predominantly provided by alternation of lithic fragments, which are closely related to the depositional facies.

Mineralogically, the grain coats could be formed either by authigenic or allogenic process. Many minerals can form grain coats mainly including smectite, illite/smectite, illite, chlorite and microcrystalline quartz (**Figure 2.13**). The positive effect on porosity preservation in deeply buried sandstones due to grain coating chlorite and microcrystalline quartz has been

reported in many studies (e.g. Pittman and Lumsden, 1968; Ehrenberg, 1993; Berger et al., 2009; Jahren and Ramm, 2009; French and Worden, 2013; Stricker and Jones, 2016). Other coat types, have also been more or less mentioned, exerted similar effect under some special provenances and conditions (Storvoll et al., 2002; Tang et al., 2017b).

The main principle of porosity preservation of grain coatings, no matter what kind of coats, is inhibiting quartz overgrowth on the host detrital grains. When the silica is over-saturated in the formation fluid, it is easy to form the syntaxial quartz overgrowth on the detrital quartz grains. The early-formed, thick, well-developed and continuous coats can retard quartz overgrowth by masking the surface of quartz grains and prevent the nucleation of quartz overgrowth. However, the epitaxial cements, such as carbonate and sulphates, would not be affected by grain coats (Pittman, 1992).

2.3.3 Other reservoir quality controlling factors

The role of oil emplacement played on diagenesis still remains a controversial topic. The different amount of quartz cement in water leg and oil leg has been used as evidence for supporting or opposing the concept 'the oil emplacement prevents quartz cementation' and thereby the effect of porosity preservation in deeply buried sandstones (e.g. Dixon et al., 1989; Gluyas et al., 1993; Ramm and Bjørlykke, 1994; Barclay and Worden, 2000; Marchand et al., 2001; Aase and Walderhaug, 2005). The principle mechanism of oil emplacement preventing quartz overgrowth is that the quartz cementation is strictly controlled by the silica transportation rate in the water leg. When the water in the pore space is replaced by oil, the silica transport by diffusion is too slow to form quartz overgrowth and even halted when the oil saturation is high (Marchand et al., 2001). However, Barclay and Worden (2000) did not find any significant difference in quartz cement amount across oil-water contact in the Magnus Field, Block 211/12a, Northern North Sea. In the Fulmar field, it is reported that the quartz

cementation in oil leg is even higher than that of in the water leg (Saigal et al., 1992). However, the oil emplacement has exerted a minor diagenetic effect in the studied area of this research, the oil was originated from Upper Jurassic Kimmeridge Clay and filled the field by migrating a relatively long distance from north of the field (Gluyas et al., 2005). The fluid inclusions in the quartz overgrowth (with homogenization temperature from 80 to 120°C) are composed by pure brine and do not contain any organic matter. This might indicate the oil migration occurred in very recent time and does not have significant impact on diagenesis. Therefore, the effect of oil emplacement will not be discussed in the later chapters.

Overpressure is another frequently mentioned factor affecting diagenesis and reservoir quality. It is defined as the amount of pressure that exceeds the calculated hydrostatic pressure at a specific depth (Osborne and Swarbrick, 1997). Over-pressured pore fluids are common in sealed or semi-sealed geological systems where pore fluids are trapped and unable to circulate (Jeans, 1994; Osborne and Swarbrick, 1997). It could usually be produced by: 1). Increase of compressive stress especially due to the rapid burial process; 2). Variations in the volume of the pore fluid or rock matrix, and 3). Fluid movement or buoyancy (Osborne and Swarbrick, 1997). Other processes, such as aqua-thermal expansion, clay dehydration, hydrocarbon generation and cracking to gas may also create overpressure but in a limited effect and the geological system need to be strictly closed (Barker, 1972; Flemings, 1998). The main porosity preservation mechanisms by overpressure are: 1). The primary porosity, which would otherwise be lost to compaction, is kept open by overpressures; and 2). Inhibiting pressure solution in sandstones by decreasing the effective stress at grain contacts therefore eliminating a presumed primary source of silica (Taylor et al., 2010). However, the mineral composition and formation time of overpressure are also critical for an effective overpressure (Bloch et al., 2002). Lander and Walderhaug (1999) and Bloch et al. (2002) used artificial rigid and ductile models to demonstrate the importance of mineral composition and formation

time of overpressure on its porosity preservation. The results show that: 1). For both rigid and ductile sands, the early-formed overpressure, which is usually earlier than mechanical compaction occurred, provides a depth window of potential porosity preservation until temperatures reach the point where significant quartz cementation can occur (~90°C), but late development of overpressure has small or negligible effect on preserving porosity; and 2). The porosity preservation effect of overpressure, compared with hydrostatic pressure, is more obvious in ductile sands (14% and 3% intergranular porosity preserved by early and late overpressure, respectively) than in rigid sands (5% and 1% intergranular porosity preserved by early and late overpressure, respectively). In this study, the burial history shows that the Devonian Formation was indeed rapidly buried, however, the Devonian strata are not a completely closed system which is pressure communicated with overlying Permian Rotliegend, Permian Zechstein and Jurassic formations (Gluyas et al., 2005), and the presence of stylolite and extensive quartz overgrowth also indicate the overpressure does not have significant impact on diagenetic process. Therefore, the effect of overpressure on reservoir quality will not be discussed in this study.

CHAPTER 3: FACIES AND PETROGRAPHY ASSESSMENT OF THE BUCHAN FORMATION (UPPER DEVONIAN) OUTCROPS, DUNNET HEAD AND ORKNEY, NORTHERN SCOTLAND

---

*This chapter has been submitted to the **Scottish Journal of Geology** and is now under journal's review.*

Outline of this chapter

Summary

The Buchan Formation (Upper Devonian) comprises of non-marine deposited sandstones and intercalated siltstones and mudstones. It occurs in the Central and Northern North Sea and crops out in coastal exposures in north-eastern Scotland. Although the offshore unit has been locally proven as an important hydrocarbon reservoir, the sparse and limited core coverage in the North Sea means that the Buchan Formation is poorly understood. This study uses two localities with excellent Buchan Formation exposures in Caithness and Orkney, the main aims are to describe the detailed facies and investigate the mineralogical composition and porosity variations using detailed petrographic analyses. The results identify that the Buchan Formation is formed by braided fluvial and aeolian dune deposits. The aeolian sandstones have higher compositional/textural maturity and porosity than fluvial sandstones. The main control of porosity is the different facies types which result in different sedimentary structures, grain size and abundance of rock fragments. With the similar palaeo climate, depositional environment, comparable lithology and characteristic petrography evidence, these outcrops can be considered an excellent analogue for the Buchan Formation reservoirs in the North Sea.

3.1 Introduction

The term 'Buchan Formation' was first introduced by Cameron (1993) for the sandstone-dominated strata of Late Devonian to Early Carboniferous age in the Central and Northern North Sea. The term was initially used in the areas of the Buchan Field (UK Blocks 20/5a and 21/1a) and it is now largely used for Upper Devonian strata in the North Sea. Equivalent on-shore strata are present along the margins of the Moray Firth, in Caithness and on Orkney (Whitbread and Kearsey, 2016). The Buchan Formation is generally dominated by fine- to medium-grained sandstones, with minor pebbly sandstones, conglomerates, siltstones and mudstones (Cameron, 1993). The main depositional environments are suggested to have been easterly-flowing fluvial systems stretching from the Central North Sea to the Shetland Islands (Hunter and Easterbrook, 2004). Fluvial systems are generally regarded as broad sandy braided rivers, which were locally associated with aeolian dune systems and to a lesser extent sabkha depositional environment (Trewin, 2002).

Until now, the Buchan Formation sandstone has been perceived to have little potential as effective hydrocarbon reservoir (e.g. Glennie, 2009). There are a few oil fields in both UK and Norwegian North Sea that have reserves and have produced oil from the Buchan Formation sandstones (Bifani and Smith, 1985; Edwards, 1991; Robson, 1991; Trewin and Bramwell, 1991; Knight et al., 1993; Gambaro and Currie, 2003; Gluyas et al., 2005). However, the Buchan Formation has never been the main exploration target. As a consequence, the cores of offshore Buchan Formation are few and typically short in amounts recovered.

On the contrary, there are excellent coastal exposures of Buchan Formation at Dunnet Head and on the nearby Orkney Islands. These exposures provide an ideal opportunity to study facies, petrography and porosity of these Upper Devonian non-marine facies. The main aims of this research are to identify and describe the facies types in details, quantify the petrology and

porosity of the Buchan Formation using samples from these two localities and determine the main controls on porosity evolution. Outcrop data have also been used to measure the proportion, connectedness of the fluvial sand bodies and compared them with the offshore Buchan Formation sandstone reservoirs. We complete the study by discussing the potential of selected outcrop as possible analogues for the offshore Buchan Formation reservoirs in the North Sea.

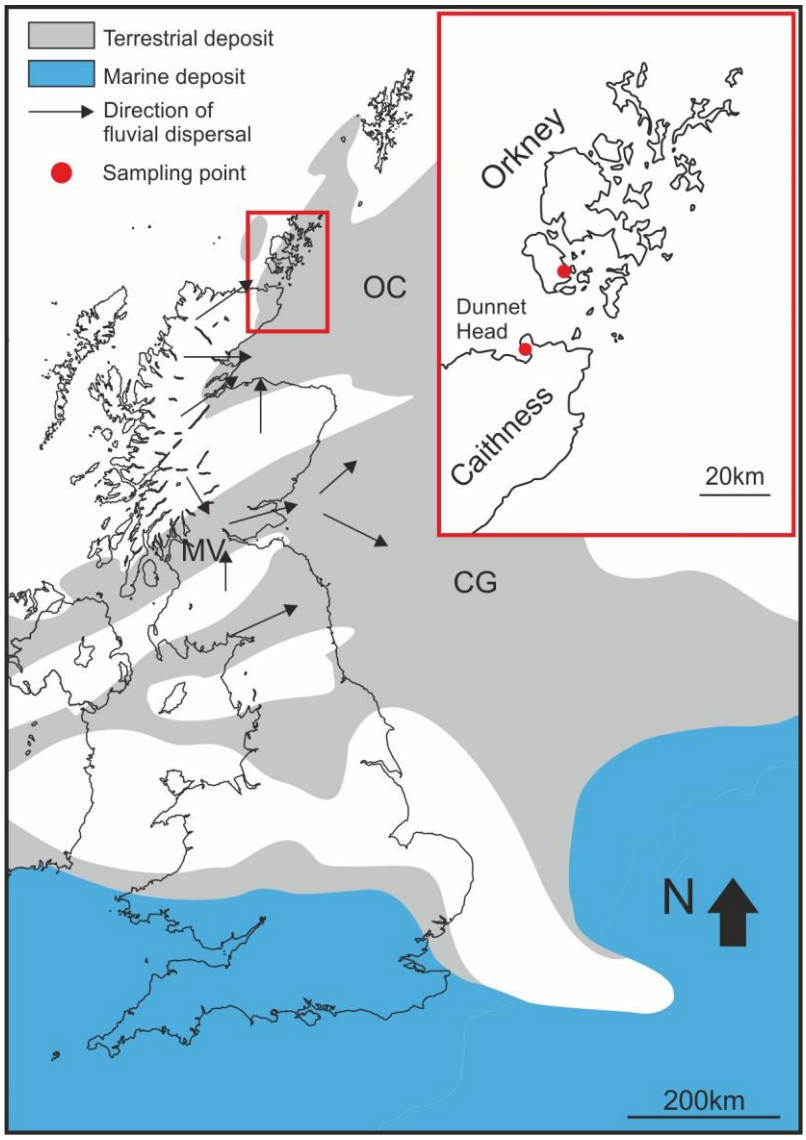

Figure 3.1 The sketched paleogeography map of British Islands and North Sea areas in the late Devonian age, and the locations of selected outcrops for this study, after Glennie (2009).

3.2 Geological background

Palaeo-magnetic data show that during the latest Middle to Late Devonian, the British Isles and North Sea areas were located in near equatorial latitudes around 15°S to 10°S, and the local climate was warm to hot and generally arid to semi-arid (Tarling, 1985; Witzke and Heckel, 1988). During the Early to Middle Devonian, continuous extension of Caledonian Orogeny created several important depo-centres for the Old Red Sandstone (Middle-Late Silurian to Earliest Carboniferous) deposits such as North Sea Basin and Orcadian Basin (Marshall and Hewett, 2003). From latest Middle Devonian to the end of Late Devonian, a continent-size braided system stretched from what are now the Central North Sea to the Northern North Sea, Orcadian Basin, western coast of Norway, Orkney, Shetland and its northernmost part probably reached the eastern Greenland (Ziegler, 1990; Friend et al., 2000) (**Figure 3.1**). The high relief areas, which were created by Caledonian Orogeny such as Southern Upland, Grampian Mountains and Northwest Highlands, are hypothesised as the main sediment source areas (Bradshaw et al., 1992). The general flowing directions of this braided system are suggested to be eastwards and north-eastwards (Ziegler, 1990). The wide distribution has made these fluvial sediments generally correlatable in the Central/Northern North Sea, Caithness and Orkney (**Figure 3.2**). The Buchan Formation was initially termed within the Buchan Field area, and now it is the representative Upper Devonian unit in the Central and Northern North Sea (Cameron, 1993b). It is partially equivalent to the Upper Eday Sandstone Formation and Hoy Sandstone Formation of Orkney Islands, and the Dunnet Head Sandstone Formation of Caithness (Kearsey et al., 2015).

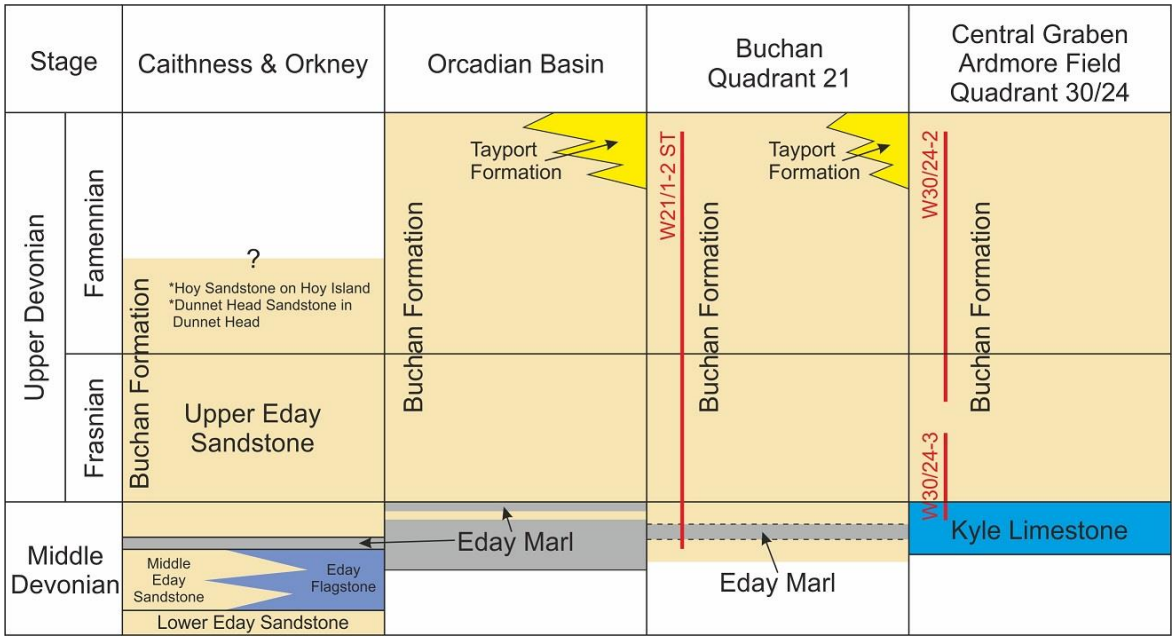

Figure 3.2 Stratigraphic correlations of Buchan Formation in the Central/Northern North Sea (with key wells), Orcadian Basin, Caithness and Orkney, after Graham et al. (2003).

The Buchan Formation in the Central and Northern North Sea is dominated by fine- to medium-grained sandstones, with minor pebbly sandstone, conglomerate, siltstone and mudstone (Cameron, 1993b). The succession represents a regional development of fluvial depositional systems across the former Orcadian Basin and Central Graben (Kearsey et al., 2015). The fluvial facies are dominated by low sinuosity sandy braided rivers; aeolian activities have been locally reported in the Ardmore Field (Gluyas et al., 2005; Tang et al., 2017a), Midland Valley of Scotland (Chisholm and Dean, 1974), Caithness and Orkney (Mykura, 2002).

The onshore Buchan Formation has excellent outcrops in Dunnet Head of the north-eastern Scotland and on the Orkney Islands. These localities have already attracted attentions and basic studies. An early study by Crampton et al. (1914) has described the sandstones in Dunnet Head as the 'Upper Old Red Sandstone' composed of major pink and yellow sandstones, minor shales, marls and mudstones. McAlpine (1977) recognized two major facies including braided river and aeolian in Dunnet Head and Hoy Island, respectively. Trewin and Hurst (2009) have made a preliminary study summarizing the outcrops displaying a typical Upper

Devonian fluvial sandstones with a general north-eastwards flowing direction. While the Upper Devonian outcrops in the Orkney Islands only distributed in the middle part of Hoy (Astin, 1990), despite the reports regarding exposed volcanic horizon at the base of the Hoy Sandstone (Upper Devonian) at a few localities (Storetvedt and Meland, 1985), the sandstones are interpreted as aeolian in origin (McAlpine, 1977; Friend and Williams, 1978; Trewin, 2002).

3.3 Materials and methods

In the northern Scotland, the Dwarwick Pier in the Dunnet Head (UK grid reference ND 207 713) has an excellent exposure of Upper Devonian sandstone which is large enough to permit collection of samples for petrography and porosity measurements. The sampling point on Orkney is located near Mill Bay on the east coast of Hoy Island (58°50'19.7"N 3°12'36.2"W), a small but typical aeolian facies exposure. A total of 25 samples (23 from Dunnet Head, 2 from Hoy) were collected by using a handheld rock drill. The samples were collected from discrete portions of the exposure and usually from less weathered parts of the outcrop.

All 25 samples were made into thin sections for petrographic examination and impregnated with blue epoxy to facilitate the identification of porosity. Petrographic examination was performed on a Leica DM2500P standard microscope to identify textures and mineral composition. Photomicrographs were taken using an attached Leica DFC420C digital camera. Estimation of the percentages of detrital grains, cements and porosity was made on an automated point counting stage with analysis of 300 counts per thins section. A HITACHI SU70 scanning electron microscope (SEM) equipped with energy-dispersive X-ray detector (EDX) was employed for a high-magnitude observation and semi-quantitative recognition of clay minerals.

3.4 Results

3.4.1 Description of sandstone bodies and depositional environment

3.4.1.1 Dwarwick Pier, Dunnet Head (Figures 3.3 and 3.4)

Description: the locality is at the northwest of the pier and displays typical fluvial sandstones of the Upper Devonian Formation (Trewin and Hurst, 2009). The outcrop mainly comprises pink, red to buff coloured, predominantly fine to medium grained sandstones. The sandstones are in sheet-like geometry and range in thickness from 0.2 m to 0.75 m, the thickness varies considerably due to erosion from the overlying sand sheets, up to a few centimetres thick at the flanks of sand body may be preserved locally between the individual sheets. Each sand body extends across the length of exposure with maximum 57.5 m in width (**Table 3.1**). Vertically the sand sheets stack to form a multi-storey sandstone bodies with about 6 m thickness. Based on differences in the sedimentary structures, three different types of sandstones have been recognized.

Sandstones with trough cross beddings (St) are the predominant type, consist of medium-grained sandstones with grouped sets of trough cross laminations. The sets are generally medium scale and range in thickness from approximately 10 cm – 30 cm. Some conglomerate-sized muddy clasts are scattered at the bases of the trough, soft sediment deformation and convolute beddings can be sighted towards the top of beds. Inclined beddings (Sl) and low-angle parallel laminations (Sh) are subordinate sedimentary structures. Sandstones are fine to medium grained with well-developed millimetre scale laminations and display current lineation. Silty or muddy layers are typically not observed.

Interpretation: based on the previous studies by McAlpine (1977) and Trewin and Hurst (2009), these sandstones are interpreted as the deposits in a low-sinuosity braided fluvial system possibly on a low-angle alluvial fan with the general transport direction from SW to NE.

This is inferred from the common presence of trough cross-bedding, tabular inclined beddings, low-angle parallel laminations and no presence of conglomerate and overbank fines, which are interpreted as within-channel sand deposits. The occurrence in places of laterally adjacent and coeval channel sand bodies indicates braided rivers (Tirsgaard and Øxnevad, 1998). Soft sediment deformation and convolute bedding on the top of beds are interpreted as the subsequent sediment reworking from the overlying layers or the rapid deposition of fine-grained sediment, thereby causing excess pore pressure (Bridge et al., 2000a). This combination of sedimentary structures strongly suggests an ephemeral braided system with a fluctuating water level, variations in flow velocity and periods of subaerial exposure (Tirsgaard and Øxnevad, 1998). The sheet-like sand body is also a characteristic feature of channels in a wide and shallow geometry with rapid lateral migration, the consequent sediment reworking resulted in the absence of fine-grained sediments.

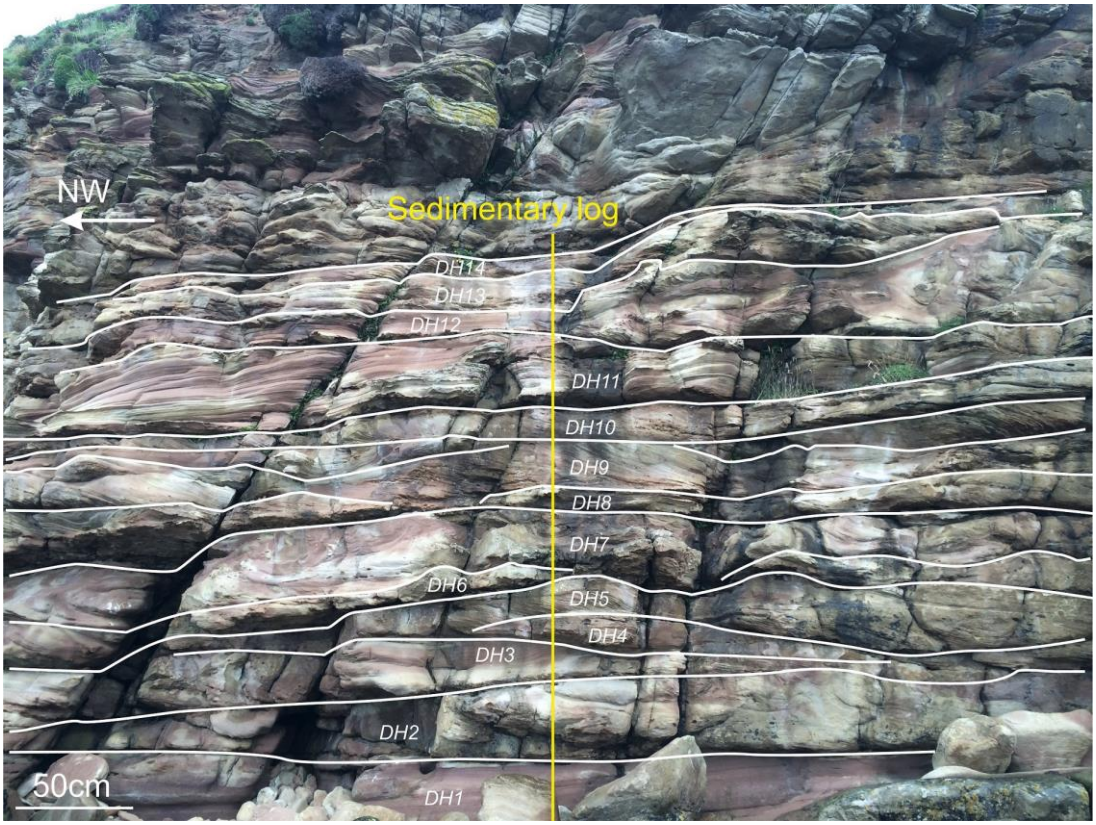

Figure 3.3 Fluvial profile in the Dunnet Head with 14 recognized sandstone units.

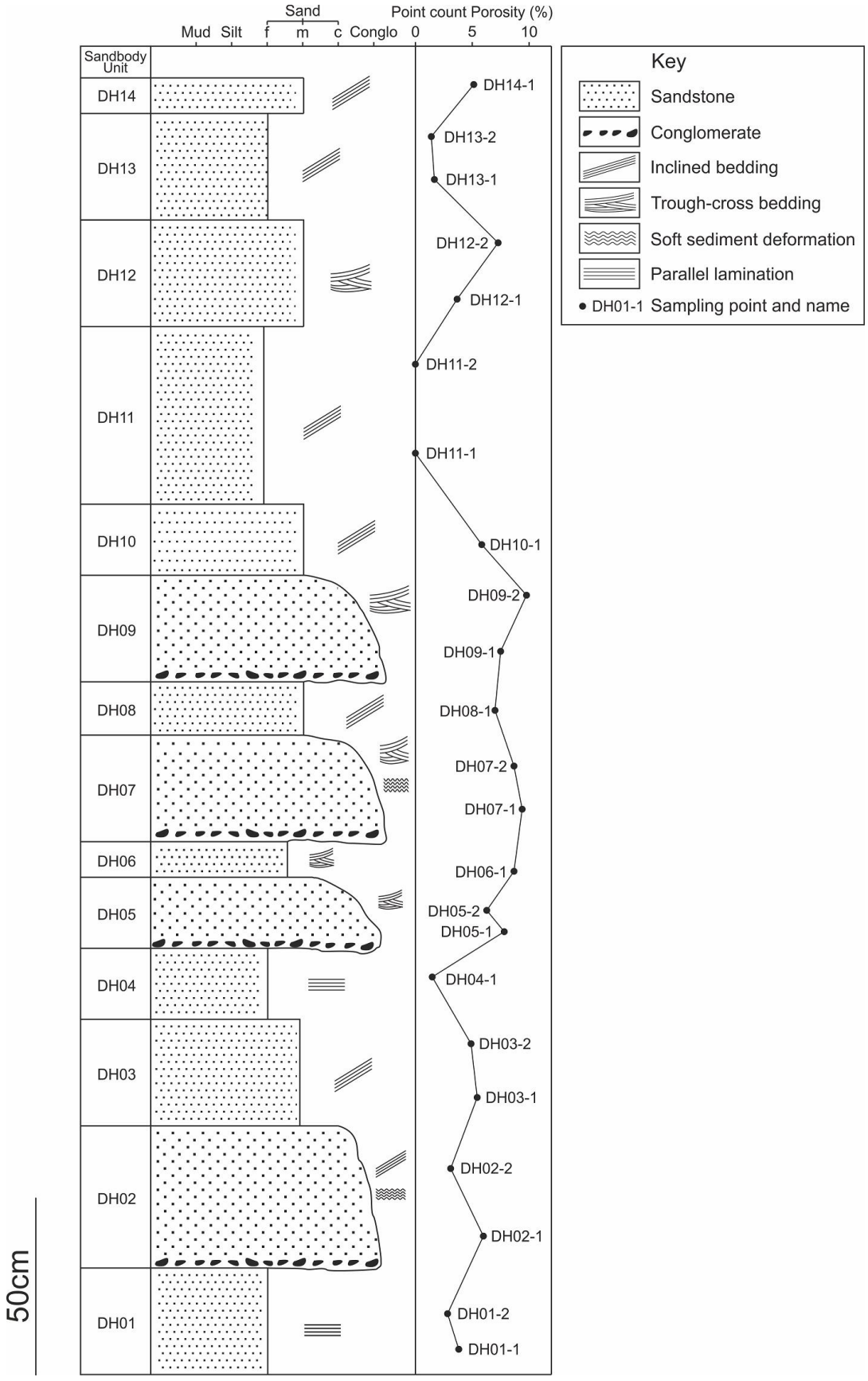

Figure 3.4 The sedimentary logs of the profile in Figure 3.3 with point count porosity.

3.4.1.2 Hoy Island, Orkney

Description: according to the BGS geological map of Hoy (sheet number 117W), the exposure located near Mill Bay on the east coast of Hoy Island (58°50'19.7"N 3°12'36.2"W) is a good outcrop for the Buchan Formation aeolian deposits. The main sedimentary structures are low-angle, asymptotic to base planar cross-beddings in a medium to large scale with wind ripples (S_{wr}) and thin parallel laminations (S_{pl}) (**Figure 3.5**). Wind ripple-laminated sandstones are at the base of the beds and gradually changed upward to thin and parallel laminated sandstones. Each lamination has thickness ranges from 1 cm to 5 cm with moderate to good continuity. Sandstones are yellow coloured, medium-grained and well sorted with no presence of conglomerates and fine-grain sediments.

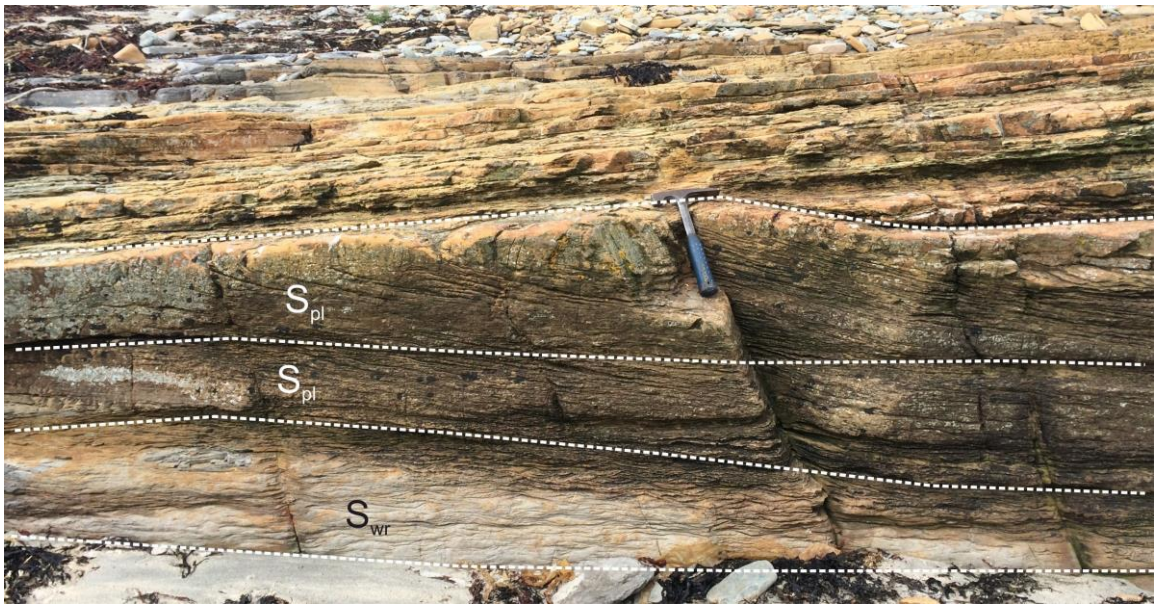

Figure 3.5 The aeolian exposures on the Hoy Island, Orkney. Swr – wind rippled sandstones; Spl – aeolian sandstone with thin parallel laminations. The length of hammer is 35 cm.

Interpretation: the large-scale planar cross bedding with thin parallel laminations indicates a stable and consistent sediment supply from the same direction. The occurrence of wind rippled laminated sandstones may indicate a damp interdune environment. The sandstones changes upward to the thin and parallel laminated sandstones which probably represents a

facies variation to the dune deposit. The well sorted sands and no presence of conglomerates and fine-grain sediments are also good indicators that these sediments were formed by aeolian process. The petrographic features (reported below) can also support this interpretation.

3.4.2 Petrography and porosity

3.4.2.1 Fluvial sandstones

According to the Folk (1957) classification, the point-count data (**Table 3.2**) indicate that the fluvial sandstones are litharenite ($Q_{52.1}F_{2.4}R_{45.5}$) and have a low textural/compositional maturity and low porosity (average ϕ = 5%). The sandstones are generally fine to medium grain size, sub-angular to sub-round with poor to moderate sorting (**Figures 3.6a – 3.6d**). Detrital quartz has a range of 33.6 % to 55.6%. The major type is the monocrystalline (**Figure 3.6b**) with subordinate amounts of quartz grains with undulose extinction (**Figure 3.6d**). Feldspar grains occur in minor amounts from trace and up to 4%, with most of the feldspar grains being microcline displaying polysynthetic twinning (**Figure 3.6d**). Rock fragments are particularly abundant (24% to 60%) and mainly consist of mica, chert and fine grained volcanic clasts (**Figures 3.6b, 3.6d**). Authigenic minerals mainly include calcite and kaolinite. The calcite cements show patchy distributions in the pore space with poikilotopic cementation (**Figure 3.6b**). Authigenic kaolinite mainly occurs in the intergranular space as vermicular aggregates. Some of the aggregates occur as infills in weathered feldspar grains (**Figures 3.6b, 3.6d**). There is a very limited amount of syntaxial macro quartz overgrowths. The point-count porosities of all 23 fluvial sandstone samples are very poor, from zero visible porosity up to 10% with an average value of 5% (**Table 3.2**).

3.4.2.2 Aeolian sandstones

Although there are only two aeolian sandstone samples, the point-count results (**Table. 2**) show contrasting features compared with fluvial sandstones. Both samples are medium

grained sub-litharenite ($Q_{89.0}F_{1.0}R_{10.0}$). The grains are moderate to very well sorted and sub-rounded to rounded (**Figure 3.6e**). Detrital quartz grains show major monocrystalline and minor undulose extinction (**Figure 3.6f**) and are coated by clay minerals. The grain coating clays are dense and continuous with strong birefringence (**Figure 3.6f**). SEM microscopy has shown that grain coating clays have 5 µm – 10 µm thickness, by using the EDX spectrum these clays are interpreted as illite/smectite (**Figure 3.7**). Feldspars, quartz overgrowths and pore-filling kaolinite are all in trace amount (< 1%). Carbonate cements are in minor abundance around 3%. The porosity of aeolian sandstone samples is higher than the fluvial sandstones and ranges from 11% to 14% (**Table 3.2**).

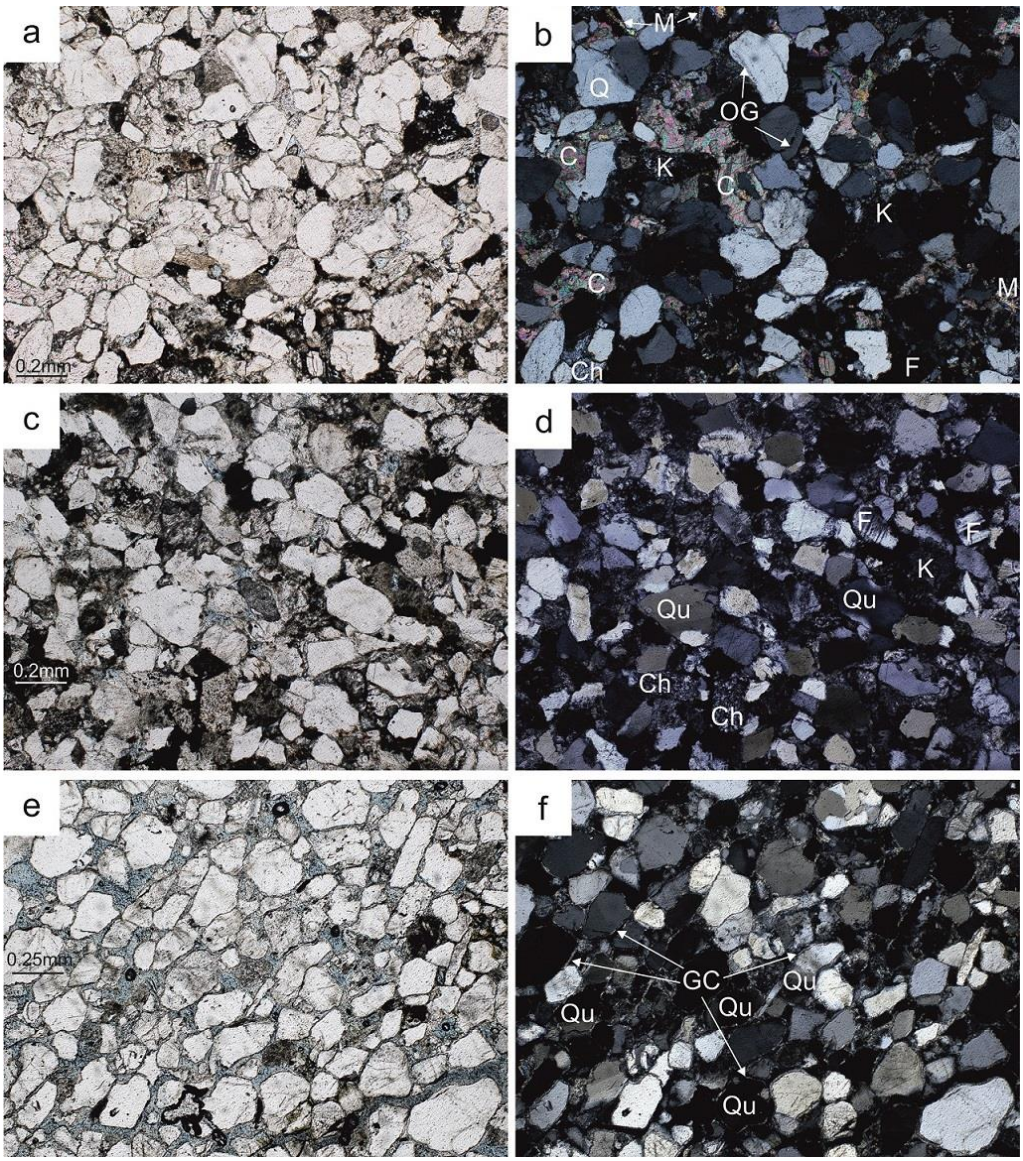

Figure 3.6 Thin section photos of fluvial and aeolian samples: (a) and (b): Plane-polarized and cross-polarized light photomicrographs of sample DH05-2, note the patchy distribution of carbonate cements and the presence of quartz overgrowth; (c) and (d): Plane-polarized and cross- polarized light photomicrographs of sample DH07-1, note the presence of quartz grains with undulose extinction; (e) and (f): Plane-polarized and cross- polarized light photomicrographs of sample OR01-1, note the high compositional and textural maturity, and the extensive distribution of grain coating clays on the quartz grains.

Q-quartz; OG-quartz overgrowth; K-kaolinite; C-carbonate cements; Ch-chert; Qu-quartz with undulose extinction; F-feldspar; GC-grain coatings.

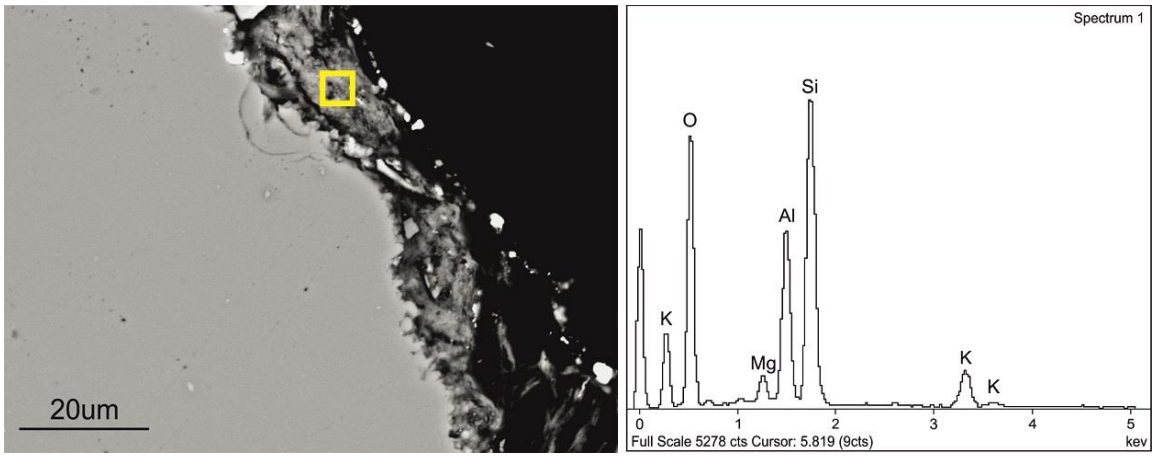

Figure 3.7 SEM image of the grain coating clay and its corresponding EDX spectrum, sample OR01-1.

3.4.3 Controls on porosity

Figure 3.8 is the scattered distribution of 23 fluvial samples from Dunnet Head with point-count porosity versus abundance of rock fragments. The data are categorised by grain sizes and sedimentary structures. The correlation between porosity and abundance of rock fragments shows an obvious inverse relationship (R^2 = 0.85). Apart from the abundance of rock fragments, the different grain size and sedimentary structures also have significant impact on porosity: the medium-grained samples have clearly higher porosity than fine-grained samples; while within the same grain size grade, sandstones with trough cross beddings (St) have higher porosity than those with inclined bedding (Sh) and parallel laminations (Sl). The different grain size, sedimentary structures and abundance of rock fragments are all closely faci-

es-related to channel; therefore we proposed that the primary and main controls of porosity in fluvial sandstone samples are the different fluvial micro-environments.

Aeolian samples have better porosity than fluvial samples (**Table 3.2**). Due to the limited sample quantities, the good porosity could preliminarily be attributed to good sorting and roundness with high content of quartz grains. Grain coating I/S also occurs at the grain contact areas, indicating early formation before the start of the mechanical compaction. Such grain coating clays may also have inhibited subsequent quartz overgrowth (e.g. Ehrenberg, 1993; Storvoll et al., 2002; Tang et al., 2017b).

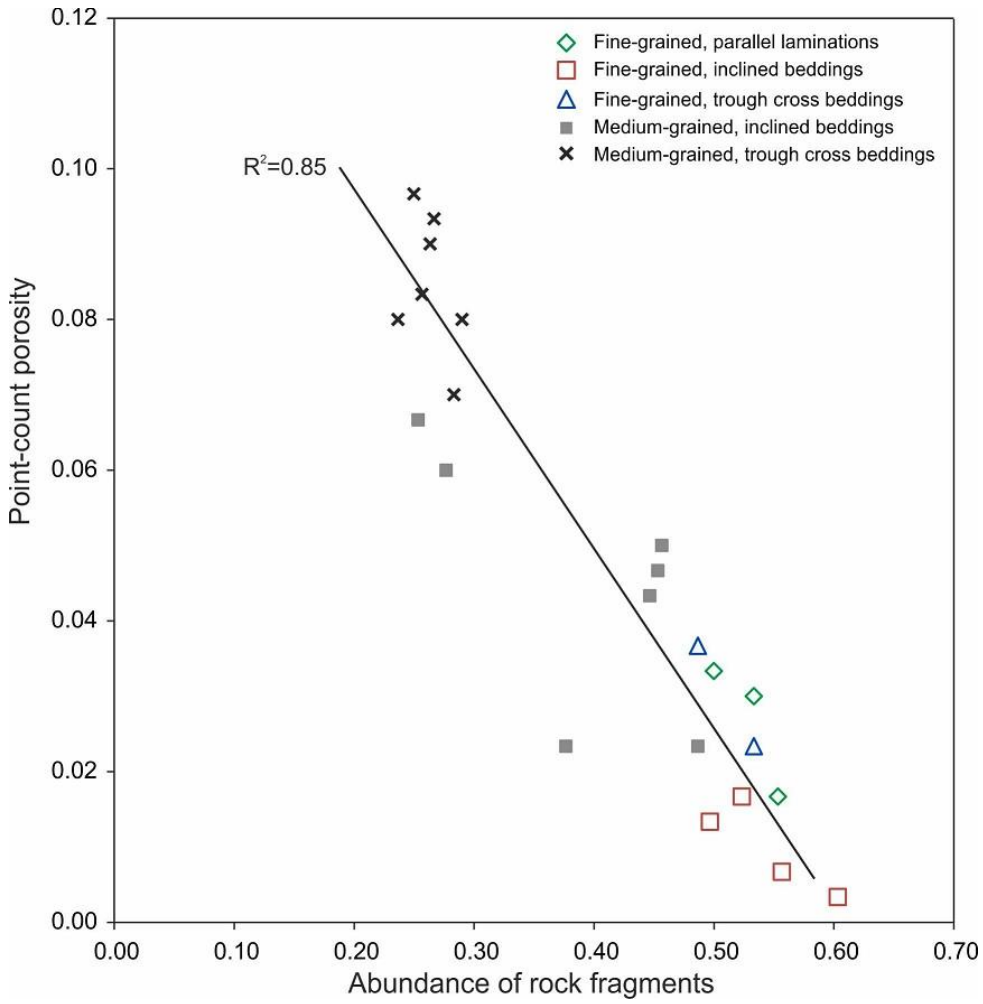

Figure 3.8 Scattered map of point-count porosity versus abundance of rock fragments, makers are differentiated by different grain size and sedimentary structures. Note the remarkable inverse correlation between porosity and the abundance of rock fragments (R^2 = 0.85).

3.5 Proportion and connectedness of fluvial sandstone bodies

The channel-deposit proportion (CDP) is one of the key factors determining whether the sand bodies are interconnected (e.g. Bridge, 1993; Bridge et al., 2000a; Bridge and Tye, 2000). It is proposed that if CDP is less than 0.4, channel belts are unconnected; while if CDP is greater than 0.75, all channel belts are connected. In our study, the proportion of sandstone bodies is very high both vertically and laterally within the outcrop. Channel sandstone proportion is generally greater than 0.95, explaining why most sandstone bodies are connected. The relatively thin, channel-form sandstone bodies are the deposits of the braided channels that migrated across the ancient low-angle alluvial plain. Vertical superimposed channel bars and fills are common, indicating a multiple episodes of fluvial channel depositions. Laterally adjacent sandstone bodies have been interpreted as the coeval channels. With the given width/thickness ratio (50:1 to 155:1, average 100:1) (**Table 3.1**) and sheet-like channel sand body geometry, the fluvial system is interpreted to have been wide and shallow channels with little confinement from river banks, this may also attribute to the lack of rooted vegetation in the Middle to Late Devonian (e.g. Davies and Gibling, 2010; Davies and Gibling, 2011; Gibling and Davies, 2012).

3.6 Comparison with subsurface sandstone bodies

The appropriate use of fluvial outcrops as an analogue for subsurface reservoirs is well documented (e.g. Miall, 1988; Howell et al., 2014; Pranter et al., 2014; Romain and Mountney, 2014). Buchan Formation is locally important reservoir rock in the Central and Northern North Sea (e.g. Marshall and Hewett, 2003; Glennie, 2009). The sandstone bodies in the outcrops need to be compared with subsurface sandstones in order to evaluate whether they can be useful analogues.

Detailed analysis of the thickness, width, proportion and connectedness of the offshore Buchan Formation reservoir has yet to be done. A preliminary attempt of comparing subsurface and outcrop data can be made using the summaries from Edwards (1991), Gambaro and Currie (2003), Gluyas et al. (2005) and Tang et al. (2017a). Subsurface sandstone lithologies, sedimentary structures, and interpretations are summarized in **Table 3.3**. Sandstone thickness was derived from cores and wireline logs. The lateral extent of sandstone bodies were established by well log correlation between neighbouring wells.

It is suggested that the thickness range, lithology and depositional environment of the selected offshore Buchan Formation sandstones are similar to that observed in the outcrops. In addition, more specific evidence is from the detailed petrography study which has clearly identified the presence of grain coating I/S in the Hoy aeolian samples. The grain coating I/S has also been found in the aeolian sandstones of Buchan Formation intervals in the Ardmore Field (Tang et al., 2017b). It is interpreted as the product of sediments in the distal sectors of fluvial distributary system. In the Ardmore Field, the fluvial-aeolian intercalated sediments were deposited under an arid climatic setting, the grain coating I/S was formed when the fluvial system retreated and aeolian deposition was dominant. The detrital clay-bearing waters of fluvial-origin may accumulated in the topographically lower interdune areas and would flow into the underlying, dry, porous and permeable aeolian sands by mechanical infiltration (Tang et al., 2017b).

In this study, the grain coating I/S widely occurs within grain contact area meeting the criteria of identifying an early-formed infiltrated clays (**Figures 3.6e, 3.6f**) (Wilson and Pittman, 1977; Moraes and De Ros, 1990). The fluctuating water level and variations in flow velocity have been interpreted from the Dunnet Head fluvial outcrop. Within the given fluvial-aeolian setting, rainfall variations in the hinterland high relief areas were the main control of the low sinuosity fluvial system (Nichols, 2005). With the suggested fluvial flowing direction to-

wards NE, the Hoy Island was farther to the fluvial system than the Dunnet Head. The aeolian exposure may represent a period of less developed braided system. In this case, only finer grained sediments, such as smectitic clays could be transported to Hoy.

By considering the highly similar palaeo-climate, sedimentary environment, lithology and petrography features, we recommended that the studied outcrops are good analogues to the offshore Buchan Formation in the Central and Northern North Sea.

3.7 Conclusions

This study has investigated the Buchan Formation sandstone outcrops from two selected localities at Dunnet Head and on Hoy, Orkney Islands to characterise their facies, petrography and porosity. The Hoy exposure on the Orkney Islands is an aeolian dune and interdune succession; sandstones are medium-grained, well sorted and sub-round to round with point-count porosity from 11% to 14%. In comparison the outcrop at Dunnet Head has been interpreted as a typical braided fluvial system with superimposed different types of channel deposits with trough cross bedding, inclined bedding and parallel laminations. The sandstones are fine to medium grained, poorly to moderately sorted and sub-angular to sub-round with point-count porosity from 0% to 10%. The main controls on porosity are the grain size, compositional and textural maturity, and the abundance of rock fragments, which are directly linked to the depositional environments. Channel sand bodies show a flat and thin geometry with a great width/thickness ratio about 100:1. The high fluvial channel sand body proportion in both vertical and lateral directions indicate that these sand bodies are likely to be interconnected.

The regional-scale depositional and climatic settings, lithological properties and sedimentary structures between selected outcrops and offshore Buchan Formation reservoir are highly comparable. In addition with the evidence that the outcrops and offshore Buchan Formation

reservoir both contain grain coating mixed layer illite/smectite that formed in the very early stage of burial by mechanical infiltrations. We recommended that the selected outcrops are excellent analogues to the Buchan Formation reservoir in the offshore oil fields of Central and Northern North Sea.

Acknowledgment

This paper is produced from doctoral research conducted at the Durham University. The author thanks Enquest PLC for financially supporting this research by covering all the costs for the field trip; Mr Ian Chaplin (Department of Earth Sciences, Durham University) for the preparation of thin section samples.

Table 3.1 The measured thickness and width of channel sand bodies from Dunnet Head profile and their corresponding width/thickness ratio.

Sand body unit	**Thickness (m)**	**Width (m)**	**Width/thickness ratio**
DH1	0.3	40	133.3
DH2	0.35	35.5	101.4
DH3	0.3	46.5	155.0
DH4*	0.2	10	50.0
DH5*	0.3	26	86.7
DH6	0.25	24	96.0
DH7	0.4	49.5	123.8
DH8*	0.25	19.5	78.0
DH9*	0.35	34	97.1
DH10	0.25	33	132.0
DH11	0.55	57.5	104.5
DH12*	0.75	51	68.0
DH13*	0.3	22	73.3
DH14	0.25	28.5	114.0
Average	0.34	34.1	100.9

Note: the sand bodies marked by * are significantly truncated by the overlying unit, so the measured results might be underestimated.

Table 3.2 Facies, lithology and point-counting mineralogical data of the samples taken from outcrops.

Sampling point	Sand body unit	Sample No.	Sedimentary Structures	Grain size	Q	F	R	Carbonate cement	Quartz cement	Kaolinite	Porosity	Facies
Dunnet Head	DH01	DH01-1	Parallel lamination	fine	0.38	0.02	0.50	0.03	0.01	0.02	0.03	Fluvial
		DH01-2			0.37	0.02	0.53	0.03	0.01	0.01	0.03	
	DH02	DH02-1	Inclined bedding; wavy lamination	medium	0.45	0.01	0.46	0.03	0.00	0.00	0.05	
		DH02-2			0.42	0.01	0.49	0.03	0.01	0.02	0.02	
	DH03	DH03-1	Inclined bedding	medium	0.44	0.02	0.45	0.03	0.01	0.01	0.04	
		DH03-2			0.43	0.01	0.45	0.04	0.02	0.00	0.05	
	DH04	DH04-1	Parallel lamination	fine	0.36	0.02	0.55	0.04	0.01	0.00	0.02	
	DH05	DH05-1	Trough cross bedding	medium	0.56	0.03	0.29	0.03	0.01	0.00	0.08	
		DH05-2			0.54	0.04	0.28	0.04	0.01	0.02	0.07	
	DH06	DH06-1	Trough cross bedding	medium	0.56	0.03	0.26	0.03	0.01	0.01	0.09	
	DH07	DH07-1	Trough cross bedding; wavy lamination	medium	0.57	0.03	0.27	0.02	0.01	0.01	0.09	
		DH07-2			0.57	0.02	0.26	0.05	0.02	0.00	0.08	
	DH08	DH08-1	Inclined bedding	medium	0.52	0.02	0.25	0.10	0.01	0.03	0.07	
	DH09	DH09-1	Trough cross bedding	medium	0.51	0.02	0.24	0.12	0.01	0.02	0.08	
		DH09-2			0.57	0.02	0.25	0.04	0.00	0.02	0.10	
	DH10	DH10-1	Inclined bedding	medium	0.52	0.02	0.28	0.09	0.01	0.03	0.06	
	DH11	DH11-1	Inclined bedding	fine	0.34	0.01	0.60	0.03	0.01	0.01	0.00	
		DH11-2			0.36	0.01	0.56	0.05	0.01	0.01	0.01	
	DH12	DH12-1	Trough cross bedding	fine	0.40	0.02	0.53	0.02	0.00	0.00	0.02	
		DH12-2			0.42	0.02	0.49	0.02	0.01	0.01	0.04	
	DH13	DH13-1	Inclined bedding	fine	0.38	0.03	0.50	0.06	0.01	0.00	0.01	
		DH13-2			0.37	0.03	0.52	0.05	0.01	0.00	0.02	
	DH14	DH14-1	Inclined bedding	medium	0.45	0.03	0.38	0.07	0.02	0.03	0.02	
Orkney		OR1-1	Large-scale planar cross beddings with pin-stripe laminations	medium	0.75	0.01	0.07	0.02	0.00	0.01	0.14	Aeolian
		OR1-2			0.74	0.01	0.10	0.03	0.00	0.01	0.11	

Table 3.3 Lithology, sedimentary facies and interpretation of subsurface sandstone bodies compared with studied outcrops.

Field & Outcrop	Location	Rock type	Grain size	Sedimentary structures	Sedimentary facies	Possible sediment source area	Flowing direction	Individual sand body thickness	Sand body ratio
Dunnet Head/Hoy	Caithness	Sandstone	fine to medium	St, Sh, Sl	Braided-fluvial	Northwest highlands	north-eastwards	0.2 m to 0.75 m	> 95%
	Hoy		medium	Swr, Spl	Aeolian	-	-	0.3 m to 0.5 m	> 95%
Ardmore	Block 30/24, UKCS	Sandstone	fine to medium	St, Sp, Sh, Sl	Braided-fluvial	Southern Uplands	eastwards	0.2 m to 1.5m	72.30%
		Sandstone	medium	Swr, Sps	Aeolian	-	westwards	0.5 m to 2 m	> 95%
Buchan	Blocks 20/5a, 21/1a, UKCS	Sandstone	fine to medium	-	Braided-fluvial	Grampian Mountains	eastwards or south-eastwards	-	-
Stirling	Block 16/21, UKCS	Sandstone	-	-	Braided-fluvial	Grampian Mountains	-	-	-

Sedimentary structures: St-trough cross bedding sandstone; Sh-low angle horizontal laminated sandstone; Sl-inclined bedding sandstone; Swr-wind rippled sandstone; Spl-parallel laminated sandstone; Sp-planar cross bedding sandstone; Sps-pin stripe laminated sandstone.

CHAPTER 4: FACIES ARCHITECTURE OF THE FLUVIAL–AEOLIAN BUCHAN FORMATION (UPPER DEVONIAN) AND ITS IMPLICATIONS ON FIELD EXPLORATION: A CASE STUDY FROM ARDMORE FIELD, CENTRAL NORTH SEA, UK

---

*This chapter has been published in the **International Journal of Geosciences** (July 2017)*

Tang, L., Jones, S. and Gluyas, J. (2017) Facies Architecture of the Fluvial-Aeolian Buchan Formation (Upper Devonian) and Its Implications on Field Exploration: A Case Study from Ardmore Field, Central North Sea, UK. International Journal of Geosciences, 8, 902-924.

doi: 10.4236/ijg.2017.87052

Chapter outline

Summary

The Upper Devonian Buchan Formation in the Central North Sea is a typical terrestrial deposit and predominantly comprises fine to medium-grained sandstones with occasional conglomerates and mudstones. The Buchan Formation has been previously described as being made up mostly of braided fluvial sandstones; however, this study confirms the presence and significance of aeolian sandstones within this fluvial-dominated sequence. Facies architecture is investigated through analogue outcrop study, well log curves and numerical facies modelling, and the results show contrasting differences between fluvial and aeolian facies. The fluvial facies is composed of multiple superimposed sand-dominated fining-upward cycles in the vertical direction. Individual sand body has a large width/thickness ratio but shows no correlation between wells. The high channel deposition proportion (CDP, average value = 72%) in fluvial-dominated intervals means that it is likely all the sand bodies are interconnected. Aeolian facies comprise superimposed dune and interdune depositions and can be laterally correlated over considerable distances (over 1 km). Although the aeolian sandstones are volumetrically minor (approx. 30%) within the whole Buchan Formation, they have very high porosity and permeability (14.1% – 28%, 27 mD – 5290 mD) and therefore are excellent potential reservoirs. The fluvial sandstones are significantly cemented by quartz overgrowth and dolomite and by comparison with the aeolian sandstones are poor reservoirs. Aeolian sandstones can be differentiated from fluvial sandstones using several features: pin-stripe lamentation, good sorting, high visible porosity, friable nature and lack of muddy or conglomeratic contents. These characteristics allow aeolian sandstones can be tentatively recognized by low gamma ray values, high sonic transit time and low density in uncored wells. The thin, laterally correlatable and permeable aeolian sandstones within the Buchan Formation are effective reservoirs and could form important exploration targets when the Devonian is targeted elsewhere in the Central and Northern North Sea.

4.1 Introduction

The hydrocarbon reservoirs of the Ardmore Field (previous name 'Argyll', now part of 'Alma/Galia project') in the UK Central North Sea comprise Upper Devonian Buchan Formation, Permian Rotliegend Sandstone and Permian Zechstein Carbonate (Bifani and Smith, 1985; Robson, 1991; Gluyas and Hichens, 2003). The Permian Rotliegend and Zechstein groups are important reservoirs in the North Sea and have been researched by numerous studies (e.g. Nagtegal, 1979; Glennie and Provan, 1990; Purvis, 1992; George and Berry, 1993; Howell and Mountney, 1997; Sweet, 1999). For the Devonian strata, the reservoir properties of Buchan Formation are highly variable, the depositional facies were poorly understood and briefly described as fluvial deposition under a semi-arid to arid setting (Robson, 1991; Gluyas et al., 2005). Until now, no report has focused on detailed facies analysis, how the facies architecture of Buchan Formation displays in the subsurface and the relationship between different facies and highly variable reservoir properties.

In this study, we have re-examined the cores and re-interpreted depositional facies of Buchan Formation in the Ardmore Field. The results show that the Buchan Formation is composed of mixed fluvial-aeolian sandstones. The aeolian sandstone intervals have the best reservoir quality among the Buchan Formation. Facies architectures and porosity/permeability relationships of fluvial and aeolian intervals show distinct differences which are responsible for the highly variable reservoir properties. The main aims of this paper are: (1) To characterize and interpret the main facies associations; (2) To simulate the facies architecture based on analogue outcrop study and the well log data; (3) To propose facies model for the fluvial–aeolian deposition of the Buchan Formation; and (4) To set several tentative criteria for recognizing aeolian sandstones in uncored wells. This is the first study on the fluvial-aeolian facies architecture of the offshore Upper Devonian reservoirs in the UK North Sea. The results provide insights into facies architecture of Buchan Formation, improve the knowledge of poorly un-

derstood Devonian in the North Sea and are useful for forecasting the quality of Upper Devonian reservoirs in the Central North Sea and other areas ahead of drilling.

During this study, lithofacies description and facies identification were carried out on cores from six wells in the Ardmore Field. Study on the analogue outcrops provides useful information of the geometry and lateral extent of the fluvial facies associations. The facies architecture in the subsurface was achieved by the facies modelling module of the Schlumberger Petrel software based on the integration of outcrops study, core data and well logging interpretation.

4.2 Geological background

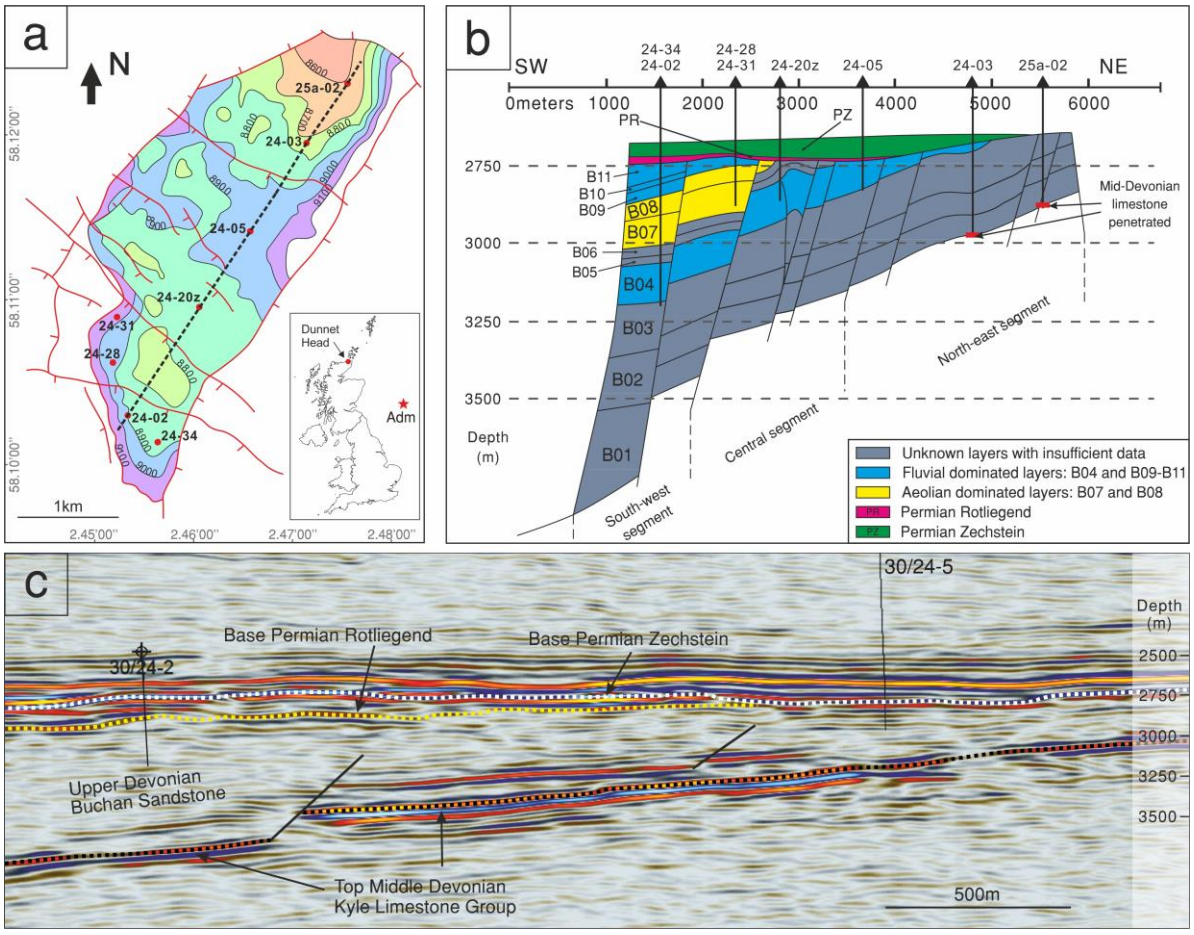

Figure 4.1 Geological maps showing: (a) Location and main structure elements of Ardmore (Adm) Field, note the location of the studied outcrop (Dunnet Head); (b) Vertical section of an SW-NE profile (dashed line in 1a); (c) Seismic section of an SW-NE profile (part of dashed line in 1a).

4.2.1 Tectonic setting of the Ardmore Field

The Ardmore Field is located on the Argyll Ridge, a large SW-NE trending Palaeozoic age tilted fault block on the south-western flank of the Central Graben in Block 30/24, UK North Sea, about 350 km south-east from Aberdeen. The field is a horst feature with the crest in the north and fault closure to the north-east. It measures 2.5 km wide and 6 km long (**Figure 4.1A)**. A combination of dip and faulting defines the limits of the field on the north-west and south-east flanks, while dip closure defines the southern limits of the field. The major fault trends are in two main directions, WNW–ESE cut by NW-SE faults (**Figure 4.1B**). Top seal of the field is provided by Triassic shale to the far west, Jurassic shale in the mid-part of the field and impermeable Chalk at the north-eastern crest (Gluyas et al., 2005). The trap relies heavily on the major SW-NE trending graben edge faults to the northeast and southwest of the field while dip closure occurs to the northwest and west.

4.2.2 Stratigraphy of the Buchan Formation

The Devonian sequence in the Ardmore Field comprises a succession of the Middle Devonian Kyle Limestone and Upper Devonian Buchan Sandstone. The succession dips to the south-west, and is separated from the Permian by a palaeo-topographic unconformity, in which successively younger stratigraphic units in the Devonian sub crop towards the south-west. Although the pre-Permian surface has topography also dips to the SW, this has the effect of making the oldest part of the Buchan Sandstone subcrop the unconformity in the NE of the field and thus the youngest Devonian in the SW slightly deeper (**Figure 4.1B**).

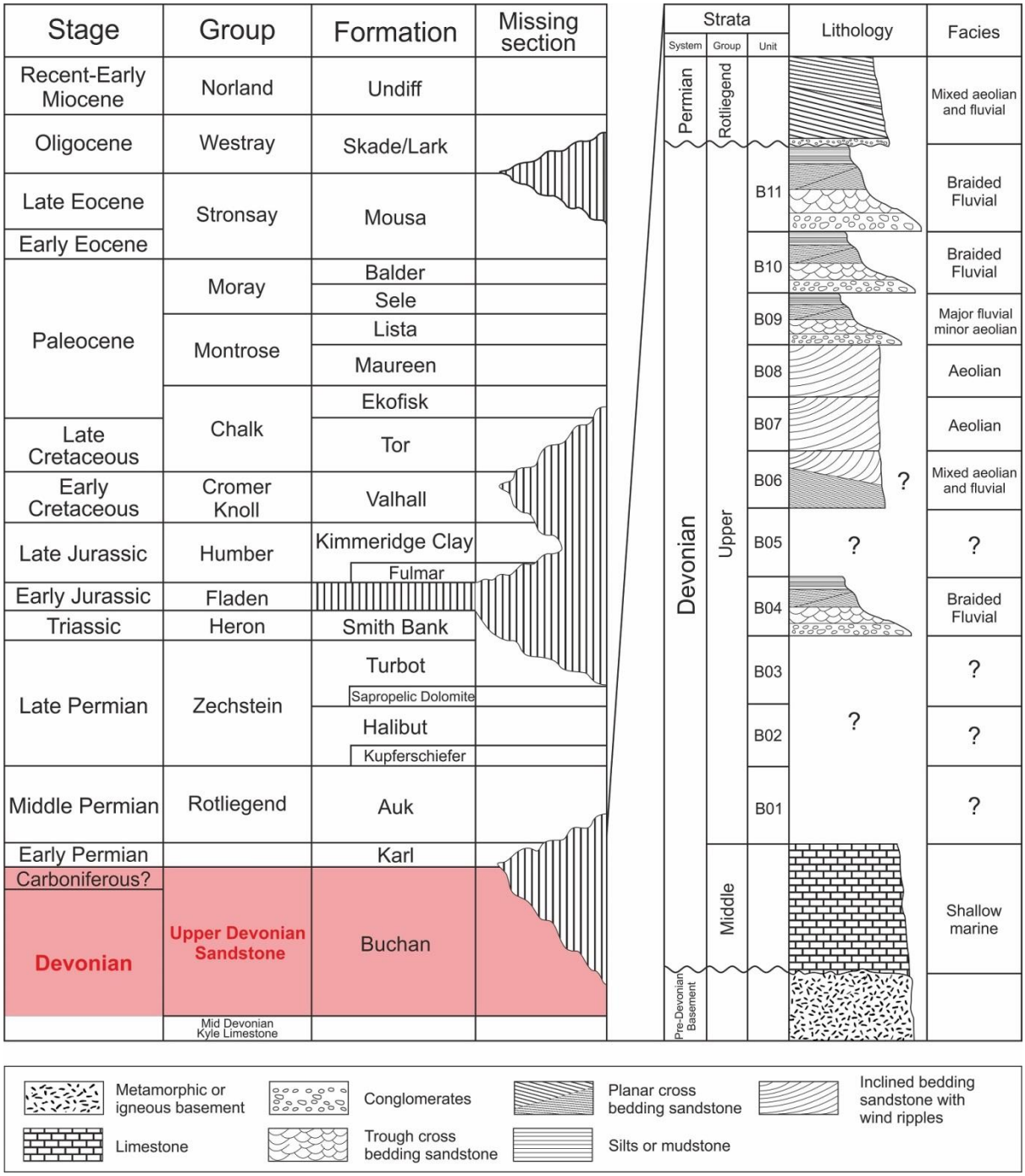

Figure 4.2 Stratigraphy column and sedimentary logs of the Ardmore Field.

The Middle Devonian Kyle Group is a fairly thin unit (c. 105 m. thick, **Figure 4.1C**) comprising limestones and minor evaporates (Graham et al., 2003). In the adjacent Auk Field, this succession rest unconformably on pre-Devonian basement (Trewin and Bramwell, 1991); this might be similar in Ardmore as inferred from seismic interpretation. The Middle Devonian limestone is mainly encountered in Ardmore wells 30/24-03 and 30/25a-02 (**Figure 4.1B**),

and forms a strong intra-Devonian seismic reflector throughout the area of the field (**Figure 4.1C**).

The Upper Devonian Buchan Formation comprises a thick, generally upward-coarsening succession of shales of mixed shallow marine and sabkha environment at the base, passing upwards into mainly fluvial and aeolian sandy sediments (**Figure 4.2**). The whole Buchan succession lacks clear seismic stratigraphic markers, a combination of log and core data has been used to divide the stratigraphic units for the Upper Devonian Group: B01 is the oldest unit overlying the Middle Devonian Limestone, and B11 is the youngest unit (Gluyas et al., 2005). In the absence of bio-stratigraphic data, sedimentary structures and lithofacies associations have been applied to help correlation (Gluyas et al., 2005). The total thickness of the Buchan Formation is nowhere documented due to the combination of erosion below the Devonian-Permian unconformity, lateral thickness variation and incomplete well penetrations. The estimated thickness is about 500 – 800 m according to the seismic profile (**Figure 4.1C**).

4.3 Facies analysis

The detailed lithofacies study forms the basis of this paper, six wells were chosen because they comprises important fluvial and aeolian intervals in the Ardmore Field, and have a good data availability (drilled cores with good recovery and well log data).

The lithofacies in the Ardmore Field can be roughly divided into three associations according to the dominant grain size grades: conglomerates (G), sandstones (S) and fine-grain sediments (F). The further detailed lithofacies identification has confirmed eight sub-types (**Table. 4.1**), the classification of lithofacies is mainly based on the original scheme of Miall (1977).

4.3.1 Fluvial facies association

Table 4.1 The lithofacies types in the Ardmore field and the corresponding descriptions, sedimentary structures, interpretations and appearances.

Facies	Lithofacies code	Lithology description	Structures	Interpretation	Appearances
Fluvial	Gm	0.5 – 1 m thick, sandy matrix-supported, red brown intra-formational mudstone or grey to white-grey quartz pebbles conglomerates, pebbles are around 1 - 3 cm in diameter.	Massive to crudely bedding	Basal lag deposits	B04, B09, B10, B11
	St	0.5 – 1.5 m thick, fine to medium-grained sandstones, containing grouped or solitary sets of trough cross laminations	Trough cross-bedding	Downstream migration of sinuous-crested dunes in fluvial channels (lower flow regime)	B04, B09, B10, B11
	Sp	0.5 – 1 m thick, fine to medium-grained sandstone with solitary sets of planar cross laminations, better sorted and cleaner than St and lack mudstone or quartz pebbles	Planar cross-bedding	Transverse and linguoid sand bars in fluvial channels (lower flow regime)	B04, B09, B10, B11
	Sh	0.2 – 0.5 m thick, red-brown, fine-grained sandstones with millimetre-scaled thin laminations.	Horizontal lamination	Flash floods deposits (lower flow regime)	B04, B09, B10, B11
	Fl	0.2 – 1 m thick, argillaceous and micaceous, very fine-grained sandstones to siltstones.	Thin laminations with soft sediment deformation	Temporary floodplains and inactive or abandon channels	B04, B09, B10, B11
	Fm	0.2 – 0.5 m thick, micaceous dark red-brown silty mudstones and mudstones	Massive bedding	Overbank	B04, B09, B10, B11
Aeolian	Sps	0.5 – 1 m thick, upper fine- to medium-grained, well sorted, well rounded sandstones. High visible porosity, friable nature and the absence of muddy or conglomeratic intra-clasts.	Pin-stripe lamination	Dune	B07, B08
	Sw	1 – 2 m thick, very fine- to medium-grained sandstones, moderately to well sorted, locally developed mud desiccation, de-water structure, cross-bedding ripples and argillaceous streaks	Discontinuous wavy lamination with several local structures	Interdune with fluctuating dry and wet conditions	B07, B08

The fluvial facies is volumetrically major (approx. 70%) in the whole Buchan Formation of the Ardmore Field and composed of multiple fining-upward cycles (see details in facies architecture part). In this study, two types of fluvial facies are identified: fluvial channel deposit and flood plain deposit.

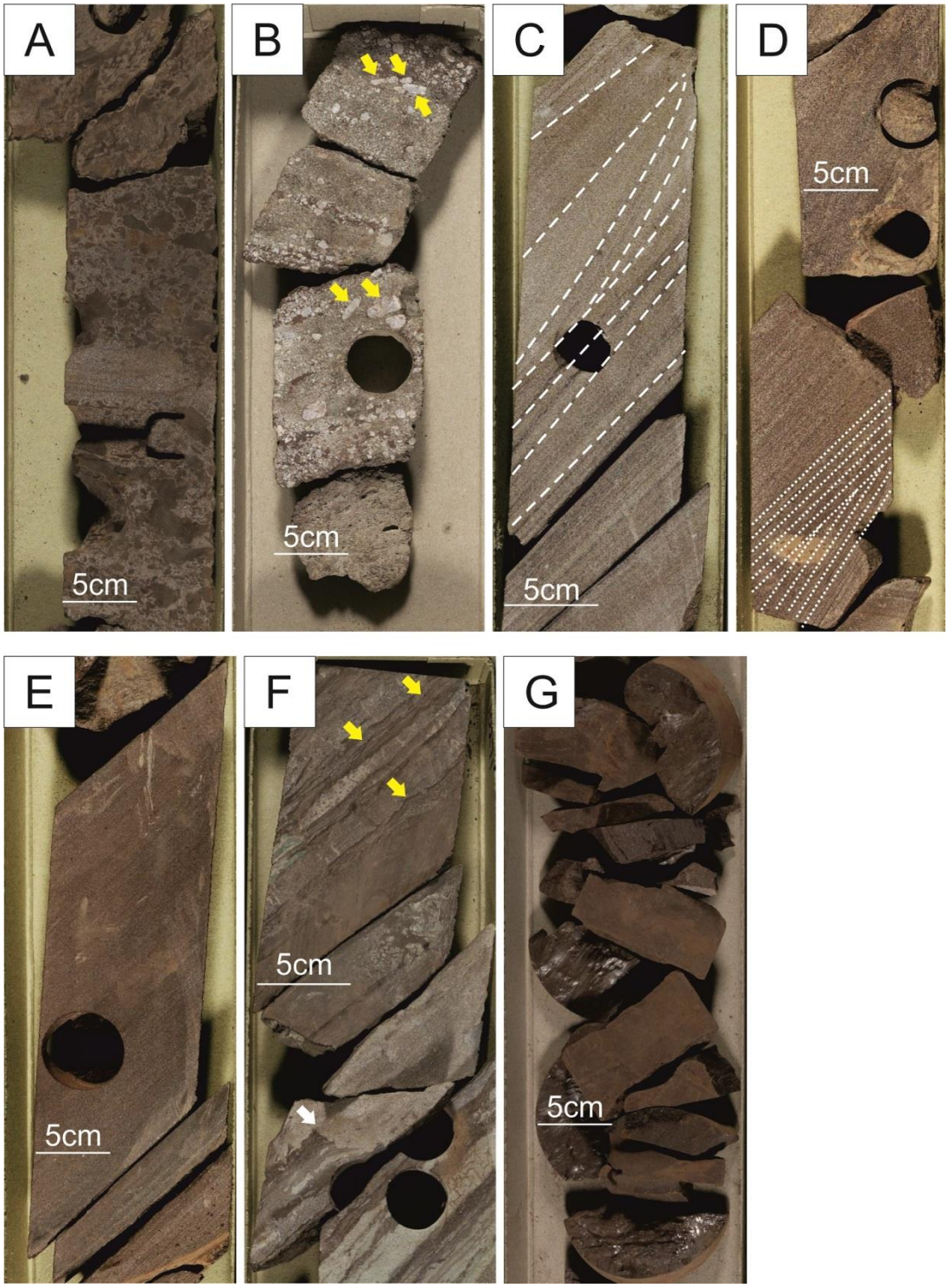

Figure 4.3 Core photos of fluvial-associated lithofacies. (A) Lithofacies Gm. Dark red-brown muddy cobbles with 0.5 cm - 2.5 cm grain size in a sandy supported matrix. Well 30/24-20z, 3159.1 m, Layer B04. (B) Lithofacies Gm. White and grey, sub-angular to sub-rounded quartz pebbles with 1 cm – 2 cm grain size in a sandy supported matrix, the platy ones are aligned or display crude imbrication (yellow arrows). Well 30/24-34, 2972.1 m, Layer B11. (C) Lithofacies St. Trough cross-bedded, medium to fine sandstones, note the white dash lines indicate the trough sets. Well 30/24-20z, 3121.7 m, Layer B04. (D) Lithofacies Sp. Planar cross bedding, medium to fine sandstones; note the white dot line indicate the interface between two planar bedding sets, Well 30/24-20z, 3172.7 m, Layer B04. (E) Lithofacies Sh. Red-brown fine-grained sandstones with millimetre-scale laminates. Well 30/24-20z, 3164 m, Layer B04. (F) Lithofacies Fl. Laminated very fine grain sandstones and silts with ripples or soft sediment deformation (yellow arrows) and the muddy desiccation cracks (white arrow). Well 30/24-20z, 3129.8 m, Layer B04. (G) Lithofacies Fm. Dark brown mudstones with no obvious beddings. Well 30/24-34, 2945.3 m, Layer B11.

4.3.1.1 Fluvial channel facies

a. Conglomerate (Gm)

Description: this lithofacies occurs in a minor proportion (< 10%). It is commonly developed as thin lags (0.5 m – 1 m) on erosional planes. The conglomerates are generally composed of red brown intra-formational mudstone clasts (**Figure 4.3A**) or grey to white-grey quartz pebbles (**Figure 4.3B**) up to 3 cm in diameter with a fine to medium grained sandy matrix. The muddy clasts and quartz pebbles are sub-angular to sub-round (**Figures 4.3A and 4.3B**), and the platy ones are often aligned or display crude imbrication (**Figure 4.3B**). This lithofacies generally occurs at base of the fining-upward cycle.

Interpretation: this lithofacies represents a depositional setting with very high energy, which can be explained as the fluvial basal lag deposition. The wide range of sediment grain size (from fine sand to conglomeratic grade) represents a clast-rich debris flow (Miall, 2013).

b. Sandstones (St, Sp and Sh)

Description: fine to medium-grained sandstone bodies up to 10 m thick comprise the main lithology type (approx. 80%) of fluvial channel facies, various sedimentary structures have

been recognized (**Table 4.1**). Typically the sandstone bodies are organized into three lithofacies: 1) Trough cross-bedding (St); 2) Planar cross bedding (Sp); and 3) Inclined horizontal lamination (Sh).

Lithofacies St (**Figure 4.3C**) is common within the whole fluvial interval (approx. 30% – 40%) and it consists of 0.5 m – 1.5 m thick, fine to medium-grained sandstones with grouped or solitary sets of trough cross laminations. The sets generally range in thickness from approximately 10 cm – 30 cm. The sedimentary structures are defined by argillaceous laminae. This lithofacies forms an important unit within fining-upward cycle and commonly passes transitionally upwards into lithofacies Sp, Sh, Fl or Fm.

Lithofacies Sp (**Figure 4.3D**) is also common (approx. 20% – 30%) and consists of 0.5 m – 1 m thick, fine to medium-grained sandstone with solitary sets of planar cross beddings. The sandstones are better sorted and cleaner than lithofacies St and lack mudstone or quartz pebbles. This lithofacies also forms an important unit within fining-upward cycle and commonly passes transitionally upwards into lithofacies Sh, Fl or Fm.

Lithofacies Sh (**Figure 4.3E**) is subordinate (10% – 20%) and consists of 0.2 m – 0.5 m thick, fine-grained sandstones with well-developed inclined horizontal laminations. The millimetre-scaled thin laminations are defined by dense concentrations of fine-grained detrital rock fragments in red-brown colour, and the coarser and cleaner laminates show lighter colour. This lithofacies occurs towards the upper part of fining upward cycles.

Interpretation: the fine- to medium-grained sandstones with various sedimentary structures record the different types of channel migration and accretion. The trough cross bedding represents the result of downstream migration of sinuous-crested dunes, which was usually formed by braided channel-fill deposits under a lower flow regime (Miall, 2013). The planar cross bedding usually represents the transverse and linguoid sand bars in fluvial channels, and

this could be either the result of lateral or downstream accretions (Miall, 2013). The inclined horizontal laminations could be interpreted as the plane-bed flow and was probably formed by the flash floods deposits within a distal sheet-flood sand-bed river system.

4.3.1.2 Flood plain facies (Fl and Fm)

Description: the flood plain facies consists of very fine laminated sandstones to siltstones with soft sediment deformation (Fl) and massive silty mudstones and mudstones (Fm). The lithofacies Fl (**Figure 4.3F**) consists of 0.2 m – 1 m thick, argillaceous and micaceous, very fine-grained sandstones to siltstones. The argillaceous content occurs as inclined parallel laminae, small ripple cross laminae, and discontinuous steaks and mud curls. Soft sediment deformation structures are common, some occasional desiccation cracks with infilled sands are also recorded (**Figure 4.3F**). The lithofacies Fm (**Figure 4.3G**) consists of 0.2 m – 0.5 m thick, micaceous dark red-brown silty mudstones and mudstones with massive beddings, and usually occurs at the top of fining-upward cycles.

Interpretation: these finer-grained sediments record flood plain deposition resulting from overbank flood event (McKee et al., 1967). The lithofacies Fl might be the temporary flood-plains and inactive or abandon channels. The desiccation cracks with infilled sands indicate the occasional exposed setting under arid climate. The mudstones (Fm) were accumulated in the lowest energy zones which represent a quite standing water condition following flooding events.

4.3.2 Aeolian facies association

The aeolian facies is volumetrically minor in the whole Buchan Formation of the Ardmore Field (approx. 30%). In this study, two types of aeolian deposit are identified: the pin-stripe laminated dune and discontinuous wavy laminated interdune sandstones.

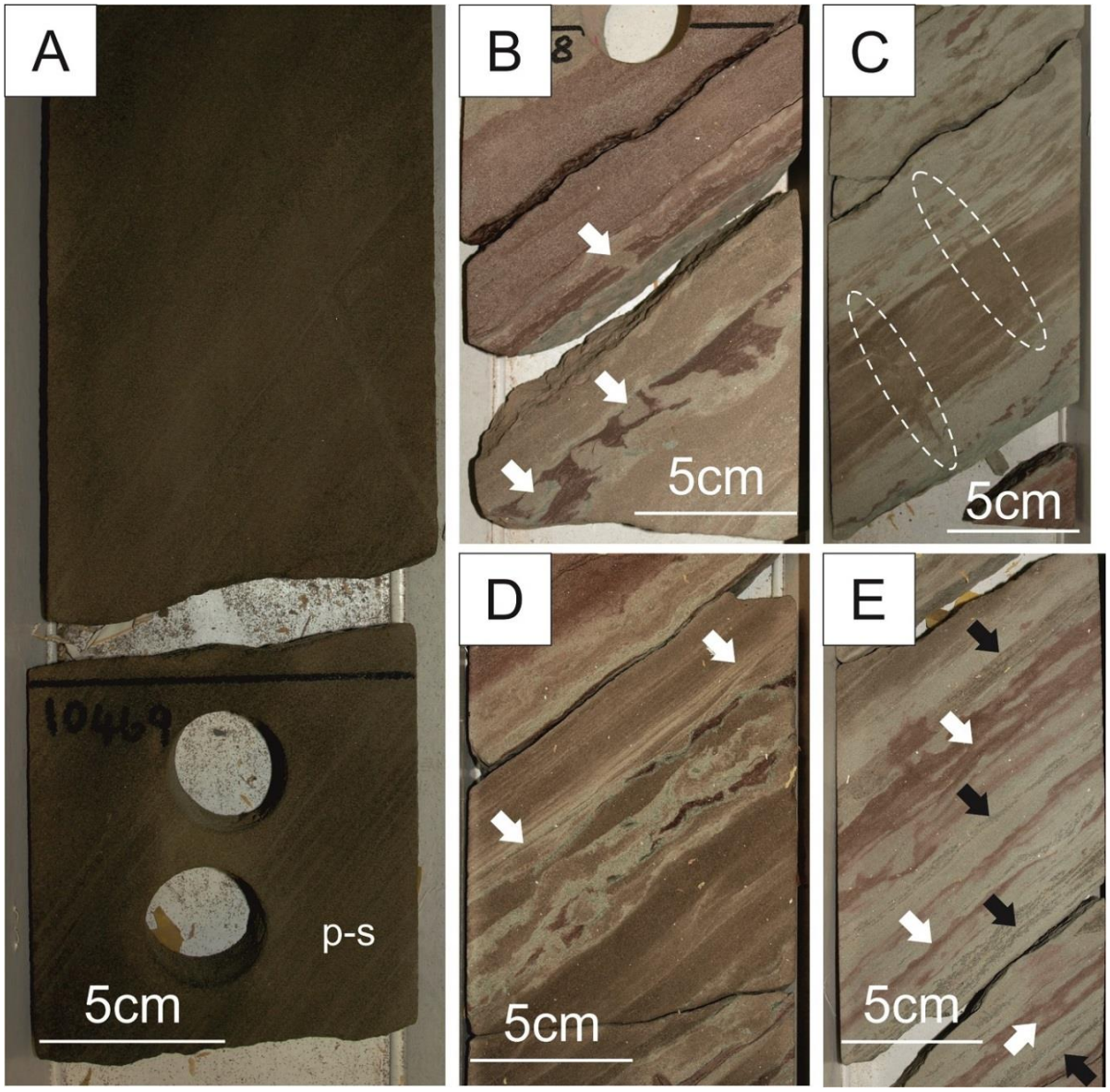

Figure 4.4 Core photos of aeolian-associated lithofacies. (A) The oil-stained, medium-grained, pin-stripe (p-s) aeolian dune sandstones, Well 30/24-31, 3191 m, Layer B08. (B) Muddy-rich fine–grained interdune sandstones with muddy desiccation cracks (white arrows), Well 30/24-31, 3184.7 m, Layer B08. (C) The de-watering (white dashed ellipse) sighted in a sandy-dominated interdune deposit, Well 30/24-31, 3187.8 m, Layer B08. (D) Centimetre-scale cross-bedding ripples (white arrows) sighted in a sandy-dominated interdune deposit, note the underlying soft sediment deformation. Well 30/24-31, 3183.8 m, Layer B08. (E) The discontinuous wavy laminations (white arrows) and argillaceous streaks (black arrows) sighted in a sandy-dominated interdune deposit. Well 30/24-31, 3189.3 m, Layer B08.

4.3.2.1 Lithofacies Sps: pin-stripe laminated sandstones (Figure 4.4A)

Description: this lithofacies forms the major component (approx. 70%) of aeolian facies and are characterized by 0.5 m – 1 m thick, upper fine- to medium-grained, well sorted sandstones. The grains are well rounded and the thin pin-stripe laminates are commonly exhibited. The sandstones display large-scale cross-bedding organized into 0.5 m to 1 m-thick sets, and the dip angle is about 35°. Additionally, there are several secondary features possessed by these deposits contrast them with the fluvial facies: high visible porosity, friable nature and the absence of muddy and/or conglomeratic intra-clasts.

Interpretation: the presence of well-rounded and sorted, upper fine- to medium-grained, muddy or conglomeratic clast-free sandstones with pin-stripe laminates are typical features of the aeolian dune deposits (Hunter, 1977; Kocurek and Dott Jr, 1981; Fryberger and Schenk, 1988). The high-angle, relatively stable graded laminates are interpreted as sand-flow deposits, formed by avalanching of non-cohesive sands on dune slip faces (Hunter, 1977). The highly friable nature suggests the low cementation, which is probably responsible for the high visible porosity.

4.3.2.2 Lithofacies Sw: discontinuous wavy laminated sandstones

Description: this lithofacies is the minor type (approx. 30%) in aeolian association and occurs interbedded with the dune sandstones. It is dominantly composed of 1 m – 2 m thick, very fine- to medium-grained sandstones that are moderately to well sorted, with low-angle discontinuous wavy laminates. Several local sedimentary structures can be sighted, including the mud desiccation infilled by sands (**Figure 4.4B**), de-water structure (**Figure 4.4C**), cross-bedding ripples (**Figure 4.4D**) and argillaceous streaks (**Figure 4.4E**). Vertically, there is no obvious boundary between Sps and Sw.

Interpretation: the discontinuous wavy laminates with several local sedimentary features suggest that this lithofacies represents the interdune environment. The interdune is usually located in low-relief areas of a dune system (Langford, 1989). In the given fluvial-presented setting, the interdune area would be affected by fluvial depositions. The mud desiccation infilled by sands and de-water structures indicate dry condition, while the cross-bedding ripples and argillaceous streaks can represent a wet and damp condition (Kocurek and Dott Jr, 1981). The variation between dry and wet conditions could be associated with the fluctuated development of the fluvial system.

4.4 The analogue outcrop in Dunnet Head, Northeast Scotland

The appropriate use of outcrop data is a good way to study the behaviour of subsurface reservoirs when wells are sparse and high resolution seismic survey is missing (Bridge et al., 2000b; Howell et al., 2014; Pranter et al., 2014; Romain and Mountney, 2014). The onshore Upper Devonian strata (equivalent to Buchan Formation) are present in the Midland Valley, along the margins of the Moray Firth, in Caithness and on Orkney (Gatliff and Survey, 1994; Hunter and Easterbrook, 2004).

In the Dunnet Head of Northwest Scotland, a good outcrop of Upper Devonian strata is cropping at the Dwarwick Pier (see **Figure 4.1A** for location) and it has already attracted a number of researches. The outcrop has been generally described as the Upper Devonian braided fluvial sandstones (Crampton et al., 1914; McAlpine, 1977; Trewin and Hurst, 2009) but none of them has linked it with the offshore Upper Devonian reservoirs. Tang et al. (2018) studied the facies and petrography of this outcrop and compared it with the subsurface Buchan Formation reservoirs (see Chapter 3 for details). They proposed that with the similar climatic and depositional setting and comparable lithology types, this outcrop could be good analogue of offshore Buchan Formation. They also measured the scale of channel sand bodies

and the data shows that the sand bodies typically display a flat and wide geometry with an average width/thickness ratio of 100:1 (see Table 3.1). For the purpose of numerical simulation of subsurface channel sand bodies, this would be a useful reference to determine the geometrical parameters.

4.5 Facies architecture analysis

The study on the lithofacies has revealed that the Buchan Formation in Ardmore Field is composed by sandstones mainly deposited in fluvial-braided and aeolian dune/interdune settings. By using the well logging data, geometry knowledge from analogue outcrop study and the facies modelling module in Schlumberger Petrel software, it is possible to study the facies architecture in both vertical and lateral directions. The selected profile is roughly perpendicular to the fluvial flowing (NW to SE) and palaeo wind blowing (E to W) directions (Hall and Chisholm, 1987). Wells are in relatively close spacing (approx. 500 m) which will be helpful on increasing accuracy of lateral correlation (Miall, 1988). The main parameters for Petrel facies modelling are listed in **Table 4.2** (at the last page of this chapter).

4.5.1 Fluvial association (Layer B10 as example)

4.5.1.1 Vertical architecture

In the Ardmore Field, layers B04, B10 and B11 are fluvial-dominated and composed of conglomerates, sandstones and fine grain sediments. **Figure 4.5A** is the detailed lithology log for three wells containing Layer B10 (see **Figure 4.1A** for well locations). The Layer B10 in all three wells is composed by superimposed fining-upward cycles, each with 5 m – 8 m thick. Each cycle generally comprises minor lithofacies Gm at base, succeeded by predominant lithofacies St, Sp and Sh in the middle and minor Fl/Fm on the top. The fluvial types could be classified as the combination of high-energy sand-rich and sheet-flood distal braided deposi-

tions according to the classification scheme of Miall (2013). The occurrence of fining-upward cycle indicates the deposition within channel streams (Bridge and Lunt, 2006; Bongiolo and Scherer, 2010). Therefore, the superimposed fining-upward cycles in each well represent the multi-stage developments of braided channels.

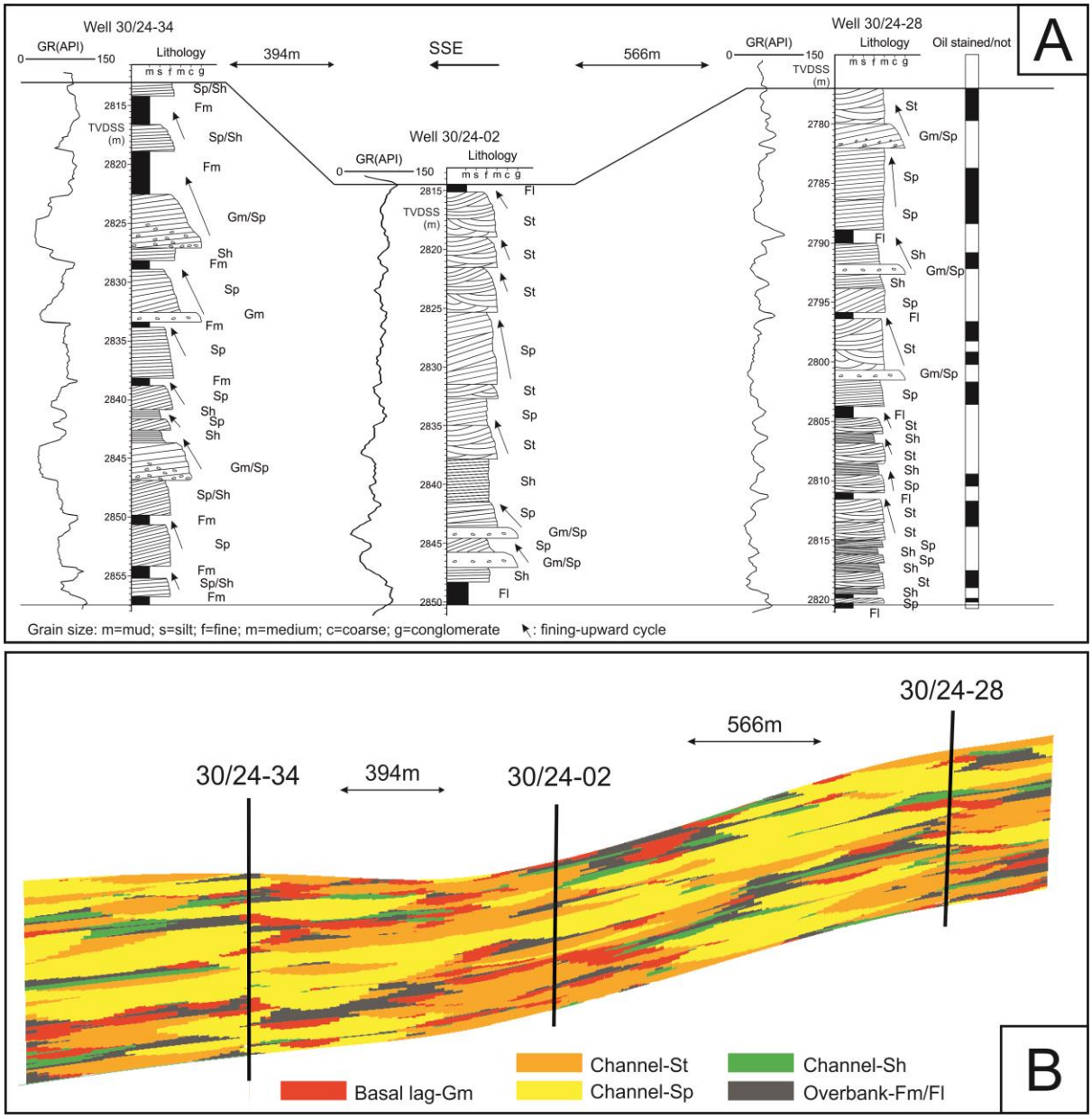

Figure 4.5 Well logging profile and facies modelling result of a typical fluvial association Layer B10. (A) The lithology log of selected wells, note the superimposed fining-upward cycles. (B) Petrel simulation result of the selected profile.

Within an individual fining-upward cycle, the lithofacies Gm usually forms the cycle base with thickness around 0.5 m – 1 m, indicates the thin basal lag deposit within a channel. The dominant lithofacies St, Sp and Sh are the most common types and form the main part of the fining-upward cycle, representing residual dunes, linguoid and transverse bars, and planar bed flows, respectively, and were produced in a low flow regime (Miall, 1977). The finer grained sediments Fl and Fm indicate the decrease of flow velocity or channel abandonment (Miall, 2013), and separate the channel deposits and usually occur at the top of the cycle with 0.5 m and up to 4 m thick. The stained oil is mainly distributed within the lithofacies St and Sp, indicates that braided channel sands are likely to be effective reservoirs.

4.5.1.2 Lateral architecture

The parameters for facies modelling are integrated by analogue outcrop study and depended on the actual well log correlation in Ardmore wells. In the lateral direction, the well log curve and detailed lithofacies log for three wells are not laterally correlatable, which indicate that the deposition was multiple braided channels rather than a single channel with kilometre-scale width.

The facies modelling result for Layer B10 (**Figure 4.5B**) shows a high gross sand ratio in the profile, the channel sand bodies are closely superimposed with adjacent ones both in vertical and lateral directions. According to the relationship between sand body connectivity and channel deposit proportion proposed by Karssenberg and Bridge (2008), the high gross sand ratio (67.18% for B04, 71.5% for B10 and 77.7% for B11) has increased the possibility that the superimposed sand bodies are almost inter-connected with each other, and only some thick muddy layers (> 2 m) could form local flow barriers.

4.5.2 Aeolian association (Layer B08 as example)

4.5.2.1 Vertical architecture

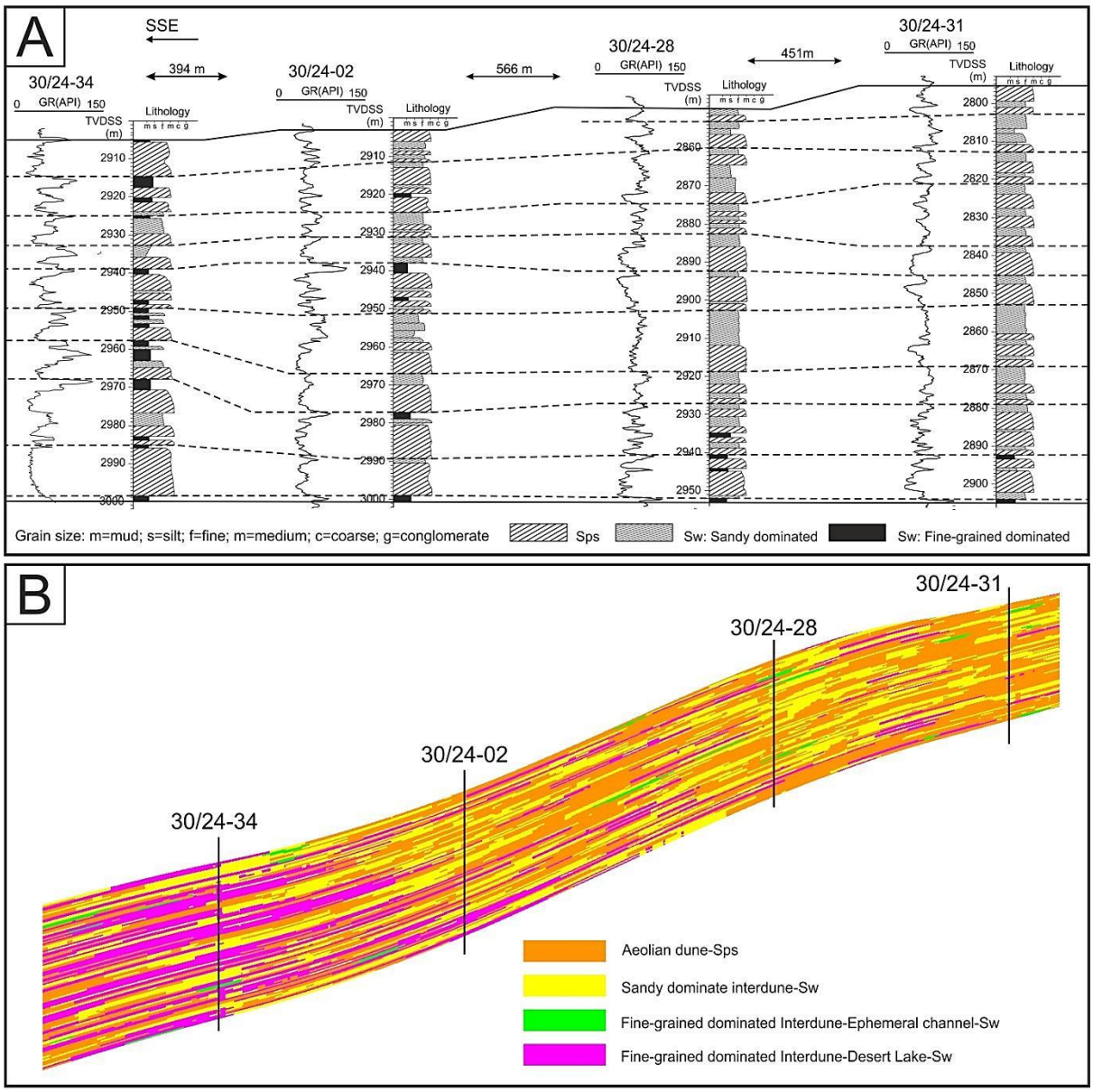

Figure 4.6 Well logging profile and facies modelling result of the typical aeolian association Layer B08. (A) The lithology log and lateral correlations of selected wells. (B) Petrel simulation result of the selected profile.

In the Ardmore Field, Layers B07 and B08 are aeolian-dominated units and mainly composed by upper fine to medium-grained and well sorted sandstones and minor fine-grained sediments. **Figure 4.6A** is the detailed lithology log for four adjacent wells containing Layer B08

(see **Figure 4.1A** for well locations). In the vertical direction, aeolian association shows a relatively simple architecture composed by superimposed dune and interdune depositions, there is no significant grain size variation in the vertical direction. The coarse grain sediments, such as conglomerates, are absent in the association, and the fine grain sediments occur consistently minor in four wells and increase south-eastwards.

4.5.2.2 Lateral architecture

The close spacing (around 500 m) of development wells in Ardmore Field permits the lateral correlation of aeolian units with reasonable confidence. By comparing the well log data of selected wells, the aeolian association comprises a number of laterally correlatable horizons over kilometre scale across the profile and generally shows a tabular geometry (**Figures 4.6A, 4.6B**). Dune sand bodies pinch out into finer grained interdune deposits, in this case the desert lake association, towards south-east, and the bounding surfaces of each horizon are commonly the overlain interdune deposits.

4.6 Discussion

4.6.1 Depositional pattern for the Ardmore Field area in the Late Devonian age

The aforementioned lithofacies and facies architecture studies have revealed that the Upper Devonian Buchan Formation in the Ardmore Field comprises a succession of thick terrestrial sandstones, mainly fluvial and subordinately aeolian depositions under a semi-arid to arid climate. The climatic changes, in this case the rainfall variations in the hinterland high relief area, were the main control of fluvial distributary system (Nichols and Fisher, 2007), and would occur uniformly across the basin-scale area at the same time (Nichols, 2005). Therefore, the changes from fluvial to aeolian facies between B04 and B07/B08 (B05 and B06 are not clear), and the reverse transition from aeolian to fluvial between B07/B08 and B09-B11 may be expected to have occurred across the basin-scale area at about the same time, and pre-

sented a general progradation-retreat-progradation cycle of the alluvial fan-based braided system with aeolian deposits occurred mainly between two main progradation periods.

Therefore this study proposed a depositional pattern for the Ardmore Field area in the Late Devonian age (**Figure 4.7**). The lithofacies database is restricted to the Ardmore Field and the areas beyond that are conjectured based on previous studies on related areas.

The braided fluvial fan system was possibly sourced from high-relief uplands in Scotland Midland Valley, and flowed south-eastwards to the Central North Sea area (Bluck, 2000; Graham et al., 2003). The Ardmore Field is believed locating near the margin of the braided fluvial fan system (**Figure 4.7**), as the presence of aeolian and associated desert lake sediments became established during more arid periods. It could be generally divided into two patterns: the fluvial dominated and aeolian dominated patterns. The bird-eye view slices of facies modelling results demonstrate more details of fluvial and aeolian dune geometry:

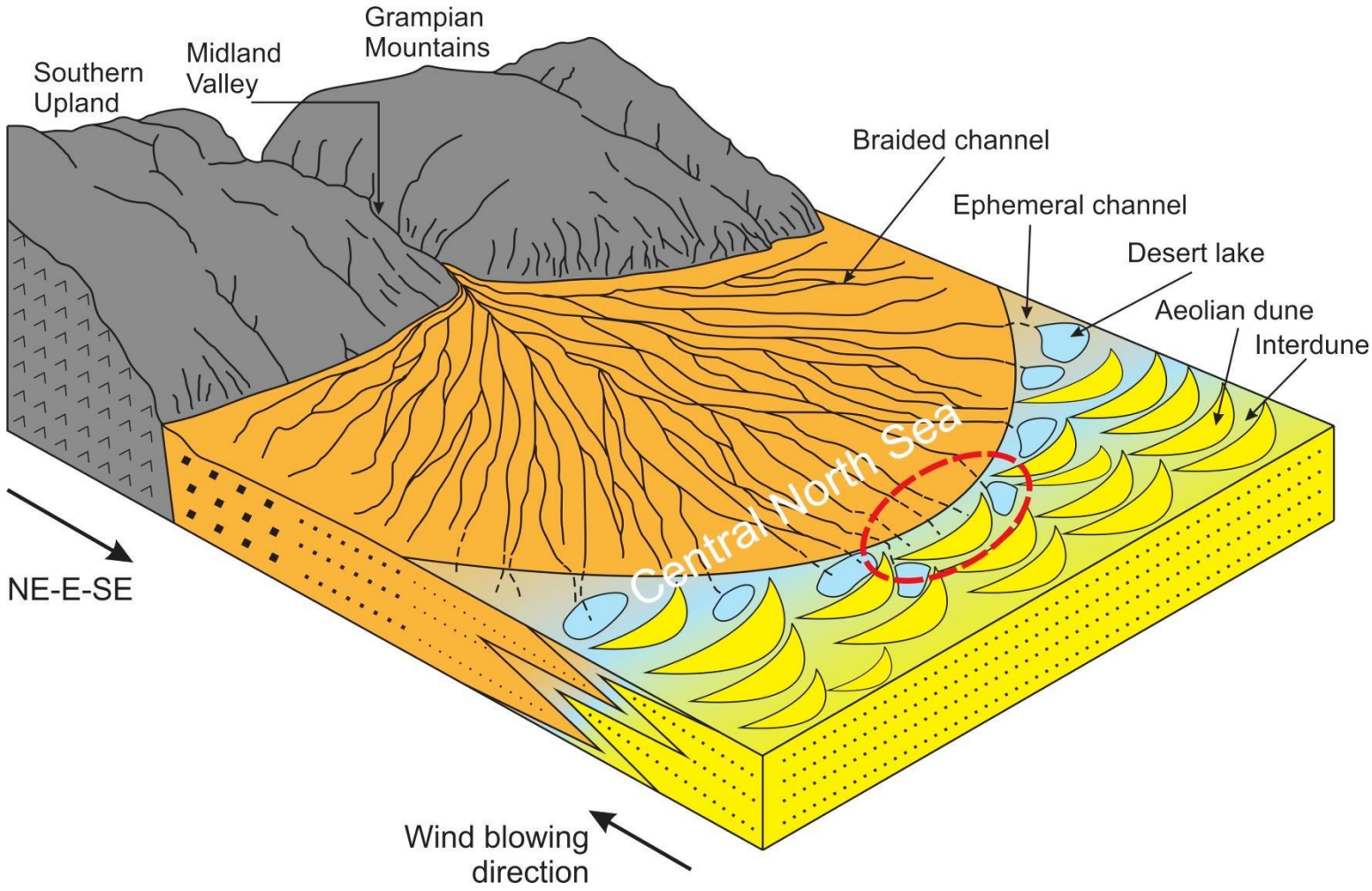

Figure 4.7 Schematic depositional pattern for the Ardmore Field and its adjacent areas (Figure not for scale). Note the red dashed ellipse indicate the location of Ardmore Field.

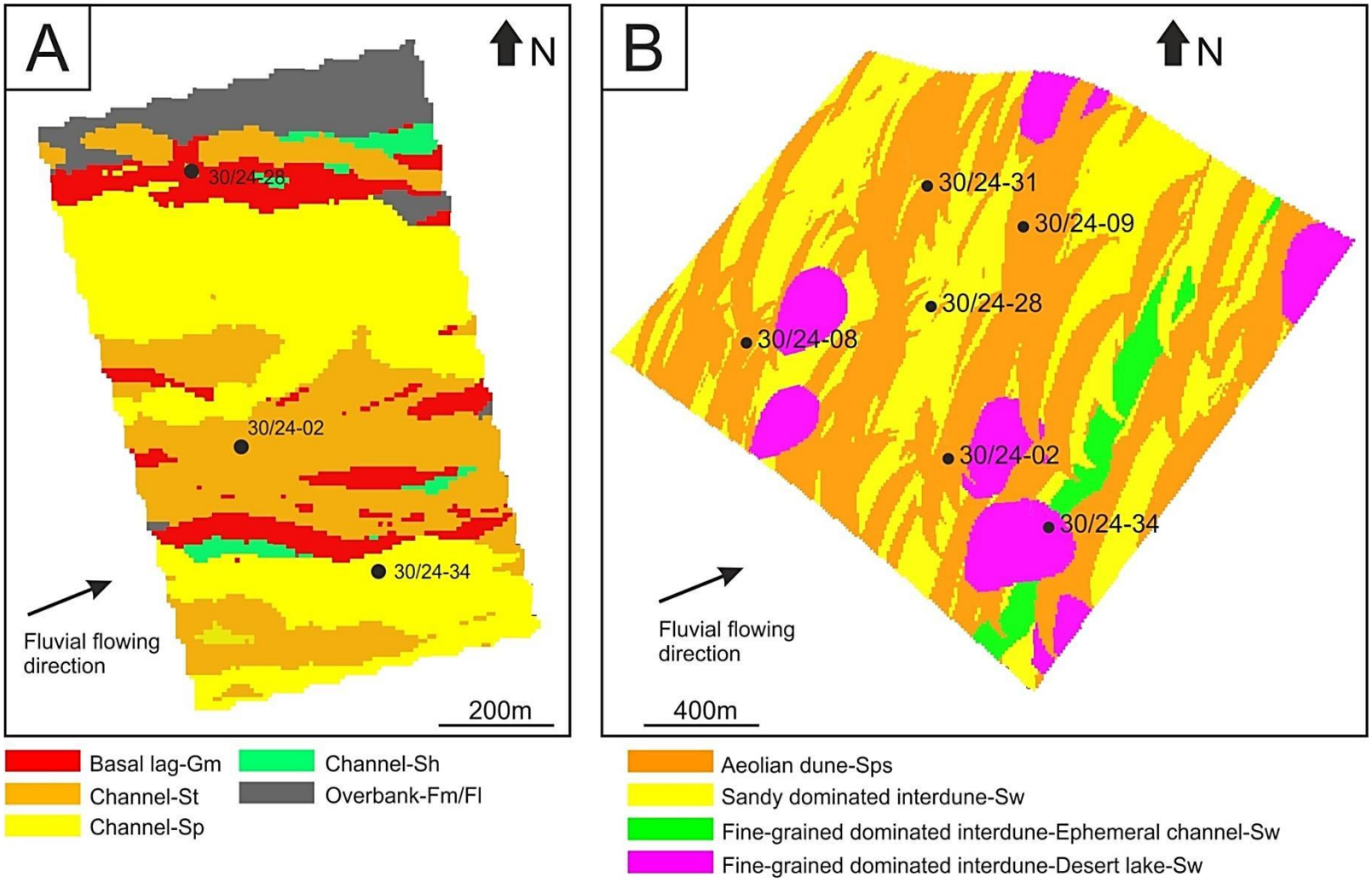

Figure 4.8 Bird-eye view slices generated by Petrel facies modelling for: (A) Layer B10, typical fluvial-dominated unit. (B) Layer B08, typical aeolian-dominated unit.

I. During the fluvial-dominated period, the Ardmore Field was located in a braided fluvial fan with multiple conglomeratic-sandy channels and minor overbank/flood plain depositions (**Figure 4.8A**). The braided fluvial sedimentation was featured as poorly confined channels with rapid and frequent lateral migrations, the cross section of a single channel, according to the analogue outcrops, shows a sheet-like sand body with high width-thickness ratio. This could be explained by the weak riverbank stability due to the lack of deeply rooted vegetation in the Devonian age (Davies and Gibling, 2010; Gibling et al., 2014) and overall arid climate which enabled the frequent lateral migration of channel deposits.

II. During aeolian-dominated period, the dune and interdune deposits were predominated and the general wind direction was suggested as blowing from east to west (Hall and Chisholm, 1987). Clearly not all the interdune deposits were aeolian origin, but also the modification by the loading occasional fluvial deposits. There were no conglomeratic-sandy channel deposits during this period, and only some distal fluvial deposits (e.g. sheet flood, floodplain) could affect the study area (**Figure 4.8B**). The fluvial-origin fine grained sediments were deposited in the topographically lower area, in this case, the interdune facies. During this period, occasional desert lakes could exist when the water table was high. The dune and interdune facies are laterally extensive which suggests the stable development of aeolian deposition, either as the consequences of major channel switching and/or the regionally significant hiatus of fluvial activity.

4.6.2 Significance of identifying aeolian deposits

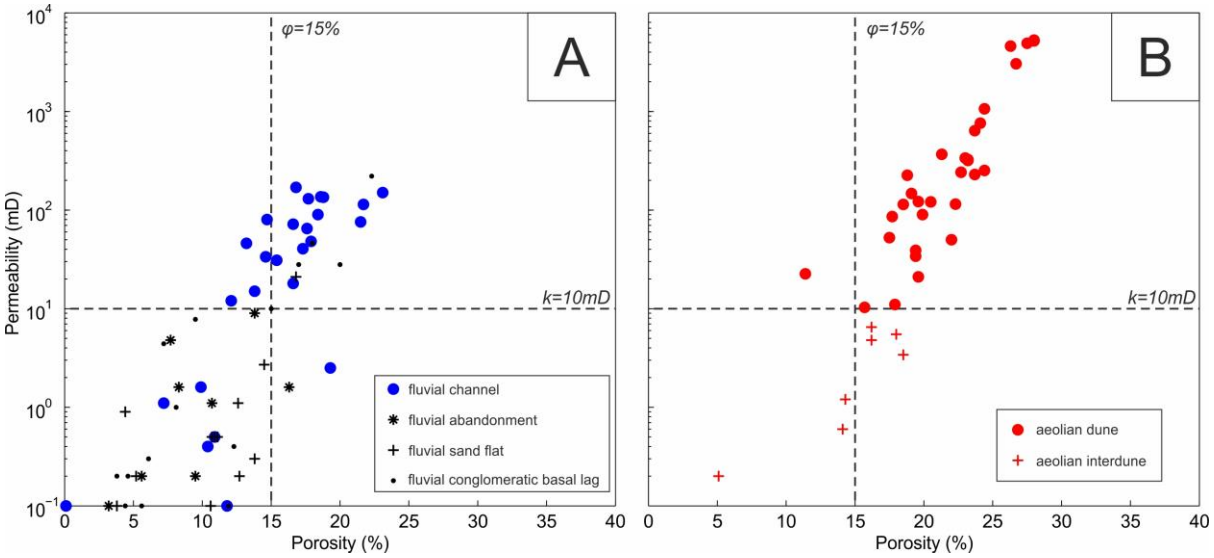

Figure 4.9 The scattered porosity and permeability maps for: Fluvial-associated sandstones. (B) Aeolian-associated sandstones. Note porosity = 15% and permeability = 10 mD are set as the lower limits of effective reservoir.

Aeolian facies is commonly featured as widespread occurrence and good reservoir properties, which usually make aeolian sandstones attractive exploration targets (Ahlbrandt and Fryberger, 1982). In the Ardmore Field, the reservoir quality of volumetrically major fluvial sandstones was significantly suffered by cementation of extensive quartz overgrowths and authigenic dolomites (Bifani and Smith, 1985), porosity ranges from 6% to 24%, but permeability never exceeded 400 mD (**Figure 4.9A**). Conversely, aeolian deposits possess volumetrically minor component but both dune and interdune facies show good reservoir quality (**Figure 4.9B**).

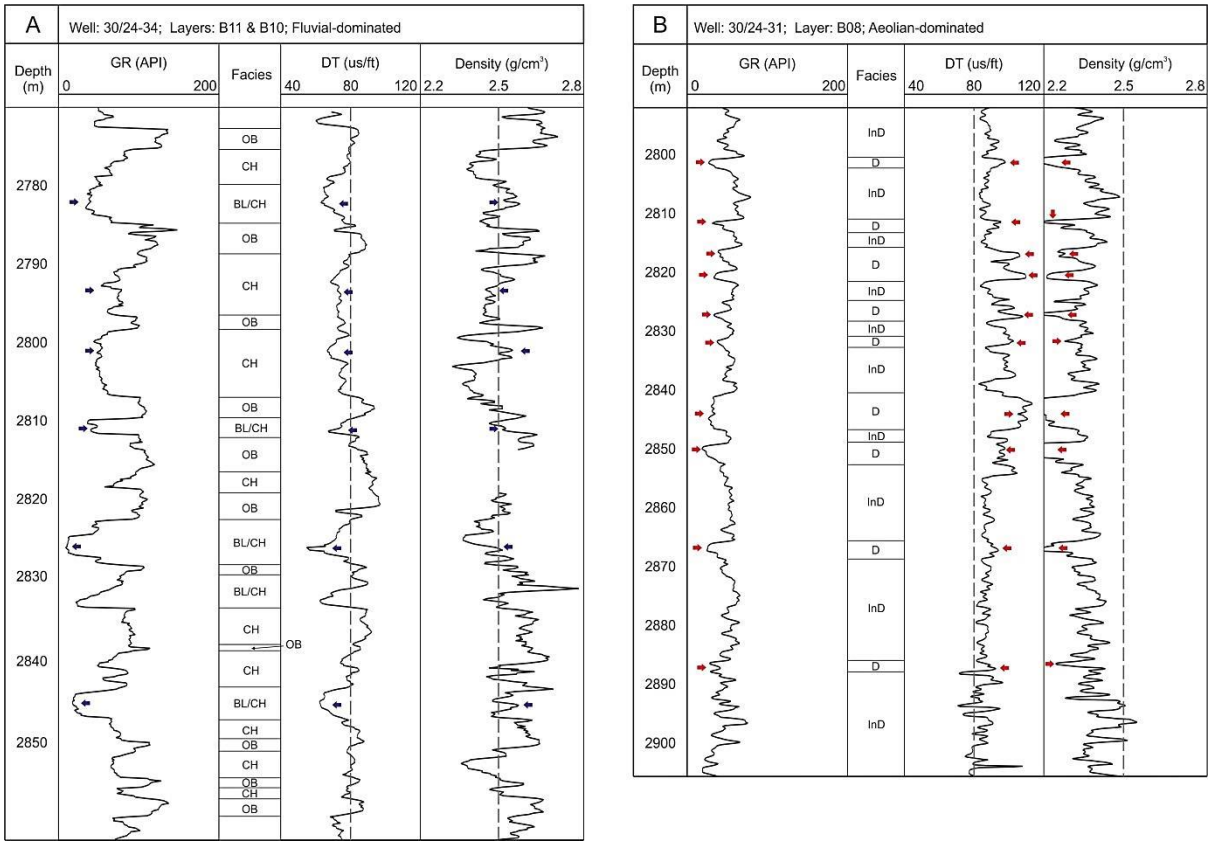

Figure 4.10 Different well log responses for (A) Fluvial-dominate intervals, note in blue arrows indicate the features of low gamma ray, low sonic log and high density in fluvial channel sandstones, BL=basal lag, CH=channel, OB=overbank. (B) Aeolian-dominated interval, note the red arrows indicate the features of low gamma ray, high sonic log and low density in aeolian dune sandstones, D=dune, InD=interdune.

Therefore, it is important to identify the aeolian association as early as possible during exploration or development. Due to the presence of conglomerates and highly cemented sandstones, the well log responses of fluvial sandstones are commonly featured as medium-low gamma ray value (50 API – 80 API), low sonic transit times (< 75 μs/ft.) and medium-high density (> 2.5 g/cm^3), and each conglomerate-sandstone group is separated by an overbank-associated muddy layer whose gamma ray value is greater than 100 API (**Figure 4.10A**). The aeolian deposits are sandy-dominated with high compositional and textual maturity, high porosity, low cementation and absence of conglomerates and muddy contents, these features can be manifested on well log curves by low gamma ray value (consistently less than 75 API), high

sonic transit times (consistently greater than 80 μs/ft.) and low density (< 2.5 g/cm^3). These featured well log responses, combined with uniform dipmeter patterns (not shown in the Figure), make it possible to tentatively identify aeolian facies in uncored wells (**Figure 4.10B**).

4.6.3 Implications on Devonian-associated reservoir explorations

Devonian strata in the North Sea have been perceived little hydrocarbon potential for a long time (Downie, 2009), several fields in both UK and Norwegian North Sea have confirmed the industrial oil productions from Devonian-associated reservoirs in recent decades (Edwards, 1991; Knight et al., 1993; Gambaro and Currie, 2003; Gluyas et al., 2005).

In this study, we confirm that the Buchan Formation in Ardmore Field is composed not only of fluvial deposits but also the presence of aeolian components. Aeolian components possess volumetrically minor percentage (approx. 30%) but show the best reservoir quality among the whole Buchan Formation: in fluvial sandstones, the extensive quartz and dolomite cementation reduces permeability by 1 – 2 orders of magnitude. However, quartz overgrowth is absent in aeolian sandstones. Given the same tectonic setting and burial process, these contrasting differences have two implications: 1). The relationship of porosity and permeability is different in fluvial and aeolian sandstones; and 2). The fluvial and aeolian sandstones have undergone different diagenesis processes. These make the sandwiched aeolian sandstones can still keep good porosity/permeability even the surrounding fluvial sandstones were significantly cemented.

In the Ardmore Field, aeolian sandstones are thin, laterally extensive, poorly cemented and permeable, and interbedded with thick, cemented and low-permeability fluvial sandstones. Since the North Sea area had similar depositional setting in the Late Devonian age, careful facies identification is important for determining the presence of aeolian sandstones. This study has improved the knowledge of depositional setting in the study area and provided sev-

eral tentative criteria for recognizing aeolian sandstones for the uncored wells. The results can have broad applications on future exploration in Devonian targets of the North Sea or other places with similar provenance.

4.7 Conclusions

A renewed attempt on facies identification and modelling has been made by using lithofacies, analogue outcrops, well logging data and software simulation. This study has announced the presence of aeolian sandstones within the fluvial-dominated Buchan Formation in the Ardmore Field, which has not been clearly identified in the previous time.

Fluvial-associated sandstones are volumetrically major facies type (approx. 70%) and typical braided origin. They are composed of superimposed fining-upward cycles, and each cycle represents a deposition of channel bar or channel fills. None of channel deposits can be correlated among the inter-well distance, but the high channel deposition proportion indicate that the channel sandstones are likely to be interconnected with each other.

Aeolian-associated facies form a volumetrically minor (approx. 30%) but important reservoir in the studied field. It comprises superimposed dune and interdune sandstones and is laterally correlatable over kilometre scale. Both dune and interdune sandstones have good reservoir quality as a consequence of good sorting, roundness, absence of muddy and conglomeratic contents, and low cementation. These features allow them to be tentatively identified, especially for those uncored wells, by using the combination of well log responses such as low gamma ray, high sonic transit time and low density.

Understandings on the scheme of this fluvial-aeolian facies system demonstrate the possibility of effective reservoir potential in Devonian strata. Sandstones deposited in different facies would undergo different diagenesis, in this case, the sandwiched aeolian sandstones could

still hold good reservoir property even the surrounding fluvial sandstones were highly cemented. This should have an important impact on reservoir identification, appraisal and discovery.

Acknowledgement

The authors thank Enquest PLC for supporting this research through access to core, seismic sections and other data and financial support for field work and petrographic analyses; Dr Bernard Besley for providing data and helpful discussions; Mr Russel Ball (San Leon Energy PLC) for providing helpful skills on facies modelling in Petrel; BGS (British Geological Survey) for its assistance in facilitating the examination of Devonian cores.

Table 4.2 The main parameters of Petrel facies modelling for the selected layers

Layer	Sandstone-body type	Simulation method	Main constraints						Background sediment type
			Lithology-Lithofacies elements		Proportion (%)	Orientation (Compass degrees)	Mean width(m)	Mean thickness(m)	
Fluvial-dominated association									
B10	Fluvial channels	Object modelling	Conglomerate	Gm	7.86	240-240	80	1	Mud
			Medium sand	St, Sp	56.84		400	4	
			Fine sand	Sh	14.5		180	1.5	
			Mud	Fl, Fm	20.8		250	1.5	

Layer	Sandstone-body type	Simulation method	Main constraints						Background sediment type
			Lithology-Lithofacies elements		Proportion (%)	Orientation (Compass degrees)	Mean width(m)	Mean thickness(m)	
Aeolian-dominated association									
B08	Aeolian dunes	Object modelling	Medium sand	Sps	41.7	140-140	700	2	Fine sand
			Fine sand	Sw	52.2		1000	4	
	Aeolian interdunes		Silt	Sw	1.47	240-240	100	1	
			Mud	Sw	14.64		150	1.5	

CHAPTER 5: POROSITY PRESERVATION DUE TO GRAIN COATING ILLITE/SMECTITE: EVIDENCE FROM BUCHAN FORMATION (UPPER DEVONIAN) OF THE ARDMORE FIELD, UK NORTH SEA

---

*This chapter has been accepted by the **Proceedings of the Geologists' Association** and is now in press.*

Chapter outline

Summary

The Buchan Sandstone reservoirs (Upper Devonian) from the Ardmore Field in the UK Central North Sea are fluvial-aeolian deposits and provide examples of porosity preservation in deeply-buried reservoirs (2.7 km – 3.2 km) caused by grain-coating illite/smectite. Here, high reservoir quality commonly correlates with the occurrence of grain-coating illite/smectite and consequent inhibition of quartz cementation in the aeolian dune and interdune sandstones; while porosity is lower in fluvial sandstones lacking grain coating illite/smectite but with intense quartz overgrowths. We propose that the presence of illite/smectite content reflects syn-depositional concentration of the smectitic-rich clay bearing water which would have been the deposits of the interdune and/or distal sector of fluvial distributary system. The smectitic clays were introduced into porous aeolian deposits by mechanical infiltration. Petrographic relationships indicate that these coatings grew mainly before the beginning of mechanical compaction as the presence of clays occurs at grain contacts. An empirical model is applied to calculate the effect of these coatings and the results suggested that about 6% – 7% porosity has been preserved. The burial and thermal history of the Ardmore area contributed to preservation of high quality reservoir because throughout much of the time since deposition the Devonian sandstones have been little buried. Only in the Tertiary have reservoir temperatures exceeded about 70°C. A consequence is that the minor amounts of pore-filling smectitic clays have only minor negative effect on reservoir quality while at the same time they inhibited quartz cementation. The circumstances of porosity preservation in the Buchan Formation aeolian sandstones of the Ardmore Field may be unusual, but nonetheless have profound consequences for exploration. It may be possible to identify new Buchan Formation prospects in areas hitherto dismissed because they were assumed to contain none effective reservoir.

5.1 Introduction

Quartz cement is one of the dominant porosity reducing agents in many reservoir sandstones, but other factors such as grain size, sorting, clay content, mechanical compaction, pore fluid pressure, early cementation and authigenic clay minerals also play a critical role (Worden and Morad, 2000). Different types of grain coatings have been identified to inhibit or reduce quartz cementation. The basic mechanism of inhibiting quartz overgrowth is that the grain coatings covered the nucleation site on the host grains and the authigenic quartz could not nucleate on or through the coatings (Pittman, 1972). The most effective grain coating mineral is said to be micro-quartz (Aase et al., 1996) and for the grain coating clays, authigenic chlorite is commonly reported as a preserver (e.g. Pittman and Lumsden, 1968; Ehrenberg, 1993; Berger et al., 2009; Stricker and Jones, 2016). Illite is less frequently reported as grain coatings that preserve porosity (Storvoll et al., 2002) but frequently cited as the cause of permeability destruction (Robinson et al., 1993). Smectitic clay is commonly regarded as having negative effects on reservoir quality due to its water-sensitive swelling property (Gray and Rex, 1965), and it commonly transforms to fibrous/hairy illite in a potassium-rich pore fluids. Precipitation of illite usually causes significant permeability reduction (Almon and Davies, 1981; Le Gallo et al., 1998; Wilson et al., 2014).

The oil reservoirs in the Ardmore Field, UK Block 30/24, Central North Sea, are hosted in Permian Zechstein carbonates, Permian Rotliegend sandstones and Upper Devonian Buchan Formation sandstones (Gluyas et al., 2005). The two Permian units have been studied in a number of publications (e.g. Nagtegal, 1979; Glennie and Provan, 1990; Purvis, 1992; Howell and Mountney, 1997; Leveille et al., 1997; Sweet, 1999); however, the deeper and older Buchan Formation sandstones (2.7 km – 3.2 km TVDSS) are poorly understood but have also been proven to be an important hydrocarbon reservoir in the Central North Sea (Edwards, 1991; Knight et al., 1993; Gambaro and Currie, 2003; Gluyas et al., 2005). The

Buchan Formation is composed chiefly of a sand-dominated unit deposited in a braided fluvial and aeolian environment during a hot and semi-arid to arid period (Gluyas et al., 2005; Kearsey et al., 2015). Gluyas et al. (2005) reported the conventional core analysis data for Buchan Formation sandstones, porosity ranges between 1% and 28% while permeability varies between < 1 mD and > 5000 mD. The main influences on reservoir quality reduction were mechanical compaction, extensive quartz overgrowth and dolomite cementation (Bifani and Smith, 1985). However, many of the Buchan Formation sandstones have little cement and are excellent reservoirs. Why some of these ancient sandstones remain high quality reservoirs has not previously been reported.

In this study, we discovered that the aeolian-associated sandstones with grain coating illite/smectite (I/S) usually have anomalously high porosity and permeability, while quartz overgrowth is almost absent in this sandstone type. Conversely, the fluvial facies sandstones without thick and continuous I/S coatings are usually cemented by extensive quartz overgrowth, and commonly show poor, or at best, moderate reservoir quality. Therefore, this study focused on the following points and questions: 1). Why is the grain coating I/S only presented in aeolian sandstones and how did it form? and 2). Is it possible to quantitatively evaluate the porosity preserving effect of I/S grain coatings? The positive effect of grain coating I/S can be expected to occur only under particular circumstances, but in such cases it can have profound consequences for exploration. This study has broad implications for future exploration, appraisal and production of Devonian reservoirs within this area.

5.2 Geological Setting

5.2.1 Tectonic setting

The Ardmore Field is located on the Argyll Ridge, a large SW-NE trending Palaeozoic age tilted fault block on the south-western flank of the Central Graben in Block 30/24, UK North

Sea, about 350 km south-east from Aberdeen. The field is located in a horst feature with the crest in the north and fault closure to the north-east. It measures 2.5 km wide and 6 km long (**Figure. 5.1a**). A combination of dip and faulting defines the limits of the field on the north-west and south-east flanks, while dip closure defines the southern limits of the field. The major fault trends are in two main directions, WNW–ESE cut by NW-SE faults (**Figure. 5.1b**). The top seal is provided by Triassic shale in the far west, Jurassic shale in the mid-part of the field and impermeable Chalk at the north-eastern crest (Gluyas et al., 2005). The trap relies heavily on the major NW-SE trending graben edge faults to the northeast and southwest of the field while dip closure occurs to the northwest and west.

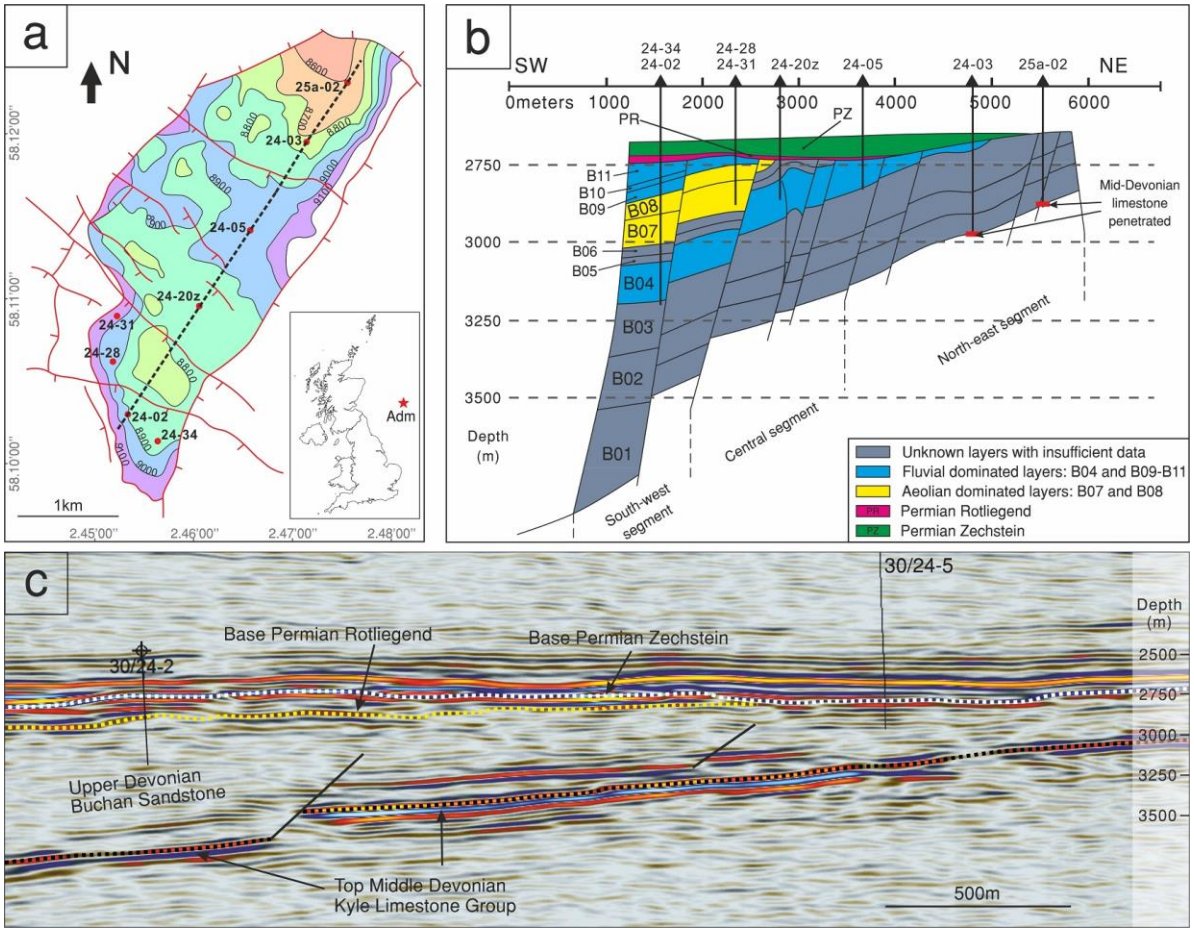

Figure 5.1 Geological maps showing: (a) Location and main structure elements of Ardmore (Adm) Field; (b) Vertical section of an SW-NE profile (dashed line in 1a); (c) Seismic section of an SW-NE profile (part of dashed line in 1a).

5.2.2 Stratigraphy

The Devonian sequence in the Ardmore Field comprises a succession of the Middle Devonian Kyle Limestone and Upper Devonian Buchan sandstone. The succession dips to the south-west, and is separated from the Permian by a palaeo-topographic unconformity, in which successively younger stratigraphic units in the Devonian sub crop towards the south-west. Although the pre-Permian surface has topography it also dips to the SW, this has the effect of making the oldest part of the Buchan sandstone subcrop the unconformity in the NE of the field and thus the youngest Devonian in the SW slightly deeper (**Figure. 5.1b**).

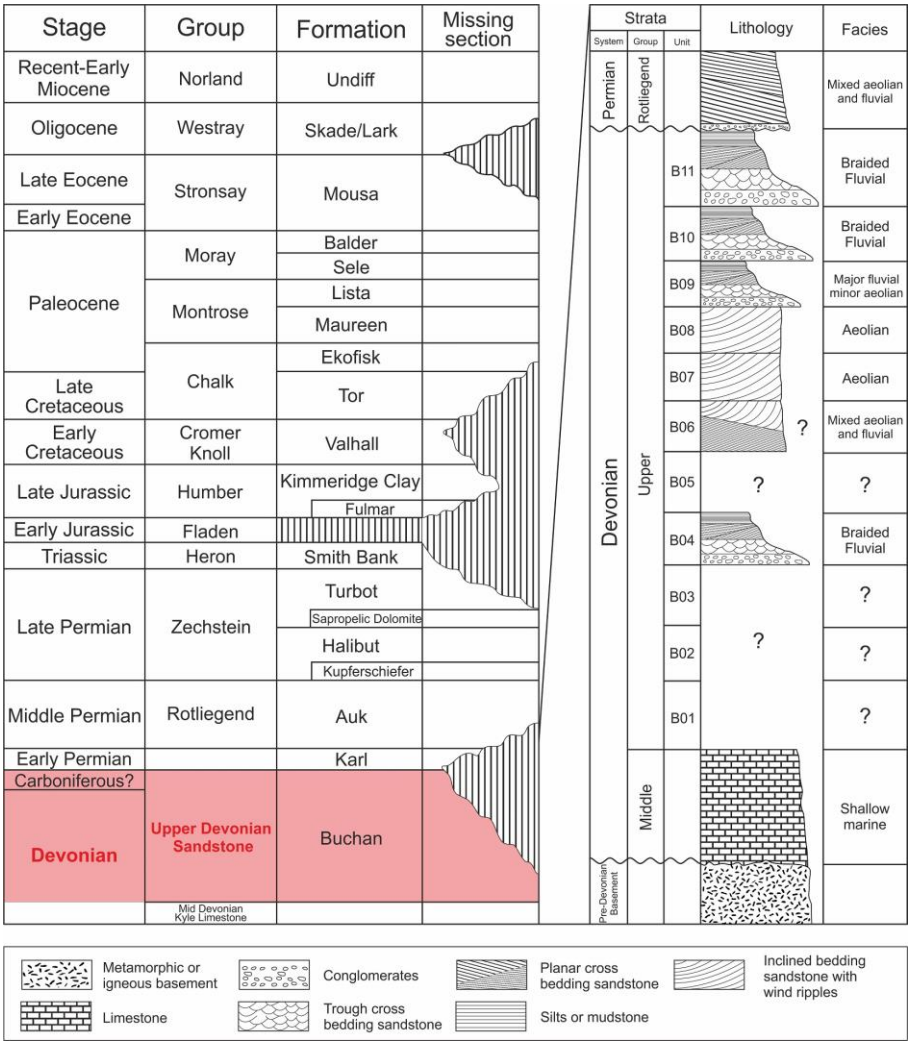

Figure 5.2 General stratigraphy of the Ardmore Field and a schematic stratigraphic log of the Buchan Formation.

The Upper Devonian Buchan Formation comprises a thick, generally upward-coarsening succession of shales of mixed shallow marine and sabkha environment at the base, passing upwards into mainly fluvial and aeolian sandy sediments (**Figure. 5.2**). The whole Buchan succession lacks clear seismic stratigraphic markers, a combination of log and core data has been used to divide the stratigraphic units for the Upper Devonian Group: B01 is the oldest unit overlying the Middle Devonian Limestone, and B11 is the youngest unit (Gluyas et al., 2005). In the absence of bio-stratigraphic data, sedimentary structures and lithofacies associations have been applied to help correlation (Gluyas et al., 2005). The total thickness of the Buchan Formation is not documented due to the combination of erosion below the Devonian-Permian unconformity, lateral thickness variation and incomplete well penetrations. The estimated thickness is about 500 m – 800 m according to the seismic profile (**Figure. 5.1c**).

Units B01, B02, B03, B05 and B06 are equivocal about their origin due to the insufficient core coverage. The core description revealed the presence of two main sedimentary facies within the Buchan formation (Robson, 1991; Gluyas et al., 2005). Braided fluvial facies is the volumetrically major type (approx. 70%) and consists of multiple fining-upward sequences (not shown in the Figure. 5.2), each sequence is commonly composed of: a). Sand-supported conglomerates at the cycle base with thickness around 0.5 m – 1 m, the quartz and muddy clast pebbles (1 cm – 3 cm in diameter) are sub-angular to sub-rounded and show roughly imbricated alignment, which indicates the thin basal lag deposit within a channel (CHC); b). Fine to medium-grained, moderately sorted sandstones with trough cross bedding, planar cross bedding and horizontal laminations are the dominant type within the fining-upward cycle, representing various channel bar deposits (CHB) such as residual dunes, linguoid and transverse bars, and planar bed flows; and c). Laminated fine-grained sediments with soft sediment deformation usually form the top of the sequence, which indicate the decrease of

flow velocity such as sand flat (SF) or channel abandonment (CHA) and usually occur at the top of the cycle with 0.5 m and up to 3 m thick.

The aeolian facies is the volumetrically minor type (approx. 30%) and composed of well sorted, medium-grained, pin-stripe laminated sandstones and fine-grained, discontinuous wavy laminated sandstones, which represents an interbedded dune (AD) and interdune (ID) deposits. Overall, the known units comprise a vertically fluvial (B04, approx. 100 m)-aeolian (B07 and B08, approx. 50 m)-fluvial (B09, B10 and B11, approx. 240 m) variation, which generally represents a progradation-retreat-progradation cycle of the alluvial fan-based braided system with aeolian deposits occurring mainly between two main progradation periods.

5.3 Dataset and Methodology

A total of 190 samples were taken from BGS and EnQuest core stores. Cores from five wells (30/24-05, 30/24-20z, 30/24-28, 30/24-31, 30/24-34) in the Buchan Formation ranging from 2650 m to 3150 m (TVDSS) were logged (**Appendix I**). The porosity and permeability data were provided by EnQuest internal reports, porosity was determined via direct measurement of grain volume and bulk volume by helium expansion in a Boyle's Law porosimeter. The permeability data was determined by use of a nitrogen permeameter at a confining pressure of 400 psig and are Klinkenberg-corrected.

Thin-section petrography was used to determine the rock mineralogy, diagenetic features, pore types and clay distribution in the pore spaces. One hundred and one thin sections (14 from well 30/24-05, 16 from well 30/24-20z, 38 from well 30/24-28, 16 from well 30/24-31 and 17 from well 30/24-34) were used for petrographic analysis and point counting. The samples were impregnated with blue-dyed resin in order to identify porosity.

At least 300 points were counted in each thin section to identify detrital and authigenic phases, including the clay aggregates which are larger than 0.05 mm in size (pore space is excluded). This number of point counts per thin section has a standard deviation of 5.5% or less (at the 95% confidence level) for any measured volumetric percentage of mineral or porosity components (Stanton, 1994). The point count results, petrographic information, and laboratory measured porosity/permeability are presented in **Appendix II-1**.

Microstructural observation was obtained in both secondary and backscattered electron imaging, with a Hitachi SU70 scanning electron microscope (SEM). Typical voltage for thin sections was obtained at 15 kV, 0.73 nA together with an analytical working distance of 15 mm. The electron microscope is equipped with an Oxford Instrument Aztec microanalysis system and Silicon Drift (SDD) EDX detector X-max 50. Rock chip samples from both fluvial and aeolian sandstones were Au/Pd coated with 35 nm thick (Cressington Scientific 108 Auto sputter coater) for optimum imaging resolution at 5 KeV and 8 KeV. Thin sections were carbon coated with 30 nm thick (Cressington Scientific 108 evaporating system A) in order to obtain large area "Phase Maps" which were achieved using Phase ID within Aztec 3.3 software.

To identify and quantify the clay mineralogy, six samples were chosen for XRD analysis (4 from grain coated aeolian sandstone samples, 2 from fluvial sandstone samples with quartz and dolomite cements and without grain coatings). The bulk rock was disaggregated by gentle crushing and suspend in distilled water. After allowing the coarse grains to settle for 3 hours, the clay in suspension was decanted in the centrifuge for 4.8 minutes at 1000 rpm, and this process is performed 3 times. Clay with less than 2 microns was tested after being air dried, solvation with glycerol and heating at 500°C for 2 hours.

5.4 Results

5.4.1 Porosity and permeability

The Buchan Formation sandstones have a wide range of porosity and permeability (ϕ = 1% – 28% and K= 0.1 mD – 5290 mD). Porosity and permeability are well correlated in most of the samples (in fluvial samples, R^2 = 0.68; in aeolian samples, R^2 = 0.89; in all samples, R^2 = 0.74) inferred that the factors affecting porosity would also affect permeability (**Figure. 5.3a**).

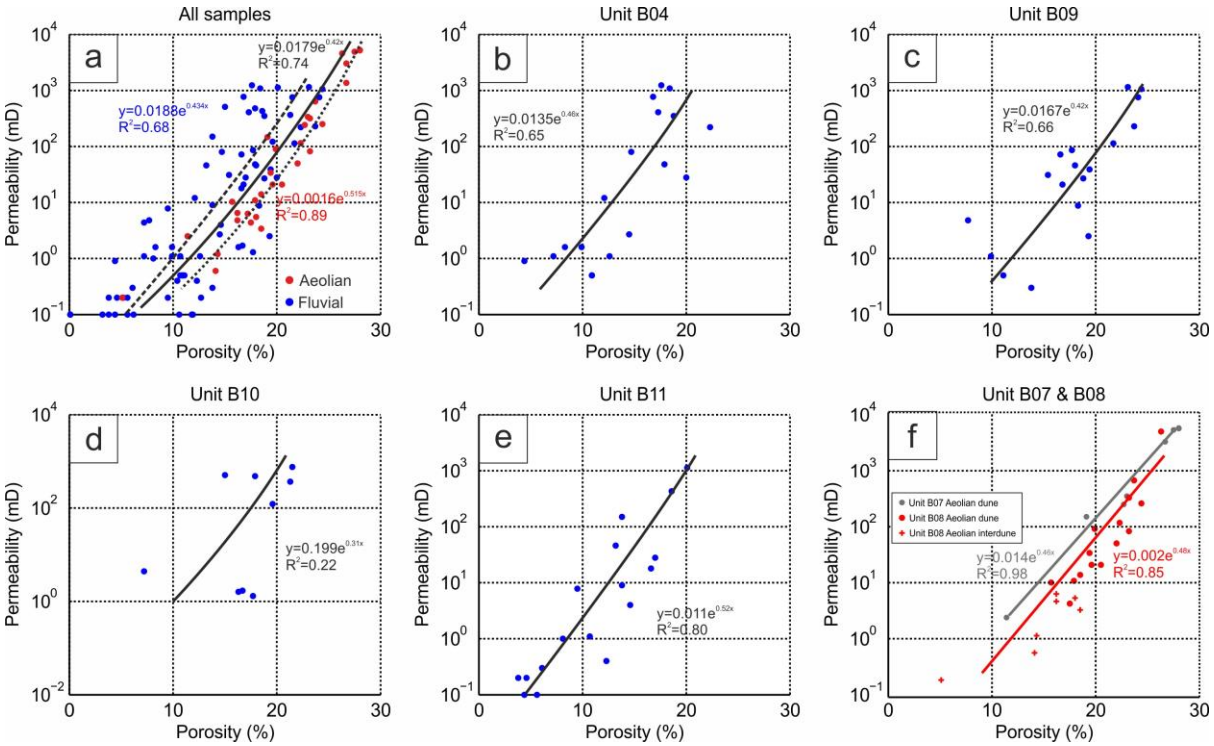

Figure 5.3 Porosity and permeability distributions and correlation coefficients for: (a) All the samples; (b) Stratigraphic unit B04; (c) Stratigraphic unit B09; (d) Stratigraphic unit B10; (e) Stratigraphic unit B11; (f) Stratigraphic units B07 and B08.

For the fluvial units including B04, B09, B10 and B11 (**Figure. 5.3b – 5.3e**), the porosity ranges from 0.1% to 23.1% (arithmetic mean 12.7%), and the permeability ranges from 0.2 mD to 1240 mD (arithmetic mean 147.7 mD, geometric mean 5.41 mD). For the aeolian units B07 and B08 (**Figure. 5.3f**), the porosity ranges from 5.1% to 28% (arithmetic mean 20.2%),

and the permeability ranges from 0.2 mD to 5290 mD (arithmetic mean 740.6 mD, geometric mean 64.9 mD).

5.4.2 General petrographic descriptions

5.4.2.1 Detrital mineralogy

The studied Buchan sandstone samples are litharenite to sub-litharenite and minor quartz-arenite based on Folk (1957), with an overall average composition of $Q_{78.3}F_{2.9}R_{18.8}$. The average composition for fluvial sandstones is $Q_{76.1}F_{3.3}R_{20.7}$ (**Figure. 5.4a**); aeolian sandstones have an average composition of $Q_{82.1}F_{2.4}R_{15.6}$ (**Figure. 5.4b**). Texturally, the fluvial sandstones are relatively immature and fine to medium grained, sorting ranges from poor to moderate and roundness of grains varies from sub-angular to sub-rounded, grains are tightly compacted showing curved and concavo-convex grain contacts. Conversely, the fine to medium grained aeolian sandstones are more mature, sorting ranges from moderate to good and roundness of grains varies from sub-rounded to rounded, and the grain contacts are commonly point to linear.

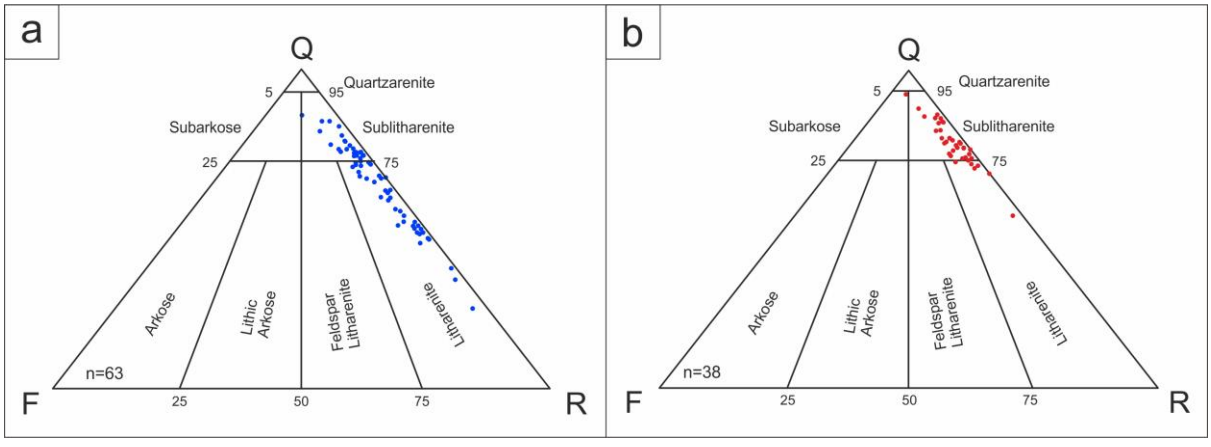

Figure 5.4 (a) QFR charts for fluvial sandstone samples; (b) QFR charts for aeolian sandstone samples.

In all samples, quartz is the dominant grain type (41% – 95%). Most quartz grains are monocrystalline (**Figure 5.5a**), some of them showing little to moderate undulose extinction (**Fig-**

ure 5.5b). Polycrystalline quartz is a minor constituent and only found in conglomerate-size quartz grains (**Figure 5.5c**). Feldspar is commonly present in trace amount and up to 7%, the main type is microcline with polysynthetic twinning (**Figure 5 5d**), the feldspars occur as both fresh (**Figure 5.5d**) and kaolinitized grains (**Figure 5.5e**). Most mica grains are muscovite presenting in all the samples and comprising up to 13%. Micas show variable amounts of distortions (**Figure 5.5b**). Rock fragments (**Figure 5.5f**) are mainly micaceous and illitic mud clasts, fine-grained metamorphic and volcanic fragments are present in trace quantities. The abundance of rock fragments is highly variable (1% – 69%) and related to each sub-facies: CHB has the lowest average rock fragments (11%) among all fluvial sub-facies (15% in CHC, 16% in SF and 27% in CHA). While in the aeolian facies, aeolian dune has a lower average rock fragments (13%) than interdune deposits (16%).

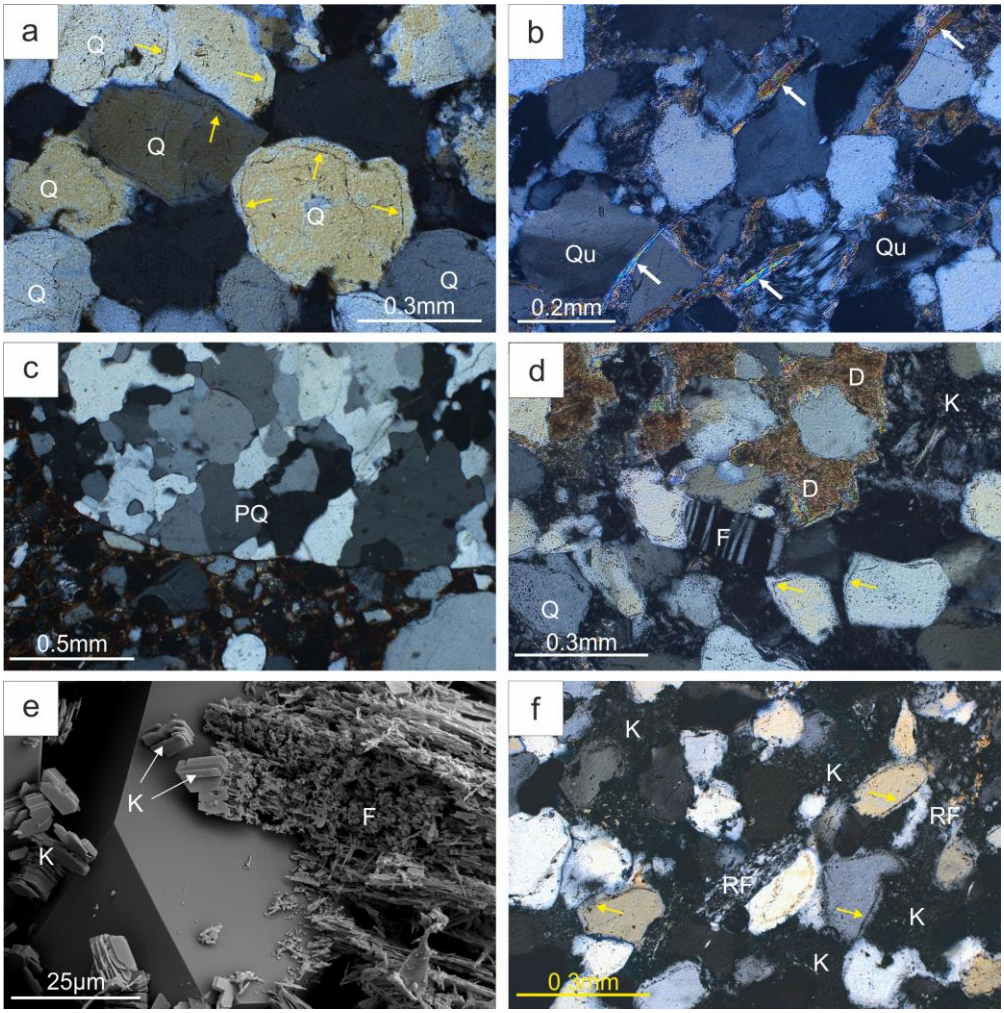

Figure 5.5 Photomicrographs of sandstone detrital minerals. All thin section images were produced under cross-polarized light. (a) Monocrystalline quartz grain with quartz overgrowth and visible dust rims (yellow arrows) on the original detrital grain. Well 30/24-34, 2967.8 m, unit B11, fluvial facies; (b) Bended muscovite grains (white arrows) and quartz grains with undulose extinction. Well 30/24-20z, 3125.4 m, unit B04, fluvial facies; (c) Polycrystalline quartz in conglomeratic-sized grains. Well 30/24-28, 2791.5 m, unit B10, fluvial facies; (d) Microcline with polysynthetic twinning, notes the presence of carbonate cement and pore-filling kaolinite. Well 30/24-05, 2846.4 m, unit B04, fluvial facies; (e) SEM image of severely dissolved feldspar and authigenic kaolinite. Well 30/24-20z, 3125.4 m, unit B04, fluvial facies; (f) Possible volcanic-origin rock fragments, note the pore-filled kaolinite aggregates and quartz overgrowth (yellow arrows). Well 30/24-05, 2847 m, unit B04, fluvial facies;

Q-quartz; Qu- quartz grains with undulose extinction; PQ- Polycrystalline quartz; F-feldspar; C-carbonate cement; K-kaolinite; RF-rock fragment

Pore space mainly consists of primary intergranular pores, secondary inter- and intragranular pores and intra-crystalline micro pores. The polygonal intergranular pores are the main type (more than 90% among all pore space) and range in sizes from 5 μm to 200 μm. The secondary pores (less than 10% among all pore space) are mainly contributed from framework-grain dissolution, i.e. the dissolution of detrital feldspars. Dissolution of dolomite cement can be found in trace amounts. The intra-crystalline micro pores (negligible among all pore space) mainly consist of micro pores in clay minerals (e.g., kaolinite, illite, smectite) and range in size from 0.1 μm to 5 μm.

5.4.2.2 Authigenic mineralogy

Authigenic minerals in the studied sandstones are mainly dolomite, quartz overgrowth, kaolinite, illite and I/S. The kaolinite, illite and quartz overgrowth are usually associated with fluvial sandstones, while I/S are only found in aeolian sandstones.

Dolomite is the prevalent cement in the Buchan sandstones ranging from 0% – 36% with an average value of 5.7%, and are commonly iron-stained. It is usually presented as thin bands of disseminated red-brown stained nodules in hand specimen with a size of up to 2 mm (**Fig-**

ure 5.6a). Thin section observation reveals a rhombic shape with clear rims and cloudy centre (**Figure 5.6b**) and poikilotopic structure (**Figure 5.6C**).

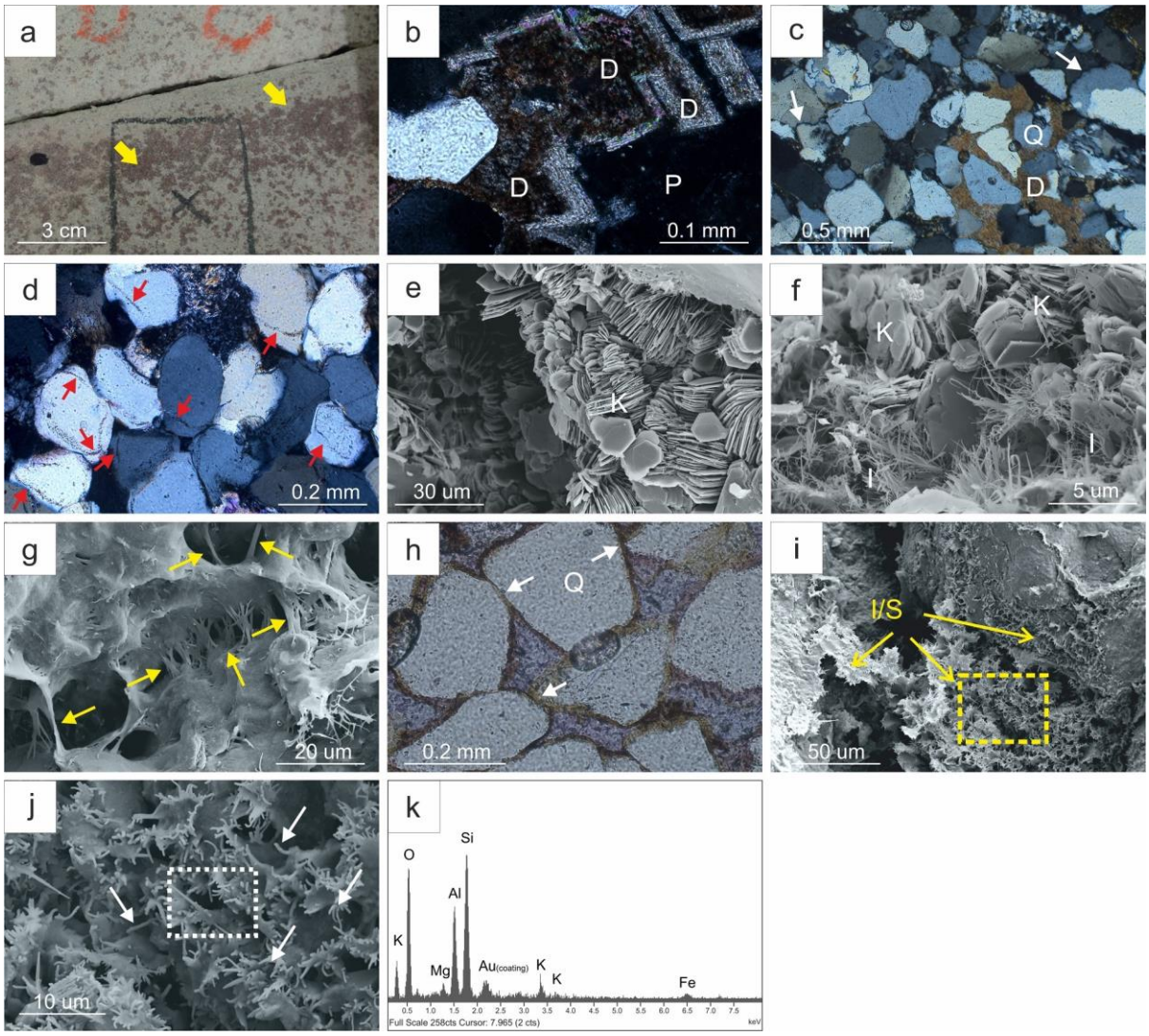

Figure 5.6 Photomicrographs showing different diagenetic minerals. (a) Thin bands of 'spotty' red-brown stained cements (yellow arrows) in the cores. Well 30/24-05, 2849.1 m, unit B04, fluvial facies; (b) Dolomite cements in the pore space showing well rhombic shape with cloudy core and light rims, cross-polarized light. well 30/24-05, 2849.1 m, unit B04, fluvial facies; (c) Quartz grains floating in the dolomite cements and well compacted (white arrows) without pore-filling dolomite cements, cross-polarized light, well 30/24-20z, 3126 m, unit B04, fluvial facies; (d) Extensive quartz overgrowth (red arrows) on the detrital quartz grains, cross-polarized light, well 30/24-20z, 3126 m, unit B04, fluvial facies; (e) Kaolinites showing pseudo-hexagonal plates and vermicular and booklet morphologies under SEM. Well 30/24-20z, 3176.6 m, unit B04, fluvial facies; (f) Fibrous/hairy authigenic illite based on kaolinite under SEM. Well 30/24-20z, 3126 m, unit B04, fluvial facies; (g) SEM image showing pore-bridging habit of authigenic illite (yellow arrows). Well 30/24-20z, 3165.3 m, fluvial

facies; (h) Grain coating clays existing between grain contact areas (white arrows), plane- polarized light ,well 30/24-31, 3197.7 m, unit B08, aeolian facies; (i) Pore-filling and grain coating smectite-illite mixed layers showing honeycomb or cornflake morphology under SEM. Well 30/24-28, 2891.1 m, unit B07, aeolian facies; (j) Enlarged view of the rectangle area in Fig. 6i, note the filamentous terminations (white arrows) indicates the illitization occurred; (k) EDX spectrum of the rectangle area in Fig. 5.6j, note the small peak of potassium indicates the partial illitization.

D-dolomite; P-pore space; K-kaolinite; I-illite; I/S-illite/smectite

Quartz overgrowth is present primarily as syntaxial cement forming incomplete or complete rims around quartz grains (**Figures 5.5a and 5.6d**). Boundaries between detrital grains and overgrowth cements are visible due to the presence of inclusions along grain boundaries. Quartz overgrowths are widely distributed in the fluvial sandstone samples (up to 6%, average 3%). While the quartz overgrowth is typically absent in most of the aeolian samples, except a few samples (5 out of 36) have trace amount of quartz overgrowth up to 1% (**Appendix II-1**). Kaolinite and authigenic illite are the two main clay types in fluvial sandstones. Kaolinite mainly occurs as euhedral pseudo-hexagonal plates and vermicular or booklet aggregates filling primary pores (**Figure 5.6e**). Illite occurs as fibrous or hairy crystals mainly nucleated on kaolinite (**Figure 5.6f**) and shows a pore-bridging habit (**Figure 5.6g**).

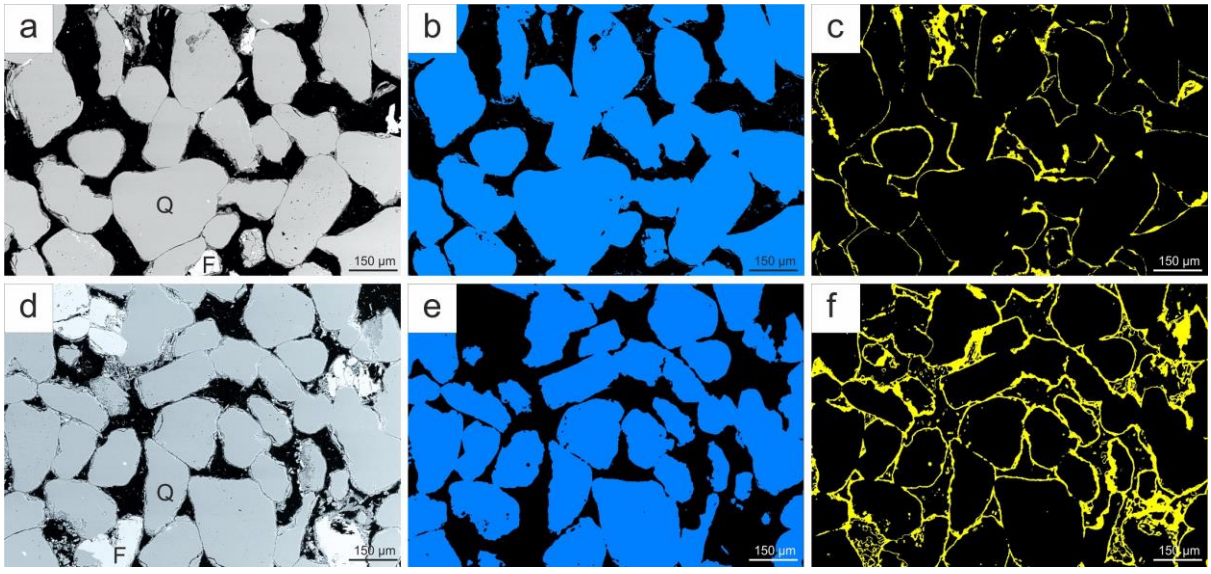

Figure 5.7 The mineral phases maps for two typical aeolian sandstone samples which contain well-developed and continuous grain coating clays. (a) (b) (c) BSEM image, quartz-facies map and grain coating facies map of sample from Well 30/24-31, 3197.7 m, unit B08, aeolian facies; (d) (e) (f) BSEM image, quartz-facies map and grain coating facies map of sample from Well 30/24-28, 2891.1 m, unit B07, aeolian facies.

I/S has been identified by XRD (**Table. 5.1,** at the end of this chapter) and EDX analysis (**Figure 5.6k**) and it is the most important clay type in the studied aeolian sandstones although it is only present in minor amounts (0.5% – 5%). The thin section and SEM observations illustrate that the I/S is presenting in two forms: a). Grain coating I/S (**Figures 5.6h and 5.6i**) commonly occurs as cornflake or honeycomb morphology with filamentous terminations, and consists of a 1 μm – 5 μm thick rim coating all the detrital grains in aeolian facies sandstones; it is absent in fluvial facies sandstones. It is also observed that quartz overgrowth are absent in aeolian facies sandstones where uniform and robust grain coating I/S has developed; and b). Pore-filling I/S (**Figure 5.6i and 5.6j**), commonly presenting as flocculent aggregates existing in the intergranular pore space of aeolian facies sandstones, and is also absent in fluvial facies sandstones. To evaluate the development, coverage and continuity of the grain coating I/S, the mineral phases map has been created for two aeolian dune samples (**Figure 5.7**). Figures 5.7c and 5.7f clearly displayed that nearly all the grains are coated by well-developed and continuous grain coating I/S, the visual grain coating coverage is nearly 100%.

In both sandstone types, chlorite is subordinate and present in trace amounts (0.1% – 0.5%) which is confirmed by XRD analysis (**Table 5.1**).

5.4.3 Porosity loss evaluation

Calculation on porosity loss from compaction (COPL) and cementation (CEPL) is a good way to calculate the effect of compaction and cementation on reducing porosity. These two

parameters were firstly proposed by Lundergard (1992), and a useful parameter compaction index (Ic), can be calculated using following equations:

$$\mathrm{COPL} = \mathrm{P_i} - (\frac{(100-\mathrm{P_i})*\mathrm{IGV}}{100-\mathrm{IGV}}). \quad (1)$$

$$\mathrm{CEPL} = (\mathrm{P_i} - \mathrm{COPL}) * (\frac{\mathrm{C}}{\mathrm{IGV}}). \quad (2)$$

$$\mathrm{Ic} = \frac{\mathrm{COPL}}{\mathrm{COPL+CEPL}}. \quad (3)$$

Where P_i is the assumed initial porosity, the intergranular volume (IGV) is calculated by adding up the measured porosity and the total cement volume *C*. The calculation of COPL and CEPL are only accurate when three conditions are met: 1). The assumed initial porosity *Pi* is appropriate; 2). The amount of cement produced by local grain dissolution is negligible or known; and 3) The amount of framework exported by dissolution is negligible or known (Lundergard, 1992). The compaction index (Ic) equals 1.0 when all porosity loss is due to mechanical compaction, and equals 0 when all porosity loss is due to cementation.

In this study, we employ the estimated Pi for loose sands according to Beard and Weyl (1973), the assumed Pi for the fine-medium grained, moderately sorted fluvial sandstones is 34.8%, and for the fine-medium grained, well sorted aeolian sandstones, Pi is 37.8%.

The results (**Appendix II-2**) show that compaction has reduced more porosity in aeolian sandstones than in fluvial sandstones: the COPL value is 14.82% (accounted for 39.21% on initial porosity, average Ic = 0.73) in aeolian sandstone samples and 10.06% (accounted for 28.91% on initial porosity, average Ic = 0.44) in fluvial sandstone samples, respectively. It is also worthy to note that the COPL of fluvial samples has a larger range (0% – 29%) than aeolian samples (3.5% – 22.8%).

The CEPL results suggest that fluvial sandstones suffered much more porosity loss from cementation (average 12.71%, accounted for 36.52% on initial porosity) than aeolian sandstones (average 5.63%, accounted for 14.89% on initial porosity).

5.4.4 Burial-thermal history

The 1D burial history was modelled using Schlumberger petroleum systems modelling software PetroMod (V2014.1). Several heat flow histories of the Central Graben and, more specifically, of UK Quadrant 30 in the Central North Sea (Swarbrick et al., 2000; Carr, 2003; Di Primio and Neumann, 2008) have been employed for the modelling. **Figure 5.8** is a burial-temperature history for the Buchan Formation in the Ardmore Field which is generally similar to burial histories presented in other studies of Central Graben (Nguyen et al., 2013). The Buchan Formation in the Ardmore Field was at consistently shallow burial depth and low temperature (< 1.5 km and < 60°C) until Paleogene, and then rapidly buried into current maximum depth and reached higher temperature within a short time.

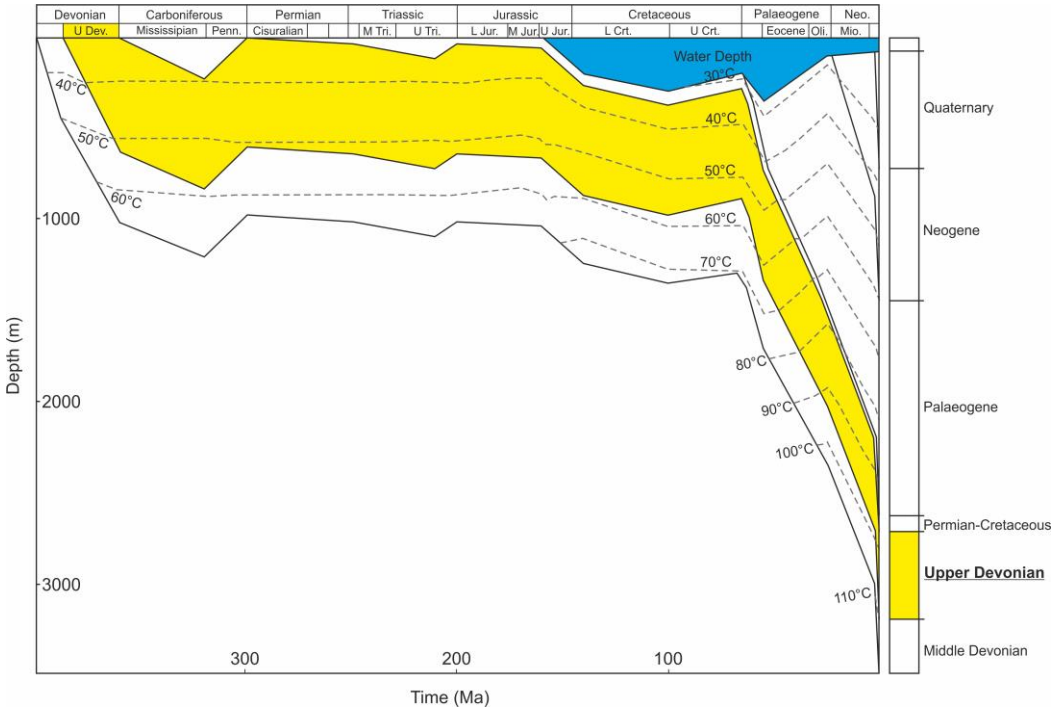

Figure 5.8 1D burial depth curves with geothermal isochore lines of Buchan Formation.

5.5 Discussion

5.5.1 Paragenesis

The relative timing of the main diagenetic features can be reconstructed by considering the relationships between the different diagenetic events (**Figure 5.9**). However, there are some diagenetic differences between fluvial and aeolian sandstones.

The earliest diagenetic event was the formation of grain coating clays in aeolian deposits, which is considered to be introduced from the infiltration of clay-bearing groundwater through the sands. This event was prior to the compaction and could be proved by the presence of grain coating clays between grain contact areas (**Figure 5.6h**).

Mechanical compaction in both aeolian and fluvial deposits followed after clay infiltration, during which mica flakes were deformed around quartz and feldspar grains (**Figure 5.5b**). In both fluvial and aeolian samples, an early dolomite cementation occurred at this time, as in some samples the detrital grains appear to float and point grain contact is preserved within the poikilotopic dolomite cement (**Figure 5.6c**). Where dolomite is not present, grains are well compacted (**Figure 5.6c**). The presence of euhedral dolomite with cloudy centres and clear rims (**Figure 5.6B**) might be an indicator of dolomitization occurred on calcrete precursor. Pressure dissolution at the quartz grain contacts would have occurred as compaction increased due to the weight of overburden. This is more common in fluvial sandstones possibly due to the greater number of rock fragments, such as ductile micaceous clast, may promote the compaction in the fluvial sandstones and resulted in concavo-convex grain contacts **(Figure 5.6c**). This is also supported by greater maximum COPL in fluvial samples ($COPL_{max}$ = 29%) than in aeolian samples ($COPL_{max}$ = 22.8%).

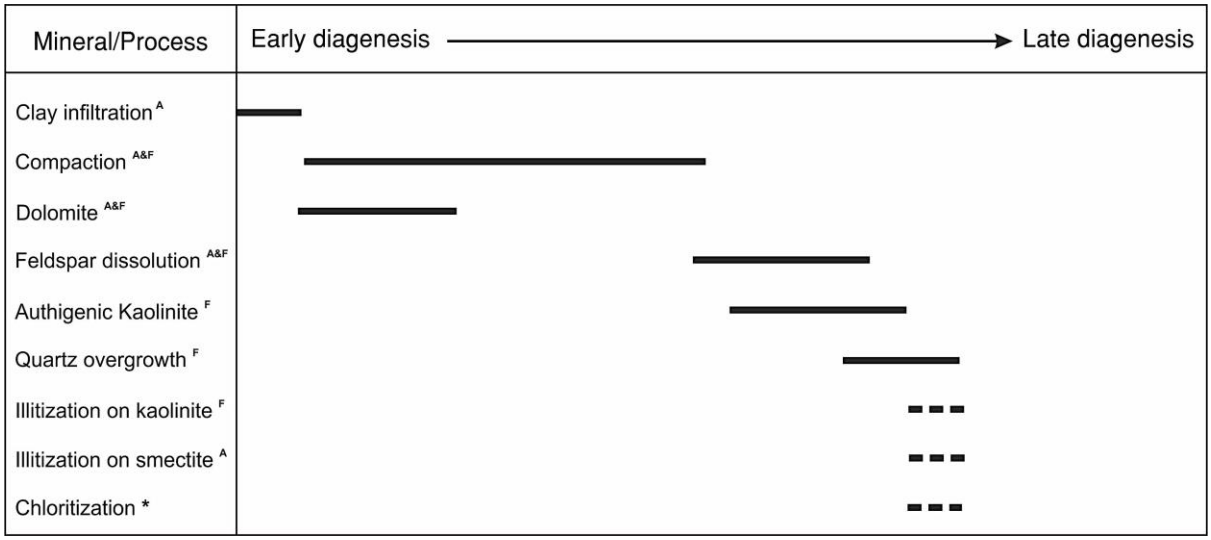

*Figure 5.9 Paragenetic sequences of the Buchan Formation, the solid/dash lines represent the major/minor events. Note the superscripts at the end of each event represent: A – the event mainly occurred in aeolian sandstones; F – the event mainly occurred in fluvial sandstones; A&F – the event mainly occurred in both aeolian and fluvial sandstones; * – the event is not observed under either thin section or SEM, but confirmed by XRD.*

A subsequent event was the dissolution of feldspar in both aeolian and fluvial deposits which generated authigenic kaolinite (**Figure 5.5e**). Considerable silica ions were released into solution, this would form quartz overgrowth in fluvial sandstones, this is usually suggested to be occur in middle to late diagenesis stage (Worden and Morad, 2000). While in the aeolian sandstones, the presence of early-formed grain coating clays provided no site on the grain surface for nucleation of silica ions, quartz overgrowth is thereby not observed.

The whole diagenetic setting might become more alkaline during late diagenesis. In the fluvial sandstone, illitization occurred on kaolinite displaying a fibrous/hairy morphology (**Figure 5.6f**). While in the aeolian sandstones, illitization is observed both on grain-coating and pore-filling smectite (**Figure 5.6i**), and the presence of pore-bridging habit of illite is often regarded to be an indicator of intermediate to deeper burial (Jiang, 2012). It can also be supported by XRD data (**Table 5.1**), the I/S is in R1 ordered interstratification and the percentage of illite within I/S is around 70% – 80%, this usually occurred at 100°C – 110°C (Hoffman and

Hower, 1979; Huang et al., 1993). There are also minor chloritization possibly due to the presence of Mg^{2+} and ferroan ions in the formation water.

5.5.2 The grain coating I/S

5.5.2.1 Source of grain coating I/S

The cornflake or honeycomb morphology observed under SEM suggests that the grain coating I/S (also the pore-filling I/S) was transformed from smectite precursor, as illite originated from kaolinite is more possible to show sheet-like morphology (Pollastro, 1985). Mineralogically, Pittman (1992) deduced that smectite could form an effective dense and continuous grain coat because they nucleate flatly attached to the detrital grain surface and curl away from that surface. The clay developed initially as clay wisps and progressed to clay platelets that formed a root zone, then to an open polygonal box-work and finally to a denser polygonal box-work.

In this study, the grain coating I/S has a contrasting distribution pattern that it is only found in aeolian facies sandstones and absent in fluvial sandstones. Within the given arid/semi-arid aeolian-dominated setting, the fine-grained sandstones with discontinuous wavy laminations commonly indicate a wet interdune or desert lake deposits, which were possibly charged by distal sector (i.e. sand flat) of fluvial distributary system during fluvial-retreat period. As a consequence, the fine-grained sediments, in this case the smectitic clays, would be accumulated in this setting and flow into aeolian dune by mechanical infiltration, which is suggested to be a likely main source of grain coating (also the pore-filling) I/S.

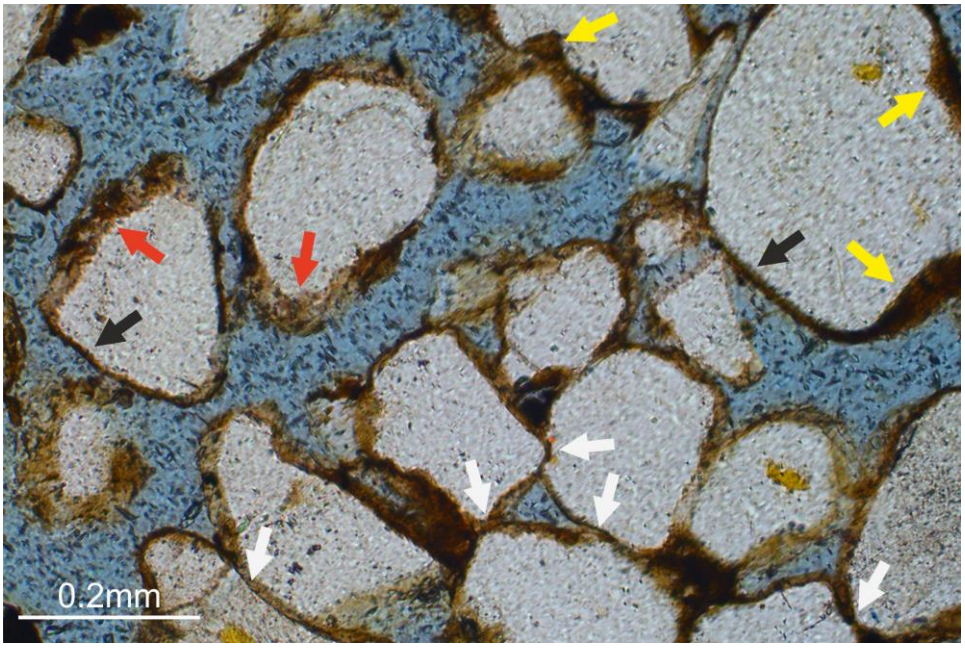

Figure 5.10 The photomicrograph (plane-polarized light) illustrates the presence of grain coating I/S in the grain contact areas (white arrows), thicker coats in grain surface depressions (yellow arrows) and grain rough surface (red arrows), and thinner coats in non-depression areas (black arrows). Sample from well 30/24-31, 3190.6 m, unit B08, aeolian dune sands.

Petrographic evidences also support this idea. Wilson and Pittman (1977) has set several criteria for recognizing mechanically infiltrated clay rims in aeolian and shallow marine sandstones: 1). Presence at grain contact areas; 2). Increased thickness in depressions on framework-grain surface; and 3). More extensive development in finer grained laminae or beds. In this study, the petrographic features of grain coating I/S meet the recognition criteria of mechanical infiltration, it occurs commonly at the grain contact areas of aeolian sandstones, and generally shows a thicker I/S coating in the framework-grain depressions and rough surfaces than the non-depression and smooth areas (**Figure 5.10**). Additionally, **Figure 5.11** clearly displays that more extensive development of grain coating and pore filling I/S in finer-grained aeolian sands than in medium-grain aeolian sands.

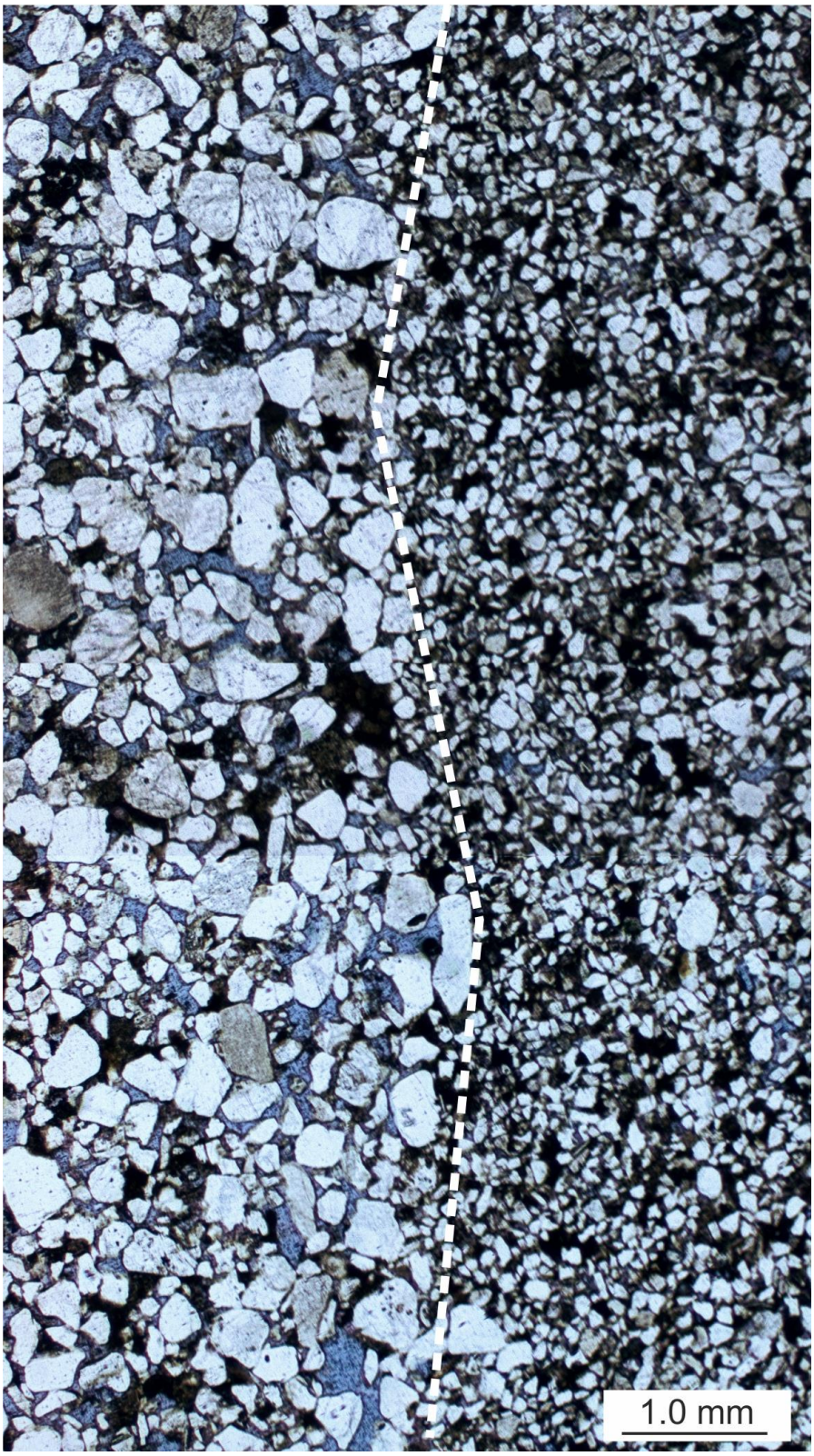

Figure 5.11 Photomicrograph illustrating different abundance of infiltrated clays in representative pin-stripe lamination dune sandstones. Note the finer grain-size lamentation (right) contains more pore-filling clays. Well 30/24-31, 3190.6 m, unit B08, aeolian dune sands.

5.5.2.2 Effect of grain coating I/S on reservoir quality

The sum of total cements (dolomite, quartz overgrowth and authigenic clays) clearly has an inverse relationship (R^2 = 0.47) with porosity (**Figure 5.12**). This at least indicates that the various types of cementation are jointly the main control of reservoir quality. As the dolomite and authigenic kaolinite occurred in both fluvial and aeolian sandstones, the most remarkable difference between two sandstone types is the quartz overgrowth which is extensively distributed (up to 6%) in fluvial sandstones and nearly negligible in aeolian sandstones.

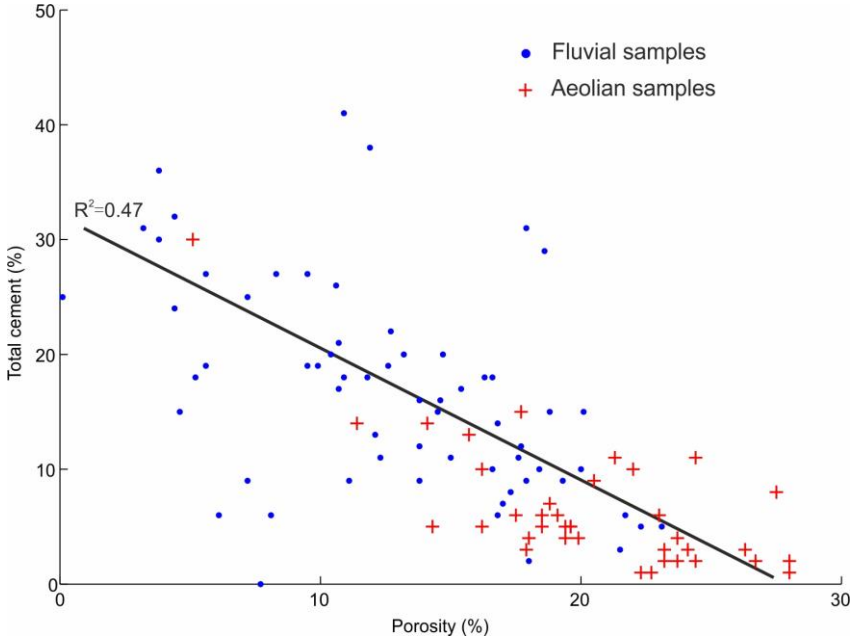

Figure 5.12 The scattered image of porosity and total cements showing a clearly inverse relationship. The data is categorized by aeolian and fluvial facies.

Continuous grain coating minerals are often the key factor for high porosity in deeply buried (> 2.5 km) sandstones (Pittman, 1992). Amongst the numerous studies, the grain coating chlorite and microcrystalline quartz are most frequently mentioned. In our study, the grain coating I/S is also effective on inhibiting quartz overgrowth thus preserving porosity.

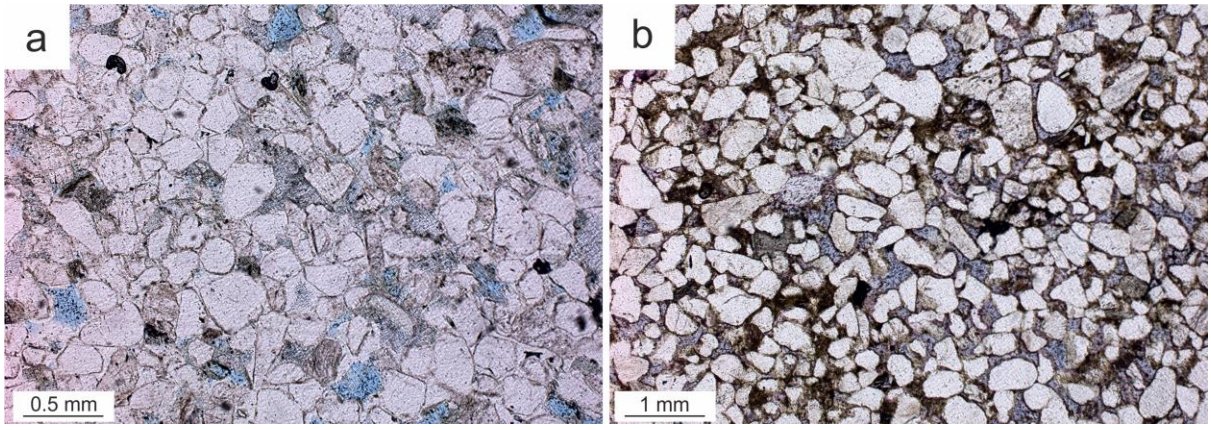

Figure 5.13 Comparison between: (a) fluvial channel sandstone without clay coatings which is extensively cemented by quartz overgrowth, the clay coating coverage is 0%, and about 95% of grains have quartz overgrowth, n = 89. Well 30/24-20z, 3117.8 m, unit B04; (b) aeolian sandstone with very high clay coating coverage (100%, n = 212) with no quartz overgrowth. Well 30/24-31, 3202 m, unit B08. Both figures are taken under plane-polarized light.

In the Buchan Formation, the amount of quartz cement in all the samples is clearly linked to the presence and coverage of grain coating I/S. The fluvial sandstones do not contain any type of continuous and well developed clay coatings around quartz grains (grain coverage is nearly 0%, n = 89) and are hence 95% of grains (84 out of 89) are cemented by quartz overgrowth in variable amount (**Figure 5.13a**). Conversely, grain coating I/S are well developed in almost all the aeolian sandstone samples with good coverage (grain coverage = 100%, n = 212) and continuity, and the quartz cementation is almost absent (**Figure 5.13b**).

To quantitatively evaluate the effect of grain coating I/S, we employ the algorithm of Walderhaug (1996) to calculate the theoretical amount of quartz cementation in upper fine to medium-grained (grain size = 0.25 mm – 0.3 mm) aeolian sandstones if the grain coating I/S were absent (parameters and functions of the algorithm see **Appendix III**). With the assumed duration of 70 million years from beginning of Paleogene, the result shows there would be about 6% – 7% porosity has been preserved by grain coating I/S (**Figure. 5.14**).

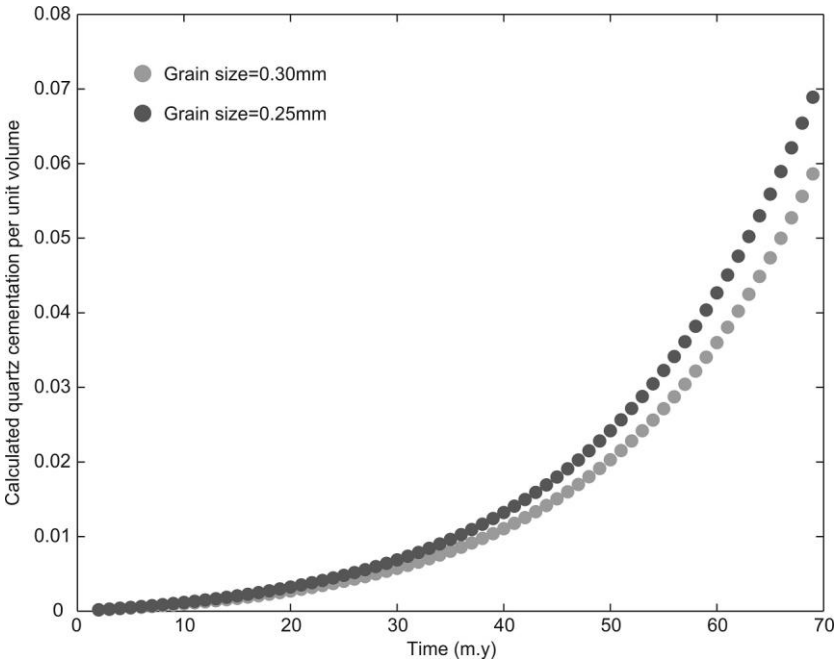

Figure 5.14 Empirical calculations of possible quartz overgrowth amounts for sand grain size in 0.25 mm and 0.30 mm during 70 million years. The algorithm is after Walderhaug (1996).

The grain coating I/S in this study was transformed from a smectitic precursor. For the reservoir quality, smectitic clay usually has two shortcomings: 1). Smectite would transform to mixed layer smectite-illite and finally illite when the K^+ is enriched in the fluid and temperature reaches around 70°C – 80°C or higher. The hairy/fibrous morphology of illite would reduce the pore and throat space, thus significantly decreasing reservoir quality, especially permeability (Almon and Davies, 1981; Wilson, 1994; Le Gallo et al., 1998); 2). Smectite has a high water sensitivity thus could easily swell and occupy the pore space (Gray and Rex, 1965).

However, these two shortcomings have very limited negative impact on reservoir quality in this study. Huang et al. (1993) and Wilson (1994) suggested that the kinetics of illitization of precursor detrital smectitic clays not solely depends on temperature but potassium concentration and total time-temperature exposure. In the Buchan Formation, feldspar dissolution might provide considerable amount of K^+. The burial history has illustrated that the Buchan

Formation was consistently at shallow depth (< 1.5 km, temperature < 60°C) until the Palaeogene and was then rapidly buried to present day maximum burial depth. This rapid burial would only provide short thermal exposure which is insufficient for full and complete illitization. Secondly, the amount of pore-filling I/S are commonly less than 5% in each aeolian sandstone sample and this would not significantly occlude the pore space.

5.6 Conclusions

The grain coatings observed in the fluvial-aeolian Buchan Formation sandstones of the Ardmore Field have been identified as illite/smectite (I/S) which were transformed from smectite precursor. The effect of porosity preservation due to grain coating chlorite and microcrystalline quartz has been demonstrated in a number of publications, however this study shows that I/S grain coatings can also be very effective in preventing quartz cementation under specific conditions, and thereby help preserving primary porosity.

In the fluvial sandstones, the precursor material has been absent resulting in the absence of clay coatings on the sand grains, and thereby quartz cementation is extensively developed and reservoir quality is poorer.

The thick and continuous grain coating I/S with extensive and good grain coverage is only observed in aeolian sandstones and this clay coating has inhibited quartz overgrowth and hence high porosity values have been persevered at more than 2.5 km depth. The illitization on smectite occurred limitedly thus would not significantly reduce reservoir quality. This is mainly due to the featured burial history: the Buchan formation was at consistently shallow depth and low temperature until Palaeogene which is not kinetically favourable to activate the smectite illitization. After the Palaeogene, the Buchan Formation was buried to today's maximum depth and temperature rapidly, the short time-temperature exposure is insufficient for

full and complete illitization. The I/S coatings were generated from smectitic precursor. It is possible that the precursor has been formed by mechanical infiltration from associated wet interdune deposits charged by clay-bearing water representing more distal sector of fluvial distributary system during aeolian-dominated period.

The understanding of the positive effect on porosity preservation from grain-coating I/S may aid predictions of high quality Devonian-hosted reservoirs in the Central North Sea. Such sandstones could form attractive exploration targets that hitherto may have been ignored because they would be expected to have low porosity on the basis of regional trends.

Acknowledgments

The author thanks CGG for providing the seismic data; Enquest PLC for supporting this research through access to core and financial support of analytical work; X-ray Mineral Services Ltd for processing the XRD analysis; Dr Bernard Besley for providing data and helpful discussions; BGS (British Geological Survey) for its assistance in facilitating the examination of Devonian cores; We are all grateful for the expertise and general assistance offered by Mr Ian Chaplin (Department of Earth Sciences, Durham University) and Mr Leon Bowen (Department of Physics, Durham University) in the preparation of samples.

Table 5.1 XRD data for < 2 µm size mineral fraction in selected samples.

Well	Depth (m)	Facies	Wt.%	Illite/smectite				Illite			Kaolinite			Chlorite			Quartz		Calcite		Dolomite	
			<2um	% A	% B	Order	% I	% A	% B	Crys	% A	% B	Crys	% A	% B	Crys	% A	% B	% A	% B	% A	% B
30/24-28	2790.1	AD	1.9	34.4	0.7	O	70-80	58.3	1.1	P	0.0	0.0	-	7.1	0.1	P	0.3	0.1	0.0	0.0	0.0	0.0
30/24-28	2829.8	AD	3.0	46.3	1.4	O	70-80	25.9	0.8	P	22.6	0.7	M	2.9	0.1	M	2.4	0.1	0.0	0.0	0.0	0.0
30/24-28	2844.1	AD	3.0	50.5	1.5	O	70-80	32.7	1.0	P	7.5	0.2	M	3.5	0.1	M	5.8	0.2	0.0	0.0	0.0	0.0
30/24-31	3190.3	AD	2.0	44.8	0.9	O	70-80	34.9	0.7	P	10.7	0.2	M	5.1	0.1	P	4.5	0.1	0.0	0.0	0.0	0.0
30/24-28	2794.7	CHB	3.3	TR	TR	-	-	22.0	0.7	P	58.7	1.9	M	15.8	0.5	M	3.6	0.1	0.0	0.0	0.0	0.0
30/24-05	2849.3	CHB	3.2	TR	TR	-	-	8.5	0.3	P	72.6	2.3	M	5.3	0.2	P	3.1	0.1	0.0	0.0	10.6	0.3

Facies: AD = aeolian dune; CHB- channel bar
A = Weight% relevant size fraction; B = Weight% bulk sample;
Mixed-layer Ordering: RI= Randomly Interstratified (R0); O = Ordered Interstratification (R1); LR = Long-range Ordering (R3);
Crystallinity: VW = Very Well Crystallised; W = Well Crystallised; M = Moderately Crystallised; P = Poorly Crystallised.

CHAPTER 6: DIAGENETIC AND GEOCHEMICAL STUDIES OF THE BUCHAN FORMATION (UPPER DEVONIAN) IN THE CENTRAL NORTH SEA

---

*This chapter has been accepted by the **Petroleum Science** and is now in press.*

Chapter outline

Summary

The Upper Devonian Buchan Formation sandstone reservoirs in the UK Central North Sea are litharenite/sublitharenite and were deposited in fluvial/aeolian settings. The grain-coating clays in the aeolian sandstones has effectively inhibited quartz overgrowth, the reduction of reservoir quality is mainly due to mechanical compaction and early dolomite precipitation in both fluvial and aeolian sandstones; quartz overgrowth and kaolinite illitization in fluvial sandstones; and limited smectite illitization in aeolian sandstones.

The carbon/oxygen stable isotopes of dolomite cements suggest a predominantly marine carbon source and precipitation temperature at between 25°C – 58°C indicating a shallow burial depth during dolomite precipitation. The temperatures and the dolomite distribution indicate that the cements originated from the overlying Upper Permian Zechstein carbonates. Extensive quartz overgrowths formed at 80°C – 120°C in the late and deep diagenetic burial history. The most probable silica source was from feldspar kaolinitization and pressure dissolution of quartz grains. Through detailed petrography and geochemical analyses the burial-paragenesis-thermal history of Buchan Formation has been constructed.

Similar diagenetic processes are likely to have occurred in the Buchan Formation in other parts of the Central and Northern North Sea. This study may allow new petroleum plays to be considered in areas previously thought to have poor hydrocarbon potential.

6.1 Introduction

The Upper Devonian Buchan Formation have a wide distribution in the Central and Northern North Sea (Ziegler, 1990) but are usually perceived to have little hydrocarbon potential (Downie, 2009). Despite this, a number of discoveries both in UK and Norwegian North Sea have confirmed considerable, but highly variable hydrocarbon reserves in the Buchan Formation sandstones (Edwards, 1991; Trewin and Bramwell, 1991; Knight et al., 1993; Gambaro and Currie, 2003; Gluyas et al., 2005). Until now, the Buchan Formation sandstones have been poorly understood due to the fact that the Devonian Formations were never considered as the main exploration targets for petroleum. Previous studies of the Upper Devonian reservoirs have concentrated on the sedimentology, describing the strata as deposits of fluvial-braided and aeolian systems (Graham et al., 2003; Downie, 2009).

The reservoir quality of these typically terrestrial deposits is highly heterogeneous and varies from nearly impermeable (less than 0.1 mD) up to Darcy level (Gluyas et al., 2005). It is reported that the cementation by authigenic carbonate and quartz overgrowth are the principle causes of poor reservoir quality (Downie, 2009). However, no detailed report has explained the sources of these cements, when and under what conditions they were formed and how the cements control the reservoir quality.

To achieve a better understanding on these problems, the Ardmore Field (previous name 'Argyll') was selected as the main research target due to it possessing extensive core coverage of the Buchan Formation interval. The Ardmore Field has multiple reservoirs: Permian Zechstein carbonate, Permian Rotliegend sandstone and Upper Devonian Buchan Formation sandstones all of which are in communication, together with minor, isolated oil accumulations in Upper Jurassic Fulmar Sandstones and Upper Cretaceous Chalk (Bifani and Smith, 1985; Robson, 1991; Gluyas et al., 2005). The properties of the former two Permian units have been recognised in numerous studies (e.g. Nagtegal, 1979; Glennie and Provan, 1990; Purvis, 1992;

Howell and Mountney, 1997; Leveille et al., 1997; Sweet, 1999; Heward et al., 2003; Gluyas, 2016); but this is the first time a study has been reported on the combined diagenetic and geochemical analyses of the Buchan Formation sandstone reservoirs. The results provide new insights into these poorly-understood Devonian reservoirs. We investigate the sources of cements, diagenetic history and evaluate their influences on reservoir quality. Additionally, the outcomes have broad implications for the future petroleum explorations of Devonian age reservoirs in the Central and Northern North Sea.

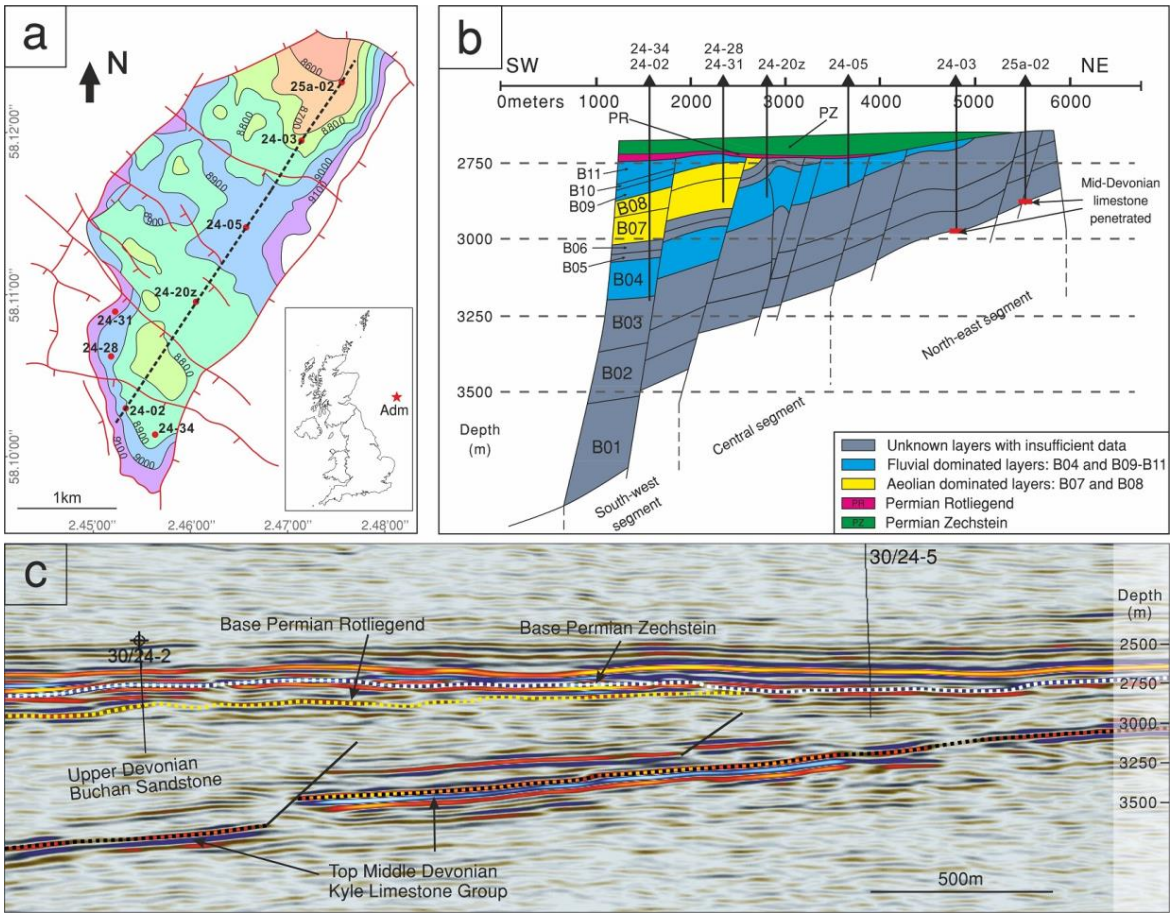

Figure 6.1 Geological maps showing: (A) Location and main structure elements of Ardmore (Adm) field. (B) Vertical section of an SW-NE profile a-b in Figure 6.1A. (C) Seismic section of a-b profile.

6.2 Geological setting

The Ardmore Field is located on the Argyll Ridge, a large NE-SW trending Palaeozoic-age tilted fault block on the south-western flank of the Central Graben in Block 30/24, UK Conti-

nental Shelf, about 300 km east from Edinburgh, the field measures 2.5 km wide and 6 km long (**Figure 6.1A**). It is a horst feature with the crest in the north and fault closure to the north-east. A combination of dip and faults defines the limits of the field on the north-west and south-east flanks, while dip closure defines the southern limits of the field. The major fault trends are in two main directions, WNW–ESE cut by NW-SE faults. As the Devonian is steeply dipping within the Ardmore Field, it is further dissected by those NW-SE oriented faults, which divide the field into three parts: the NE, Central and SW segments (**Figure 6.1B**).

The Middle Devonian Kyle Limestone and overlying Upper Devonian Buchan Formation sandstones are the oldest strata penetrated in the Ardmore Field. The Kyle Limestone shows strong seismic reflection which provides a good lower limit and its upper boundary is a conformable transition to the Buchan Formation sandstones (**Figure 6.1C**). The uppermost Buchan Formation sub-crops at the Base Permian unconformity, the oldest stratigraphic units sub-crop in the NE segment with progressively younger stratigraphic units sub-cropping towards the SW segment. Eleven units (named as B01 to B11 from base to top) have been divided within the formation based on well logs utilising laterally correlative shale beds (Gluyas et al., 2005). The interpretation is controlled by available core data, although this provides limited stratigraphic control, as core coverage per unit is sparse. The lowest units (B01 to B03) are of poor reservoir quality, as they are shaley relative to the overlying reservoirs. These older units are oil-bearing in the NE segment of the field but few wells have penetrated them and only minor oil production has occurred. The reservoir quality of Buchan Formation sandstones improves towards the south-west, with the central and south-west segments containing better reservoir quality intervals.

We are uncertain about the depositional facies for sandstones in stratigraphic units B01, B02, B03, B05 and B06 due to the poor core coverage; while the units B04, B09, B10 and B11 are

dominated by fluvial braided deposits, and units B07, B08 and some minor portions in B09 and B10 contain significant aeolian deposits (**Figure 6.2**) (Tang et al., 2017a). The overall known units comprise a fluvial (B04)-aeolian (B07 and B08)-fluvial (B09, B10 and B11) variation and generally represent a progradation-retreat-progradation cycle of the alluvial fan-based braided system with aeolian deposits occurring mainly between two main progradation periods (Tang et al., 2017a). The total thickness of Buchan Formation sandstones is nowhere fully penetrated but based on seismic interpretation we estimate it to be up to 800 m.

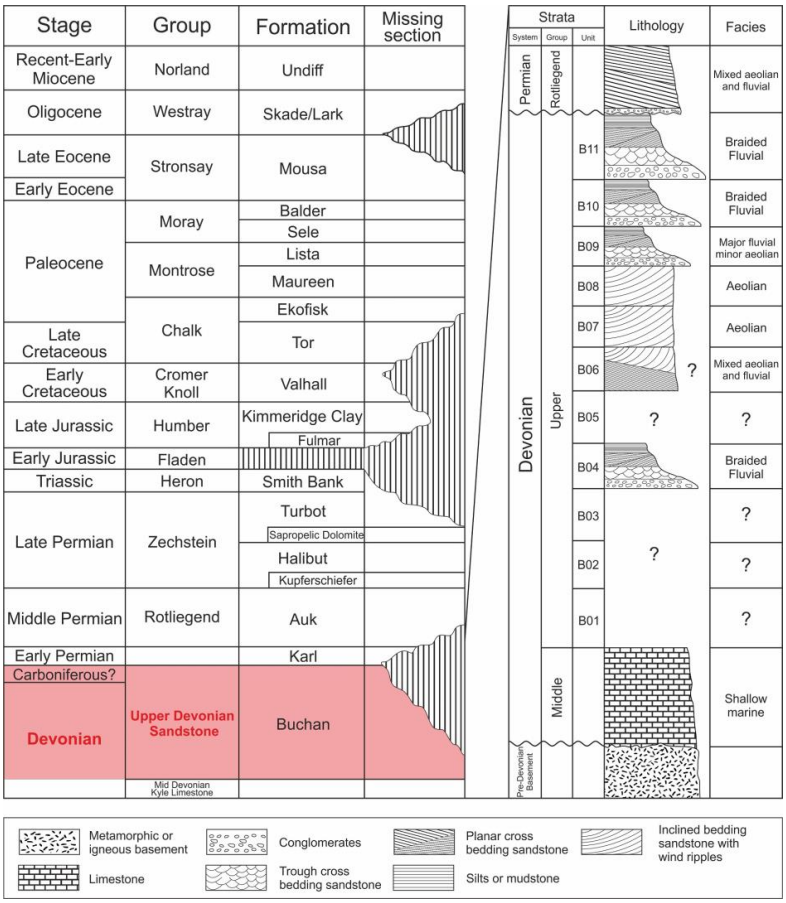

Figure 6.2 Stratigraphy and sketched sedimentary log of the Ardmore Field.

The Buchan Formation sandstones in the Ardmore Field are heterogeneous and hence the reservoir quality is highly variable. Net to gross ratio is commonly greater than 70% in the better quality zones, the better developed braided channels and aeolian dune sand bodies achieve porosity between 12% to 28%, and the typical porosity values of North Sea oil-

bearing sandstones at this depth is around 16% (Selley, 1978). Net sand permeability reaches 5 Darcies, though 10's mD and 100's mD are typically average values in the fluvial and aeolian sand packages, respectively.

6.3 Database and methods

One hundred and one Buchan Formation sandstone core samples were collected from five wells (14 from well 30/24-05, 16 from well 30/24-20z, 38 from well 30/24-28, 16 from well 30/24-31 and 17 from well 30/24-34). Care was taken to minimize breakage and thereby preserve cements, textures, and fabrics. Thin sections for petrographic examination, fluid inclusion wafers, and other analytical analysis were prepared. Samples for thin-section petrography were impregnated with blue epoxy to facilitate the identification of porosity. Petrographic examination was performed on a Leica DM2500P standard polarising microscope to identify textures and mineral composition as well as characterize the relationships between different cement types. Photomicrographs were taken using an attached Leica DFC420C digital camera. Estimation of the percentages of detrital grains and cements was made on thin sections by point counting analysis (n = 300). The measured porosity and permeability data were provided by EnQuest internal reports.

Based on the microscopic petrography examinations, representative samples were selected for Hitachi SU70 scanning electron microscope (SEM) observation. The electron beam has acceleration energy of 10 kV – 20 kV. The technique relies on backscattered electrons on polished sections to define mineral grain boundaries, and then analyses X-ray emission with an energy-dispersive X-ray detector (EDX) to assign the mineral compositions. Cathodoluminesence (CL) was employed for recognizing different quartz overgrowth generations and performed on a Hitachi SU70 electron microscope equipped with a Gatan Mono CL Digiscan II, operated at 12 kV for panchromatic imaging.

To identify and quantify the clay mineralogy, six samples were chosen for XRD analysis (4 from grain coated aeolian sandstone samples, 2 from fluvial sandstone samples with quartz and dolomite cements and without grain coatings). The bulk rock was disaggregated by gentle crushing and suspended in the distilled water. After allowing the coarse grains to settle for 3 hours, the clay in suspension was decanted into a tube for centrifuging. Clay with less than 2 microns was tested after being air dried, solvation with glycerol and heating at 500°C for 2 hours.

A very fine-grained sample (siltstone) was selected for QEMSCAN (quantitative evaluation of minerals by scanning electron microscopy) analysis with the aim to provide a quantitative petrographic characterisation. The sample was cut to give a flat surface and impregnated with Struers Epofix resin within a 30 mm diameter mould. The sample was polished, carbon coated and measured using automated mineral analysis at the Rocktype QEMSCAN facility. The FEI QEMSCAN technique combines SEM and X-ray (EDX) technology to provide automated petrographic description of geological samples in the form of high resolution images and spatially resolved compositional and textural data.

Doubly polished wafers for fluid inclusion analysis were prepared from eleven samples selected from sandstones with extensive quartz overgrowth. The aim is to investigate the precipitation temperature of the quartz overgrowth. Homogenization temperatures (T_h) of fluid inclusions were measured by the Linkam THMS600 Cooling-Heating Stage in State Key Laboratory of Oil and Gas Reservoir Geology and Exploitation, Chengdu University of Technology (CDUT). The temperature range of the instrument is from −196°C to 600°C with a precision of < 0.1°C. The rate of temperature increase can be controlled to within 1°C/min when approaching the critical point.

The carbon- and oxygen-isotopic analysis on carbonate cements was measured by the Scottish Universities Environmental Research Centre (SUERC) in the University of Glasgow.

Seventeen sandstone samples with variable amounts of dolomite cements were gently disaggregated with a hammer and then crushed in a mortar, at least 1 mg of dolomite powder is obtained for each sample. The value of $\delta^{13}C$ and $\delta^{18}O$ were determined on CO_2 liberating from dolomite cements dissolved by 100% H_3PO_4 at 50°C. The isotopic composition of CO_2 is reported in units of ‰ relative to Pee Dee belemnite (PDB).

Burial history and thermal condition of the Ardmore Field have been analysed using data from exploration wells by the Schlumberger software PetroMod (V2014.1). In the studied area, there are several stratigraphic hiatuses between Devonian and Palaeogene, with the estimated thicknesses calculated by using data from adjacent fields (Graham et al., 2003; Hayward et al., 2003; Glennie, 2009). The maximum burial depth of the Upper Devonian Buchan Formation in the Ardmore Field occurs today at approximately 2.7 km to 3.2 km. The present day geothermal gradient is around 34.6°C/km (Graham et al., 2003) with an average surface temperature of 12°C, and the present day maximum temperature in the field is around 115°C – 120°C at 3.2 km burial depth.

6.4 Results

6.4.1 Petrography

Petrographic examination indicates that the fluvial and aeolian sandstones have different features for both mineral composition and grain texture. Generally the sandstone samples are classified as litharenite to sublitharenite according to Folk (1957), with the total average composition of $Q_{78}F_3R_{19}$, and the aeolian sandstones have a more mature composition ($Q_{82}F_2R_{16}$, **Figure 6.3B**) than fluvial sandstones ($Q_{76}F_3R_{21}$, **Figure 6.3A**). Texturally, except the minor thin-bedded (less than 1 m) and sandy-clast supported conglomerates (less than 10% among all fluvial deposits) and mudstones (less than 10% among all fluvial deposits), the fluvial sandstones are relatively immature and fine to medium grained. Sorting ranges from poor

to moderate and roundness of grains varies from sub-angular to sub-rounded. Quartz grains are tightly compacted usually showing curved and rare concavo-convex grain contacts. The fine to medium grained aeolian sandstones have a higher textural maturity, sorting ranges from moderate to good and roundness of grains varies from sub-rounded to rounded. The grain contacts are commonly point to long.

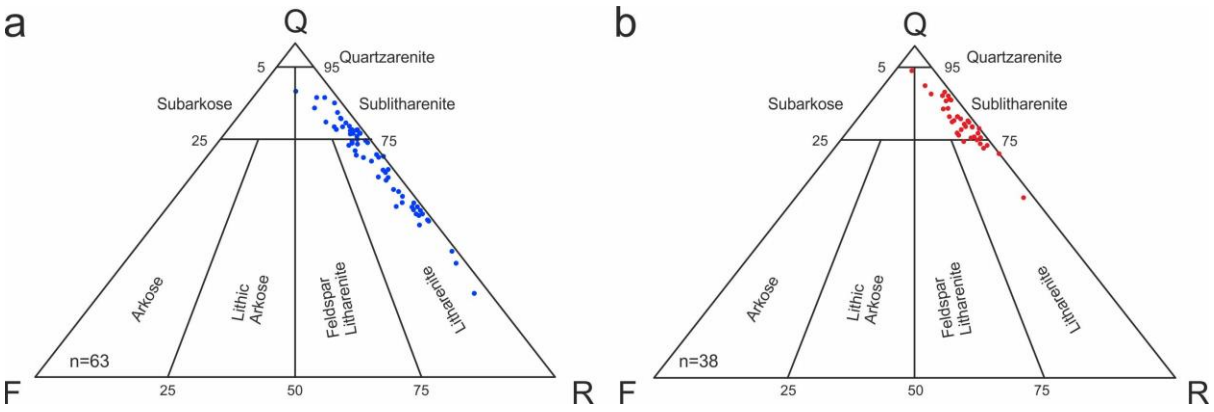

Figure 6.3 The QFR ternary charts for (A). Fluvial sandstone samples; and (B). Aeolian sandstone samples.

Detrital quartz is the dominant mineral type (41% – 95%) in all samples. Most quartz grains are monocrystalline with 0.15 mm to 0.3 mm grain size (**Figure 6.4A**) and can exhibit undulose extinction (**Figure 6.4B**). Detrital feldspar occurs from trace amounts up to 7% with the main feldspars commonly demonstrating polysynthetic twinning microcline (**Figure 6.4C**). The feldspars occur as both fresh grains and dissolved grains with relic outlines (**Figures 6.4C and 6.4D**). Other major identified minerals include mica comprising up to 13%, and show variable amounts of distortions and grain breaking (**Figure 6.4E**). Rock fragments are in variable quantities and include micaceous and illitic mud clasts and fine-grained metamorphic and volcanic fragments to a lesser quantity (**Figure 6.4F**).

Diagenetic minerals in Buchan Formation sandstones include dolomite, quartz overgrowth, kaolinite, illite and illite/smectite (I/S). Dolomite occurs in both fluvial and aeolian sandstones (up to 28%, mean value 7.5%) showing sporadically ‘spotty’ purple-red stained ce-

ments and sometimes in irregular band distribution in hand specimen (**Figure 6.5A**). Under thin section observation, the poikilotopic dolomite cements commonly show typical structure of 'light rims and cloudy core' in a well-developed rhombic shape and size ranges from 20 μm – 200 μm (**Figure 6.5B**). Chlorite occurs in both fluvial and aeolian sandstones with a trace amount (up to 0.5%), confirmed by XRD analysis (see **Table 6.1**).

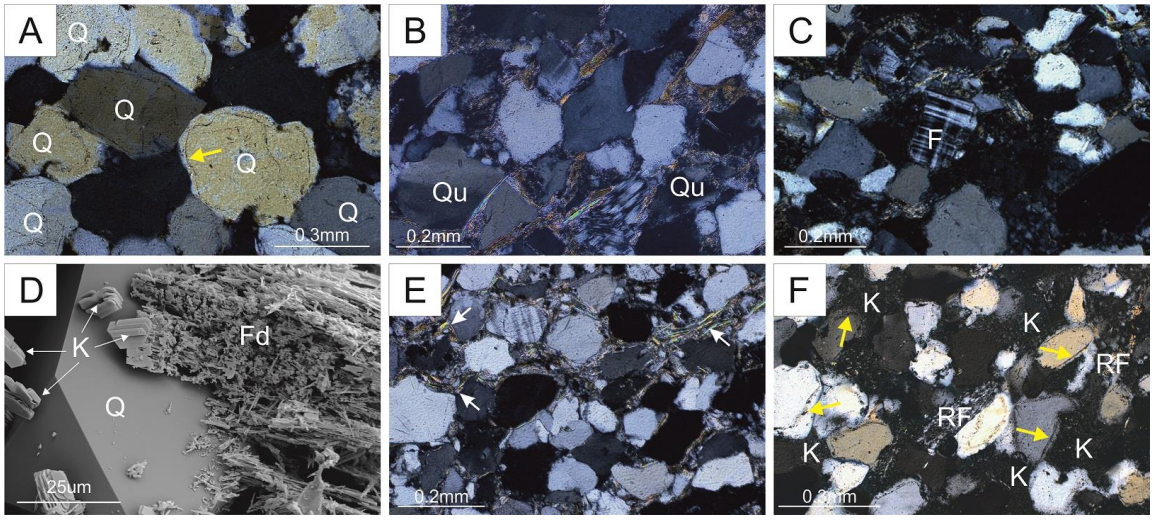

Figure 6.4 Photomicrographs of sandstone compositions. (A) Monocrystalline quartz grain with quartz overgrowth and visible dust rims (yellow arrows) on the original detrital grain. Well 30/24-34, 2967.8 m. (B) Quartz grains exhibiting undulose extinction. Well 30/24-20z, 3125.4 m. (C) Microcline showing polysynthetic twinning. Well 30/24-05, 2846.4 m. (D) SEM image of feldspar dissolution and presence of authigenic kaolinite. Well 30/24-20z, 3126 m. (E) Bended mica (white arrows) between quartz grains. Well 30/24-20z, 3125.4 m. (F) Possible volcanic-origin rock fragments, notes the pore-filled kaolinite aggregates and quartz overgrowth (yellow arrows). Well 30/24-05, 2847 m.

Q-quartz; Qu-quartz with undulose extinction; F-feldspar; K-kaolinite; Fd-dissolved feldspar; RF-rock fragments; D-dolomite; P-porosity.

Apart from the prevalent dolomite cements, fluvial sandstones are featured as containing dense authigenic kaolinite aggregates and extensive quartz overgrowths. The authigenic kaolinite is present as densely-packed pseudo-hexagonal booklets and platelets as grain-shaped masses and the pore-filling aggregates in the interstices (**Figure 6.5C**). The quartz overgrowth (1% – 7%, mean value 4.5%) occur as syntaxial cements forming incomplete or complete rims around quartz grains with the thickness ranging from 10 μm to 50 μm. Boundaries

between detrital quartz grains and overgrowth are visible due to the presence of 'dust' lines (**Figure 6.4A**). The SEM-cathodoluminescence (CL) analysis revealed that the quartz overgrowths were probably formed by several stages (**Figures 6.5D and 6.5E**), which corresponds to the range of measured homogenization temperature in the fluid inclusion (80°C – 120°C). Authigenic illite can be found under SEM and mainly occurs as fibrous or hairy crystals (**Figure 6.5F**).

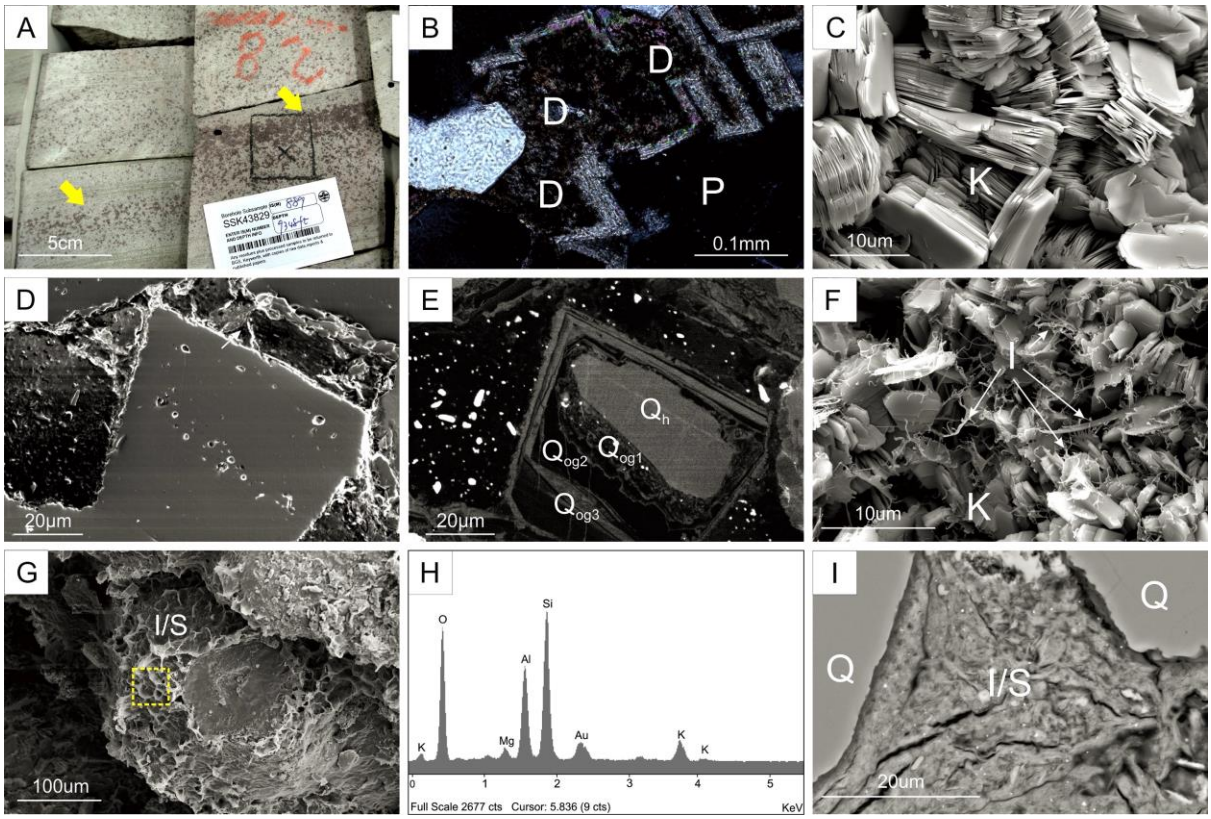

Figure 6.5 Photomicrographs and EDX spectrums of authigenic minerals. (A) Thin bands of 'spotty' red-brown stained cements (yellow arrows) in the cores. Well 30/24-05, 2849.1 m; (B) Dolomite cements in the pore space showing well rhombic shape with cloudy core and light rims under microscope. Well 30/24-05, 2849.1 m; (C) SEM image of authigenic kaolinite presents in densely-packed pseudo-hexagonal booklets and platelets. Well 30/24-05, 2849.1 m; (D) A quartz grain with intense quartz overgrowth under SEM, Well 30/24-34, 2976.4 m; (E) A quartz grain with intense quartz overgrowth under CL, note multiple stages of overgrowth sighted around the host grain. Well 30/24-34, 2976.4 m; (F) SEM image of authigenic illite occurs as fibrous and hairy crystals based on the associated with kaolinite precursor aggregates. Well 30/24-05, 2850.9 m; (G) SEM image of grain-coating illite/smectite showing cornflake-honeycomb morphology. Well 30/24-31, 3190.6 m; (H) The EDX spectrum of grain coating I/S (the dashed square area in Fig. 5G). Well 30/24-31, 3190.6 m; (I)

BSEM image of pore-filling illite/smectite occurred as flocculent aggregates existing in the intergranular pore space. Well 30/24-31, 3190.6 m.

Qh-host quartz grains; Qog-quartz overgrowth; K-kaolinite; I-illite; I/S-illite/smectite; gc-grain coating; pf-pore filling.

Conversely, quartz overgrowth is absent and kaolinite is subordinate in aeolian sandstones. Illite/smectite (I/S) has been identified by EDX spectrum (**Figure 6.5H**) and XRD analysis (**Table. 6.1**) which is the unique and most important clay type in aeolian sandstones although it is present in minor amounts (0.5% – 5%). Thin section and SEM observations illustrate that the I/S occurs in two forms. a) The grain coating I/S (**Figure 6.5G**) commonly occurs as cornflake and/or honeycomb morphology with short filamentous terminations, and consists of 1 μm – 5 μm thick rim coating all detrital grains in the aeolian sandstones. These grain coatings are absent in fluvial sandstones. Quartz overgrowths are noticeably absent in the aeolian sandstone facies where uniform and robust grain coating I/S has developed. b) Pore-filling I/S can occur (< 5%) as aggregates existing in the intergranular pore space of aeolian sandstones, and is absent in the fluvial sandstones (**Figure 6.5I**).

6.4.2 Fluid inclusions

Fluid inclusion thermometry can provide useful temperature information for the authigenic mineral precipitation (Robinson and Gluyas, 1992). The fluid inclusions in the selected samples primarily occur in two forms: a) The belt-like distribution along the healed microfractures within quartz grains (Type I, **Figure 6.6A**); and b) Between the host quartz grain and their surrounding overgrowths (Type II, **Figure 6.6B**). The size of fluid inclusions is about 2 μm – 8 μm in diameter and most of them have gas bubbles and fluid phases with a gas/liquid ratio less than 5% at room temperature (15°C).

The measured homogenization temperature (T_h) of the two types fluid inclusions are shown in **Table 6.2**, and the **Figure 6.6** presents the T_h distribution of fluid inclusions both in Type I

and Type II. The T_h in the healed micro-fractures mainly ranges from 110°C – 140°C and a few of them are under 110°C and over 140°C. For the Type II fluid inclusions, T_h has a relatively uniform range from 80°C to 120°C with a mean value of 101.2°C. More than half (56.3%) measured T_h values are located between 81°C to 100°C, which might imply the temperature condition for precipitation of the primary quartz overgrowth.

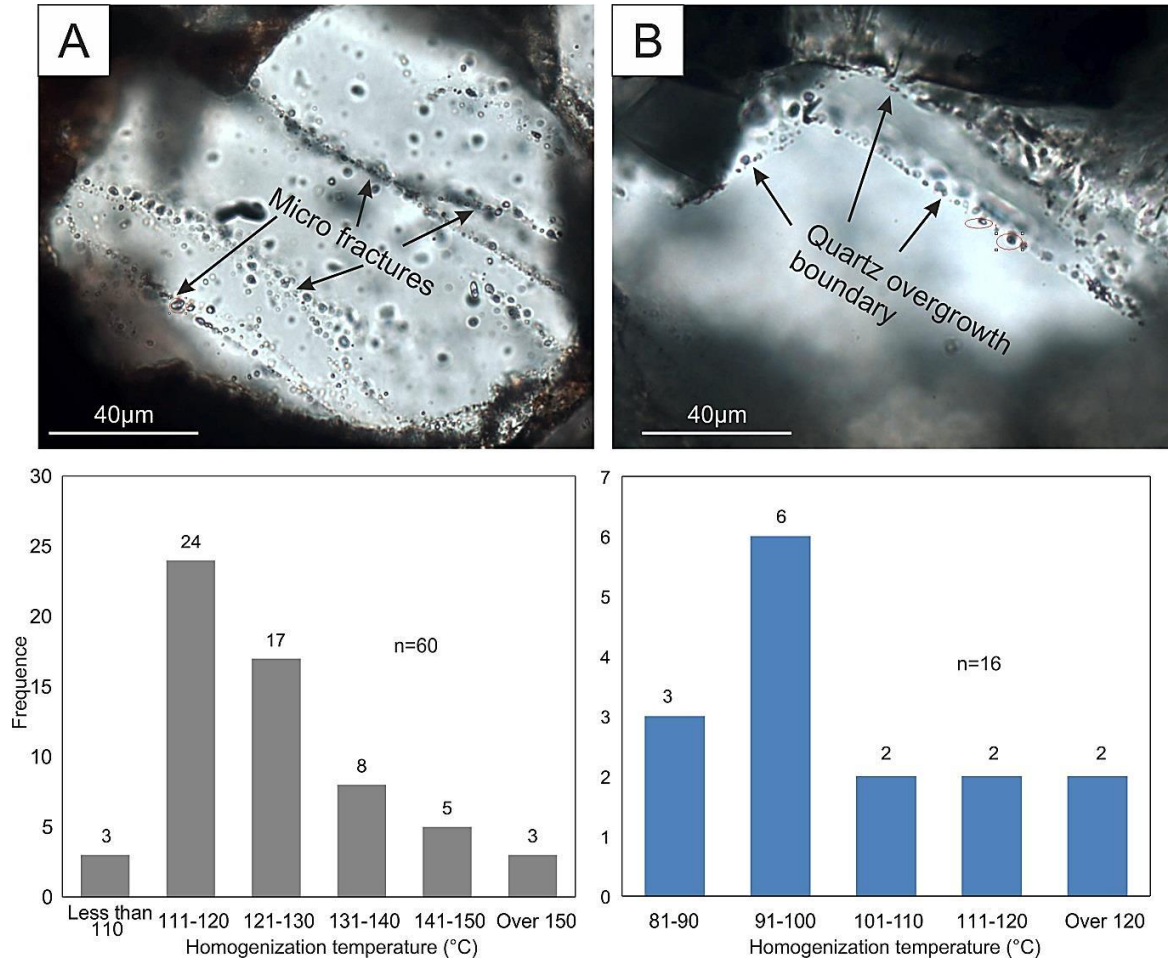

Figure 6.6 Photomicrographs and temperature distribution charts of fluid inclusions (A) In the micro fractures within quartz grains (Type I); and (B) between host quartz grains and overgrowth (Type II), note at least two stages quartz overgrowths have been sighted.

6.4.3 Isotopic composition of dolomite cements

The carbon and oxygen isotopic compositions of dolomite cements were measured in 17 sandstone samples (**Table. 6.3**). The results show that most dolomite cements have a relatively wide range of $\delta^{18}O_{PDB}$ values from -6‰ to 0.8‰ but are mainly allocated between -3‰ to

0‰ with an average value of -1.8‰. The values of $\delta^{13}C_{PDB}$ vary from -3.1‰ to 1.6‰. The calculated value of $\delta^{18}O_{SMOW}$ is derived from: $\delta^{18}O_{SMOW} = 1.03091\times \delta^{18}O_{PDB} + 30.91$ (Coplen et al., 1983), and the temperature is calculated by using fractionation equation between carbonate and water: $1000\times \ln\alpha_{dolomite\text{-}water} = 3.06 \times 10^6/T^2 - 3.24$ (Matthews and Katz, 1977).

6.5 Discussion

6.5.1 Sources of the authigenic minerals

6.5.1.1 Authigenic kaolinite and quartz overgrowth

Precipitation of authigenic kaolinite and formation of quartz overgrowth occurred relatively late in the diagenetic history. For the deeply buried sandstones, the concentration of SiO_2 (aq) (< 100 ppm) and Al^{3+} (< 10 ppm) is commonly low (Bjorlykke and Jahren, 2012; Yuan et al., 2015). In such a condition with considerable heterogeneity in porosity and permeability, none of the advective flow, thermal convection and diffusion is capable for long-distance and massive transfer of SiO_2 (aq) and Al^{3+} from the remote external sources (Bjørlykke et al., 1988; Yuan et al., 2015).

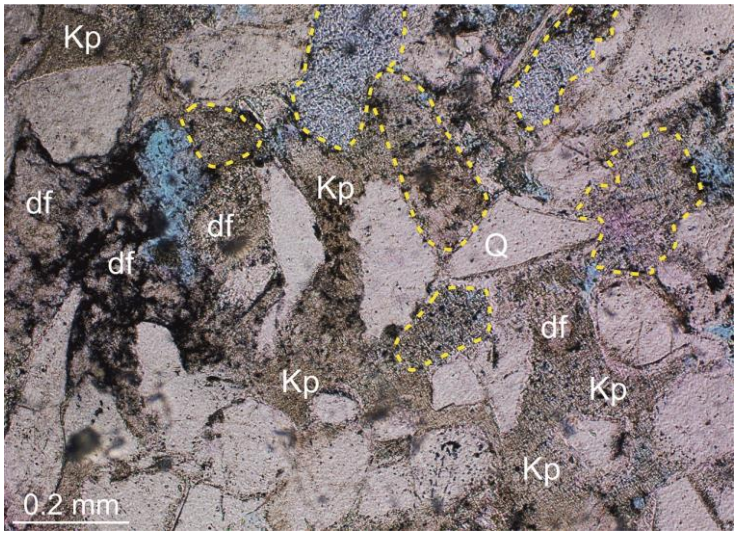

Figure 6.7 The different occurrences of authigenic kaolinite aggregates which may indicate at least two different sources, note the recognizable relic shape of seriously dissolved feldspar grains (yellow dash circles), Well 30/24-34, 2887.7 m. df-dissolved feldspar; Kp- pore filling kaolinite; Q-quartz.

For the authigenic kaolinite in sandstones, Shelton (1964) suggested three possible sources: 1) Crystallization of introduced material from solutions and/or deposition of material from colloidal suspensions; 2) Alteration in place of some parent minerals; and 3) Recrystallization of fine-grained detrital kaolinite clay. In this study, the authigenic kaolinite mainly presents in two forms (**Figure 6.7**): 1) Relatively isolated patches of pore-filling aggregates; and 2) Aggregates with a recognizable precursor grain shape. With the observed petrographic features and no obvious clue of external source, the most possible source for authigenic kaolinite should be the dissolution of feldspars within the sandstones. On the thin section scale, an inverse correlation could be identified between quantity of remained feldspar and kaolinite (**Figures 6.8B**): that is little remained feldspars are commonly accompanied with massive kaolinite, and massive remained feldspars are commonly accompanied with little kaolinite. The inverse correlation between remained feldspar and kaolinite suggests that the most possible source of kaolinite is the dissolution of local feldspars and/or the dissolved solution from the nearby sandstones. At the same time, the authigenic kaolinite content increases slightly with the increasing burial depth (**Figure 6.8A**), this suggests that the higher temperature and deeper burial depth would probably promote the feldspar dissolution and therefore generate more kaolinite.

In quartz-dominated sandstones with quartz overgrowths, the most probable source of silica is from quartz dissolution along grain contacts (commonly stylolite) and feldspar dissolution (Walderhaug, 2000; Tournier et al., 2010). The feldspar alteration, in this case the kaolinitization, could release considerable amount of silica ions (Bjørlykke, 1983). In this study, the sandstones experienced minor pressure dissolution. Additionally, both the authigenic kaolinite and released silica are the products of feldspar dissolution, and there is indeed a positive correlation between authigenic kaolinite and quartz overgrowth (**Figure 6.8C**). It is proposed

in this study that the most probable silica source for quartz overgrowth is the dissolution of local feldspars and pressure dissolution has provided a minor contribution.

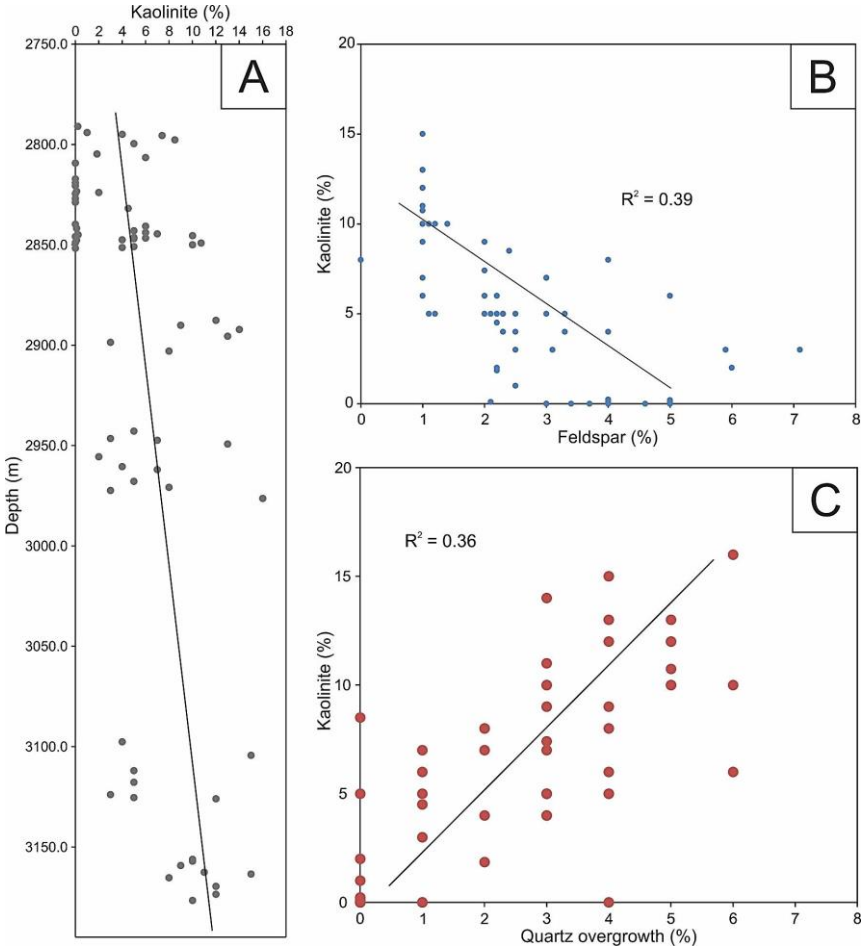

Figure 6.8 Scattered diagrams showing relationship between: (A) kaolinite and depth; (B) kaolinite and feldspar; and (C) kaolinite and quartz overgrowth. Database is from fluvial sandstone samples.

6.5.1.2 Dolomite

Syn-depositional dolomite commonly occurs in sabkha deposits when the Mg/Ca ratio in the brines increased with a consequent Ca^{2+} removal from solution (Evans et al., 1969; Kinsman, 1969). If this was the case for the dolomite in the Buchan Formation, the distribution of dolomite cements would expect to be highly facies-related, such as with the interdune sabkha and desert lakes. However, the dolomite cements are found throughout the cored intervals, regardless of lithofacies, and occur in both aeolian and fluvial sandstones.

The $\delta^{13}C_{PDB}$ values are largely but slightly negative and restricted near 0‰ (14 out of 17 are between -3.0 ‰ and 1 ‰, mean value -1.2 ‰, **Table 6.3**) which may indicate a major contribution from marine carbon source (Keith and Weber, 1964) and minor from other sources. Talbot (1990) has suggested that the correlation coefficient between $\delta^{13}C_{PDB}$ and $\delta^{18}O_{PDB}$ is a useful tool to discriminate the water setting is open or closed, that is high ($r > 0.7$) and low ($r < 0.4$) coefficients indicate closed and open settings, respectively. The measured samples have a quite low correlation coefficient between $\delta^{13}C_{PDB}$ and $\delta^{18}O_{PDB}$ ($r = 0.46$) which would imply a generally open settings, where the fresh sea water was commonly introduced. Therefore the $\delta^{18}O_{SMOW}$ value of 0‰ of formation water in eodiagenetic stage is acceptable. By employing the oxygen isotope fractionation factor for dolomite/water (Matthews and Katz, 1977), the calculated precipitation temperatures for dolomite cements range mainly from 25°C to 58°C (**Table. 6.3**), which could indicate that these dolomite cements were formed at relatively shallow burial depth.

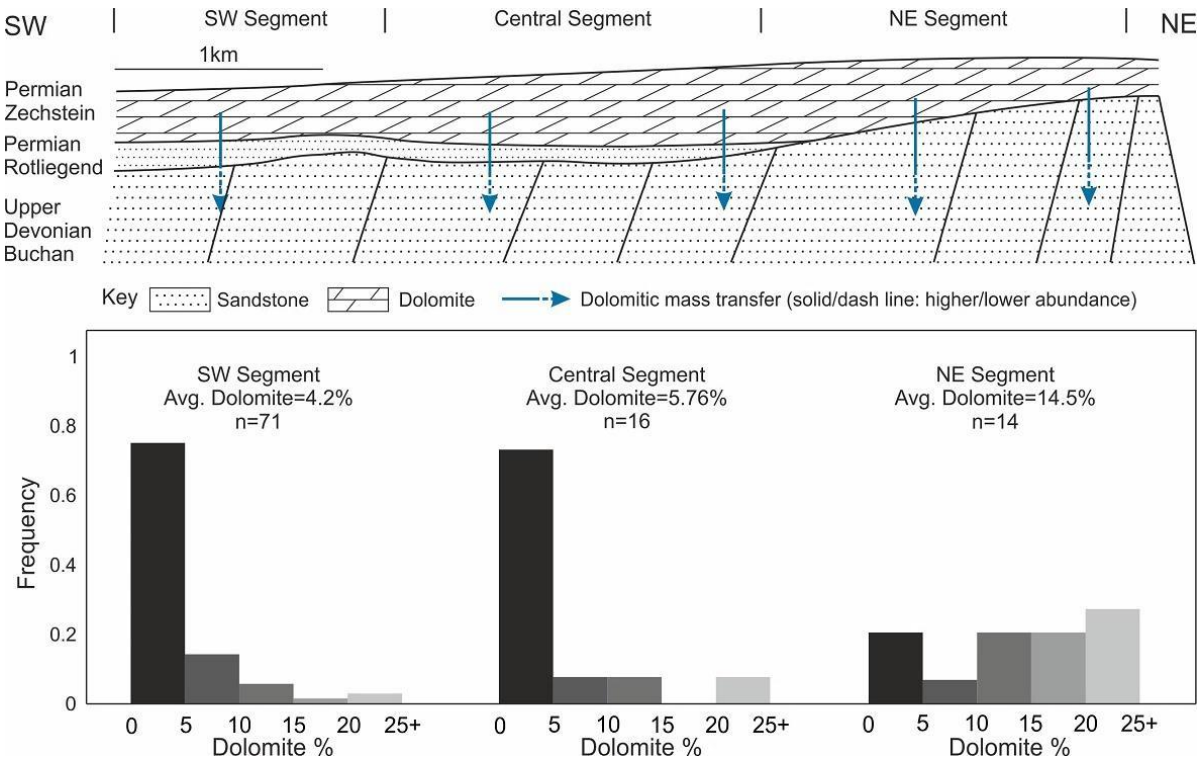

Figure 6.9 Sketched map showing dolomite precipitation from Zechstein and the statistics of the dolomite abundance in three segments. Note the vertical thickness is not for scale.

Although there were several major marine incursions in the study area during Carboniferous, Late Permian, Late Triassic, Cretaceous, Palaeogene and Quaternary age (Bradshaw et al., 1992), this study proposes that the overlying Late Permian Zechstein carbonates would be the most likely source of carbonate cements. A number of comparable cases were reported in the Southern North Sea, the dolomite cements (also some other evaporates) are prevalent in the underlying Permian Rotliegend sandstones, and were precipitated by percolating brines originating directly from the overlying Permian Zechstein carbonates (e.g. Pye and Krinsley, 1986; Glennie and Provan, 1990; Purvis, 1992). It is proposed that this situation would also have occurred in the Ardmore Field. The Upper Devonian Buchan Formation sandstones, Permian Rotliegend sandstones and Permian Zechstein carbonates jointly form the reservoir, and they were all charged with oil by the stratigraphically younger Jurassic Kimmeridge Clay (Gluyas et al., 2005). This would imply that these three units are in fluid communication. Across the field, the Rotliegend sandstones vary in thickness. It is thicker (around 20 m) in the southwest and centre of the field and thins to the far NE pinching out onto what were pre-Permian (Devonian) topographic highs during deposition (**Figure 6.9**). Thus the Permian Zechstein carbonates directly overlie Buchan Formation over much of NE segment of the field. After the Zechstein marine incursion, the Mg^{2+}-rich marine water flowed downwards through the Rotliegend and entered Buchan Formation, displacing and mixing with the groundwater already present and precipitated dolomite in the interstices. The mixing of the marine and groundwater probably occurred by a combination of salinity/density differences and diffusion (Purvis, 1992). This explanation is strengthened by the distribution pattern of dolomite abundance in these three segments (**Figure 6.9**), the NE segment has the highest dolomite cements, while intermediate and minor dolomite cements are shown in the central and SW segments due to part of dolomite has been precipitated in the Permian Rotliegend (**Figure 6.9**). Within the Upper Devonian sequence, there is no clear relationship between abundance of dolomite

and the distance between samples and Devonian/Permian unconformity. This may be attributed to the presence of transmissive faults and fractures. Also, it is unlikely that the post-Permian meteoric water could have entered the Buchan Formation later, owing to the thick Zechstein sediments.

6.5.1.3 Illite/smectite (I/S)

The cornflake and honeycomb morphology with boxwork structure and curved edges is a good indicator implying that these I/S clay were transformed from smectitic precursors (e.g. Wilson and Pittman, 1977; Burley, 1984; Keller et al., 1986; Vitali et al., 1999; Wilson et al., 2014). Both the grain-coating and pore-filling I/S, though the average amount is around 5%, are the featured clay types in aeolian sandstones. There are several petrographic features can be characterized including: 1) The general occurrence at the grain contact areas; 2) Thicker I/S coating in the framework-grain depressions and rough surfaces, and 3) Thinner I/S coating in the non-depression and smooth areas (**Figure 6.10**). These features closely conform to the criteria set by Wilson and Pittman (1977) for recognizing mechanical infiltrated clays.

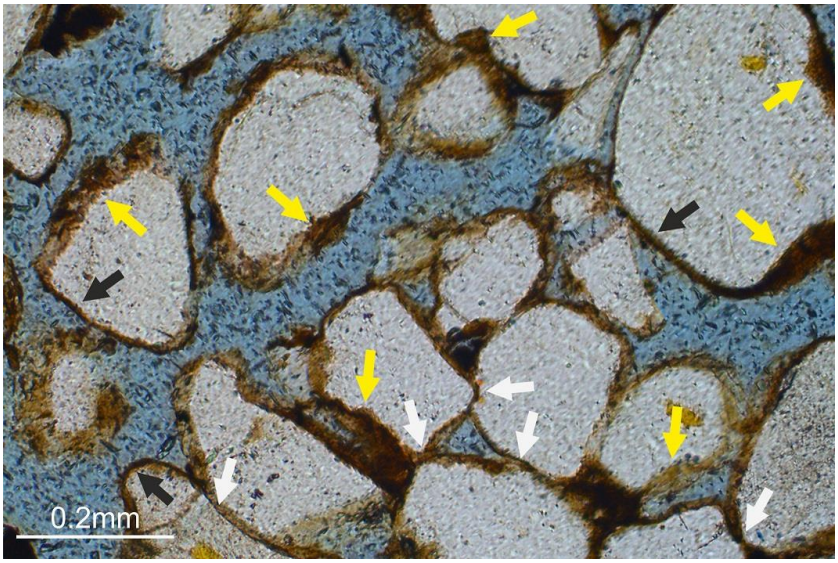

Figure 6.10 Photomicrograph showing I/S occurred at the grain contact areas (white arrows), thicker I/S coating in the framework-grain depressions and rough surfaces (yellow arrows), and thinner I/S coating in the non-depression and smooth areas (black arrows). Well 30/24-31, 3190.6 m.

In such a fluvial-aeolian mixed setting, especially during the aeolian-dominated period, the fluvial system retreated and only distal sectors of fluvial distributary system could affect the study area (e.g. sheet flood and floodplain). Additionally, the smectitic clays are usually extremely fine grained and therefore could be carried further than other sediment grains (McKinley et al., 2003). This observation is supported by the XRD analysis where smectite (shown in illite/smectite) only occurs as trace amounts in the fluvial channel samples (**Table. 6.1**).

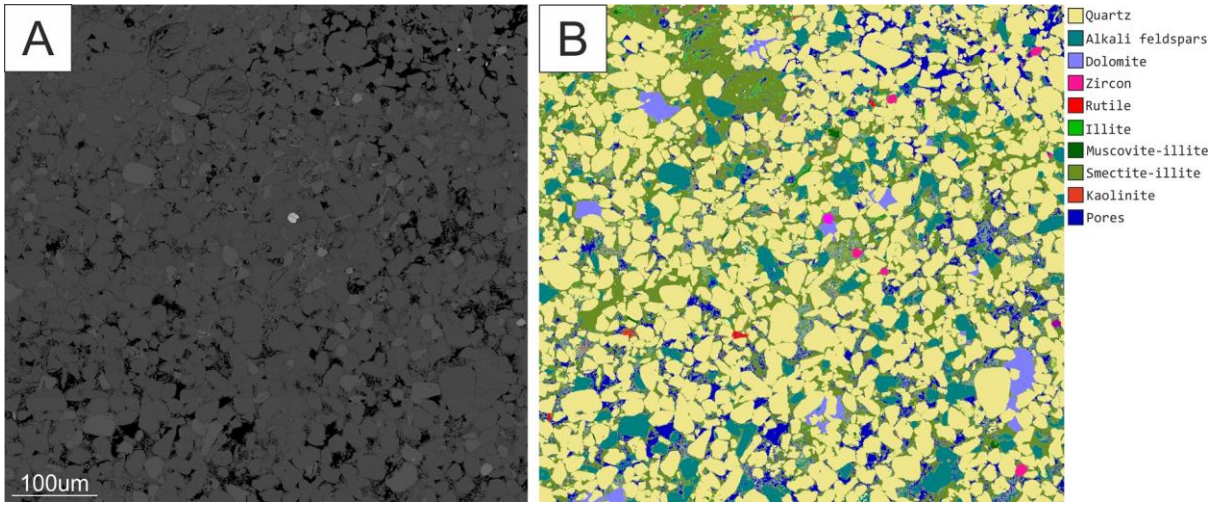

Figure 6.11 The BSEM (A) and QEMSCAN (B) images of a sheet flood deposits; this silty sample contains a higher concentrated illite/smectite which mainly presented as the pore-filling aggregates. Sample from well 30/24-05, 3163.5 m.

The most likely source of smectite is the fluvial-origin clay-bearing waters which represent the sheet flood and/or flood plain deposits. In the aeolian dominated period, these sediments could be accumulated in the interdune and/or desert lake environments. The dune sands were dry, porous and permeable shortly after deposition, this clay-bearing water could easily move into grain interstices by downward or lateral migration and form grain coating and pore filling clay aggregates before compaction. This interpretation can be reinforced by the QEMSCAN technique undertaken on a sheet flood siltstone sample (**Figure 6.11**), which contains

higher concentrated illite/smectite content (15.5%) and mainly presents as the pore-filling aggregates.

6.5.2 Paragenesis and burial history

The relative sequence of the major diagenetic events of the Buchan Formation sandstones in the Ardmore Field can be determined from thin sections and SEM observations based on the textural relationships. With the constraints set by the clay mineral XRD analysis, calculated temperatures from isotopic composition of dolomite cements, homogenization temperature of fluid inclusions in the quartz overgrowths, and the thermal conditions of Ardmore exploration well, a joint paragenesis-burial-thermal history can be generated (**Figure 6.12**).

In summary, before mechanical compaction, the earliest event was the infiltration of clay which only occurred in the aeolian sandstones. The dominant eogenetic processes in both fluvial and aeolian sandstones were compaction and dolomite cementation. The burial curves show that the Upper Devonian intervals were consistently at shallow burial depth (< 1 km) until Palaeogene and then rapidly buried to today's maximum depth around 2.7 km to 3.2 km. The subsequent mesogenetic events mainly occurred since the Palaeogene and include: 1) For the aeolian sandstones, compaction continuously reduced porosity with the increasing depth. Illitization might be the final event in the aeolian sandstones. This is supported by the XRD analysis: there are 70% – 80% of illite within I/S which are in ordered interstratification (R1 order) and this usually indicates the temperature is greater than 100°C (Hoffman and Hower, 1979; Huang et al., 1993); and 2) For the fluvial sandstones, it is not easy to determine the accurate sequence of the quartz pressure dissolution and feldspar dissolution/authigenic kaolinite generation. As the most possible source of silica, these processes are certainly prior to the quartz overgrowths which occurred in a formation temperature range of 80°C to 120°C. The dissolution of feldspar can provide considerable amounts of potassium, and the higher temperature conditions corresponded with increasing burial depth. The illitization of the flu-

vial sandstones is likely to occur in the late burial-diagenetic history and can usually be regarded as an indicator of formation temperatures greater than 100°C (Bjørlykke et al., 1986; Ehrenberg and Nadeau, 1989; Bjorkum et al., 1993).

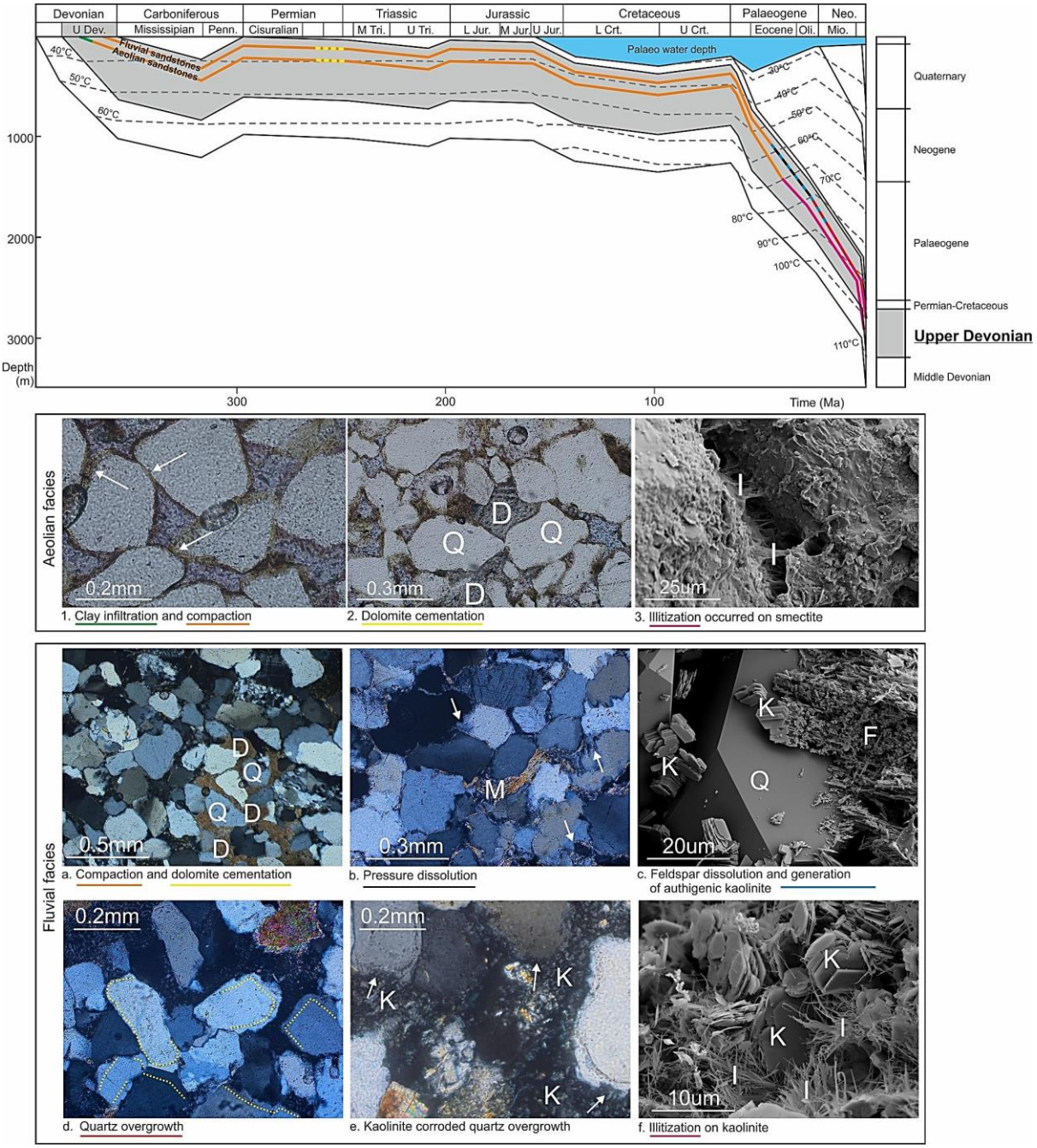

Figure 6.12 Paragenesis-burial-thermal history of Upper Devonian Buchan Sandstone in Ardmore Field with corresponded petrographic evidences.

Q-quartz; D-dolomite; M-mica; F-feldspar; K-kaolinite; I-illite.

6.5.3 Facies and diagenetic controls on reservoir quality

The porosity versus permeability diagrams show that aeolian sandstones generally have a better reservoir quality than fluvial sandstones (**Figure 6.13A**). This is partly due to the higher compositional and textural maturity of aeolian deposits, while the fluvial deposits are poorly to moderately-sorted, sub-angular to sub-rounded and contain abundant ductile rock fragments. Within each facies, the inter-granular porosity of most fluvial channel samples range between 10% and 20% with a mean value 15.1%. While other non-channel deposits, such as sheet flood and overbank, have lower porosity ranged from 0.1% to 15%, and most of them are less than 10% (**Figure 6.13B**). It is also noticed that the reservoir quality is closely correlatable to the lithology variations: channel sandstones which are close to the channel/non channel interface (< 2 m) contain more rock fragments (**Figure 6.14A**) and show less porosity (**Figure 6.14B**). While the channel sandstones which have a considerable distance to the channel/non-channel interface (> 2 m) commonly possess better reservoir quality (**Figure 6.14**). Within aeolian facies, the dune deposits possess an excellent reservoir quality. Nearly all the dune sandstone samples have porosity greater than 15% (**Figure 6.13C**). However, the reservoir properties of each sub-facies still show considerable heterogeneity, this heterogeneity is suggested to be induced by the subsequent diagenetic processes, which resulted in various diagenetic alterations that controlled reservoir quality (Salem et al., 2005).

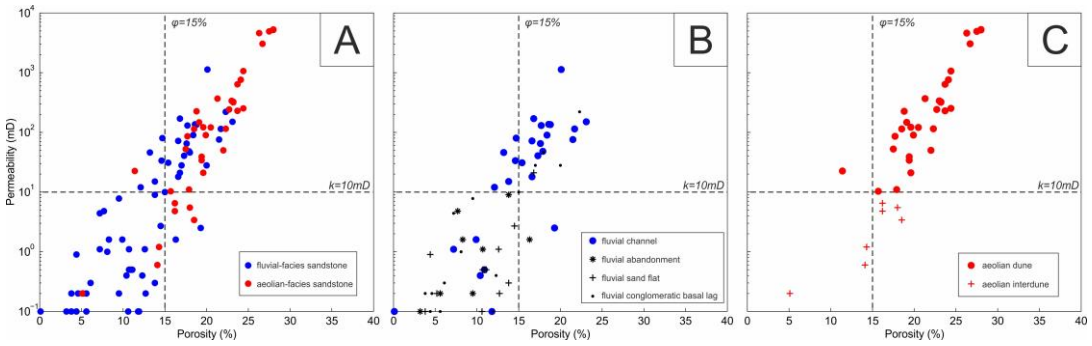

Figure 6.13 Porosity-permeability diagrams of: (A) all samples; (B) fluvial-associated samples; and (C) aeolian-associated samples. Note that porosity = 15% and permeability = 10 mD are set as the lower limit of an effective reservoir.

Compaction and cementation are two main processes reducing reservoir quality during burial diagenesis (Houseknecht, 1987; Ehrenberg, 1989; Gluyas and Cade, 1997). The relative importance of compaction and cementation on porosity reduction can be quantified using 'measured intergranular porosity-intergranular volume-total cements' diagram. This diagram can be used to evaluate which diagenetic processes have been most influential to porosity reduction (Houseknecht, 1987). For this study, the intergranular volume-cement diagram in **Figure 6.15** shows Buchan Formation data, the total cements include authigenic kaolinite, illite, illite/smectite, dolomite and quartz overgrowth, and the initial porosity is set as 40%.

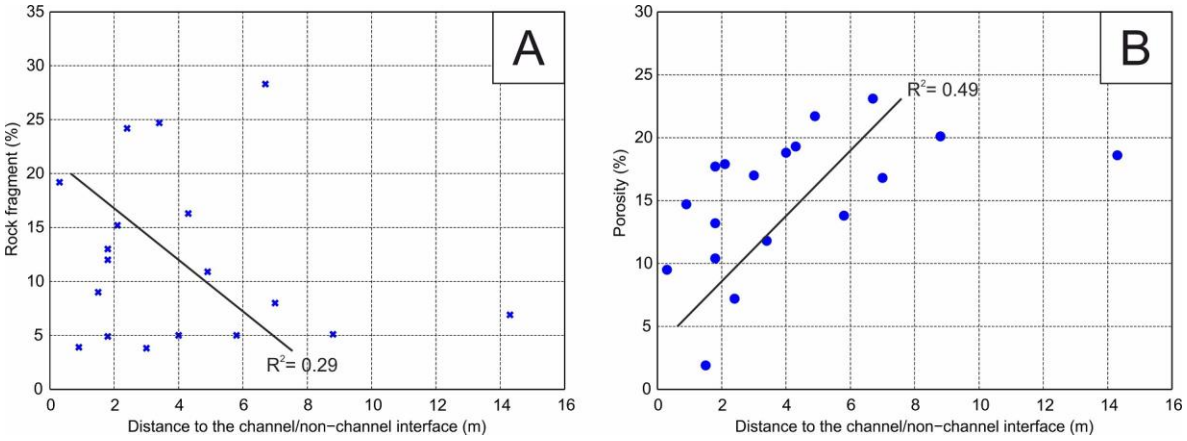

Figure 6.14 The diagrams showing relationships: (A) sample point distance to the channel/non channel interface and amount of rock fragment; and (B) sample point distance to the channel/non channel interface and porosity.

Compaction exerted a similar average reduction of porosity in both facies sandstones. The mean value 30.97% and 33.18% of the initial porosity has been decreased by compaction in fluvial and aeolian facies, respectively **(Figure 6.15**). However, evidence from petrographic observations reveal that the fluvial sandstones have undergone highly various degrees of compaction from moderate to intense (1.5% to 80.75% of the original porosity has been destroyed by compaction, **Figure 6.15A**). This is supported from the presence of long and concavo-convex grain contacts in the fluvial sandstones. The aeolian sandstones have only experienced a low to moderate compaction (11.25% to 51.5% of the original porosity has been

destroyed by compaction, **Figure 6.15B**), as they commonly display point to long grain contacts.

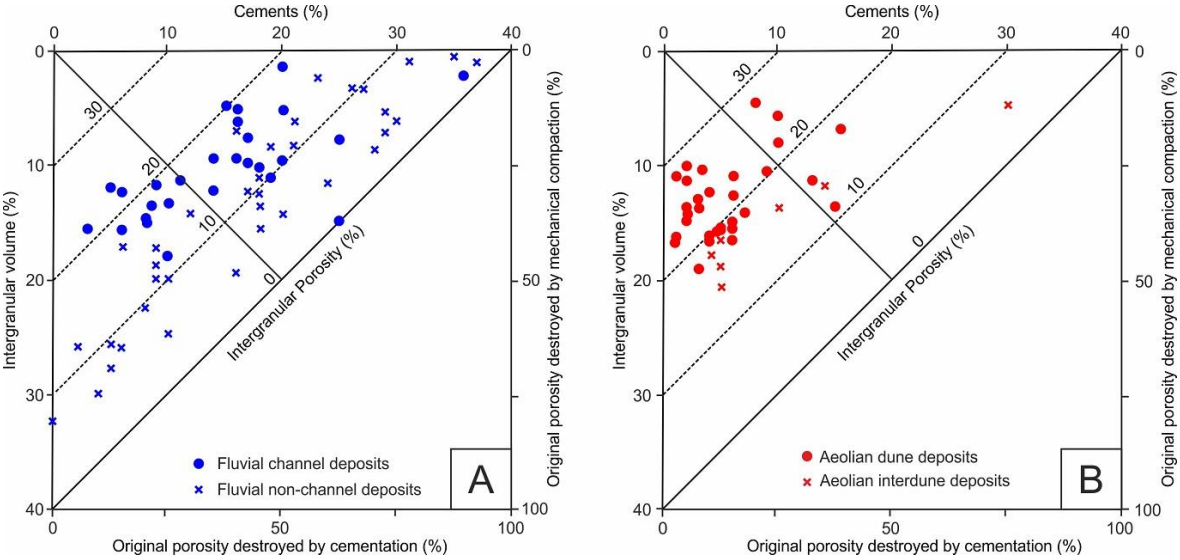

Figure 6.15 Intergranular volumes versus cement with the importance of compaction/cementation on reducing porosity in different Buchan Sandstone facies. (A) Fluvial-associated samples; and (B) Aeolian-associated samples.

Cementation clearly shows different development in fluvial and aeolian sandstones. Tang et al. (2017b) have reported that the primary porosity of aeolian sandstones has been preserved by the early mechanical infiltration of grain coating illite/smectite, which has inhibited quartz overgrowth development. The calculated results suggest that in the aeolian sandstones, there were only 13% and 26% porosity reduction of dune and interdune facies respectively by cementation (**Figure 6.15B**). In comparison, the dolomite cements, authigenic kaolinite and quartz overgrowth in the fluvial sandstones have significantly occupied the pore space. The fluvial channel and non-channel deposits have undergone 36.4% and 42.9% of the original porosity loss by cementation, respectively (**Figure 6.15A**).

Compaction and cementation have exerted the major porosity loss in the Buchan Formation sandstone reservoirs. Aeolian sandstones maintained a better reservoir quality due to the higher compositional and textural maturity, this would be helpful on keeping primary porosi-

ty from mechanical compaction. Additionally, with the absence of abundant kaolinite aggregates and the presence of grain coating illite/smectite which has effectively prevented quartz overgrowth, only sparse dolomite cements have a subordinate effect on reducing porosity. For the fluvial sandstones, lower grain maturity and extensive cementation have significantly reduced porosity. The fluvial intervals with relatively good reservoir quality are mainly composed of the channel sand packages that tended to be insolation from other channel facies.

6.6 Conclusions

This research of the Upper Devonian Buchan Formation has investigated the source of various cements, reconstructed the sequence of diagenetic events, and evaluated their effects on reservoir quality by using diagenetic and geochemical methods. Mechanical compaction exerted similar porosity loss on both aeolian and fluvial sandstones. However, cementation of various authigenic minerals shows contrasting differences. Dolomite cementation is prevalent in both sandstone facies: the stable isotope analysis suggested a major marine carbon source and the precipitation at a shallow burial depth. The overlying Upper Permian Zechstein carbonate is suggested as the most probable source. The aeolian sandstones contain grain coating clays that have restricted quartz overgrowth development. Conversely, the fluvial sandstones suffered higher degrees of porosity loss from quartz cementation due to the lack of grain coating clays. The extensive quartz overgrowths in the fluvial sandstones probably originated from feldspar kaolinitization and pressure dissolution. The homogenization temperature of fluid inclusions (80°C – 120°C) between the quartz overgrowths and host grains indicates this process occurred at a relatively late stage of burial. Illitization occurred in both aeolian and fluvial sandstones and was suggested to be the last diagenetic event.

This research has important implications for the hydrocarbon exploration of mixed fluvial – aeolian reservoir sandstones where there can be considerable variations in reservoir quality

controlled primarily by early grain coating clays. The results highlight the immense potential for exploration in Devonian mixed fluvial-aeolian reservoirs of mature hydrocarbon provenances such as the Central and Northern North Sea.

Acknowledgements

The author thanks Enquest PLC for supporting this research through access to the internal data and financial support of analytical work; BGS (British Geological Survey) for its assistance in facilitating the examination of Devonian cores. We are all grateful for the expertise and general assistance offered by Ian Chaplin (Department of Earth Sciences, Durham University); and the assistance on preparing isotopic samples from Dr Geoff Nowell (Department of Earth Sciences, Durham University). Thanks too are given to Adrian Boyce of SUERC for undertaking the isotope analysis and Jenny Omma of Rocktype for undertaking the QEM-SCAN analysis.

Table 6.1 XRD data for < 2 µm size mineral fraction from selected samples.

Well	Depth (m)	Wt.%	Illite/smectite				Illite			Kaolinite			Chlorite			Quartz		Calcite		Dolomite	
		<2um	% A	% B	Order	% Illite	% A	% B	Crys	% A	% B	Crys	% A	% B	Crys	% A	% B	% A	% B	% A	% B
30/24-28	2790.14	1.9	34.4	0.7	O	70-80	58.3	1.1	P	0.0	0.0	-	7.1	0.1	P	0.3	0.1	0.0	0.0	0.0	0.0
30/24-28	2829.76	3.0	46.3	1.4	O	70-80	25.9	0.8	P	22.6	0.7	M	2.9	0.1	M	2.4	0.1	0.0	0.0	0.0	0.0
30/24-28	2844.09	3.0	50.5	1.5	O	70-80	32.7	1.0	P	7.5	0.2	M	3.5	0.1	M	5.8	0.2	0.0	0.0	0.0	0.0
30/24-31	3190.34	2.0	44.8	0.9	O	70-80	34.9	0.7	P	10.7	0.2	M	5.1	0.1	P	4.5	0.1	0.0	0.0	0.0	0.0
30/24-18	2794.71	3.3	TR	TR	-	-	22.0	0.7	P	58.7	1.9	M	15.8	0.5	M	3.6	0.1	0.0	0.0	0.0	0.0
30/24-05	2849.27	3.2	TR	TR	-	-	8.5	0.3	P	72.6	2.3	M	5.3	0.2	P	3.1	0.1	0.0	0.0	10.6	0.3

A = Weight% relevant size fraction; B = Weight% bulk sample;
Mixed-layer Ordering: RI= Randomly Interstratified (R0); O = Ordered Interstratification (R1); LR = Long-range Ordering (R3);
Crystallinity: VW = Very Well Crystallised; W = Well Crystallised; M = Moderately Crystallised; P = Poorly Crystallised.

Table 6.2 Thermometry data of fluid inclusions in Buchan Formation sandstone samples from Ardmore Field. T_h-Homogenization temperature

Sample		Type	Distribution	Shape of FI	Gas/Liquid ratio	Homogenization phase	Th (°C)		Salinity (wt.% NaCl)
Well	**Depth (m)**						**Type I**	**Type II**	
30/24-05	2840.1	Brine	Belt	Regular	≤ 5%	Liquid	117-130	83	6.88
	2844.7	Brine	Belt	Regular	≤ 5%	Liquid	110-135	97	12.68
	2846.5	Brine	Belt	Regular	≤ 5%	Liquid	109-131	87	11.61
	2846.8	Brine	Belt	Regular	≤ 5%	Liquid	109-149	101	10.62
		Brine	Belt	Regular	≤ 5%	Liquid		92	11.58
		Brine	Belt	Regular	≤ 5%	Liquid		93	4.8
		Brine	Belt	Regular	≤ 5%	Liquid		121	2.74
	2848.1	Brine	Belt	Regular	≤ 5%	Liquid	109-141	118	8.35
		Brine	Belt	Regular	≤ 5%	Liquid		94	2.74
	2849.6	Brine	Belt	Regular	≤ 5%	Liquid	114-146	123	4.96
		Brine	Belt	Regular	≤ 5%	Liquid		87	11.61
	2850.8	Brine	Belt	Regular	≤ 5%	Liquid	118-146	103	3.87
30/24-28	2795.0	Brine	Belt	Regular	≤ 5%	Liquid	112-137	91	11.05
30/24-34	2903.8	Brine	Belt	Regular	≤ 5%	Liquid	111-117	94	8.19
	2903.8	Brine	Belt	Regular	≤ 5%	Liquid		117	2.74
	2933.9	Brine	Belt	Regular	≤ 5%	Liquid	112-157	118	3.55

Table 6.3 Stable isotopic data and calculated formation temperature of dolomite cements in the Buchan Sandstone samples

Well	Depth (m)	Carbonate cement type	Carbonate cement%	$\delta^{18}O_{PDB}$ (‰)	$\delta^{13}C_{PDB}$ (‰)	$\delta^{18}O_{SMOW}$ (Calculated, ‰)	Temp (°C) $\delta^{18}O_{SMOW}$ = 0‰
30/24-03	2692.0	dolomite	20	0.5	0.0	31.4	24.0
30/24-03	2692.3	dolomite	5	0.6	1.0	31.5	23.5
30/24-03	2697.8	dolomite	10	-0.1	1.2	30.8	26.6
30/24-05	2844.7	dolomite	20	-1.0	-2.4	29.9	30.8
30/24-05	2846.5	dolomite	3	-2.4	-2.6	28.4	37.7
30/24-05	2848.1	dolomite	10	-2.7	-3.0	28.1	39.2
30/24-05	2849.3	dolomite	10	-0.8	-2.4	30.1	29.9
30/24-05	2850.2	dolomite	20	-1.3	-3.1	29.6	32.2
30/24-05	2850.8	dolomite	10	-0.7	-2.1	30.2	29.4
30/24-18	2797.8	dolomite	40	-1.7	-0.1	29.2	34.2
30/24-18	2798.4	dolomite	15	-0.5	-0.3	30.4	28.5
30/24-20z	3120.8	dolomite	7	-2.1	-1.5	28.8	35.9
30/24-20z	3129.9	dolomite	5	-2.1	-2.3	28.8	36.1
30/24-20z	3131.2	dolomite	10	0.8	-2.1	31.7	22.8
30/24-20z	3174.5	dolomite	5	-6.0	-2.9	24.7	57.6
30/24-28	2795.0	dolomite	10	-0.9	1.6	30.0	30.2
30/24-34	2903.8	dolomite	10	-1.7	0.6	29.2	34.2

Note: the calculated $\delta^{18}O_{SMOW}$ (‰) is derived from $\delta^{18}O_{PDB}$ (‰) by the equation: $\delta^{18}O_{SMOW} = 1.03091 \times \delta^{18}O_{PDB} + 30.91$ (Coplen, 1983); the equations used for fractionation between carbonates and water are: $1000 \times \ln\alpha$ dolomite/ankerite-water $= 3.06 \times 10^6/T^2 - 3.24$ (Matthews and Katz, 1977), T is in Kelvin unit.

CHAPTER 7: THE ALMA FIELD (FORMERLY ARGYLL/ARDMORE), BLOCKS 30/24 & 30/25A, UK NORTH SEA – A REVIEW

---

*This chapter has been accepted by the **Geological Society of London** and will be published in the **GSL Memoir Book 'United Kingdom Oil and Gas Fields 50 Years Commemorative Atlas'.***

Chapter outline

Summary

The Alma Field (initial name was Argyll from 1975 – 1992 and then Ardmore from 2003 – 2005) is located within Block 30/24 (one well in 30/25a flowed oil on test but was not put on production) in the UK North Sea, on the western margin of the Central Graben. The block was awarded in 1969 to a Hamilton operated partnership, and the first discovery well 30/24-1 was drilled in 1969. A converted semi-submersible drill rig (Transworld 58) was installed in 1975 and oil production started up the following year. The 2D and 3D seismic surveys were shot over the field in 1980 and 1991, respectively. Oil was produced from four reservoirs: Devonian Buchan Formation sandstones, Permian Rotliegend sandstones, Zechstein carbonates and minor production from Jurassic sandstones until the October 1992 when the field was abandoned for economic reasons. In 2002, Tuscan Energy and Acorn Oil & Gas were awarded the licence to redevelop the Argyll Field and they renamed it as Ardmore since on abandonment and return of the licence to the UK government Argyll had ceased to exist from a legal perspective. The first Ardmore well was drilled in 2003 and oil flowed in again in September 2003. A further 5 million barrels were produced at high rate before commercial considerations once again forced abandonment despite the technical success. In 2013, the licence was once again issued to EnQuest; the company renamed it as Alma and drilled 6 new high angle wells. First oil from the Alma development was achieved in October 2015 and the field is currently producing oil.

Commercial hydrocarbons mainly occur in reservoirs ranging in age from Late Devonian to Late Jurassic together with untested oil in parts of the Cretaceous Chalk. Total ultimate recovery for all reservoirs in the field is expected to be about 100 million barrels of oil (MMBBL). As of end 2005, the field had produced 77.6 MMBBL. A further 3.8 million barrels has been produced from the Alma Field to April 2017 (includes about 0.5 MMBBL from a long reach well drilled into the Duncan/Galia Field immediately west of Alma).

The field has been described previously by Bifani and Smith (1985), Robson (1991), Heward et al. (2003), Gluyas et al. (2005) and Gluyas et al. (2018). This review of the Alma Field includes new information on the volumetrically largest reservoir, the Upper Devonian Buchan Formation sandstones. Research conducted on the facies and reservoir quality of these Devonian Buchan Formation sandstones has been added to update the previous field descriptions. The research has allowed a better understanding of the Devonian reservoir, its distribution and properties.

The aim of this paper is to describe the geology, development and production history of the Argyll Field in UK Blocks 30/24 and 30/25a (**Figure. 7.1**). Argyll is unique. Not only was it the first field to be produced for oil in the North Sea, it also has a peculiar history insofar as the field has been developed on three separate occasions by completely different partnership and it has been twice abandoned, ceasing to exist from a legal perspective. It is thus the only field in the UK North Sea which as existed as three legal entities: first it was Argyll (production 1976 – 1992), then Ardmore (production 2003 – 2005) and now Alma (production from 2015). The understanding of the field has been dramatically changed since it was first discovered.

7.1 History

The development of Block 30/24 started in 1969 under Licence P.073 issued in 1965. The first well (30/24-1) of Argyll discovery was drilled for a Tertiary target. The Tertiary was dry (reservoir absent) but the deeper Permian Zechstein had oil shows. A second well, 30/24-2, was drilled in 1971 and just 400 m SW of the 30/24-1, its target was an identified horst at Base Cretaceous. It found Zechstein and Devonian reservoirs and 4300 BOPD were produced from Zechstein carbonates after acidising. Three subsequent wells (30/24-3, 5 and 6) were drilled and also found oil in what were termed Zechstein and Rotliegend reservoirs. It was

several years later that much of the so-called Rotliegend interval proved to be Old Red Sandstone and hence Devonian.

Following an appraisal programme, the initial reserves estimate for the Argyll Field were 25 mmstb (Methven, 1993). In June 1975, a converted semi-submersible drill rig, the Transworld 58, was used to begin production from the Argyll Field. The initial production was all from Zechstein completions, though well 30/24-3 was completed as a Devonian producer.

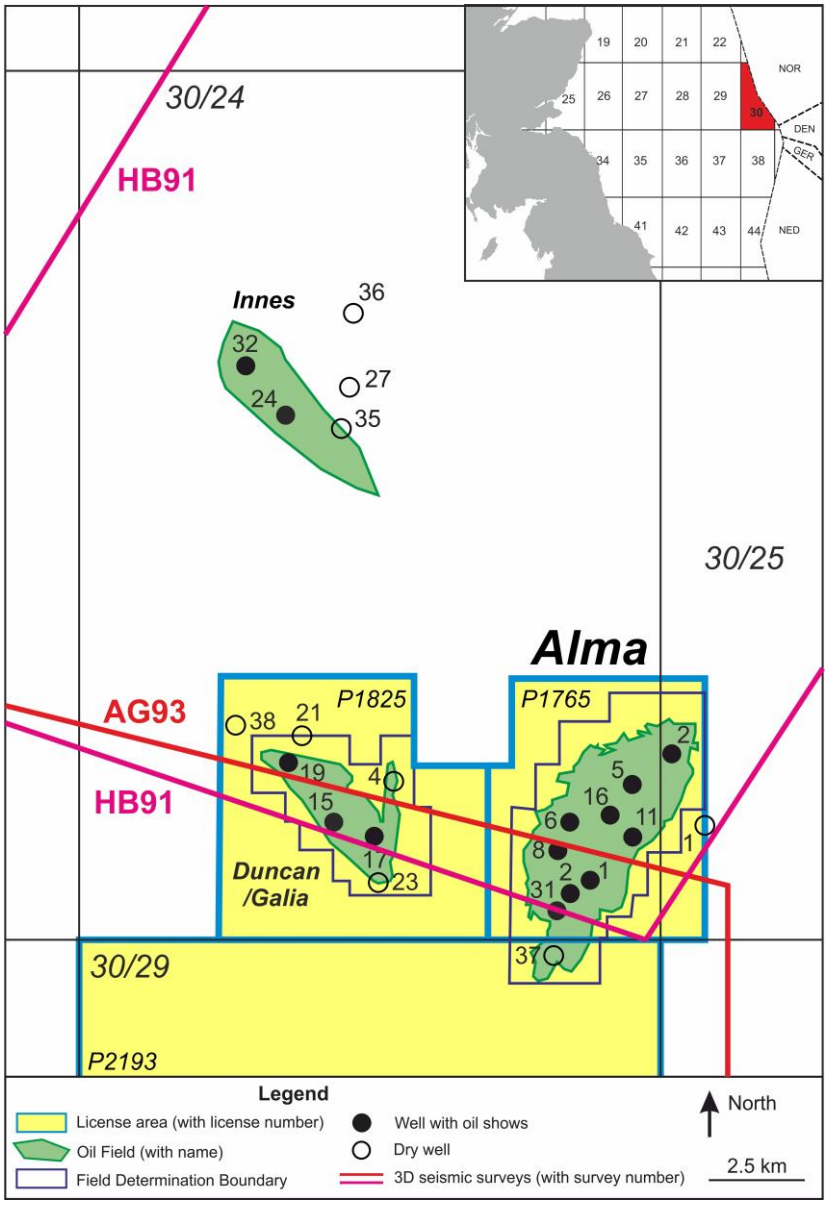

Figure 7.1 The location map of Alma Field.

Drilling on the Argyll Field continued until 1986. The process can be roughly divided into three stages: Zechstein development until 1979, Rotliegend development between 1979 and 1982, and finally Devonian development from 1983 onwards. Two wells, 30/24-6 and 30/24-8 produced small quantities of oil from Upper Jurassic marine sandstones found on the western flank of the field and likely connected with the Duncan (now Galia) Field immediately east of Argyll. The final well to be drilled during the Argyll phase was 30/24-39 in 1989. It targeted possible Jurassic sandstones on the southern flank of the field. The well found a thin and wet Jurassic sandstone package. A total of 23 wells were drilled in the field during this period.

From 1983 it became difficult to sustain production from natural flow. This was caused by falling reservoir pressure and increasing water cuts. The gas lift system helped maintain production, however as time went on it became increasingly difficult to start up wells after shutdowns. The problem was a lack of gas to start up the system.

Hamilton continued to pursue exploration prospects in the late 1980s; however they increasingly met with failure. In 1985 they drilled two wells elsewhere on the block (30/24-34 and 37) both of which tested oil at ~1000 BOPD, but neither was capable of sustaining flow without gas lift. In 1991 Hamilton shot a 3D seismic survey in Block 30/24, this survey was designed to look for other prospects in the area, though it did cover the northern part of the field. Argyll continued production until October 1992 then the field was abandoned.

In 2002, two new oil companies, Tuscan Energy and Acorn Oil & Gas were awarded the licence to redevelop Argyll Field and they renamed it as ‘Ardmore’. The first Ardmore well was drilled in the summer of 2003 and oil flowed in again in September 2003, a further 5 mil-

lion barrels were produced at high rate. The field was then abandoned again due to commercial considerations despite the technical success.

Ten years after cessation of production from Ardmore, the licence was once again issued to EnQuest. The company renamed it as 'Alma' and drilled 6 new high angle wells. First oil from the Alma development was achieved in October 2015; the estimated amount is c.26 MMBOE (million barrels of oil equivalent) of net 2P (proven and probable) reserves. Only 30% has so far been recovered from Alma STOIIP of 307 million barrels (EnQuest, 2015).

7.2 Structure, stratigraphy and trap

The Alma Field is located on the Argyll Ridge, a large SW-NE trending Palaeozoic-age tilted fault block on the south-western flank of the Central Graben. The field is a horst feature with the crest in the north and fault closure to the north-east (**Figures 7.2A and 7.2B**). A combination of dip and faulting defines the limits of the field on the north-west and south-east flanks, while dip closure defines the southern limits of the field. Truncation of the post Devonian reservoirs at the crest of the field also provides a potential trapping mechanism. As the Devonian does not act as a base seal, the trapping relies on the major NW-SE trending graben edge faults to the northeast of the field. The major NW-SE faults are pre-Permian in age.

7.2.1 Devonian

The Middle Devonian Kyle Limestone is the oldest strata penetrated in the Alma Field (**Figure. 7.2C**). The overlying Upper Devonian is assigned to Buchan Formation, where its base part is dated a late Givetian to early Frasnian age by palynological evidence (Gluyas et al., 2005). There is no palynological age control for upper part of Buchan Formation: the topmost part of Buchan Formation may extend to the earliest Carboniferous. The Buchan Formation has a dip at 7° – 10° to the SW, and thus the oldest stratigraphic units sub-crop in the NE with

progressively younger stratigraphic units sub-cropping the Base Permian Unconformity towards the SW. Eleven units (named as B01 to B11 from base to top) have been divided within the formation based on well logs utilizing laterally correlative shale beds (Gluyas et al., 2005). Deposition of the Buchan Formation occurred in a fluvial-aeolian mixed depositional setting (Tang et al., 2017a).

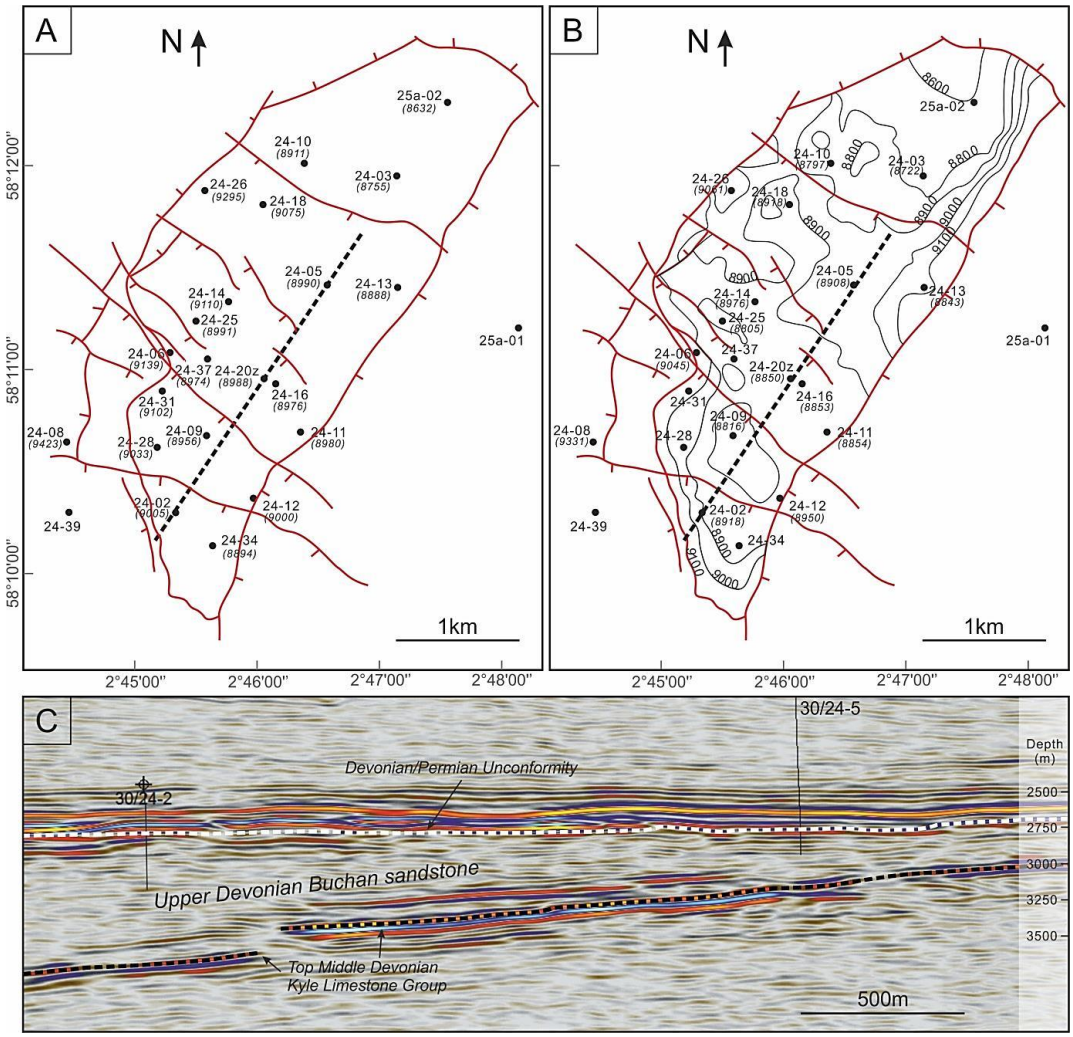

Figure 7.2 The structure contour maps and seismic profile of the Alma Field. (A): Top Upper Devonian depth structure; (B): Top Zechstein depth structure; and (C) The seismic image of the SW-NE dash line shown in Fig. 7.2A and 7.2B. Note the well names in Figs. 7.2A and 7.2B are associated with top depth of corresponding layers shown in feet.

At the top of the Devonian sequence is a major angular unconformity (the Hercynian unconformity) (**Figure. 7.2C**). The nature of this erosion and resulting palaeo-topography controls

the distribution of all later sediments. Therefore, Permian Rotliegend, Permian Zechstein and minor Cretaceous Chalk were all deposited onto the Devonian in different parts of the field. Regionally, the Devonian sequence can be divided into three segments (**Figure. 7.3**):

- The northeast segment: Cretaceous Chalk and Permian Zechstein overlie Devonian;
- The central segment: Permian Zechstein and thin Permian Rotliegend overlie Devonian;
- The southwest segment: thicker Permian Rotliegend overlies Devonian.

7.2.2 Permian Rotliegend and Zechstein

The Middle-Late Permian Rotliegend is assigned to Auk Sandstone, overlies the Devonian in the central and SW parts of the field (**Figure. 7.3**). The distribution of this unit is limited and its distribution controlled by local pre-Permian palaeo-topography. The Auk Sandstone consists of aeolian and fluvial sandstones. They are interpreted to have been deposited from southeasterly directed palaeo-winds and easterly flowed fluvial system. Locally an altered volcanic horizon occurs at the Devonian/Permian boundary. These rocks have been dated as Permian- Carboniferous in age, and it is likely that they are related to the thick sequences of volcanic which occur farther south (Robson, 1991).

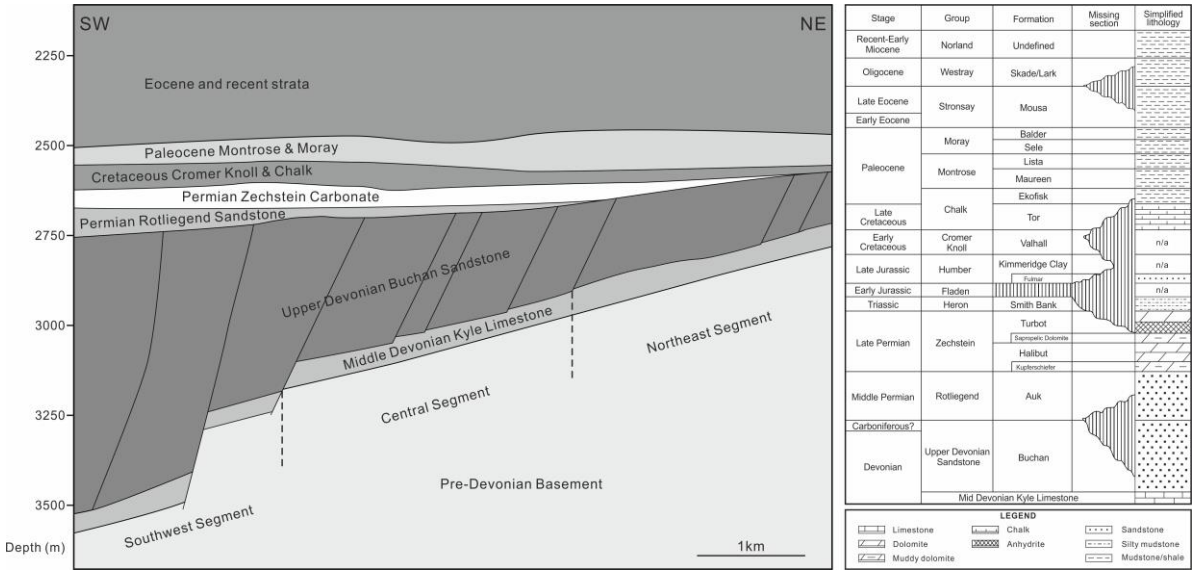

Figure 7.3 The sketched SW-NE cross section and general stratigraphy column of the Alma Field.

Late Permian Zechstein carbonates directly overlie the Rotliegend reservoir and can be further divided into four units from bottom to top: Kupferschiefer, Halibut Bank Formation, Sapropelic Dolomite and the Turbot Bank Formation (**Figure. 7.3**). The whole Zechstein interval in Alma is assigned to Z2, Z3 and Z4 subunits (Taylor, 1990a).

A thin Kupferschiefer marks the onset of the Zechstein transgression, with suggestions of the uppermost parts of the Rotliegend sequence was reworked by marine. Subsequent Zechstein carbonates conformably overlie the Kupferschiefer. These carbonate sediments are of a marginal marine facies and consist of a lower dolomitic horizon, assigned to the Halibut Bank Formation and an overlying sequence of anhydrite, dolomite and claystone assigned to the Turbot Bank Formation. An organic matter-rich dolomitic interval known as the Sapropelic Dolomite separates the upper and lower parts of the Zechstein interval (Robson, 1991).

7.2.3 Triassic Heron Group

The Smith Bank claystones (Triassic Heron Group) cover the Zechstein as continental conditions become established. These Triassic siltstones/claystones partly contribute as the seal on the Zechstein reservoir in the western fringe of the Alma Field (not shown in Figure 7.3).

7.2.4 Upper Jurassic

Major unconformities resulted in the absence of the Lower and Middle Jurassic in the Alma Field area, along with severe truncation of other post-Devonian sediments at the crest of the field. Thin Upper Jurassic shallow marine sandstones are present over the rest of the field and are equivalent to the Fulmar Formation sandstones as seen in the Fulmar Field 50 km to the NW (not shown in Figure. 7.3).

7.2.5 Cretaceous

The Lower Cretaceous Cromer Knoll Group sediment and Upper Cretaceous Chalk Group chalks blanket the Alma Field and provide an ultimate top seal for the hydrocarbon accumulation (**Figure. 7.3**).

7.2.6 Paleogene to recent strata

The Paleogene, Neogene and Quaternary strata in the Alma are thick (over 2000 m) are largely argillaceous and not considered to have any hydrocarbon potential.

7.3 Database

The three-stage development has made the well and core database comprehensive. A total of fifty-three wells have been drilled, thirty-two of them were cored.

Many 2D seismic lines across Block 30/24 are available. A 3D seismic survey was shot over the northern half of the Alma area in 1991 by BHP. An Agip 3D seismic survey covered the southern half of the field in 1993.

The authors of this paper have done extensive research on the Buchan Formation sandstone reservoirs of the Alma Field. This new information was not available for the previous publications on the field. The new information reported here includes data from one hundred and one petrographic thin sections, data from core chips examined using a scanning electron microscope, fluid inclusion micro-thermometry of quartz overgrowth, stable isotope data from dolomite cement and XRD analysis of clay minerals.

7.4 Reservoirs

Alma contains four reservoir units (Upper Devonian-Buchan, Permian-Rotliegend, Permian-Zechstein and Upper Jurassic). The former three units are in pressure and fluid communica-

tion, while the Upper Jurassic is independent (Gluyas et al., 2005). The 1D burial-thermal history (**Figure. 7.4**) indicates that the stratigraphic units between Devonian and Palaeocene were little buried until the Paleogene and contain many unconformities due to multiple episodes of tectonic uplift and erosion.

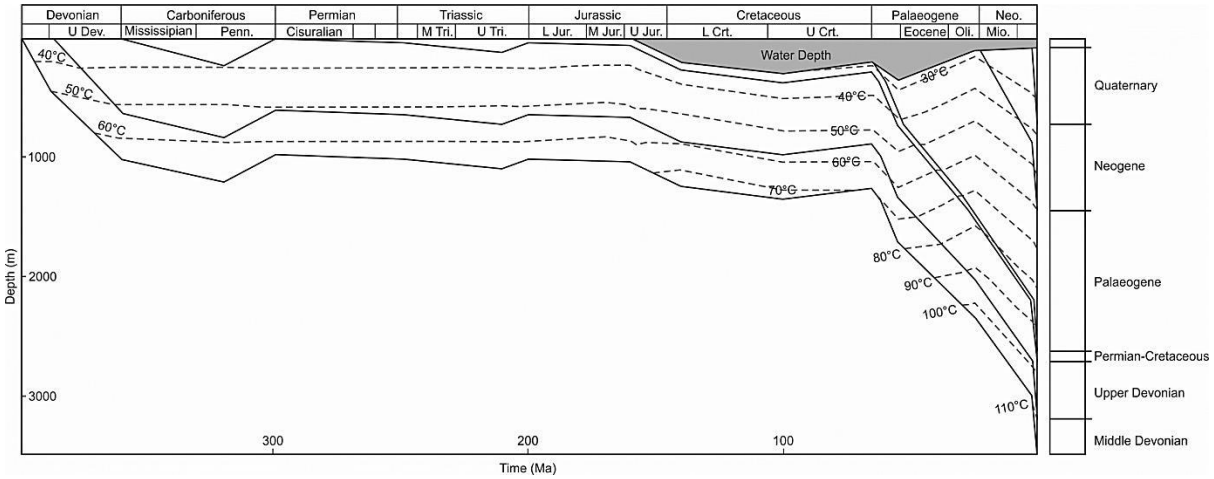

Figure 7.4 The 1D burial-thermal history of stratigraphic units in Alma Field.

7.4.1 Upper Devonian Buchan Formation

The Upper Devonian Buchan Formation comprises predominantly sandstones with minor siltstone, mudstones and conglomerates. The main deposition facies are braided-fluvial and aeolian sandstones. However, for units B01, B02, B03, B05 and B06 there is only very poor core coverage and hence uncertainty about the exact depositional environments in which their sediments formed. The remaining units vary in the dominant facies: fluvial (B04), aeolian (B07 and B08) and fluvial (B09, B10 and B11) representing a progradation-retreat-progradation cycle of the alluvial fan-based braided system with aeolian deposits occurred mainly between two main progradation periods (Tang et al., 2017a). Wells can be correlated by aeolian sand packages (**Figure. 7.8A**) but the correlations between fluvial intervals are difficult and may not be reliable.

The commonest sedimentary structures include: trough and planar cross bedding in fluvial sandstones (**Figures 7.5A and 7.5B**), and the large scale planar cross bedding with pin-stripe and discontinuous wavy lamination in aeolian sandstones (**Figures 7.5C and 7.5D**). Most of the sandstones are litharenite to sublitharenite with fine to medium grain size. Both compositional and textural maturities of aeolian sandstones are higher than fluvial sandstones.

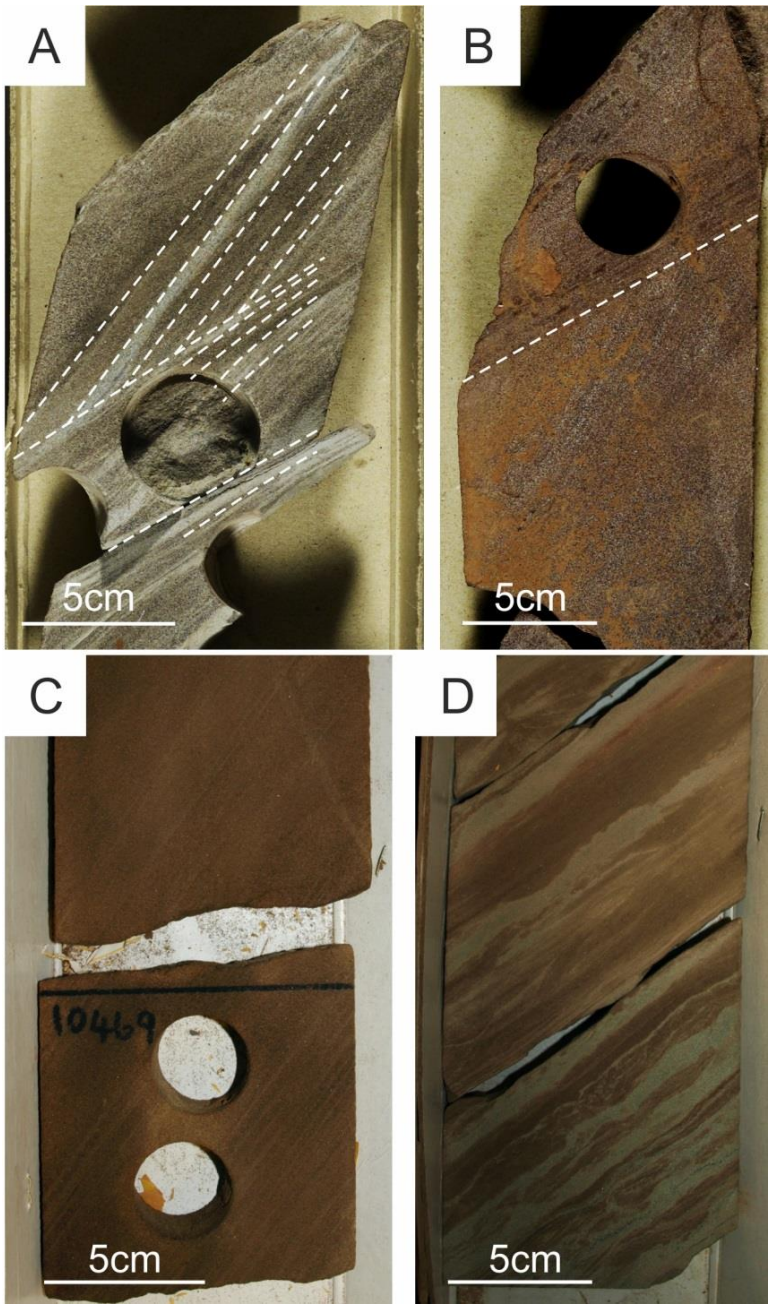

Figure 7.5 Typical core photos of Buchan Sandstone fluvial and aeolian deposits: (A): Trough cross-bedded, medium to fine sandstones, Well 30/24-20z, 3121.7 m; (B): Planar cross bedding, medium to

fine sandstones, Well 30/24-20z, 3172.7 m; (C): The oil-stained, medium-grained, pin-stripe aeolian dune sandstones, Well 30/24-31, 3191 m; and (D): The fine-medium grained sandstone with discontinuous wavy lamination. Well 30/24-31, 3183.8 m.

The braided channel and aeolian dune deposits mainly form the reservoir, while the facies with finer grain size, such as fluvial abandonment, overbank and aeolian interdune, are typically non-reservoir and form significant formation heterogeneity. The reservoir quality of fluvial reservoir sandstones is suffered from significant dolomite cementation and quartz overgrowth. While the early formed grain coating illite/smectite in the aeolian sandstones has effectively inhibited quartz overgrowth and the aeolian sandstones therefore have better reservoir quality than fluvial sands (Tang et al., 2017b).

The reservoir quality of Buchan Formation has a large range, porosity and permeability of fluvial and aeolian sandstones varied from 0.1% to 23.1% & 0.2 mD to 1240 mD and 5.1% to 28% & 0.2 mD to 5290 mD, respectively (**Figures 7.7A and 7.7B**).

7.4.2 Middle-late Permian Rotliegend

A more detailed description of the Rotliegend reservoir can be found in Heward et al. (2003). The Rotliegend deposition is confined to the SW and central areas of the field. The Rotliegend consists of good quality medium-grained dune slipface sands and coarse water-lain sands (Weissliegend unit) which were deposited on the denuded Devonian surface, the dune slipface sandstones are consolidated to poorly consolidated, and the cementation is limited (**Figure. 7.6A**). The coarse water-lain sandstones contain conglomeratic quartz pebbles with sandy-supported matrix (**Figure. 7.6B**). The sands dominated by wind ripple laminated facies are relatively tight and have characteristically high water saturations. These differences can be picked out in core or on the sonic log. Occasionally the wind ripple laminated facies can be seen as potential barriers to flow. Porosity and permeability ranges from 18% – 25%

and 10 milli-Darcies and up to 10 Darcies (**Figure. 7.7C**). Net to gross is from 70% – 98%, and the sandstones can be well correlated between selected wells (**Figure. 7.8B**).

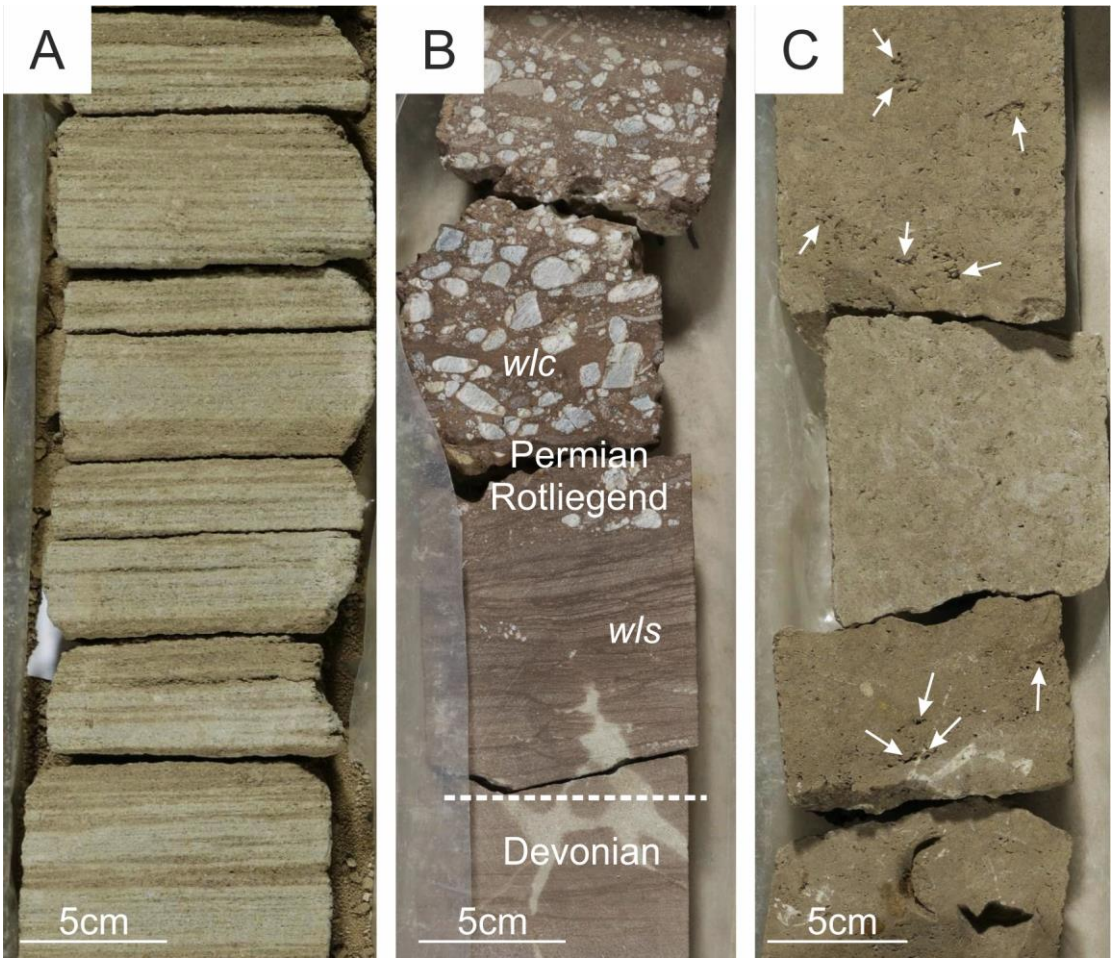

Figure 7.6 Typical core photos of Permian examples: (A): Permian Rotliegend aeolian sandstone, Well 30/24-18, 2780.7 m; (B) Permian Rotliegend waterlain conglomeratic sandstone, Well 30/24-18, 2788.9m; and (C) Zechstein dolomite with visible vugs (white arrows), Well 30/24-18, 2751.4 m.

7.4.3 Late Permian Zechstein

A comprehensive description of Zechstein dolomite reservoir are made by Bifani and Smith (1985), Gluyas et al. (2005) and Gluyas et al. (2018). The Zechstein here is subdivided into three cycles, the Halibut Bank Formation (Z2) and the Turbot Bank Formation (Z4) separated by the easily correlatable Sapropelic Dolomite (Z3) (**Figure. 7.8C**). The reservoir possesses a dual porosity system of large pores visible to naked eyes (**Figure. 7.6C**) and microscopic-scale pores. The large pores include tectonic-origin fractures and dissolved vugs, the vugs are

100 µm to 5 mm in diameter (**Figure. 7.6C**). The Lower Halibut Bank is a calcite cemented dolomite and generally exhibits poorer reservoir qualities than the Upper Turbot Bank Formation. This is overlain by an organic rich dolomite interval, the Sapropelic Dolomite which could act as a vertical permeability barrier. The better quality Upper Turbot Bank Formation consists of interbedded anhydrites, clays and dolomite. The dolomite has undergone extreme karstification resulting in vuggy porosity and collapse breccias. Porosity and permeability are poorly correlated, a typical porosity ranges from 5% – 20% but the permeability ranges from hundreds milli-Darcies and up to 1 Darcy which is locally enhanced by vugs and fractures.

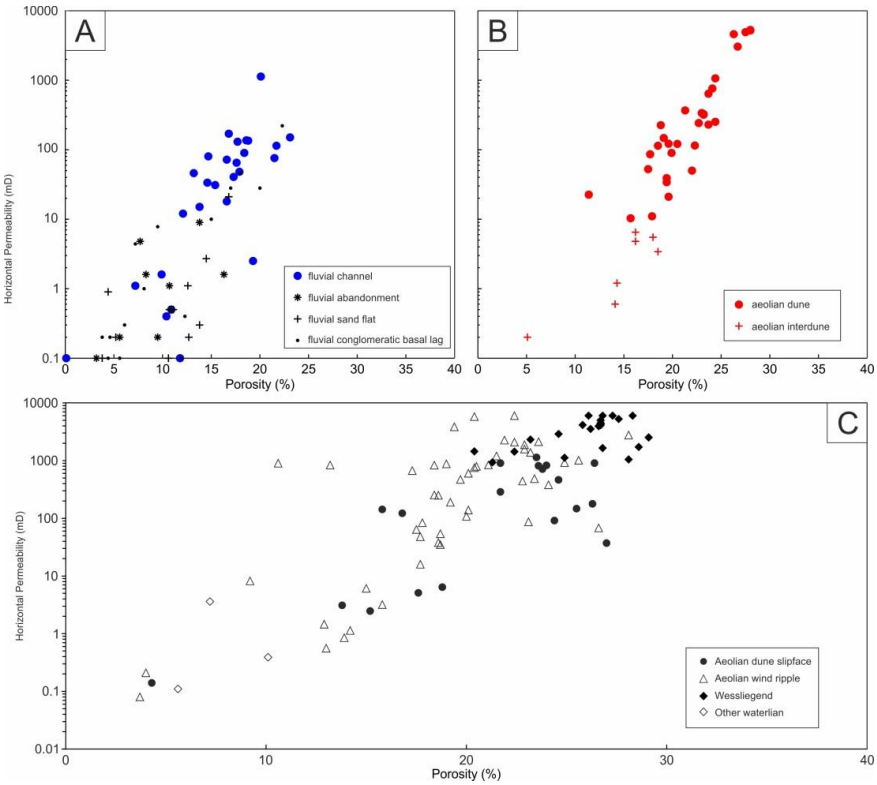

Figure 7.7 The porosity and permeability crossplots of (A): Fluvial samples of Buchan Sandstone reservoir; (B): Aeolian samples of Buchan Sandstone reservoir; and (C) Rotliegend Auk Formation reservoir.

Figure 7.8 The well correlations of three main reservoirs among selected wells

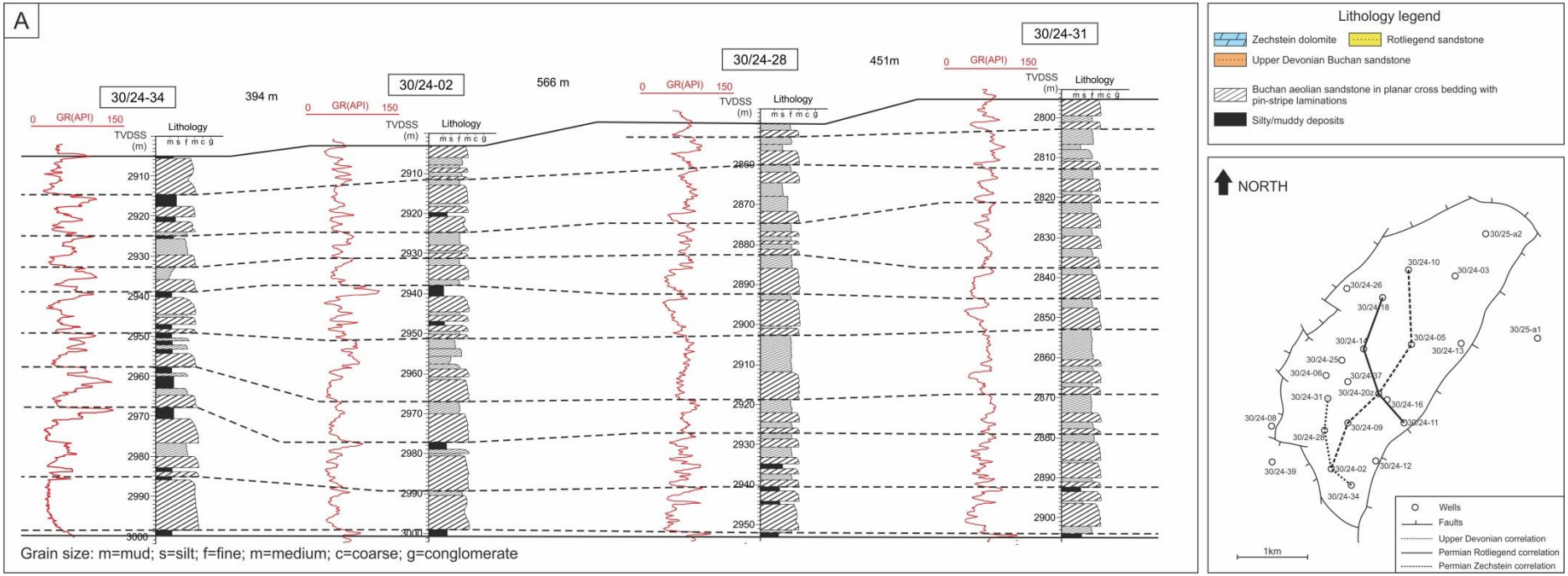

(A): Aeolian dominated layer B08 of Devonian Buchan Formation (Tang et al., 2017a).

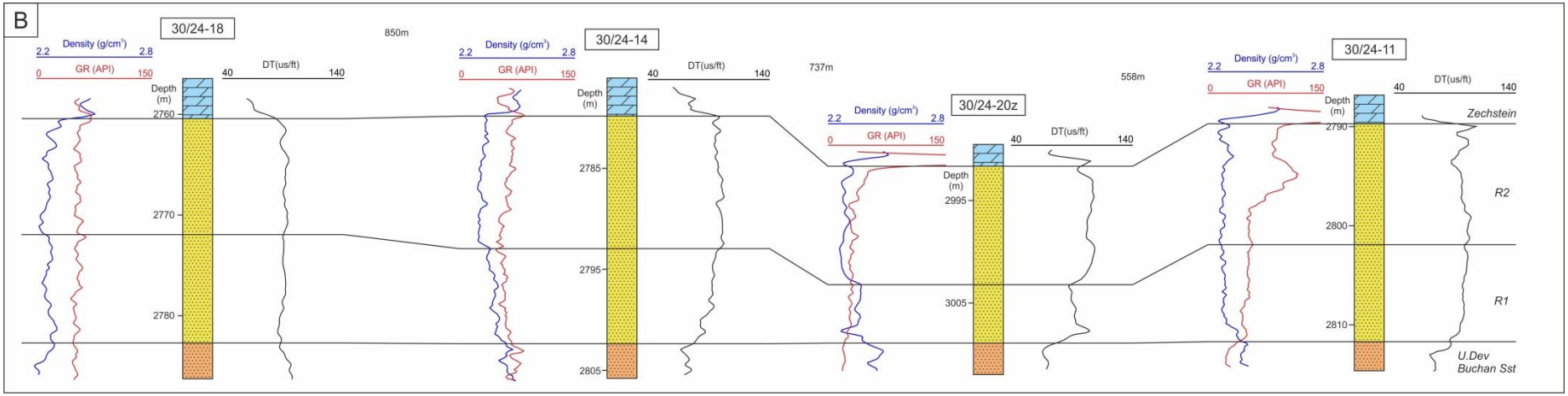

(B): Rotliegend sandstone unit.

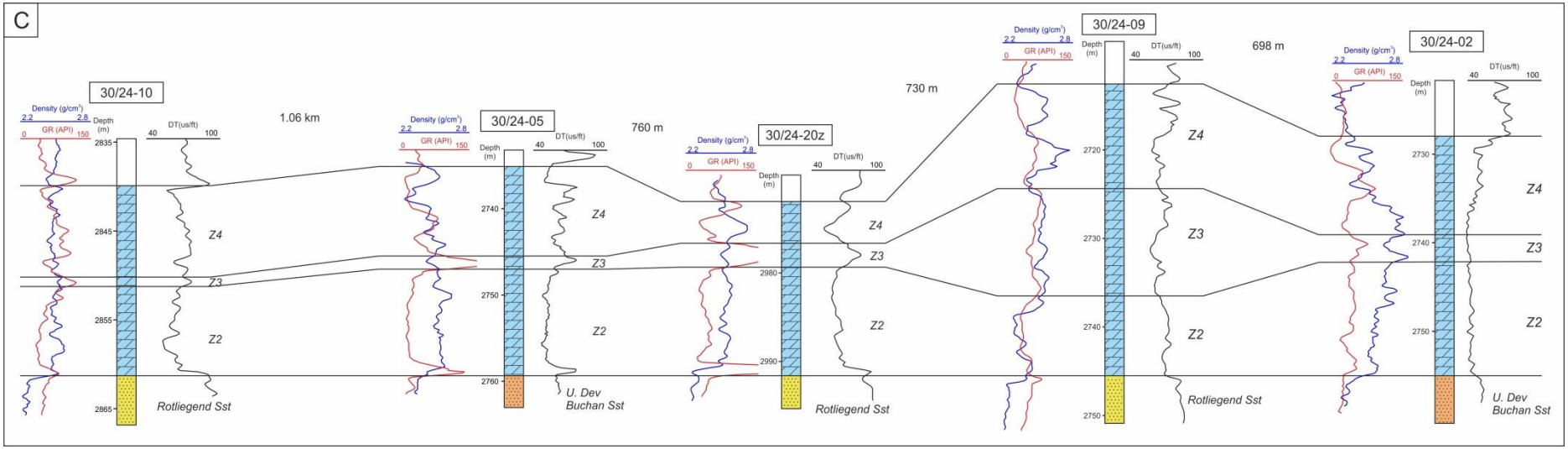

(C): Zechstein dolomitic unit

7.4.4 Upper Jurassic

An overall fining upwards sequence is recognized varying from coarse conglomeratic sandstones through pebbly sandstones into fine grained sandstones upwards. The relatively high energy conglomerate and pebbly sandstones are interpreted as representing the reworking of the top of the underlying conglomeritic unit. The sequence represents decreasing energy and increasing water depth upwards and possibly is part of an overall transgressive sequence culminating with the deposition of the Kimmeridge Clay (Bifani and Smith, 1985).

Porosity and permeability are moderate to good within the fine grained sandstones (16% – 21%, few milli-darcies to a few hundred milli-darcies). Petrographic analysis shows occlusion of porosity due to carbonate cementation. Petrographic analysis suggests that calcite cement leaching and feldspar dissolution may have occurred thus creating the secondary porosity.

7.5 Source

The deeply buried Upper Jurassic Kimmeridge Clay organic shales are the source of hydrocarbons for the Central Graben region (Gluyas et al., 2005). They are not mature in the Alma Field area, but migration is likely to have come from the deeper more basinal Central Graben from the east-northeast.

7.6 Oil in place, reserves and production

The most recent estimate for oil in place for Alma Field plus the adjacent Galia Field (formerly Duncan Field) is 307 million barrels (EnQuest, 2015). We are aware of at least ten 'different calculations' oil in place calculations. These range from 198 mmstb in the 1991 Argyll 'Cessation of Production' report by Hamilton to 375 mmstb calculated by Tuscan during the

Ardmore phase of the field (Gluyas et al., 2018). There were in total 72.6 million barrels oil has been produced during the Argyll-stage development from 1975 to 1992 (41.1 million barrels from Zechstein interval completions, 18.2 million barrels from Rotliegend interval completions, and 12.8 million barrels from Devonian interval completions. Much of the oil produced from wells completed in the Zechstein was produced from the Rotliegend and Devonian reservoirs via cross-flow (Gluyas et al., 2018). Only natural aquifer support and gas lift were used to support production of Argyll. During the Ardmore phase of the field, wells were completed in both the Zechstein and Devonian intervals and co-produced using natural flow initially and then with electro-submersible pumps. Five million barrels was produced from Ardmore between 2003 and 2005 (**Figure. 7.9**). Well workovers completed during the Ardmore phase demonstrated that the main natural aquifer was the Rotliegend sandstones with about 30 billion barrels attached to the field (Gluyas et al., 2018). Water flows from the Rotliegend into both the Zechstein above and Devonian below. Reservoir quality in the deeper Devonian is poorer and there is effectively no bottom drive. The Alma development phase has provision for water injection but as of yet has not been implemented. Alma production has delivered 3.8 million barrels including about 0.5 million barrels from a long-reach well into the adjacent Galia Field. Remaining reserves prior to Alma start-up were calculated to be about 25 MMBBL.

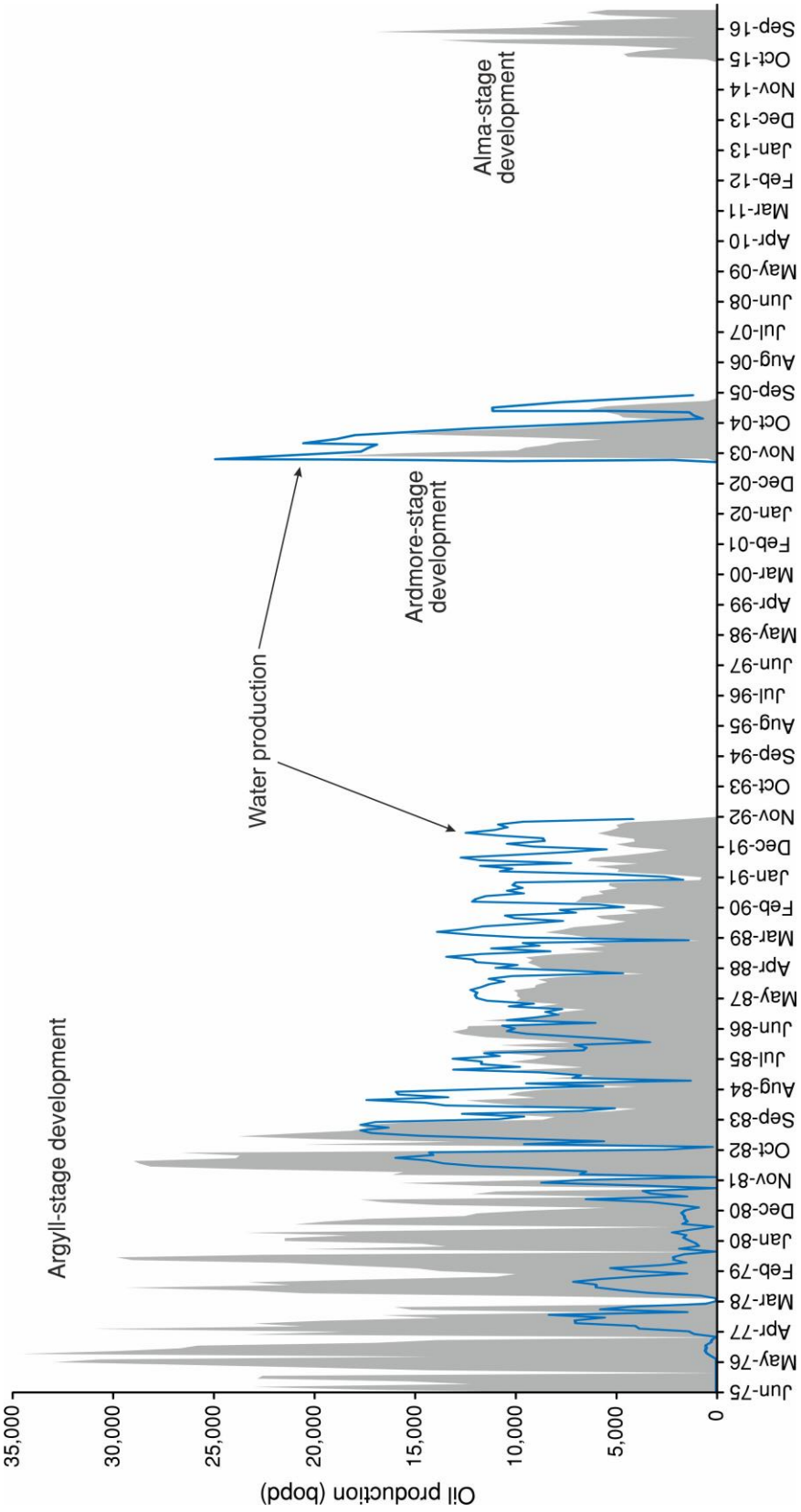

Figure 7.9 Three-stage production history of the Alma Field by the end of April 2017.

7.7 Field Summary Table

Parameter	Data and suggested Units	Author's explanatory comments
Trap		
Type	Horst block	
Depth to crest	8,600 (ft. TVDSS)	
Hydrocarbon contacts	9,360 (ft. TVDSS)	The contact is shallower in the NE crest of the field at 9150 ft. TVDSS and deepest in the far SW at 9430 ft. TVDSS
Maximum oil column thickness	860 (ft.)	Measured from NE crest to SW OWC
Maximum gas column thickness	Not applicable (ft.)	
Main Pay Zone		
Formation	1. Fulmar Formation 2. Halibut Bank, Sapropelic Dolomite, Turbot Bank formations 3. Auk Formation 4. Buchan Formation	1. Minor development on western flank 2. Zechstein Group formations 3. Rotliegend sandstone 4. Old Red Sandstone
Age	1. Upper Jurassic 2. Upper Permian 3. Lower Permian 4. Upper Devonian	4. Youngest Buchan Formation may be Lower Carboniferous in age
Depositional setting	1. Shallow marine 2. Shallow, restricted marine, evaporate basin 3. Terrestrial aeolian, fluvial & sabkha 4. Terrestrial aeolian and fluvial	
Gross/net thickness	1600 ft. to 3,300 ft.	Zechstein oversteps Rotliegend and where the latter is absent lies unconformably above Buchan sandstones; The Rotliegend sandstones infill topography in pre-Permian land surface; Buchan tilted to west with topographic erosion surface separating it from younger sediments
Average porosity (range)	Fulmar: 20 – 25% Zechstein: 5% – 20%; Rotliegend: 18% – 25%; Buchan: 0.1% – 28%;	
Average net: gross ratio	Fulmar: 0.8 - 1 Zechstein: 0.25-0.9 Rotliegend: 0.7-0.98 Buchan: 0.5-0.95	
Cutoff for net reservoir	Fulmar: 17% porosity Zechstein: 5% porosity Rotliegend: 12% porosity Buchan: 13% porosity	Argyll phase
Average permeability (range)	Fulmar: range 1mD to 100 mD Zechstein: >1D Rotliegend: 200mD range 4-5410 mD Buchan: 340 mD (arithmetic) 10.5 (geometric) range <1 to >1000 mD	Zechstein core is rubbly and vuggy, core measurements are unreliable, fracture permeability dominates
Average hydrocarbon saturation	Fulmar: 70% Zechstein: 45%	

	Rotliegend 50% Buchan 42%	
Productivity index range	Not available	
Hydrocarbons		
Oil gravity	38 (°API)	
Oil properties	Light crude with viscosity (0.58 cp to 0.7 cp)	
Bubble point (oil) Dew point (condensate)	Fulmar: 1920 psi Zechstein: 1152 psi Rotliegend: 989 to 1152 psi Buchan: 142 psi	
Gas/Oil Ratio or Condensate/Gas Ratio	267 scf/bbl	Based on cumulative production
Formation Volume Factor (oil)	1.214	
Gas gravity	n/a	
Gas Expansion Factor	n/a	
Formation Water		
Salinity	58,110 (ppm NaCl equiv.)	
Resistivity	0.141 ohm-m at 250°F	
Pressure gradient - water	0.43 psi ft^{-1}	
Reservoir Conditions		
Temperature	122 (°C)	252°F at 9000 ft. TVD datum
Initial pressure	5285 (psia at 9,000 ft. TVDSS)	
Hydrocarbon pressure gradient - oil	0.326 (psi/ft.)	
Hydrocarbon pressure gradient - gas	n/a	
Field Size		
Area	11.33 (km^2)	
Gross Rock Volume	n/a	
STOOIP	Alma 307 (mmbbl) Ardmore 375 mmbbl Argyll 198 mmbbl (range 198-342 mmstb)	Most recent update (Enquest 2015) Argyll STOIIP calculation from cessation of production report
Associated GIP	Not calculated (bcf)	
Non-associated GIP	Not calculated (bcf)	
Drive mechanism (primary, secondary)	Primary pressure depletion	
Recovery to date - oil	81.4 (mmbbl)	To April 2017
Recovery to date - gas	n/a	
Expected ultimate recovery factor/volume - oil	33 (%) / 100 (mmbbl)	Based upon 307 mmstb STOIIP
Expected ultimate recovery factor/volume - gas	(%)/(bcf)	
Production		
Start-up date	June 1975	
Number of Exploration/Appraisal Wells	1/4	
Number of Production Wells	17 Argyll 3 Ardmore 6 Alma	Appraisal wells used for production during Argyll phase
Number of Injection Wells	0	
Development scheme	Argyll converted drill ship	

	Ardmore converted jack-up Alma floating production	
Plateau rates – oil/gas	Argyll 34,500 bopd Ardmore 18,900 bopd Alma 13,000 bopd	August 1976 December 2003 May 2016
Planned abandon-ment	n/a	

CHAPTER 8: CONCLUSIONS AND FURTHER DISCUSSIONS

Chapter outline

8.1 Principle findings

8.2 Analysis of uncertainties: the architecture of fluvial channel sand body in the Ardmore Field

8.3 Implications from this study

8.4 Suggestions for the future research

8.1 Principle findings

8.1.1 Lithology, facies identification, facies architecture and sand body connectivity

- Core cut in Buchan Formation of the Ardmore Field contains three lithologies: conglomerates, sandstones and fine-grain sediments including siltstones and mudstones. They can be further classified into eight sub-types based on sedimentary structures. These deposits were formed in fluvial and aeolian systems under hot and arid conditions.
- In the Ardmore Field, the core and well log studies identify that the Buchan Formation consists of a fluvial-aeolian-fluvial succession representing a predominantly progradational sequence of the alluvial fan-based braided system with aeolian-dominated deposits between two main fluvial progradation periods.
- Facies architecture was studied using analogue outcrops, core logging data, well log correlation and basin modelling. The results demonstrate that the fluvial sequences are composed of metre scale superimposed fining-upward cycles, interpreted as high-energy fluvial braided systems. Laterally, a single fluvial channel sand body has a thin (1 m – 3 m) and sheet-like morphology with a high width/thickness ratio (80:1 – 120:1, mean value 110.7:1).The high channel deposit proportion (> 75%) indicates that nearly all the channel sand bodies were likely to be interconnected both vertically and laterally.
- The aeolian sequence has a simpler internal architecture: the interbedded occurrence of dune (good reservoir quality) and interdune (moderate reservoir quality) deposits. Individual dune and interdune deposit can laterally extend up to a kilometre scale and generally shows tabular geometry in the lateral direction. The connectivity of individual dune sand body is excellent in the lateral direction and is compartmentalized by interdune deposits in the vertical direction.

- Compared with fluvial facies sandstones, the aeolian-associated facies form a volumetrically minor (approx. 30%). They are an important reservoir in Ardmore Field due to good sorting, high grain roundness and absence of both muddy and conglomeratic contents and were little cemented. These features allow them to be tentatively identified, especially for those uncored wells, by using the combination of well log responses: low gamma ray, high sonic transit time and low bulk density.

8.1.2 Petrography, diagenesis and reservoir quality of the Upper Devonian Buchan Formation in Ardmore Field

- The main sandstone type is fine to medium-grained, moderately to well sorted litharenite and sublitharenite with anomalously good but variable reservoir quality (ϕ = 1% – 28%, K = 0.1 mD – 5280 mD). An important finding from this research is the recognition that the Upper Devonian stratigraphy of the North Sea can have good reservoir quality with hydrocarbon potential.
- The reservoirs consist of braided fluvial channel and aeolian dune sandstones. The volumetrically minor aeolian dune sandstones generally show excellent reservoir quality (ϕ = 5.1% to 28%, mean value 20.2%, K = 0.2 mD to 5280 mD, geometric mean 64.9 mD). The volumetrically major fluvial channel sandstones possess reservoir quality with a large variation (ϕ = 0.1% to 23.1%, mean value 12.7%; K = 0.2 mD to 1240 mD, geometric mean 5.41 mD).
- Both reservoir sandstone types suffered moderate porosity loss from early mechanical compaction (average 14.82% and 10.06% porosity have been reduced by compaction in aeolian and fluvial samples, respectively), but show clearly different phases of burial diagenesis and cementation (average 5.63% and 12.71% porosity have been reduced by cementation in aeolian and fluvial samples, respectively). The dolomite cementation is common in both sandstone types. In the fluvial facies sandstones, the intense quartz over-

growth is widely presented and volumetrically occupied 3% – 7% intergranular space. In the aeolian facies sandstones, the most noticeable differences are the absence of quartz overgrowth and presence of thick (1 μm – 5 μm) and continuous grain-coating clays covering nearly all the quartz grains.

- Detailed petrographic analysis has identified that grain coating clays were formed before compaction and mixed layer clay of illite/smectite (I/S). The cornflake and/or honeycomb morphology identifies that the precursor of I/S is likely to be smectite. The most probable source of these detrital clays was from the distal sector of a braided system such as flood plain deposits and the accumulations in the interdunes. When the clay-bearing water encountered the porous and permeable aeolian sands, the clays would have infiltrated into the porous intergranular space by mechanical infiltration.
- The grain coating I/S inhibited subsequent quartz overgrowth and helped to preserve primary porosity. By using the model of Ehrenberg (1993) it is proposed that 6% – 7% porosity would be occupied by quartz overgrowth if there wasn't grain coating I/S.
- Illitization of smectite has limited negative effect on reservoir quality, the 1D burial curve shows that the Buchan Formation was at consistently shallow depth (< 1.5 km) and low temperature (< 70°C) until Palaeogene and rapidly buried to today's maximum depth (2.5 km – 3.2 km). The low burial temperatures encountered for much of the geological history of the Buchan Formation sandstones has provided insufficient time for transformation of smectite to hairy/fibrous illite.

8.1.3 Results from geochemical analysis

- Quartz overgrowths show zoned structure under CL (cathodoluminescence) representing multiple stages of authigenic quartz precipitation. This corresponds to the homogenization temperature of fluid inclusions between quartz and overgrowth ranges uniformly from 80°C to 120°C. Fluid inclusions consist of pure brine water confirming that the quartz

overgrowths developed earlier than the oil migration. The most possible source of silica is from alteration (kaolinitization) of feldspars, the pressure dissolution of quartz grains also has a minor contribution.

- The temperature of precipitation and paragenesis of dolomitic cements were investigated through stable isotopic analysis. The results of $\delta^{13}C$ and $\delta^{18}O$ clearly identify a well-developed marine carbon signature ($\delta^{13}C$ = -3.1‰ to 1.6‰) forming in temperature range from ~25°C to ~58°C. It is proposed that the most likely source for such a marine signature is the overlying Zechstein carbonates.
- For the clay minerals, the XRD analysis show that the I/S is in the R1 ordered interstratification, the illite component is 70% – 80% in the mixed I/S and dickite is not found in the kaolinite aggregates. Burial history temperatures never exceeded ~130°C and the Buchan Formation is at maximum burial at present day.

8.2 Analysis of uncertainties: the architecture of fluvial channel sand bodies in Ardmore Field

The geological concept '*the present is the key to the past*' was firstly developed during the Scottish Enlightenment, which means that the processes and phenomena of occurring today have operated throughout most of the Earth's history (Mathieson, 2002). But, is it really applicable to the whole geological history? In this study, the answer is 'no'.

Fluvial systems are a common part of the landscape on Earth and its architecture is vital in the petroleum industry for estimating reservoir volumes and petroleum productivity (Miall, 2013). Both external and internal factors can have impacts on fluvial architecture including climate, tectonics, sediment supply rate, topography, sediment calibre, slope, avulsion rate, soil and vegetation (Bull, 1991; Charlton, 2007; Miall, 2013). Amongst all these factors, vegetation might be the only one with significant evolution which shows contrasting differences

between ancient and modern ages. Therefore, the morphology of ancient fluvial (early and middle Palaeozoic age) may be very different to that of today due to the absence of these river bank stabilizers.

Geologically, the most important impact of the vegetation, particularly the truly rooted vascular species, on the fluvial morphology is stabilizing river banks and forming relatively fixed channels (Gibling and Davies, 2012). The vascular plants started presenting on the land surface at approximately Late Silurian to Early Devonian and became widespread at the Late Devonian to Early Carboniferous (Małkowski and Racki, 2009; Davies and Gibling, 2010). Before the universal colonization of truly rooted vegetation on the land surface, the fluvial deposits usually demonstrate a 'sheet-like' braided style generated by wide and shallow flow with low relief margins, and the floodplain deposit was generally little preserved (e.g. Davies and Gibling, 2011; Gibling and Davies, 2012; Gibling et al., 2014).

During the Devonian the UK and especially the North Sea area were located at the 15° to 20° latitude in the southern hemisphere (Hunter and Easterbrook, 2004). The low latitude tropical position, presence of aeolian deposits and mud desiccation cracks support a palaeo-climatic setting of hot and arid to semi-arid. Any vegetation is likely to be restricted and have played a negligible role in controlling fluvial system evolution. The superimposed meter-scale fining-upward cycles imply that the discharge was the 'seasonal' flood events probably depending on the variation of rainfall in the sediment source areas, rather than a single-episode and relatively steady long-term discharge mode. A single discharge cycle might look like a thin and flat sheet flow with high width/thickness ratio. Moreover, the uncorrelated conglomeratic basal lags might be a good indicator representing multiple discharges existed contemporaneously.

So far we know that the fluvial system in the study area is a combination of the high-energy, braided-like and distal, sheet flood sand-bed styles. In this case, the main facies which could form effective reservoir are the sandy-dominated channel deposits. A good quality of estimation on the scale of these channel deposits is important for: 1). Lateral extension of single sand body in the subsurface; 2). Net-gross ratio: the key factor for calculating the approximate reservoir volume; and 3). The channel deposition proportion (CDP) which is decisive on subsurface sand body connectivity (Bridge and Tye, 2000).

To minimize the uncertainty of geometry parameters of subsurface channel sand bodies and obtain a relatively accurate width/thickness ratio, we employed both analogue outcrops with similar sedimentary facies and well logs among neighbouring wells in the Ardmore Field. The measurement of channel sand bodies at outcrops provides an approximate range of width/thickness ratio, and this could be used to decide whether the sand bodies with comparable well log responses in different wells are correlated or not. Here we propose that the combination of analogue outcrops and well logs among neighbouring wells could provide parameters for subsurface simulations. These might be the best way to study the geometry of subsurface channel sand bodies when the high resolution seismic data is not available.

8.3 Implications from this study

8.3.1 Reservoirs with possibly good potential of the Upper Devonian Buchan Formation in the Central North Sea

In the North Sea, the Permian, Mesozoic and Cainozoic reservoirs have been considerably studied and explored. However the often deeper and older objectives (Devonian and Carboniferous) have been overlooked for a long time. This study has confirmed that in the Central North Sea, the Upper Devonian Buchan Formation could form good reservoirs under specific depositional, diagenetic and burial conditions. The outcomes may stimulate further investiga-

tions on Buchan Formation and re-evaluate the potential of Upper Devonian strata in Central and Northern North Sea.

8.3.2 Survival of porous aeolian sandstones within cemented fluvial sandstones

In this study, we have found that the aeolian deposits are sandwiched by considerably cemented fluvial sandstones but show abnormally high reservoir quality and lesser cementations. The fluvial sandstones are highly cemented by authigenic dolomite and quartz overgrowth, but these aeolian deposits are free of quartz cementation. This study has proposed that the presence of early formed mechanically infiltrated grain coating clays and the featured burial history are the main key factors for the good reservoir quality in aeolian sandstones. The presence of grain coating clays is closely related to the fluvial-aeolian setting which is reportedly extensive from Midland Valley (Cameron and Stephenson, 1985; Hall and Chisholm, 1987) to the UK-Norwegian boundary areas in the North Sea (Knight et al., 1993; Graham et al., 2003; Abay et al., 2014). A number of publications have shown that the burial history with similar features may present elsewhere in the Central Graben (e.g. Swarbrick et al., 2000; Carr, 2003; Di Primio and Neumann, 2008; Nguyen et al., 2013). Based on these clues, we proposed that the Upper Devonian aeolian sandstones in the Central Graben are likely to possess good reservoir quality if they have been deposited in analogue depositional setting and experienced similar diagenetic and burial histories.

8.3.3 Positive effect of smectite (subsequently altered to I/S) on preserving porosity

The illitization of smectite is traditionally regarded to be harmful to the reservoir quality (especially on reducing permeability) due to its water and salinity sensitive swelling property. This study has demonstrated that grains coated with tangential illite/smectite can still keep high quality reservoirs if illitization has not progressed to develop to the stage of elongated filamentous illite. In the Buchan Formation of the Ardmore Field, the smectite/illite has not

fully transformed to illite despite the high reservoir temperature (approx. 120°C) because burial to such temperature only occurred in the recent geological past and provided insufficient time-temperature exposure for illitization. Based on the numerous reports on the positive effect of porosity preservation by grain coating chlorite and microcrystalline quartz overgrowth, this study has confirmed that the grain coating I/S, with particular depositional, diagenetic and burial conditions, can also be a good porosity preserver which has been rarely realized before.

8.4 Suggestions for future research

During this research, a number of questions and ideas turned up. These ideas are presented below and may represent opportunities to expand on the research reported here and to further develop the research into related areas.

8.4.1 Aeolian dune deposits of Upper Devonian Buchan Formation in the Central North Sea: is it a new hope in the old strata?

The excellent reservoir quality of aeolian dune sandstones has been confirmed in this study and this was largely unidentified in previous research. It shows that the high compositional and textural maturity, early-formed grain coating clays and the featured burial history are the key points determining high reservoir quality in late Palaeozoic sediments of the North Sea. We suggest that the future research and exploration of Devonian targets should consider these aeolian sandstones associated with fluvial deposits if they are at low temperatures or only recently heated. Since the aeolian deposits were not well identified in Devonian strata of the North Sea, a critical revisit on drilled Devonian intervals and careful explanation of any new encountered Upper Devonian Formation should be made in the future.

8.4.2 Source area of the fluvial sediments

Mykura (2002) illustrated that in the Midland Valley and Southern Upland, the Late Devonian fluvial systems generally flowed eastwards into the Central North Sea. In the further north area, the Upper Old Red Sandstone in the Buchan Field (UK Block 21/1) was originated from igneous rocks in the Grampian Region (Richards, 1985b). However, there is no direct evidence could prove these localities were true sediment source areas, and the exact scale of the fluvial systems existed during Late Devonian is still unclear. We suggest that the further investigations can be made by studying polycrystalline quartz grains, smectite aggregates, different quartz colours under cathodoluminescence, heavy minerals to achieve a better understanding of the sediment provenance (Haughton and Farrow, 1989).

8.4.3 Quantitative petrography analysis on the quartz overgrowth

In this study, fluid inclusions have been used to determine the precipitation temperature of quartz overgrowth and cathodoluminescence analysis has identified the multiple stages of quartz cementation. To constrain the rates and mechanisms of quartz cementation and quantify changes in the physical properties of sandstones during burial, we suggest that the situ secondary ion mass spectrometry (SIMS) can be used in the future to quantitatively determine the quartz cementation histories.

8.4.4 Recognition of open fractures in uncored wells.

Downie (2009) has mentioned the important role of open fractures on assisting the flow of hydrocarbons in the Devonian reservoir rocks. By investigating the existed cores, the fractures are not widely distributed. Less than 10% cores have visible fractures presenting in sealed and open types (**Figures 8.1A and 8.1B**). The open fractures are likely to be recognizable according to a couple of well log responses including: 1). The high value and ‘cycle skip’ shape of acoustic log due to the contrasting sonic propagation velocity in the air and

rocks (Gao and Xie, 2007); and 2). Rapid decrease of ILM (medium-depth induction) while the ILD (deep-depth induction) varies stably and smoothly (Cancan, 2003) (**Figure 8.1B**). We suggest that these characteristics can be used for recognizing open fractures in the uncored wells.

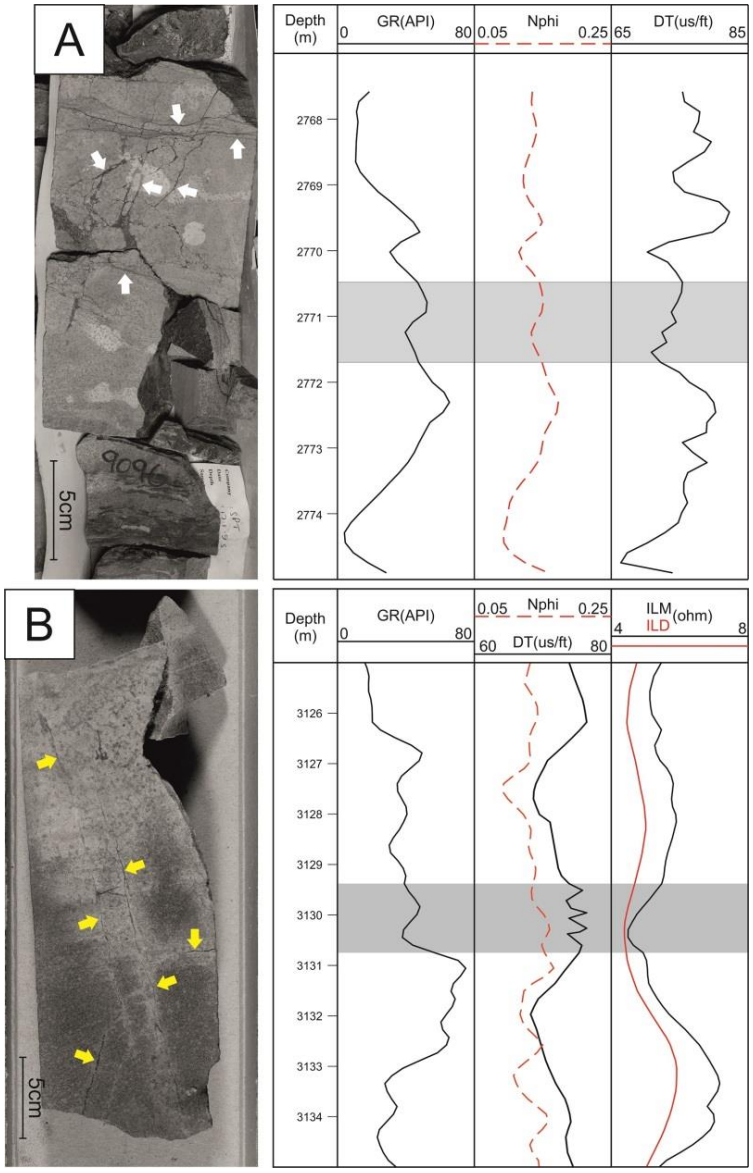

Figure 8.1 The presence and well log response of two types' fractures. A. the sealed fractures in the Upper Devonian fluvial sandstones, well 30/24-05, 2772.5 m. B. the open fractures in the Upper Devonian fluvial sandstones, well 30/24-20z, 2835.6 m.

REFERENCES

Aase, N.E., Bjorkum, P.A. and Nadeau, P.H., 1996. The effect of grain-coating microquartz on preservation of reservoir porosity. AAPG bulletin, 80(10): 1654-1673.

Aase, N.E. and Walderhaug, O., 2005. The effect of hydrocarbons on quartz cementation: diagenesis in the Upper Jurassic sandstones of the Miller Field, North Sea, revisited. Petroleum Geoscience, 11(3): 215-223.

Abay, T., Karlsen, D. and Ohm, S., 2014. Vertical variations in reservoir geochemistry in a palaeozoic trap, Embla field, offshore Norway. Journal of Petroleum Geology, 37(4): 349-372.

Abbotts, I., 1991. United Kingdom oil and gas fields: 25 years commemorative volume. Geological Society Publishing House.

Ahlbrandt, T.S. and Fryberger, S.G., 1982. Introduction to eolian deposits, Sandstone Depositional Environments. AAPG Special Volumes pp. 11-47.

Ajdukiewicz, J.M. and Lander, R.H., 2010. Sandstone reservoir quality prediction: The state of the art. AAPG bulletin, 94(8): 1083-1091.

Ali, S.A., Clark, W.J., Moore, W.R. and Dribus, J.R., 2010. Diagenesis and reservoir quality. Oilfield Review, 22(2): 14-27.

Allen, J., 1983. Studies in fluviatile sedimentation: bars, bar-complexes and sandstone sheets (low-sinuosity braided streams) in the Brownstones (L. Devonian), Welsh Borders. Sedimentary Geology, 33(4): 237-293.

Allen, J.R.L., 1965. Upper Old Red Sandstone (Farlovian) paleogeography in south Wales and the Welsh borderland. Journal of Sedimentary Research, 35(1).

Allen, P.A. and Mange-Rajetzky, M.A., 1992. Devonian-Carboniferous sedimentary evolution of the Clair area, offshore north-western UK: impact of changing provenance. Marine and Petroleum Geology, 9(1): 29-52.

Almon, W.R. and Davies, D.K., 1981. Formation damage and the crystal chemistry of clays. Short course in clays and the resource geologist: Montreal, Mineralogical Association of Canada, 7: 81-102.

Andrews, I., Long, D., Richards, P., Thomson, A., Brown, S., Chesher, J. and McCormac, M., 1990. The geology of the Moray Firth. United Kingdom Offshore Regional Report, 3. HMSO.

Armstrong, M. and Paterson, I.B., 1970. The Lower Old Red Sandstone of the Strathmore region. HM Stationery Office.

Astin, T., 1990. The Devonian lacustrine sediments of Orkney, Scotland; implications for climate cyclicity, basin structure and maturation history. Journal of the Geological Society, 147(1): 141-151.

Barclay, S. and Worden, R., 2000. Geochemical modelling of diagenetic reactions in a sub-arkosic sandstone. Clay Minerals, 35(1): 57-57.

Barker, C., 1972. Aquathermal Pressuring-Role of Temperature in Development of Abnormal-Pressure Zones: Geological notes. AAPG Bulletin, 56(10): 2068-2071.

Beard, D. and Weyl, P., 1973. Influence of texture on porosity and permeability of unconsolidated sand. AAPG bulletin, 57(2): 349-369.

Berger, A., Gier, S. and Krois, P., 2009. Porosity-preserving chlorite cements in shallow-marine volcaniclastic sandstones: Evidence from Cretaceous sandstones of the Sawan gas field, Pakistan. AAPG bulletin, 93(5): 595-615.

Besly, B., 2011. Reservoir geology studies of Argyll Field. Personal Communication.

Bifani, R. and Smith, C., 1985. The Argyll field after a decade of production, Offshore Europe. Society of Petroleum Engineers.

Bjorkum, P.A., Walderhaug, O. and Aase, N.E., 1993. A model for the effect of illitization on porosity and quartz cementation of sandstones. Journal of Sedimentary Research, 63(6).

Bjørlykke, K., 1983. Diagenetic reactions in sandstones, Sediment diagenesis. Springer, pp. 169-213.

Bjørlykke, K., 1984. Formation of secondary porosity: how important is it. Clastic diagenesis: AAPG Memoir, 37: 277-286.

Bjørlykke, K., Aagaard, P., Dypvik, H., Hastings, D. and Harper, A., 1986. Diagenesis and reservoir properties of Jurassic sandstones from the Haltenbanken area, offshore mid-Norway. Habitat of hydrocarbons on the Norwegian continental shelf: 275-286.

Bjorlykke, K. and Egeberg, P., 1993. Quartz cementation in sedimentary basins. AAPG bulletin, 77(9): 1538-1548.

Bjorlykke, K. and Jahren, J., 2012. Open or closed geochemical systems during diagenesis in sedimentary basins: Constraints on mass transfer during diagenesis and the prediction of porosity in sandstone and carbonate reservoirs. AAPG bulletin, 96(12): 2193-2214.

Bjørlykke, K., Mo, A. and Palm, E., 1988. Modelling of thermal convection in sedimentary basins and its relevance to diagenetic reactions. Marine and Petroleum Geology, 5(4): 338-351.

Bloch, S., Lander, R.H. and Bonnell, L., 2002. Anomalously high porosity and permeability in deeply buried sandstone reservoirs: Origin and predictability. AAPG bulletin, 86(2): 301-328.

Bloch, S. and McGowen, J., 1994. Influence of depositional environment on reservoir quality prediction. Special Publications of SEPM, Reservoir Quality Assessment and Prediction in Clastic Rocks (SC30).

Bluck, B., 2000. Old Red Sandstone basins and alluvial systems of Midland Scotland. Geological Society, London, Special Publications, 180(1): 417-437.

Boggs Jr, S., 2006. Sedimentology and stratigraphy. Pearson Education.

Bongiolo, D.E. and Scherer, C.M., 2010. Facies architecture and heterogeneity of the fluvial–aeolian reservoirs of the Sergi formation (Upper Jurassic), Recôncavo Basin, NE Brazil. Marine and Petroleum Geology, 27(9): 1885-1897.

Bowen, J., 1975. The Brent oil-field. Petroleum and the continental shelf of north-west Europe, 1: 353-361.

Bradshaw, M., Cope, J., Cripps, D., Donovan, D., Howarth, M., Rawson, P., West, I. and Wimbledon, W., 1992. Atlas of palaeogeography and lithofacies. The Geological Society (Geological Society of London, Memoir) London, UK.

Brewster, J., 1991. The Frigg field, Block 10/1 UK North Sea and 25/1, Norwegian North Sea. Geological Society, London, Memoirs, 14(1): 117-126.

Bridge, J. and Demicco, R., 2008. Earth surface processes, landforms and sediment deposits. Cambridge University Press.

Bridge, J.S., 1993. The interaction between channel geometry, water flow, sediment transport and deposition in braided rivers. Geological Society, London, Special Publications, 75(1): 13-71.

Bridge, J.S., Jalfin, G.A. and Georgieff, S.M., 2000a. Geometry, lithofacies, and spatial distribution of Cretaceous fluvial sandstone bodies, San Jorge Basin, Argentina: outcrop analog for the hydrocarbon-bearing Chubut Group. Journal of Sedimentary Research, 70(2).

Bridge, J.S., Jalfin, G.A. and Georgieff, S.M., 2000b. Geometry, lithofacies, and spatial distribution of Cretaceous fluvial sandstone bodies, San Jorge Basin, Argentina: outcrop analog for the hydrocarbon-bearing Chubut Group. Journal of Sedimentary Research, 70(2): 341-359.

Bridge, J.S. and Lunt, I.A., 2006. Depositional models of braided rivers. Braided Rivers, Processes, Deposits, Ecology and Management, Int. Assoc. Sediment. Spec. Pub, 36: 11-50.

Bridge, J.S. and Tye, R.S., 2000. Interpreting the dimensions of ancient fluvial channel bars, channels, and channel belts from wireline-logs and cores. AAPG bulletin, 84(8): 1205-1228.

Brzesowsky, R., Spiers, C., Peach, C. and Hangx, S., 2014. Time‐independent compaction behavior of quartz sands. Journal of Geophysical Research: Solid Earth, 119(2): 936-956.

Bukar, M., 2013. Does oil emplacement stop diagenesis and quartz cementation in deeply buried sandstone reservoirs, University of Liverpool.

Bull, W.B., 1991. Geomorphic responses to climatic change. Oxford University Press., New York, NY (United States).

Burley, S., 1984. Patterns of diagenesis in the Sherwood Sandstone Group (Triassic), United Kingdom. Clay Minerals, 19(3): 403-440.

Burton, C. and Tanner, P., 1986. The stratigraphy and structure of the Devonian rocks around Liskeard, east Cornwall, with regional implications. Journal of the Geological Society, 143(1): 95-105.

Cameron, I.B. and Stephenson, D., 1985. British regional geology: the Midland Valley of Scotland. Hmso Books.

Cameron, T., 1993a. Carboniferous and Devonian of the southern North Sea. British Geological Survey.

Cameron, T., 1993b. Triassic, Permian and pre-Permian of the central and northern North Sea. British Geological Survey.

Cancan, Z., 2003. Contributing factor of sandstone fracture and its integrated identifying technology for regular logging data. Oil Geophysical Prospecting, 38(4): 425-430.

Caputo, M.V., de Melo, J.H.G., Streel, M. and Isbell, J.L., 2008. Late Devonian and early Carboniferous glacial records of South America. Geological Society of America Special Papers, 441: 161-173.

Carr, A., 2003. Thermal history model for the South Central Graben, North Sea, derived using both tectonics and maturation. International Journal of Coal Geology, 54(1): 3-19.

Carrigy, M. and Mellon, G., 1964. Authigenic clay mineral cements in Cretaceous and Tertiary sandstones of Alberta. Journal of Sedimentary Research, 34(3).

Carvalho, M.V., De Ros, L.F. and Gomes, N.S., 1995. Carbonate cementation patterns and diagenetic reservoir facies in the Campos Basin Cretaceous turbidites, offshore eastern Brazil. Marine and Petroleum Geology, 12(7): 741-758.

Charlton, R., 2007. Fundamentals of fluvial geomorphology. Routledge.

Chisholm, J. and Dean, J., 1974. The Upper Old Red Sandstone of Fife and Kinross: a fluviatile sequence with evidence of marine incursion. Scottish Journal of Geology, 10(1): 1-30.

Compernolle, T., Welkenhuysen, K., Huisman, K., Piessens, K. and Kort, P., 2016. Can combined investments reduce the impact of uncertainty? CO2 Enhanced Oil Recovery.

Coplen, T.B., Kendall, C. and Hopple, J., 1983. Comparison of stable isotope reference samples. Nature, 302(5905): 236-238.

Cornford, C., 1994. Mandal-Ekofisk petroleum system in the Central Graben of the North Sea. Memoirs-American Association Of Petroleum Geologists: 537-537.

Craig, J., Gluyas, J., Laing, C. and Schofield, P., 2013. Hardstoft–Britain's first oil field. AAPG Petroleum History Institute, Oil-Industry History: 97-116.

Crampton, C.B., Carruthers, R.G., Horne, J.S., Peach, B.N. and Flett, J.S., 1914. The Geology of Caithness:(Sheets 110 and 116, with Parts of 109, 115, and 117.), 110. HM Stationery Office.

Davies, N.S. and Gibling, M.R., 2010. Paleozoic vegetation and the Siluro-Devonian rise of fluvial lateral accretion sets. Geology, 38(1): 51-54.

Davies, N.S. and Gibling, M.R., 2011. Evolution of fixed-channel alluvial plains in response to Carboniferous vegetation. Nature Geoscience, 4(9): 629-633.

Deegan, C.t. and Scull, B.J., 1977. A standard lithostratigraphic nomenclature for the Central and Northern North Sea, 1. HMSO.

Dewers, T. and Ortoleva, P., 1991. Influences of clay minerals on sandstone cementation and pressure solution. Geology, 19(10): 1045-1048.

Dewey, J. and Strachan, R., 2003. Changing Silurian–Devonian relative plate motion in the Caledonides: sinistral transpression to sinistral transtension. Journal of the Geological Society, 160(2): 219-229.

Di Primio, R. and Neumann, V., 2008. HPHT reservoir evolution: a case study from Jade and Judy fields, Central Graben, UK North Sea. International Journal of Earth Sciences, 97(5): 1101-1114.

Dieter, R., 1967. Sedimentology and facies of the Meadfoot beds (lower Devonian) in south-east Devon (England). Geologische Rundschau, 56(1): 543-561.

Dixon, S., Summers, D. and Surdam, R., 1989. Diagenesis and preservation of porosity in Norphlet Formation (Upper Jurassic), southern Alabama. AAPG Bulletin, 73(6): 707-728.

Dominguez, G., 1992. Carbonate reservoir characterization: a geologic-engineering analysis, 30. Elsevier.

Downie, R., 2009. Devonian. Petroleum Geology of the North Sea: Basic Concepts and Recent Advances, Fourth Edition: 85-103.

Edwards, C., 1991. The Buchan Field, Blocks 20/5a and 21/1a, UK North Sea. Geological Society, London, Memoirs, 14(1): 253-259.

Ehrenberg, S., 1989. Assessing the relative importance of compaction processes and cementation to reduction of porosity in sandstones: discussion; compaction and porosity evolution of

Pliocene sandstones, Ventura Basin, California: discussion. AAPG Bulletin, 73(10): 1274-1276.

Ehrenberg, S., 1993. Preservation of anomalously high porosity in deeply buried sandstones by grain-coating chlorite: examples from the Norwegian continental shelf. AAPG Bulletin, 77(7): 1260-1286.

Ehrenberg, S. and Jakobsen, K., 2001. Plagioclase dissolution related to biodegradation of oil in Brent Group sandstones (Middle Jurassic) of Gullfaks Field, northern North Sea. Sedimentology, 48(4): 703-721.

Ehrenberg, S. and Nadeau, P., 1989. Formation of diagenetic illite in sandstones of the Garn Formation, Haltenbanken area, mid-Norwegian continental shelf. Clay Minerals, 24(2): 233-253.

EnQuest, 2015. Alma/Galia first oil. Accessed November 2017.

Erratt, D., Nicholson, P., Winefield, P., Milton-Worssell, R., Cayley, G. and Arter, G., 2005. Exploration history of the high-pressure, high-temperature plays: UK Central North Sea, Geological Society, London, Petroleum Geology Conference series. Geological Society of London, pp. 253-267.

Evans, G., Schmidt, V., Bush, P. and Nelson, H., 1969. Stratigraphy and geologic history of the sabkha, Abu Dhabi, Persian Gulf. Sedimentology, 12(1‐2): 145-159.

Fesharaki, O., García-Romero, E., Cuevas-González, J. and López-Martínez, N., 2007. Clay mineral genesis and chemical evolution in the Miocene sediments of Somosaguas, Madrid Basin, Spain.

Flemings, P.B., 1998. Generation of overpressure and compaction‐driven fluid flow in a Plio‐Pleistocene growth‐faulted basin, Eugene Island 330, offshore Louisiana. Basin Research, 10(2): 177-196.

Folk, R.L., 1957. Petrology of sedimentary rocks. Hemphill Publishing Company.

French, M.W. and Worden, R.H., 2013. Orientation of microcrystalline quartz in the Fontainebleau Formation, Paris Basin and why it preserves porosity. Sedimentary Geology, 284: 149-158.

Friend, P.F., Williams, B., Ford, M. and Williams, E., 2000. Kinematics and dynamics of Old Red Sandstone basins. Geological Society, London, Special Publications, 180(1): 29-60.

Friend, P.F. and Williams, B.P.J., 1978. A Field Guide to Selected Outcrop Areas of the Devonian of Scotland, the Welsh Borderland and South Wales: Proceedings of the Palaeontological Association International Symposium on the Devonian System (PADS 78), 1978. Palaeontological Association.

Fryberger, S.G. and Schenk, C.J., 1988. Pin stripe lamination: a distinctive feature of modern and ancient eolian sediments. Sedimentary Geology, 55(1-2): 1-15.

Gambaro, M. and Currie, M., 2003. The Balmoral, Glamis and Stirling fields, block 16/21, UK Central North Sea. Geological Society, London, Memoirs, 20(1): 395-413.

Gao, X. and Xie, Q.-b., 2007. Advances in identification and evaluation of fracture [J]. Progress in geophysics, 5: 018.

Gatliff, R., 1994. The geology of the central North Sea, 5. HM Stationery Office.

Gatliff, R.W. and Survey, B.G., 1994. The Geology of the Central North Sea. United Kingdom offshore regional report, 5. H.M. Stationery Office.

George, G.T. and Berry, J.K., 1993. A new lithostratigraphy and depositional model for the Upper Rotliegend of the UK Sector of the Southern North Sea. Geological Society, London, Special Publications, 73(1): 291-319.

Gibling, M., Davies, N., Falcon-Lang, H., Bashforth, A., DiMichele, W., Rygel, M. and Ielpi, A., 2014. Palaeozoic co-evolution of rivers and vegetation: a synthesis of current knowledge. Proceedings of the Geologists' Association, 125: 524-533.

Gibling, M.R. and Davies, N.S., 2012. Palaeozoic landscapes shaped by plant evolution. Nature Geoscience, 5(2): 99-105.

Giles, M., 1987. Mass transfer and problems of secondary porosity creation in deeply buried hydrocarbon reservoirs. Marine and Petroleum Geology, 4(3): 188-204.

Giles, M. and De Boer, R., 1990. Origin and significance of redistributional secondary porosity. Marine and Petroleum Geology, 7(4): 378-397.

Glennie, K., 2009. Petroleum Geology of the North Sea: Basic concepts and recent advances. John Wiley & Sons.

Glennie, K. and Provan, D., 1990. Lower Permian Rotliegend reservoir of the southern North Sea gas province. Geological Society, London, Special Publications, 50(1): 399-416.

Gluyas, J., 2016. Zechstein carbonates as a petroleum reservoir, Argyll/Ardmore Field, UK Continental Shelf. POUGS, 2: 39-45.

Gluyas, J. and Cade, C.A., 1997. Prediction of porosity in compacted sands. AAPG Memoir 69: Reservoir Quality Prediction in Sandstones and Carbonates, 69: 19-27.

Gluyas, J., Robinson, A., Emery, D., Grant, S. and Oxtoby, N., 1993. The link between petroleum emplacement and sandstone cementation, Geological Society, London, Petroleum Geology Conference series. Geological Society of London, pp. 1395-1402.

Gluyas, J.G. and Hichens, H.M., 2003. United Kingdom oil and gas fields: commemorative millennium volume.

Gluyas, J.G., Mair, B., Schofield, P., Arkley, P. and McRae, D., 2005. Ardmore Field: rebirth of the first offshore oil field, UKCS, Geological Society, London, Petroleum Geology Conference series. Geological Society of London, pp. 367-388.

Gluyas, J.G., Tang, L. and Jones, S.J., 2018. Argyll Field: the first oil field to be developed on the UK continental shelf, in press. Special Publication of the Geological Society of London, History of the European Oil Industry.

Graham, C., Armour, A., Bathurst, P., Evans, D. and Petroleumsforening, N., 2003. The Millennium Atlas: petroleum geology of the central and northern North Sea. Geological Society of London.

Gray, D. and Rex, R., 1965. Formation damage in sandstones caused by clay dispersion and migration. Clays and Clay Minerals: 355-365.

Grier, S. and Marschall, D., 1992. Reservoir Quality: Part 6. Geological Methods. AAPG Development Geology Reference Manual, Methods in Exploration(Geological methods).

Hall, I. and Chisholm, J., 1987. Aeolian sediments in the late Devonian of the Scottish Midland Valley. Scottish Journal of Geology, 23(2): 203-208.

Hantschel, T. and Kauerauf, A.I., 2009a. Fundamentals of basin and petroleum systems modeling. Springer Science & Business Media.

Hantschel, T. and Kauerauf, A.I., 2009b. Pore pressure, compaction and tectonics, Fundamentals of Basin and Petroleum Systems Modeling. Springer, pp. 31-101.

Harris, P.M., Kendall, C.G.S.C. and Lerche, I., 1985. Carbonate cementation—a brief review. Special Publications of SEPM, Carbonate cements(SP36).

Haughton, P. and Bluck, B., 1988. Diverse alluvial sequences from the Lower Old Red Sandstone of the Strathmore region, Scotland—implications for the relationship between Late Caledonian tectonics and sedimentation.

Haughton, P. and Farrow, C., 1989. Compositional variation in Lower Old Red Sandstone detrital garnets from the Midland valley of Scotland and the Anglo-Welsh Basin. Geological Magazine, 126(4): 373-396.

Hayes, J.B., 1979. Sandstone diagenesis - the whole truth. Special Publications of SEPM, 26: 127-139.

Hayward, R., Martin, C., Harrison, D., Van Dort, G., Guthrie, S. and Padget, N., 2003. The Flora field, blocks 31/26a, 31/26c, UK north sea. Geological Society, London, Memoirs, 20(1): 549-555.

Heald, M. and Larese, R., 1974. Influence of coatings on quartz cementation. Journal of Sedimentary Research, 44(4).

Heward, A.P., Schofield, P. and Gluyas, J.G., 2003. The Rotliegend reservoir in Block 30/24, UK Central North sea: including the argyll (renamed Ardmore) and innes Fields. Petroleum Geoscience, 9(4): 295-307.

Hoffman, J. and Hower, J., 1979. Clay mineral assemblages as low grade metamorphic geothermometers: application to the thrust faulted disturbed belt of Montana, USA. SEPM Special Publication No.26 pp. 55-79.

Holloway, S., Reay, D., Donato, J. and Beddoe-Stephens, B., 1991. Distribution of granite and possible Devonian sediments in part of the East Shetland Platform, North Sea. Journal of the Geological Society, 148(4): 635-638.

Houseknecht, D.W., 1987. Assessing the relative importance of compaction processes and cementation to reduction of porosity in sandstones. AAPG bulletin, 71(6): 633-642.

Howell, J. and Mountney, N., 1997. Climatic cyclicity and accommodation space in arid to semi-arid depositional systems: an example from the Rotliegend Group of the UK southern North Sea. Geological Society, London, Special Publications, 123(1): 63-86.

Howell, J.A., Martinius, A.W. and Good, T.R., 2014. The application of outcrop analogues in geological modelling: A review, present status and future outlook. Geological Society, London, Special Publications, 387(1): 1-25.

Huang, W.-L., Longo, J.M. and Pevear, D.R., 1993. An experimentally derived kinetic model for smectite-to-illite conversion and its use as a geothermometer. Clays and Clay Minerals, 41: 162-162.

Hunter, A. and Easterbrook, G., 2004. The geological history of the British Isles. Open University.

Hunter, R.E., 1977. Basic types of stratification in small eolian dunes. Sedimentology, 24(3): 361-387.

Jahren, J. and Ramm, M., 2009. The porosity-preserving effects of microcrystalline quartz coatings in arenitic sandstones: Examples from the Norwegian continental shelf. Quartz Cementation in Sandstones. Spec. Publ, 29: 271-280.

Jeans, C., 1994. Clay diagenesis, overpressure and reservoir quality: an introduction. Clay Minerals, 29(4): 415-424.

Jeremiah, J.M., 2000. Lower Cretaceous turbidites of the Moray Firth: sequence stratigraphical framework and reservoir distribution. Petroleum Geoscience, 6(4): 309-328.

Jiang, S., 2012. Clay minerals from the perspective of oil and gas exploration, Clay Minerals in Nature-Their Characterization, Modification and Application. InTech.

Joachimski, M., Breisig, S., Buggisch, W., Talent, J., Mawson, R., Gereke, M., Morrow, J., Day, J. and Weddige, K., 2009. Devonian climate and reef evolution: insights from oxygen isotopes in apatite. Earth and Planetary Science Letters, 284(3): 599-609.

Johnston, S.C., Smith, R.I. and Underhill, J.R., 1995. The Clair discovery, west of the Shetland Isles. Scottish Journal of Geology, 31(2): 187-190.

Kantorowicz, J., Bryant, I. and Dawans, J., 1987. Controls on the geometry and distribution of carbonate cements in Jurassic sandstones: Bridport Sands, southern England and Viking Group, Troll Field, Norway. Geological Society, London, Special Publications, 36(1): 103-118.

Karssenberg, D. and Bridge, J.S., 2008. A three‐dimensional numerical model of sediment transport, erosion and deposition within a network of channel belts, floodplain and hill slope: extrinsic and intrinsic controls on floodplain dynamics and alluvial architecture. Sedimentology, 55(6): 1717-1745.

Kearsey, T., Ellen, R., Millward, D. and Monaghan, A., 2015. Devonian and Carboniferous stratigraphical correlation and interpretation in the Central North Sea, Quadrants 25–44.

Keith, M. and Weber, J.N., 1964. Carbon and oxygen isotopic composition of selected limestones and fossils. Geochimica et Cosmochimica Acta, 28(10-11): 1787-1816.

Keller, W., Reynolds, R. and Inoue, A., 1986. Morphology of clay minerals in the smectite-to-illite conversion series by scanning electron microscopy. Clays and Clay Minerals, 34(2): 187-197.

Kiessling, W., 2002. Secular variations in the Phanerozoic reef ecosystem. Special Publications of Society for Sedimentary Geology (SEPM) 72: 625-690.

Kinsman, D.J., 1969. Modes of formation, sedimentary associations, and diagnostic features of shallow-water and supratidal evaporites. AAPG Bulletin, 53(4): 830-840.

Knight, I., Allen, L., Coipel, J., Jacobs, L. and Scanlan, M., 1993. The Embla Field, Geological Society, London, Petroleum Geology Conference series. Geological Society of London, pp. 1433-1444.

Kocurek, G. and Dott Jr, R.H., 1981. Distinctions and uses of stratification types in the interpretation of eolian sand. Journal of Sedimentary Research, 51(2).

Lander, R.H. and Walderhaug, O., 1999. Predicting porosity through simulating sandstone compaction and quartz cementation. AAPG bulletin, 83(3): 433-449.

Langford, R.P., 1989. Fluvial‐aeolian interactions: Part I, modern systems. Sedimentology, 36(6): 1023-1035.

Le Gallo, Y., Bildstein, O. and Brosse, E., 1998. Coupled reaction-flow modeling of diagenetic changes in reservoir permeability, porosity and mineral compositions. Journal of Hydrology, 209(1): 366-388.

Leder, F. and Park, W.C., 1986. Porosity reduction in sandstone by quartz overgrowth. AAPG Bulletin, 70(11): 1713-1728.

Leeder, M., 1973. Sedimentology and palaeogeography of the Upper Old Red Sandstone in the Scottish border basin. Scottish Journal of Geology, 9(2): 117-144.

Leveille, G.P., Primmer, T.J., Dudley, G., Ellis, D. and Allinson, G.J., 1997. Diagenetic controls on reservoir quality in Permian Rotliegendes sandstones, Jupiter Fields area, southern North Sea. Geological Society, London, Special Publications, 123(1): 105-122.

Loucks, R., Dodge, M. and Galloway, W.E., 1979. Importance of Secondary Leached Porosity in Lower Tertiary Sandstone Reservoirs Along Texas Gulf Coast: ABSTRACT. AAPG Bulletin, 63(9): 1606-1607.

Lundergard, P., 1992. Sandstone porosity loss. A ‘‘big picture’’view of the importance of Compactation. J Sediment Petrol, 62: 250-260.

Małkowski, K. and Racki, G., 2009. A global biogeochemical perturbation across the Silurian–Devonian boundary: Ocean–continent–biosphere feedbacks. Palaeogeography, Palaeoclimatology, Palaeoecology, 276(1): 244-254.

Marchand, A.M., Haszeldine, R.S., Smalley, P.C., Macaulay, C.I. and Fallick, A.E., 2001. Evidence for reduced quartz-cementation rates in oil-filled sandstones. Geology, 29(10): 915-918.

Marriott, S. and Wright, V., 1993. Palaeosols as indicators of geomorphic stability in two Old Red Sandstone alluvial suites, South Wales. Journal of the Geological Society, 150(6): 1109-1120.

Marshall, J., 1991. Palynology of the Stonehaven Group, Scotland: evidence for a Mid Silurian age and its geological implications. Geological Magazine, 128(03): 283-286.

Marshall, J., 1998. The recognition of multiple hydrocarbon generation episodes: an example from Devonian lacustrine sedimentary rocks in the Inner Moray Firth, Scotland. Journal of the Geological Society, 155(2): 335-352.

Marshall, J.E. and Hewett, A.J., 2003. Devonian. In: D. Evans, C. Graham, A. Armour and P. Bathurst (Editors), The Millenium Atlas: Petroleum Geology of the Central and Northern North Sea. The Geological Society of London, the Geological Survey of Denmark and Greenland and the Norwegian Petroleum Society, pp. 65-81.

Mathieson, E.L., 2002. The present is the key to the past is the key to the future, Geological Society of America 98th Annual Meeting, Cordilleran Section, Program and Abstracts, Session.

Mathisen, M.E., 1984. Diagenesis of Plio-Pleistocene Nonmarine Sandstones, Cagayan Basin, Philippines: Early Development of Secondary Porosity in Volcanic Sandstones: Part 2. Aspects of Porosity Modification.

Matthews, A. and Katz, A., 1977. Oxygen isotope fractionation during the dolomitization of calcium carbonate. Geochimica et Cosmochimica Acta, 41(10): 1431-1438.

McAlpine, A., 1977. The Upper Old Red Sandstone deposits of Hoy and Dunnet Head. Unpublished PhD Thesis. University of Newcastle-upon-Tyne.

McKee, E., Crosby, E.t. and Berryhill Jr, H., 1967. Flood deposits, Bijou Creek, Colorado, June 1965. Journal of Sedimentary Research, 37(3).

McKinley, J., Worden, R. and Ruffell, A., 2003. Smectite in sandstones: a review of the controls on occurrence and behaviour during diagenesis. Worden RH, Morad S. Clay Mineral Cements in Sandstones: International Association of Sedim-entologists Special Publication, 34: 109-128.

Methven, J., 1993. The Argyll Field Life Cycle With Cost Control as the Operator's Ethos. SPE 26690. . SPE Journal, Offshore Europe.: 167-174.

Miall, A., 2013. The geology of fluvial deposits: sedimentary facies, basin analysis, and petroleum geology. Springer.

Miall, A.D., 1977. Lithofacies types and vertical profile models in braided river deposits: a summary. AAPG Memoir 5: 597-604.

Miall, A.D., 1988. Reservoir heterogeneities in fluvial sandstones: lessons from outcrop studies. AAPG bulletin, 72(6): 682-697.

Mitra, S., 1988. Effects of deformation mechanisms on reservoir potential in central Appalachian overthrust belt. AAPG Bulletin, 72(5): 536-554.

Morad, S., 2009. Carbonate Cementation in Sandstones: Distribution Patterns and Geochemical Evolution (Special Publication 26 of the IAS), 72. John Wiley & Sons.

Morad, S., Al-Ramadan, K., Ketzer, J.M. and De Ros, L., 2010. The impact of diagenesis on the heterogeneity of sandstone reservoirs: A review of the role of depositional facies and sequence stratigraphy. AAPG bulletin, 94(8): 1267-1309.

Moraes, M.A. and De Ros, L.F., 1990. Infiltrated clays in fluvial Jurassic sandstones of Recôncavo Basin, northeastern Brazil. Journal of Sedimentary Research, 60(6).

Mykura, W., 2002. Old Red Sandstone. Geology of Scotland. The Geological Society London, 205-51 pp.

Nagtegal, P., 1979. Relationship of facies and reservoir quality in Rotliegendes desert sandstones, southern North Sea region. Journal of Petroleum Geology, 2(2): 145-158.

Nanson, G.C., Rust, B.R. and Taylor, G., 1986. Coexistent mud braids and anastomosing channels in an arid-zone river: Cooper Creek, central Australia. Geology, 14(2): 175-178.

Newman, M.S.J., Reeder, M., Woodruff, A. and Hatton, I., 1993. The geology of the Gryphon oil field, Geological Society, London, Petroleum Geology Conference series. Geological Society of London, pp. 123-133.

Nguyen, B.T., Jones, S.J., Goulty, N.R., Middleton, A.J., Grant, N., Ferguson, A. and Bowen, L., 2013. The role of fluid pressure and diagenetic cements for porosity preservation in Triassic fluvial reservoirs of the Central Graben, North Sea. AAPG bulletin, 97(8): 1273-1302.

Nichols, G., 2005. Sedimentary evolution of the Lower Clair Group, Devonian, west of Shetland: climate and sediment supply controls on fluvial, aeolian and lacustrine deposition, Geological Society, London, Petroleum Geology Conference series. Geological Society of London, pp. 957-967.

Nichols, G. and Fisher, J., 2007. Processes, facies and architecture of fluvial distributary system deposits. Sedimentary Geology, 195(1): 75-90.

Norton, M., Coney, P. and Davis, G., 1986. Collapse of the Caledonian orogen and the Old Red Sandstone. Nature, 323: 147-149.

Nyland, B., 2016. Five billion barrels of oil and gas from the Statfjord field. The Norwegian Petroleum Directorate.

O'driscoll, D., Hindle, A. and Long, D., 1990. The structural controls on Upper Jurassic and Lower Cretaceous reservoir sandstones in the Witch Ground Graben, UK North Sea. Geological Society, London, Special Publications, 55(1): 299-323.

OGA, 2017. Full List of Offshore Fields in Production. Oil & Gas Authority Open Data.

OGJ, 2017. Piper field resumes production in North Sea. Oil & Gas Journal.

Oil & Gas, U., 2012. Oil&Gas UK 2012 Economic Report. The United Kingdom Offshore Oil and Gas Industry Association Limited.

Orchard, M.J., 1978. The conodont biostratigraphy of the Devonian Plymouth Limestone, south Devon. Palaeontology, 21(4): 907-955.

Osborne, M.J. and Swarbrick, R.E., 1997. Mechanisms for generating overpressure in sedimentary basins: a reevaluation. AAPG bulletin, 81(6): 1023-1041.

Paxton, S., Szabo, J., Ajdukiewicz, J. and Klimentidis, R., 2002. Construction of an intergranular volume compaction curve for evaluating and predicting compaction and porosity loss in rigid-grain sandstone reservoirs. AAPG bulletin, 86(12): 2047-2067.

Pettijohn, F.J., Potter, P.E. and Siever, R., 2012. Sand and sandstone. Springer Science & Business Media.

Pittman, E.D., 1972. Diagenesis of quartz in sandstones as revealed by scanning electron microscopy. Journal of Sedimentary Research, 42(3).

Pittman, E.D., 1992. Clay coats: Occurrence and relevance to preservation of porosity in sandstones. Origin, Diagenesis, and Petrophysics of Clay Minerals in Sandstones. Sepm Special Publication No. 47.

Pittman, E.D. and Lumsden, D.N., 1968. Relationship Between Chlorite Coatings on Quartz Grains and Porosity, Spiro Sand, Oklahoma: NOTES. Journal of Sedimentary Research, 38(2).

Pollastro, R.M., 1985. Mineralogical and morphological evidence for the formation of illite at the expense of illite/smectite. Clays and Clay Minerals, 33: 265-274.

Pranter, M.J., Hewlett, A.C., Cole, R.D., Wang, H. and Gilman, J., 2014. Fluvial architecture and connectivity of the Williams Fork Formation: use of outcrop analogues for stratigraphic characterization and reservoir modelling. Geological Society, London, Special Publications, 387(1): 57-83.

Purvis, K., 1992. Lower Permian Rotliegend sandstones, southern North Sea: a case study of sandstone diagenesis in evaporite-associated sequences. Sedimentary Geology, 77(3-4): 155-171.

Pye, K. and Krinsley, D., 1986. Diagenetic carbonate and evaporite minerals in Rotliegend aeolian sandstones of the southern North Sea: their nature and relationship to secondary porosity development. Clay Minerals, 21(4): 443-457.

Ramm, M. and Bjørlykke, K., 1994. Porosity/depth trends in reservoir sandstones: Assessing the quantitative effects of varying pore-pressure, temperature history and mineralogy, Norwegian Shelf data. Clay minerals, 29(4): 475-490.

Richards, P.C., 1985a. A Lower Old Red Sandstone lake in the offshore Orcadian Basin. Scottish Journal of Geology, 21(3): 381-383.

Richards, P.C., 1985b. Upper Old Red Sandstone sedimentation in the Buchan oilfield, North Sea. Scottish Journal of Geology, 21(3): 227-237.

Robinson, A., Coleman, M.L. and Gluyas, J.G., 1993. The age of illite cement growth, Village Fields area, southern North Sea: Evidence from K-Ar ages and 18O/16O ratios. AAPG Bulletin, 77(1): 68-80.

Robinson, A. and Gluyas, J., 1992. Duration of quartz cementation in sandstones, North Sea and Haltenbanken Basins. Marine and Petroleum Geology, 9(3): 324-327.

Robson, D., 1991. The Argyll, Duncan and Innes Fields, Block 30/24 and 30/25a, UK North Sea. Geological Society, London, Memoirs, 14(1): 219-226.

Roels, H., 2001. Groningen field, past, present and future. Nordic Journal of Geosciences, 80(01): 12-14.

Rogers, D. and Astin, T., 1991. Ephemeral lakes, mud pellet dunes and wind-blown sand and silt: reinterpretations of Devonian lacustrine cycles in north Scotland. In: L.C.a.K.K. P. Anadón (Editor), Lacustrine Facies Analysis Blackwell Publishing Ltd., Oxford, UK. .

Romain, H.G. and Mountney, N.P., 2014. Reconstruction of three-dimensional eolian dune architecture from one-dimensional core data through adoption of analog data from outcrop. AAPG Bulletin, 98(1): 1-22.

Saigal, G.C., Bjorlykke, K. and Larter, S., 1992. The Effects of Oil Emplacement on Diagenetic Processes: Examples from the Fulmar Reservoir Sandstones, Central North Sea: Geologic Note (1). AAPG Bulletin, 76(7): 1024-1033.

Salem, A.M., Ketzer, J., Morad, S., Rizk, R.R. and Al-Aasm, I., 2005. Diagenesis and reservoir-quality evolution of incised-valley sandstones: evidence from the Abu Madi gas reservoirs (Upper Miocene), The Nile Delta Basin, Egypt. Journal of Sedimentary Research, 75(4): 572-584.

Schmidt, V. and McDonald, D.A., 1979. The role of secondary porosity in the course of sandstone diagenesis. Special Publications of SEPM 26: 175-207.

Scrutton, C.T., 1977. Facies variations in the Devonian limestones of eastern South Devon. Geological Magazine, 114(03): 165-193.

Seguret, M., Seranne, M., Chauvet, A. and Brunel, A., 1989. Collapse basin: A new type of extensional sedimentary basin from the Devonian of Norway. Geology, 17(2): 127-130.

Selley, R., 1978. Porosity gradients in North Sea oil-bearing sandstones. Journal of the Geological Society, 135(1): 119-132.

Shelton, J.W., 1964. Authigenic kaolinite in sandstone. Journal of Sedimentary Research, 34(1).

Sneider, R.M., 1990. Reservoir Description of Sandstones, Sandstone Petroleum Reservoirs. Springer, pp. 1-3.

Soper, N., Strachan, R., Holdsworth, R., Gayer, R. and Greiling, R., 1992. Sinistral transpression and the Silurian closure of Iapetus. Journal of the Geological Society, 149(6): 871-880.

Spencer, A., Leckie, G. and Chew, K., 1996. North Sea hydrocarbon plays and their resources. First Break, 14(9): 345-357.

Stanton, P.T., 1994. Measurement of Independent Variables-Composition. The Society for Sedimentary Geology (SEPM), Reservoir Quality Assessment and Prediction in Clastic Rocks (SC30).

Storetvedt, K. and Meland, A., 1985. Geological interpretation of palaeomagnetic results from Devonian rocks of Hoy, Orkney. Scottish Journal of Geology, 21(3): 337-352.

Storvoll, V., Bjørlykke, K., Karlsen, D. and Saigal, G., 2002. Porosity preservation in reservoir sandstones due to grain-coating illite: a study of the Jurassic Garn Formation from the Kristin and Lavrans fields, offshore Mid-Norway. Marine and Petroleum Geology, 19(6): 767-781.

Stricker, S. and Jones, S.J., 2016. Enhanced porosity preservation by pore fluid overpressure and chlorite grain coatings in the Triassic Skagerrak, Central Graben, North Sea, UK. Geological Society, London, Special Publications, 435: SP435. 4.

Struijk, A. and Green, R., 1991. The Brent Field, Block 211/29, UK North Sea. Geological Society, London, Memoirs, 14(1): 63-72.

Swarbrick, R., Osborne, M., Grunberger, D., Yardley, G., Macleod, G., Aplin, A., Larter, S., Knight, I. and Auld, H., 2000. Integrated study of the Judy Field (Block 30/7a)—an overpressured Central North Sea oil/gas field. Marine and Petroleum Geology, 17(9): 993-1010.

Sweet, M., 1999. Interaction between aeolian, fluvial and playa environments in the Permian Upper Rotliegend Group, UK southern North Sea. Sedimentology, 46(1): 171-188.

Talbot, M., 1990. A review of the palaeohydrological interpretation of carbon and oxygen isotopic ratios in primary lacustrine carbonates. Chemical Geology: Isotope Geoscience Section, 80(4): 261-279.

Tang, L., Jones, S.J. and Gluyas, J.G., 2017a. Facies Architecture of the Fluvial-Aeolian Buchan Formation (Upper Devonian) and Its Implications on Field Exploration: A Case Study from Ardmore Field, Central North Sea, UK. International Journal of Geosciences, 8(07): 902.

Tang, L., Jones, S.J. and Gluyas, J.G., 2017b. Porosity preservation due to grain coating illite/smectite: evidence from Buchan sandstones (Upper Devonian) of the Ardmore Field, UK North Sea. Proceedings of the Geologists' Association, Manuscript accepted with revision.

Tang, L., Jones, S.J. and Gluyas, J.G., 2018. Facies and Petrography Assessment of The Buchan Sandstone (Upper Devonian) Outcrops, Dunnet Head And Orkney, Northern Scotland. Scottish Journal of Geology, Under journal review.

Tarling, D., 1985. Palaeomagnetic studies of the Orcadian Basin. Scottish Journal of Geology, 21(3): 261-273.

Taylor, J., 1990a. Upper Permian—Zechstein. Petroleum Geology of the North Sea: Basic Concepts and Recent Advances, Fourth Edition: 174-211.

Taylor, S., Almond, J., Arnott, S., Kemshell, D. and Taylor, D., 2003. The Brent Field, Block 211/29, UK North Sea. Geological Society, London, Memoirs, 20(1): 233-250.

Taylor, T.R., 1990b. The influence of calcite dissolution on reservoir porosity in Miocene sandstones, Picaroon Field, offshore Texas Gulf Coast. Journal of Sedimentary Research, 60(3).

Taylor, T.R., Giles, M.R., Hathon, L.A., Diggs, T.N., Braunsdorf, N.R., Birbiglia, G.V., Kittridge, M.G., Macaulay, C.I. and Espejo, I.S., 2010. Sandstone diagenesis and reservoir quality prediction: Models, myths, and reality. AAPG bulletin, 94(8): 1093-1132.

Tirsgaard, H. and Øxnevad, I.E., 1998. Preservation of pre-vegetational mixed fluvio–aeolian deposits in a humid climatic setting: an example from the Middle Proterozoic Eriksfjord Formation, Southwest Greenland. Sedimentary Geology, 120(1): 295-317.

Tournier, F., Pagel, M., Portier, E., Wazir, I. and Fiet, N., 2010. Relationship between deep diagenetic quartz cementation and sedimentary facies in a Late Ordovician glacial environment (Sbaa Basin, Algeria). Journal of Sedimentary Research, 80(12): 1068-1084.

Trewin, N., 1989. The petroleum potential of the Old Red Sandstone of northern Scotland. Scottish Journal of Geology, 25(2): 201-225.

Trewin, N.H., 2002. The geology of Scotland. Geological Society of London.

Trewin, N.H. and Bramwell, M.G., 1991. The Auk Field, Block 30/16, UK North Sea. Geological Society, London, Memoirs, 14(1): 227-236.

Trewin, N.H. and Hurst, A., 2009. Excursion guide to the geology of East Sutherland and Caithness. Dunedin Academic PressLtd.

Tunbridge, I.P., 1984. Facies model for a sandy ephemeral stream and clay playa complex; the Middle Devonian Trentishoe Formation of North Devon, UK. Sedimentology, 31(5): 697-715.

Van Staal, C., Dewey, J., Mac Niocaill, C. and McKerrow, W., 1998. The Cambrian-Silurian tectonic evolution of the northern Appalachians and British Caledonides: history of a complex, west and southwest Pacific-type segment of Iapetus. Geological Society, London, Special Publications, 143(1): 197-242.

Veenhof, E.N., 1996. Geological aspects of the Annerveen gas field, the Netherlands, Geology of Gas and Oil under the Netherlands. Springer, pp. 79-92.

Vitali, F., Blanc, G., Larqué, P., Duplay, J. and Morvan, G., 1999. Thermal diagenesis of clay minerals within volcanogenic material from the Tonga convergent margin. Marine Geology, 157(1): 105-125.

Walderhaug, O., 1996. Kinetic modeling of quartz cementation and porosity loss in deeply buried sandstone reservoirs. AAPG bulletin, 80(5): 731-745.

Walderhaug, O., 2000. Modeling quartz cementation and porosity in Middle Jurassic Brent Group sandstones of the Kvitebjørn field, northern North Sea. AAPG bulletin, 84(9): 1325-1339.

Weber, K., 1980. Influence on fluid flow of common sedimentary structures in sand bodies, SPE Annual Technical Conference and Exhibition, Texas, USA, pp. 21-24.

Welton, J.E., 1984. SEM petrology atlas. American Association of Petroleum Geologists Tulsa^ eOklahoma Oklahoma.

Weyl, P.K., 1960. Porosity through dolomitization: conservation-of-mass requirements. Journal of Sedimentary Research, 30(1).

Wills, J., 1991. The Forties Field, Block 21/10, 22/6a, UK North Sea. Geological Society, London, Memoirs, 14(1): 301-308.

Wilson, 1994. Diagenetic mechanisms of porosity and permeability reduction and enhancement. The Society for Sedimentary Geology (SEPM) Reservoir Quality Assessment and Prediction in Clastic Rocks (SC30).

Wilson, M., Wilson, L. and Patey, I., 2014. The influence of individual clay minerals on formation damage of reservoir sandstones: a critical review with some new insights. Clay Minerals, 49(2): 147-164.

Wilson, M.D., 1992. Inherited grain-rimming clays in sandstones from eolian and shelf environments: their origin and control on reservoir properties.

Wilson, M.D. and Pittman, E.D., 1977. Authigenic clays in sandstones: recognition and influence on reservoir properties and paleoenvironmental analysis. Journal of Sedimentary Research, 47(1).

Winter, D. and King, B., 1991. The West Sole Field, Block 48/6, UK North Sea. Geological Society, London, Memoirs, 14(1): 517-523.

Witzke, B. and Heckel, P., 1988. Paleoclimatic indicators and inferred Devonian paleolatitudes of Euramerica. Devonian of the World: Proceedings of the 2nd International Symposium on the Devonian System — Memoir, 14: 49-63.

Wood, I., 2014. UKCS: Maximising Recovery Review. Final Report. Report for Department of Energy & Climate Change Department of Energy & Climate Change, London.

Woodcock, N.H. and Strachan, R.A., 2009. Geological history of Britain and Ireland. John Wiley & Sons.

Worden, R. and Burley, S., 2003. Sandstone diagenesis: the evolution of sand to stone. Sandstone Diagenesis: Recent and Ancient, 4: 3-44.

Worden, R. and Morad, S., 2000. Quartz cementation in oil field sandstones: a review of the key controversies. Quartz cementation in sandstones. International Association of Sedimentologists Special publication, 29: 1-20.

Worden, R. and Morad, S., 2003. Clay minerals in sandstones: controls on formation, distribution and evolution. Wiley Online Library.

Yuan, G., Gluyas, J., Cao, Y., Oxtoby, N.H., Jia, Z., Wang, Y., Xi, K. and Li, X., 2015. Diagenesis and reservoir quality evolution of the Eocene sandstones in the northern Dongying Sag, Bohai Bay Basin, East China. Marine and Petroleum Geology, 62: 77-89.

Ziegler, P.A., 1990. Geological atlas of western and central Europe. Geological Society of London.

APPENDIX I: CORE LOG DATA OF THIS PROJECT

Well list:

30/24-03

30/24-05

30/24-16

30/24-18

30/24-20

30/24-20z

30/24-28**

30/24-31**

30/24-34**

Abbreviations

Grain size: vf-very fine; f-fine; m-medium; c-coarse

Sample or not: y-8849.8-43732 (yes sample has been taken at this depth-depth in ft.-sample label number)

**All the core log works were done at BGS Core Store in Keyworth, Nottingham (30/24-03, 05, 16, 18, 20 and 20z) and EnQuest Core Store in Aberdeen (30/24-28, 31 and 34).*

***Note: the 'sample or not' column is not available for wells 30/24-28, 31 and 34, check the Appendix II-1 for sample information of wells 30/24-28, 31 and 34.*

30/24-03

Depth (ft.)	Lithology	Colour	Grain size	Sedimentary structure	Sampled or not	Other comments
8849.3-8850.5	sandstone	interbedded dark brown and light brown	f-m	parallel	y-8849.8-43742	
8850.5	mudstone	dark green grey	clay	/		fractured, oil stained
8850.8	sandstone	light grey, with seldom purple	f-m	not obvious	y-8850.8-43743	vertical fractured, but be filled
8851.2	sandstone	purple-red	f-m	not obvious, some soft sediment deformation	y-8851.0-43744	Small fractures, filled by oil?
8851.3-8851.7	sandstone	purple-red	f-m	not obvious, some soft sediment deformation	y-8851.4-43745	fractures vary in different directions, oil stained, probably heavy oil
8852	sandstone	yellow brown with part of purple red	f-m	not obvious, some soft sediment deformation	y-8851.9-43746	Small fractures, filled by oil?
8852.2-8853.7	sandstone	interbedded dark brown and light brown	m	parallel	y-8853.4-43747	small fractures
8854-8854.4	sandstone	red to yellow grey, with wide grey-white belt	f-m	not obvious	y-8854.0-43748;y-8854.3-43749	Fractures, 0.3-2mm width, various directions, infilled by dark matter.
8854.4-8855.4	sandstone	grey yellow to grey	m	parallel	y-8854.8-43750	some tilted laminate at the top
8855.5-8855.7	sandstone	purple red and brown	f-m	not obvious	n	a wide belt around 1cm width
8855.8-8856.5	sandstone	grey-white and purple brown, with black-grey laminate, at the bottom, there is a belt with 2.5cm width infilled with grey-white and green laminate	f-m	parallel	y-8856.1-43751; y-8856.4-43752	

8856.6-8858	sandstone	brown-yellow	m	not obvious	y-8856.9-43753	vertical fractures, 0.1mm width, with some branches
8858-8859	sandstone	purple red with brown-yellow laminate	m	parallel	y-8858.8-43754	reaction with HCL
8859.0-8859.6	sandstone	purple-red with light yellow brown laminate	f-m	parallel and cross bedding	y-8859.2-43755	
8859.7-8864.3	sandstone	brown-yellow	f-m	parallel	y-8859.6-43756; y-8861.5-43757; y-8863-43758	Fractures well developed, vertical, with small braches, 0.2mm width, infilled with dark matter. Especially in 8861.5, heavy smell of oil. At the 8862.8ft and bottom, wide belt infilled with dark and white-grey matter
8864.3-8864.6	sandstone	purple-red and grey	f-m	not obvious	y-8864.5-43759	small lateral fractures infilled with dark matter, with 0.5mm width
8864.7-8865.3	sandstone	grey-white with brown laminate	f-m	perfect parallel	y-8864.9-43760	the dark laminate is less than 1mm
8865.4-8867.2	sandstone	grey-white with purple-red dots	f-m	parallel	y-8865.7-43761	
8867.4-8869	sandstone	dark grey and brown	m	not obvious	y-8868.1-43762	well-developed fractures, heavy smell of oil, poorly cemented
8869.5-8871.4	sandstone	dark grey and yellow brown	f-m	parallel, and few cross bedding	y-8870.0-43763	fractures developed but infilled with grey matter, width from 0.2mm-2mm
8871.4-8871.8	sandstone	dark brown with lots of huge pink dot, diameter from 2mm-2cm	m	not obvious	y-8871.7-43764	poorly cemented, with many tiny fractures
8871.8-8873	sandstone	yellow-brown with dark grey laminate	m	not obvious, some parallel	y-8872.5-43765	
8873.4	sandstone	yellow-brown	m	parallel	y-8873.4-43766	
8873.9	sandstone	yellow-brown	m	parallel	y-8873.9-43767	
8874.5	sandstone	yellow-brown	m	parallel	y-8874.5-43768	

30/24-05

Depth (ft.)	Lithology	Colour	Grain size	Sedimentary structure	Sampled or not	Other comments
9103-9108	sandstone, high muddy content	purple red	f	approximately parallel, some soft sediment deformation	y-9103.2-43776; y-9106.5-43777	some lateral fractures, nothing infilled, 0.2-0.4mm width
9108-9110	sandstone	light grey-brown with purple laminate	f-m	parallel	y-9108.6-43778	
9110-9112	sandstone	dominated purple, with grey laminate and dark line	f-m	perfectly parallel	y-9110.7-43779; y-9111.7-43780	the dark line seems like poorly cemented with visible fractures
9112-9113	sandstone	purple-red dot and grey background, towards bottom, the purple red dot become fewer and fewer, and finally become into entire grey	f-m	parallel	y-9112.1-43781; y-9112.9-43782	
9113-9114	sandstone	light yellow brown	m	not obvious	y-9113.5-43783	
9114-9114.5	sandstone	yellow-brown	m	not obvious	y-9114.3-43784	
9114.5-9117	same to 9114-9114.5					
9117-9118	sandstone	light yellow brown with light purple red	m	approximately parallel	y-9117.3-43785	
9120-9123	sandstone	yellow-brown	m	not obvious	y-9120-43786	
9124-9130.5	sandstone	yellow-brown	m	not obvious	y-9124.3-43787	
9130.5-9133	sandstone	yellow-brown	m	not obvious, with some approximately parallel	y-9131-43793	

9133-9134	sandstone	purple-red	m	not obvious, with some approximately parallel	y-9133.5-43794	
9134-9135	sandstone	yellow-brown	m	some approximately parallel	y-9134.5-43795	
9135-9137	sandstone	purple-red	f-m	not obvious, with some approximately parallel	y-9136.5-43796	more muddy content
9137-9138.5	sandstone	purple with grey belt	m	parallel, with soft sediment deformation	y-9137.8-43797	
9138.5-9139.5	sandstone	interbedded purple and grey	m	perfectly parallel	y-9139-43798	
9140-9143	sandstone	yellow-brown	m	not obvious, with some parallel beddings	y-9140.5-43799	
9143.3-9147	sandstone	yellow-brown light	m-c	approximately parallel beddings	y-9144.0-43800	Fractures developed, indurated.
9147-9150	sandstone	brown-yellow	m	not obvious	y-9149.5-43804	
9150-9152.5	sandstone	yellow-brown	m	parallel	y-9150.8-43805	
9152.6-9155	sandstone	interbedded purple and grey	m	parallel	y-9154-43807	
9155-9157	sandstone	yellow-brown	m	approximately parallel	y-9156.5-43808	
9157-9160	sandstone	light brown	m	parallel	y-9159.5-43809	
9160-9161.5	sandstone	brown	m	not obvious	y-9161.0-43810	
9322.5-9323.8	sandstone	brown	m	parallel, with some soft sediment deformation	y-9312.8-43813	
9323.8-9324	sandstone	white-grey content significantly increased, also contains some pink content	m	not obvious	y-9323.9-43814	
9224-9328.5	sandstone	brown	m	parallel, with some soft sediment deformation	y-9224.6-43815	
9328.5-9329.5	sandstone	white-yellow light, with some purple dots	m	approximately parallel, but not very obvious	y-9329.3-43817	
9329.5-9335	sandstone	grey with lots of purple dots	m	parallel	y-9329.8-43818	

9335-9337	sandstone	light grey white with a few dark green line	m	parallel	y-9335.2-43821	
9337-9337.8	sandstone	grey with purple lines	m	parallel	y-9337.8-43823	
9337.8-9343.8	sandstone	grey with purple dots	m	dots are parallel distributed	y-9338.3-43824	many dots
9343.8-9349.5	sandstone	grey with widely distributed purple dots	m	parallel	y-9344.2-43827	a group of sudden yellow-brown laminates shown up
9349.5-9357	sandstone	grey with various quantity of purple dots	m	parallel	y-9351-43831	majorities are purple

30/24-16

Depth (ft.)	Lithology	Colour	Grain size	Sedimentary structure	Sampled or not	Other comments
9643-9644	sandstone	light brown	m	angular parallel		
9644-9645	sandstone	brown	m but coarser than previous one	not obvious		
9645-9646	sandstone	light brown	m	not obvious		
9646-9648.4	sandstone	brown	m	approximately parallel	y-9646.4-43835	vertical fractures with 0.2mm width, in-filled by dark matter
9648.4-9648.8	sandstone	brown	m	approximately parallel		with dark matters stained
9648.8-9653.5	sandstone	dark brown	m	not obvious	y-9653.0-43836	not water wettable
9653.5-9654.5	sandstone	dark brown	m	not obvious		not water wettable
9654.5-9655.75	sandstone	brown	m	not obvious		not water wettable, with fracture devel-oped, -.5-1mm width, infilled
9656-9657	sandstone	dark brown	m	not obvious		not water wettable
9657-9658	sandstone	grey	m	parallel		
9658-9659	sandstone	light brown	m	angular parallel	y-9658.2-43837	with dark matter stained
9659-9660.33	sandstone	grey-brown	m	angular parallel		with dark matter stained
9660.33-9662.9	sandstone	light brown	m	angular parallel		fewer dark matter stained
9662.9-9663.3	sandstone	dark-grey in-terbedded with yellow brown	m	parallel with high angle		
9663.3-9665.33	sandstone	light greyish yellow brown with dark lines	m	parallel with high angle		
9665.33-9666.5	sandstone	yellow brown with dark lines	m	parallel with high angle		

9666.5-9667.9	sandstone	dark yellow brown with dark matter stained	m	parallel with high angle	9667.7-43838	
9667.9-9670	sandstone	brown inter-bedded with light brown	m	parallel with soft sediment deformation		
9670-9670.8	sandstone	dark brown	m	parallel with high angle	y-9670.4-43839	not water wettable
9670.8-9671.2	sandstone	grey-brown	m	not obvious parallel, with soft sediment deformation		
9673-9676.25	sandstone	light-greyish and red brown	m	parallel with angle	y-9674-43840	

30/24-18

Depth (ft.)	Lithology	Colour	Grain size	Sedimentary structure	Sampled or not	Other comments
9153-9157	sandstone	yellow-brown with lots of black matter	m-c	perfectly parallel	y-9155.3-43842	poorly cemented, black matters everywhere
9157-9159	conglomerate	purple-red matrix, the pebble's colours contain white, pink, grey, dark grey	matrix is m-c, pebbles diameter from 1-2mm-1cm	no obvious gradient	y-9158.3-43843	
9159-9160	conglomerate	purple-red matrix, the pebble's colours contain white, pink, grey, dark grey	matrix is m-c, pebbles diameter from 1-2mm-1cm	no obvious gradient		
9160-9161.5	sandstone	purple-red	m	not obvious parallel	y-9160.5-43844	
9161.5-9162	sandstone	grey-white with brown lines	m	parallel and x bedding	y-9161.8-43845	
9162-9165.5	sandstone	light brown	m	parallel, some small cross bedding	y-9164.3-43855	
9165.5-9168	sandstone	grey with purple dots widely spread	m	purple dots parallel distributed	y-9168-43846	at 9167, small vertical fractures infilled with dark purple matters
9168-9170	sandstone	grey with purple dots widely spread	m	not obvious	y-9169.8-43847	in sampled area, there is a lateral fracture presented, infilled with the dark matter, with 0.2mm width
9170-9170.8	sandstone	purple with a few light lines interbedded	m	parallel		

9170.8-9172	sandstone	suddenly change to grey-yellow and dark grey	m	not obvious	y-9171.6-43848	
9172-9173	sandstone	purple with light lines interbedded	f-m	parallel		
9173-9174	sandstone	grey-white with dark grey matter irregularly distributed	m	not obvious, soft sediment deformation	y-9173.7-43849	
9174-9177	sandstone	grey-white matrix with abundant purple dots distributed	m	almost parallel	y-9174.2-43850	medium content of purple dots
					y-9175.2-43851	majority is purple
						at 9174.4, soft sediment deformation
						at 9176.3-9176.5, some lateral fractures, 0.2-0.3mm width, infilled with dark purple matters
9177-9178.6	sandstone	light grey white with purple dots,	m	parallel	y-9178-43852	
9178.6-9180	sandstone	purple content increased	m	parallel	y-9179-43853	sampled depth is a well-developed fractured zone
9180-9183	sandstone	grey white matrix with purple dots widely spread	m	parallel	y-9181.5-43854	

30/24-20

Depth (ft.)	Lithology	Colour	Grain size	Sedimentary structure	Sampled or not	Other comments
9877.5-9881.2	sandstone	yellow brown matrix with purple dots widely distrib-uted	m	angular parallel	y-9878-43857	
9881.2-9884	sandstone	yellow brown matrix with less purple dots widely distrib-uted	m	angular parallel	y-9883-43859	At 9883, there are many greys muddy? Content angularly parallel distributed.
9884-9887.5	sandstone	dark grey and purple	m	angular parallel	y-9885.1-43860	
9887.5-9887.8	sandstone	yellow-brown	m	not obvious	y-9887.5-43862	
9887.8-9889	sandstone	dark grey and purple	m	parallel with high angle	y-9888-43863	
9889-9891	sandstone	yellow-brown	m	not obvious	y-9890.5-43864	
9891-9891.3	sandstone	red	f-m	not obvious parallel	y-9891.1-43865	
9891.3-9895	sandstone	dark brown	m	high angle parallel	y-9893-43866	
9895-9897	sandstone	dark brown-black	m	high angle parallel	y-9896-43868	inside is black, poor cemented, brittle
9897.5-9901	sandstone	light yellow brown with purple and dark grey lines	m	high angular parallel	y-9899-43870	
9902.5-9906.5	sandstone	dark grey, yel-low-brown frequently in-terbedded	m	high angle parallel	y-9902.5-43872	much grey content
9906.4-9908.5	sandstone	light brown	m	high angle parallel	y-9908.4-43876	a few dark lines

9908.4-9911	sandstone	light brown matrix, the dark lines are signif-icantly in-creased	m	high angle parallel	y-9910-43877
9911-9913.5	sandstone	light brown	m	high angle parallel	y-9911.5-43878
9913.5-9916	sandstone	light brown matrix, the dark lines are signif-icantly in-creased	m	high angle parallel	y-9914.5-43879
9916-9923	sandstone	dark brown with yellow brown lines	m	high angle parallel	y-9916.8-43880
9923-9926.9	sandstone	light grey-brown with purple dots	m	approximately parallel, some soft sediment deformation	y-9923.7-48530
9926.9-9933.5	sandstone	light purple red with grey belts	f-m	angular parallel	y-9927-48532

30/24-20z

Depth (ft.)	Lithology	Colour	Grain size	Sedimentary structure	Sampled or not	Other comments
10156.8-10158	sandstone	brown	m	not obviously parallel		
10158-10159	sandstone	grey with purple belt	m	parallel	y-10158.8-48536	
10159-10159.2	sandstone	grey with purple dots	m	not obvious	y-10159.1-48534	
10159.2-10160	sandstone	brown	m	not obvious	y-10160-48535	
10161.6-10162	sandstone	grey	m	parallel		
10162-10165	sandstone	dark brown	m	angular parallel	y-10162.2-48537	
10166-10168	sandstone	purple grey	m	not obviously parallel	y-10167.5-48538	
10168-10169	sandstone	purple-red	f-m	not obvious, with some soft sediment deformation		contains high proportion of muddy content
10169-10169.3	sandstone	grey	f-m	not obvious		less muddy content
10169.3-10177	sandstone	brown and dark brown	m	some sections have angular parallel, whole sections are not obvious	y-10170-48539	
10177-10181.5	sandstone	light brown	m	angular parallel	y-10177.5-48542	light brown
10181.5-10186	sandstone	brown-dark brown	m	angular parallel	y-10181.5-48543	brown
10186-10186.6	sandstone	brown	m	not obvious		
10186.6-10192.8	sandstone	light brown and grey	m	approximately parallel	y-10192.4-48545	
10192.8-10202	sandstone	brown and grey	m	high angular parallel, with small scales cross bedding	y-10194.6-48546	at 10194.9-10195.2, contains some purple contents,
					y-10198.2-48547	at 10197.8, contains some purple belts
					y-10201.7-48548	at 10200-10200.8, contains small scale of cross bedding

10202-10208	sandstone	brown and grey	m	not obvious parallel	y-10203.5-48549	at 10206.3, a thin purple layer about 2cm presented
10208-10211	sandstone	brown-dark brown	m-c	not obvious parallel	y-10208.5-48550	
10211-10214	sandstone	light brown - grey brown	m	not obvious	y-10213.3-48552	at 10213.7, purple red content significantly increased
10214-10215	sandstone	dark brown	m	not obvious	y-10214.4-48553	not water wettable
10216-10216.6	sandstone	light brown - grey brown	m	parallel	y-10216.4-48554	with some black lines
10216.6-10217	mudstone	red	clay	/	y-10216.9-48555	
10217-10222.8	sandstone	light grey brown	m	not obvious		from 10220-10222.8 cores are missing
10222.8-10223.4	sandstone	brown	m	not obvious	y-10223.2-48556	
10224.6-10225	sandstone	light brown	m	approximately high angle parallel	y-10225-48557	
10228.3-10229	sandstone	grey-purple	m	not obvious	y-10228.5-48558	
10229-10235	sandstone	brown and grey interbedded	m	approximately parallel	y-10234.5-48559	
10235-10237	sandstone	purple-red and dark grey interbedded	m	approximately parallel	y-10235.5-48560	
10237-10238.5	sandstone	red-purple	m	not obvious	y-10237.6-48561	
10238.5-10238.8	sandstone	dark grey contains purple content	m	not obvious		
10238.8-10241.5	sandstone	purple interbedded with white-grey	m	approximately parallel	y-10239-48562	
10241.5-10243	sandstone	brown interbedded with white grey	m	cross bedding	y-10241.8-48563	

10243-10244.5	sandstone	dark brown with few light yellow brown lines	m	not obvious	y-10243.5-48564	
10244.5-10251.1	sandstone	light grey-brown- dark brown	m	not very obvious	y-10245-48565	At 10245.7, some small fractures developed, infilled with dark matter?
10251.1-10253	mudstone	purple red with some grey content	clay	soft sediment deformation	y-10252.8-48567	
10253-10256	sandstone	dark brown and grey	m	not obvious parallel, with soft sediment deformation	y-10253.2-48568	the grey content increased with the depth in this section
10256-10257.1	sandstone	grey and purple interbedded	m	parallel	y-10256.5-48570	the sampled area contains gradient form purple to red
10257.1-10259	sandstone	dark brown and light yellow brown interbedded	m	parallel	y-10258-48571	
10259-10260.8	missing					
10260.8-10262	sandstone	Dark grey and light grey interbedded. With moderate purple content	m	parallel and cross bedding	y-10260.5-48572	
10262-10263.5	sandstone	grey	m	parallel	y-10262.2-48573	
10263.5-10265	sandstone	orange-red and grey with grey content	m	not obvious	y-10264-48574	fractures well developed,0.1-0.3mm width, partly infilled
10265-10266.5	sandstone	orange-red with grey content	m	not obvious	y-10265.4-48575	
10266.5-10267.2	mudstone	purple-red	clay	not obvious		
10267.2-10268	sandstone	purple-red	f-m	not obvious	y-10267.9-48576	
10268-10268.8	mudstone	purple-red	clay	not obvious	y-10268.7-48577	

10268.8-10271	sandstone	lighter purple-red	f-m	not obvious, with some soft sediment deformation	y-10270.8-48578	
10271-10272.5	muddy sandstone	purple red with grey content	f-m	not obvious, with soft sedi-ment deformation	y-10271.3-48579	
10272.5-10274	sandstone	dark brown	m	not obvious	y-10273.8-48580	
10274-10360.3	sandstone	purple-red	m	approximately parallel	y-10355-48581	
10360.3-10360.5	mudstone					
10360.5-10363	sandstone	purple-red	m	not obvious	y-10361-48584	at depth 10362, there is mud concrete
10363--10366.3	sandstone with mud concrete	purple-red with grey content	sand-m	not obvious, mud concrete randomly distributed	y-10365.5-48585	
10366.3-10369.9	sandstone	grey-pink	m	angular parallel	y-10366.6-48586	
10372-10372.8	sandstone	pink-grey	m	cross bedding	y-10372.3-48587	
10372.8-10381	sandstone	purple-red	m	parallel, soft sediment defor-mation	y-10373-48588	fractures seldom developed
10381-10382	sandstone	purple-red	m	approximately parallel	y-10381.2-48592	
10382-10386	sandstone	purple-red	m	parallel	y-10385.8-48593	
10386-10391	sandstone	pink-grey	m	parallel	y-10386.4-48594	
10391-10396.5	sandstone	purple-red	m	parallel	y-10392.5-48597	
10396.5-10399.75	sandstone	dark purple red	m	parallel	y-10398.8-48599	
10399.75-10409	sandstone	purple-red	m	parallel	y-10405-48601	
10409-10418	sandstone	purple-red	m	parallel	y-10410.5-48604	
10418-10427	sandstone	lighter purple red	m	parallel	y-10422.5-48606	at depth 10426.5, cross bedding
10427-10427.5	sandstone	purple-red	m	not obvious	y-10427.2-48608	

30/24-28

Depth (ft.)	Lithology	Colour	Grain size	Sedimentary structure	Sampled or not	Other comments
9149-9153	sandstone	grey, light brown	m	low angle parallel		
9153-9158	sandstone	brown	m	low angle parallel & massive		
9158-9162	sandstone	light brown-grey	m	low angle parallel		
9162-9166.5	sandstone	brown	f-m	low angle parallel		
9166.5-9168	sandstone	brown, dark brown	m	small scale x-bedding, low angle parallel		
9168-9171	sandstone with red clast inside	light grey	f-m	massive		
9171-9173	sandstone	brown	m	low angle parallel & horizon-tal		
9173-9173.5	sandstone with red clast inside	light grey	f-m	soft sediment deformation, low angle parallel		
9173.5-9176	sandstone	dark brown	m	x-bedding		
9176-0=9180	sandstone	brown, light brown	m	low angle parallel & x-bedding		
9180-9181	sandstone	dark brown	m	low angle parallel		
9181-9190	sandstone	light brown, yellow brown	m	low angle parallel & fractures fully filled		
9190-9196	sandstone & conglomerates	brown	c	massive		
9196-9225	sandstone	light yellow brown	m	low angle parallel & massive & fractures fully filled		
9233-9236	sandstone	dark brown	m	x-bedding & soft sediment deformation		
9236-9239	sandstone with red clast inside	light grey	m	horizontal		
9239-9242	sandstone	brown, dark brown	m	massive & low angle parallel		

9242-9242.4	sandstone	light grey-brown	m	low angle parallel
9242.4-9248	sandstone	dark brown	m	low angle parallel & x bedding
9248-9262	sandstone	brown, light brown	m	massive & low angle parallel & horizontal
9262-9264	sandstone	dark brown	m	high angle parallel
9264-9266	sandstone with red clast inside	light grey	f-m	massive & soft sediment deformation
9266-9269	muddy sandstone	purple red	f-vf	horizontal & soft sediment deformation
9269-9272	sandstone	brown	m	massive
9272-9276	muddy sandstone	purple red	f-vf	horizontal & soft sediment deformation
9276-9289	sandstone	grey	m	massive, small fractures
9289-9292	sandstone	dark brown	m	massive
9292-9300	sandstone	light brown, brown	m	x-bedding & high angle parallel
9300-9305	muddy sandstone	purple red	f-m	low angle parallel & soft sediment deformation
9305-9307	sandstone	dark brown	m	massive
9307-9346	sandstone	brown, light grey brown	m	low angle parallel & soft sediment deformation & fractures fully filled
9346-9354	sandstone	dark brown	m	low angle parallel & fractures fully filled
9354-9373	sandstone	brown, light grey brown	m	low angle parallel & soft sediment deformation & fractures fully filled
9373-9375.2	sandstone	dark brown	m	low angle parallel & fractures fully filled
9375.2-9388	sandstone	light grey, purple red	f-m	low angle parallel & soft sediment deformation & horizontal
9388-9392	sandstone	dark brown	m	low angle parallel

9392-9398	sandstone	light grey, purple red	f-m	low angle parallel & soft sediment deformation & horizontal
9398-9404	sandstone	light grey, purple red	f-m	low angle parallel & soft sediment deformation & horizontal
9404-9419	sandstone	light brown and brown interbedded	m	low angle parallel & soft sediment deformation
9419-9426	sandstone	pink, light grey	f-m	massive & low angle parallel & soft sediment deformation
9426-9435	sandstone	light brown and brown interbedded	m	low angle parallel & soft sediment deformation
9435-9440.5	sandstone	pink, light grey	f-m	massive & low angle parallel & soft sediment deformation
9440.5-9446	sandstone	dark brown	m	massive
9446-9459	sandstone	light brown and brown interbedded	m	low angle parallel & soft sediment deformation
9459-9489	sandstone	pink, light grey	m-c	massive & low angle parallel & soft sediment deformation
9489-9499	sandstone	light grey	m	low angle parallel & massive
9499-9508	sandstone	pink, light grey	m-c	massive & low angle parallel & soft sediment deformation
9508-9524	sandstone	light grey	m	low angle parallel & massive
9524-9532	sandstone	pink, light grey	m-c	massive & low angle parallel & soft sediment deformation

30/24-31

Depth (ft.)	Lithology	Colour	Grain size	Sedimentary structure	Sampled or not	Other comments
10438-10444.5	sandstone	grey and light brown	m	soft sediment deformation		
10444.5-10445	sandstone	light red purple	m	parallel		lateral fractures developed, infilled by dark brown matter
10445-10447	sandstone	grey and light brown, with purple red belts	m	soft sediment deformation		lateral fractures developed, infilled by dark brown matter
10447.7-10447.9	sandstone	light brown and grey	m	parallel and soft sediment deformation		
10447.9-10449	sandstone	brown and purple interbedded	m	soft sediment deformation		purple belts 1cm width
10449-10450	sandstone	purple red, dark grey, light pink brown interbedded	m	soft sediment deformation		major colour is light pink brown, purple bels 1cm width, dark grey belts 0.5-1cm width
10450-10451.8	sandstone	purple red, light pink brown interbedded	m	parallel and soft sediment deformation		purple red content becomes major colour
10451.8-10453	sandstone	light brown and grey, with a few purple red belts, 0.5cm width	m	parallel and soft sediment deformation		
10456-10463	sandstone	grey and brown, with a few purple red belts	m	soft sediment deformation		
10463-10465	sandstone	light grey with purple belts, purple belts width range from 0.3cm-2cm	m	soft sediment deformation		lateral fractures developed, infilled with dark purple and dark grey content

10465-10466.5	sandstone	brown and light yellow brown, with purple belts and dark grey lines	m	parallel and soft sediment deformation	dark grey lines width about 0.2mm-0.8mm, purple belts width 0.5cm
10466.5-10469	sandstone	dark brown	m	not obvious	not water wettable
10469-10474	sandstone	light brown and light grey	m	not obvious, with some soft sediment deformation	at the bottom depth, the purple content obviously increased
10474-10486	sandstone	light brown and light grey interbedded	m	soft sediment deformation	lateral fractures developed, infilled with dark purple content, fractures width range from 0.2-0.5mm
10486-10488	sandstone	light brown and light grey	m	soft sediment deformation	
10489-10491	sandstone	brown to dark brown	m	not obvious	not water wettable
10491-10492	sandstone	light brown	m	parallel	
10492-10494	sandstone	brown	m	not obvious	not water wettable
10494-10495	sandstone	light brown and light grey	m	not obvious	
10495-10504	sandstone	brown-light grey	m	approximately parallel, soft sediment deformation	from 10499.5-10500 and 10501-10501.2 and 10502.5-10503, light grey contents are major colour, otherwise the major colour is brown interbedded with light grey
10504-10508	sandstone	brown	m	not obvious	
10508-10508.6	sandstone	dark brown	m	not obvious	not water wettable
10508.6-10510	sandstone	brown	m	not obvious	
10510-10512	sandstone	light brown and light grey	m	soft sediment deformation	

30/24-34

Depth (ft.)	Lithology	Colour	Grain size	Sedimentary structure	Sampled or not	Other comments
9467-9474.25	sandstone	light yellow brown	m	parallel		
9474.25-9477.5	sandstone	light yellow brown	m	parallel		some small lateral fractures developed, not infilled
9477.5-9489	sandstone	light yellow brown	m	parallel		some small lateral fractures developed, infilled by brown matter
9489-9489.4	sandstone	light yellow brown	m	parallel		lateral fractures developed
9489.4-9501	sandstone	light purple red with grey content	m	parallel		with dark grey lines
9501-9508	sandstone	purple red with parallel dark grey lines	m	parallel		fractures developed moderately
9508-9511.25	sandstone	light yellow brown	m	not obvious		at depth 9511.25, a large purple content presented, width 3cm
9511.25-9514	mudstone	dark purple red	clay	/		
9514-9517	sandstone	light yellow brown	m	not obvious		with few dark grey content
9517-9523.5	sandstone	light yellow brown	m	not obviously parallel, with dark brown lines, width 0.2mm		
9523.5-9524.7	sandstone	light red purple	m	not obvious		
9524.7-9526.25	sandstone	yellow brown and dark grey content	m	not obvious		small fracture developed, 0.1mm width, infilled
9526.25-9527	sandstone	yellow brown and dark grey content	m	not obvious		towards 9527, red purple content increased
9527-9529.1	sandstone	red purple	m	not obvious		
9529.1-	sandstone	light red purple	m	not obvious		

9651.6					
9651.6-9652	sandy conglomerates	grey purple	m-c	not obvious	fracture developed
9652-9653.2	sandstone	purple red	m	not obvious	fracture well developed, infilled by dark content
9653.2-9654.5	conglomerates	purple red matrix with white pebbles	c	not obvious	pebble width from 0.3cm-0.6cm
9654.5-9655.8	conglomerates	purple red matrix with white pebbles	c	not obvious	pebble width from 0.3cm-0.6cm
9656.7-9657.5	sandstone	yellow brown	m	parallel	with parallel dark lines
9657.5-9659	sandstone	purple red with coarse grains	m-c	nearly parallel	
9659-9659.5	conglomerates	purple red matrix with white pebbles	c	not obvious	pebble width from 0.3cm-0.6cm
9660.5-9660.7	mudstone	dark purple red	clay	not obvious	
9660.7-9661.5	matrix with white pebbles	purple red	c	not obvious	pebble width from 0.3cm-0.6cm
9661.5-9663.4	mudstone	dark purple red	clay	not obvious	
9663.4-9669.8	mudstone	dark purple red	clay	not obvious	
9669.8-9674.1	sandstone	yellow brown with purple content	m	not obvious	dark lines presented
9674.1-9674.3	sandstone	purple red	m	nearly parallel	dark grey lines, 0.2mm width
9674.3-9678.2	sandstone	yellow brown	m	not obvious	
9678.2-9682.5	sandstone	yellow brown	m	not obvious	some pebbles seldom distributed

9682.5-9687.4	conglomerates	purple red with brown content, pebbles are white and grey, width from 0.3cm-1cm	c	not obvious
9687.4-9696.5	conglomerates	purple red with brown content, pebbles are white and grey	c	not obvious

APPENDIX II: PETROGRAPHIC DATA USED IN THIS PROJECT

II-1 Point counting data

Well Name	Depth (m)	Unit	Facies	Sorting	Round-ness	GS	Detrital (%)				Authigenics (%)					Porosity (%)	Permeability (mD)
							Q	F	M	RF	K	I/S	Ch	QOG	D		
30/24-05	2840.7	B04	CHC	p	SA	f	51	5	6	28	6	tr	N	4	N	20	28
30/24-05	2841.8	B04	CHC	p	SA	f	64	4	tr	27	0	N	N	5	N	22.3	221
30/24-05	2843.0	B04	CHA	md	SR	f	51	2	tr	16	5	tr	N	4	22	17.9	48
30/24-05	2843.9	B04	CHC	p	SA	vf	46	2	2	12	5	N	N	5	28	11.9	0.12
30/24-05	2844.5	B04	SF	md	SR	f	54	3	2	17	7	1	N	3	13	4.4	0.9
30/24-05	2845.5	B04	SF	w	SR	f	53	2	3	27	10	tr	N	5	N	14.5	2.7
30/24-05	2846.4	B04	SF	md	SR	f	49	2	tr	23	5	tr	N	3	18	10.6	0.13
30/24-05	2846.7	B04	CHA	md	SR	f	36	1	2	30	6	tr	N	1	24	3.2	0.06
30/24-05	2847.0	B04	CHA	p	SR	f	46	3	5	19	5	tr	N	4	18	9.5	0.18
30/24-05	2847.6	B04	SF	md	SA	f	51	1	1	25	4	tr	N	3	15	12.7	0.19
30/24-05	2849.1	B04	CHB	md	SR	vf	51	1	4	4	11	0	N	5	25	10.9	0.49
30/24-05	2850.0	B04	CHB	md	SA	vf	48	1	2	24	10	N	N	3	12	7.2	1.1
30/24-05	2850.9	B04	CHB	md	SR	f	54	2	1	25	5	1	N	3	9	11.8	0.12
30/24-05	2851.4	B04	CHB	md	SR	f	56	2	tr	17	4	N	N	3	18	0.1	0.1
30/24-20z	3097.7	B04	CHB	mw	SR	m	77	3	2	10	4	tr	N	3	1	17.3	408
30/24-20z	3104.4	B04	CHA	p	SA	vf	48	1	1	31	15	tr	N	4	N	5.6	0.24
30/24-20z	3112.0	B04	CHB	mw	SR	m	81	3	tr	6	5	N	N	3	2	18.4	1090
30/24-20z	3117.8	B04	CHB	md	SR	vf	73	1	2	5	5	3	N	5	6	9.9	1.6
30/24-20z	3123.9	B04	CHB	w	SR	m	71	3	tr	15	3	tr	N	3	5	17.6	240
30/24-20z	3125.4	B04	CHB	md	SR	f	78	2	tr	7	4	N	N	1	8	12.1	12
30/24-20z	3126.0	B04	SF	md	SR	vf	71	1	2	7	12	1	N	1	5	12.6	1.1
30/24-20z	3156.2	B04	SF	md	SR	vf	62	1	2	14	10	N	N	3	8	10.7	0.45
30/24-20z	3157.1	B04	CHB	md	SR	f	74	1	1	4	10	tr	N	6	4	14.7	80

30/24-20z	3159.3	B04	CHA	md	SR	f	30	2	1	40	9	N	N	4	14	8.3	1.6
30/24-20z	3162.6	B04	SF	md	SR	vf	68	1	8	5	10	N	N	3	5	5.2	0.15
30/24-20z	3163.5	B04	SF	md	SR	vf	62	2	2	16	15	N	N	3	N	10.9	0.49
30/24-20z	3165.3	B04	CHB	md	SR	vf	66	0	1	13	8	N	N	4	8	10.4	0.42
30/24-20z	3169.6	B04	SF	w	SR	f	58	3	tr	3	9	N	N	5	22	3.8	0.13
30/24-20z	3173.6	B04	CHB	mw	SR	m	76	3	1	5	11	N	N	4	tr	18.8	351
30/24-20z	3176.6	B04	CHB	md	SR	m	76	1	1	8	9	tr	N	5	tr	16.8	770
30/24-28	2791.1	B10	AD	w	R	m	71	5	tr	19	0	2	N	N	2	19.6	122
30/24-28	2794.1	B10	CHB	mw	SR	m	74	3	5	16	1	1	N	N	1	21.5	75.7
30/24-28	2795.0	B10	CHC	p	A	m	50	3	1	37	4	tr	N	2	3	7.2	4.4
30/24-28	2795.6	B10	CHC	p	SA	m	60	2	1	28	7	1	N	3	N	15	510
30/24-28	2797.8	B10	CHB	w	SR	m	73	2	1	15	9	tr	N	N	N	17.9	481
30/24-28	2799.6	B10	AD	w	SR	m	73	1	N	15	5	tr	N	N	6	21.3	367
30/24-28	2804.8	B10	CHA	md	SR	vf	59	2	2	19	2	2	N	2	12	16.3	1.6
30/24-28	2806.6	B10	CHB	md	SR	f	75	2	N	11	6	tr	N	6	N	17.7	130
30/24-28	2809.3	B09	CHB	md	SR	f	65	5	N	13	0	1	N	4	12	15.4	31
30/24-28	2817.3	B09	CHB	mw	SR	m	63	5	N	27	0	1	N	1	3	23.1	150
30/24-28	2819.1	B09	CHB	w	SR	f	80	4	N	10	0	1	N	3	2	21.7	114
30/24-28	2820.6	B09	AD	w	R	m	78	4	N	15	0	1	N	N	2	24.1	59
30/24-28	2823.4	B09	AD	w	R	f	71	5	3	14	0	1	N	N	6	18.8	27
30/24-28	2824.0	B09	SF	w	SR	silt	50	2	8	31	2	5	N	N	2	11.1	0.45
30/24-28	2824.6	B09	SF	md	SR	vf	70	5	1	12	0	2	N	N	10	13.8	0.28
30/24-28	2827.0	B09	CHA	p	SA	m	25	3	5	67	0	N	N	N	N	7.7	4.8
30/24-28	2828.8	B09	CHB	md	SR	f	67	5	3	16	0	3	N	N	6	19.3	2.5
30/24-28	2831.9	B09	AD	w	R	m	84	2	1	2	5	5	N	1	N	24.4	123
30/24-28	2839.8	B09	CHB	w	SR	f	71	4	N	16	0	2	N	tr	8	16.6	72
30/24-28	2845.0	B09	AD	w	SR	f	79	3	2	1	0	12	N	tr	3	17.7	86
30/24-28	2845.9	B09	AD	w	SR	m	73	4	1	17	0	1	N	N	4	19.4	39
30/24-28	2847.7	B09	CHC	p	SA	m	72	2	2	22	0	2	N	tr	N	18	46
30/24-28	2849.0	B09	AD	w	SR	f	82	3	N	11	0	1	N	N	3	23.7	229

30/24-28	2851.7	B09	SF	md	SR	f	75	3	2	14	0	tr	N	1	5	16.8	21
30/24-28	2857.2	B08	AD	w	SR	m	84	1	1	13	N	1	N	N	N	22.3	115
30/24-28	2862.1	B08	AD	w	R	m	86	1	1	8	N	1	N	N	3	19.4	34
30/24-28	2872.2	B08	ID	md	SR	vf	71	2	3	10	5	tr	N	N	9	14.1	0.61
30/24-28	2882.2	B08	AD	mw	SR	f	85	1	2	9	N	tr	N	1	2	17.9	11
30/24-28	2884.0	B08	AD	w	R	m	73	2	2	17	N	1	N	N	5	18.5	14
30/24-28	2890.4	B08	AD	w	R	f	79	2	1	13	N	2	N	N	3	19.6	21
30/24-28	2891.6	B07	AD	mw	R	m	74	4	N	20	N	2	N	N	N	28	5200
30/24-28	2892.2	B07	AD	w	R	f	83	2	3	5	N	1	N	N	5	19.1	147
30/24-28	2893.5	B07	AD	w	R	m	77	4	N	11	6	1	N	1	N	27.5	4910
30/24-28	2894.7	B07	AD	md	R	m	87	4	1	7	N	1	N	tr	N	22.7	242
30/24-28	2899.9	B07	AD	w	R	m	92	4	N	3	tr	1	N	N	N	28	5290
30/24-28	2901.1	B07	AD	w	R	m	78	4	1	16	N	1	N	N	1	26.7	3040
30/24-28	2902.3	B07	AD	w	R	m	79	3	2	11	N	3	N	tr	3	23	337
30/24-28	2905.0	B07	AD	md	R	f	71	1	2	12	N	N	N	1	13	11.4	2.5
30/24-31	3182.1	B08	AD	w	SR	m	72	2	1	15	1	2	N	N	7	22	50
30/24-31	3183.6	B08	ID	md	SR	vf	54	2	1	13	N	1	N	tr	29	5.1	0.18
30/24-31	3186.1	B08	ID	md	SR	vf	69	2	1	18	1	4	N	tr	5	16.2	4.8
30/24-31	3186.7	B08	ID	w	SR	f	77	1	1	16	1	3	N	N	1	16.2	6.5
30/24-31	3188.8	B08	AD	w	R	m	78	2	1	10	1	2	N	N	6	20.5	21
30/24-31	3190.6	B08	AD	w	R	m	86	4	tr	7	0	3	N	N	N	26.3	4600
30/24-31	3193.4	B08	ID	md	SR	f	72	3	1	20	tr	2	N	tr	2	18	5.5
30/24-31	3195.2	B08	ID	w	SR	f	74	1	1	19	N	3	N	tr	2	14.3	1.2
30/24-31	3195.8	B08	ID	md	SR	f	75	0	tr	20	1	2	N	N	2	18.5	3.4
30/24-31	3197.4	B08	AD	w	SR	m	76	2	1	18	N	1	N	tr	2	23.2	318
30/24-31	3197.7	B08	AD	w	R	m	76	2	tr	19	tr	1	N	N	1	23.7	638
30/24-31	3199.2	B08	AD	w	SR	f	68	0	1	18	N	1	N	N	12	15.7	10.3
30/24-31	3199.9	B08	AD	md	R	f	77	1	2	16	N	2	N	N	2	19.9	90
30/24-31	3201.9	B08	AD	md	SR	m	72	1	1	23	N	1	N	N	1	23.2	82
30/24-31	3202.2	B08	AD	w	R	m	84	1	tr	13	N	1	N	N	1	24.4	252

30/24-31	3204.1	B08	AD	w	SR	f	76	1	2	15	1	2	N	N	3	17.5	4.4
30/24-34	2887.7	B11	CHB	md	SA	m	76	1	2	3	12	1	N	5	N	16.6	18
30/24-34	2890.1	B11	CHB	md	SA	m	75	1	2	6	9	2	N	3	2	14.6	33.5
30/24-34	2892.2	B11	CHA	p	SR	vf	75	2	2	4	13	1	N	3	N	10.7	1.1
30/24-34	2895.6	B11	CHC	p	SA	m	54	1	13	2	13	3	N	4	10	3.8	0.18
30/24-34	2898.6	B11	CHC	p	SA	m	77	7	3	6	4	2	N	1	N	17	28
30/24-34	2903.0	B11	CHC	p	A	m	59	4	1	4	8	N	N	2	22	4.4	0.05
30/24-34	2942.8	B11	CHC	p	A	m	57	3	1	12	5	N	N	3	19	5.6	0.1
30/24-34	2946.5	B11	CHC	p	SA	m	82	6	1	5	3	N	N	3	N	6.1	0.28
30/24-34	2947.4	B11	CHC	p	SA	m	73	3	4	5	7	7	N	1	N	4.6	0.22
30/24-34	2949.2	B11	CHB	md	SA	m	68	1	6	5	14	1	N	5	N	13.2	46
30/24-34	2955.6	B11	CHC	p	SA	m	76	6	tr	12	2	1	N	3	N	8.1	1.01
30/24-34	2960.5	B11	CHC	p	SA	m	67	4	5	13	4	4	N	3	N	12.3	0.35
30/24-34	2962.0	B11	CHA	md	SR	vf	73	1	6	11	7	0	N	2	N	13.8	9
30/24-34	2967.8	B11	CHB	md	SR	m	76	2	tr	6	6	1	N	3	6	13.8	15
30/24-34	2970.9	B11	CHB	w	SR	m	75	5	tr	5	8	tr	N	2	5	20.1	1130
30/24-34	2972.4	B11	CHC	p	SA	f	66	3	tr	12	3	0	N	5	11	9.5	7.8
30/24-34	2976.4	B11	CHB	mw	SR	m	63	1	tr	7	15	0	N	6	8	18.6	429

Facies: CHC-channel conglomeratic basal lag; CHB-channel bar; CHA-channel abandonment; SF-sheet flood; AD-aeolian dune; ID-interdune.
Sorting: p-poor; md-moderate; mw-moderate to well; w-well. Roundness: A-angular; SA-sub angular; SR-surrounded; R-rounded;
GS-Grain size: vf-very fine; f-fine; m-medium. Mineralogy: tr-trace; N-no data or zero.
Detrital: Q-quartz; F=feldspar; M-mica; RF-rock fragment
Authigenic: K-kaolinite; I/S-illite/smectite; Ch-chlorite; QOG-quartz overgrowth; D-dolomite

II-2 COPL, CEPL and Ic

Well Name	Depth (m)	Unit	Facies	C (%)	IGV (%)	COPL (%)	CEPL (%)	Ic
30/24-28	2791.1	B10	AD	4.66	24.26	17.88	3.83	0.82
30/24-28	2799.6	B10	AD	10.10	31.40	9.33	9.16	0.50
30/24-28	2820.6	B09	AD	3.00	27.10	14.68	2.56	0.85
30/24-28	2823.4	B09	AD	5.10	23.90	18.27	4.17	0.81
30/24-28	2831.9	B09	AD	10.94	35.34	3.80	10.52	0.27
30/24-28	2845.0	B09	AD	14.47	32.17	8.30	13.27	0.38
30/24-28	2845.9	B09	AD	5.00	24.40	17.72	4.11	0.81
30/24-28	2849.0	B09	AD	4.00	27.70	13.97	3.44	0.80
30/24-28	2857.2	B08	AD	1.00	23.30	18.90	0.81	0.96
30/24-28	2862.1	B08	AD	4.00	23.40	18.80	3.25	0.85
30/24-28	2882.2	B08	AD	3.10	21.00	21.27	2.44	0.90
30/24-28	2884.0	B08	AD	6.00	24.50	17.62	4.94	0.78
30/24-28	2890.4	B08	AD	5.00	24.60	17.51	4.12	0.81
30/24-28	2891.6	B07	AD	2.00	30.00	11.14	1.78	0.86
30/24-28	2892.2	B07	AD	6.00	25.10	16.96	4.98	0.77
30/24-28	2893.5	B07	AD	8.00	35.50	3.57	7.71	0.32
30/24-28	2894.7	B07	AD	1.10	23.80	18.37	0.90	0.95
30/24-28	2899.9	B07	AD	1.10	29.10	12.27	0.97	0.93
30/24-28	2901.1	B07	AD	2.00	28.70	12.76	1.74	0.88
30/24-28	2902.3	B07	AD	6.10	29.10	12.27	5.35	0.70
30/24-28	2905.0	B07	AD	14.00	25.40	16.62	11.67	0.59
30/24-31	3182.1	B08	AD	10.00	32.00	8.53	9.15	0.48

30/24-31	3188.8	B08	AD	9.00	29.50	11.77	7.94	0.60
30/24-31	3190.6	B08	AD	3.36	29.66	11.57	2.97	0.80
30/24-31	3197.4	B08	AD	3.10	26.30	15.60	2.62	0.86
30/24-31	3197.7	B08	AD	2.10	25.80	16.17	1.76	0.90
30/24-31	3199.2	B08	AD	13.00	28.70	12.76	11.34	0.53
30/24-31	3199.9	B08	AD	4.00	23.90	18.27	3.27	0.85
30/24-31	3201.9	B08	AD	2.00	25.20	16.84	1.66	0.91
30/24-31	3202.2	B08	AD	2.00	26.40	15.49	1.69	0.90
30/24-31	3204.1	B08	AD	6.00	23.50	18.69	4.88	0.79
30/24-28	2872.2	B08	ID	14.10	28.20	13.37	12.21	0.52
30/24-31	3183.6	B08	ID	30.10	35.20	4.01	28.89	0.12
30/24-31	3186.1	B08	ID	10.10	26.30	15.60	8.52	0.65
30/24-31	3186.7	B08	ID	5.00	21.20	21.07	3.95	0.84
30/24-31	3193.4	B08	ID	4.20	22.20	20.05	3.36	0.86
30/24-31	3195.2	B08	ID	5.10	19.40	22.83	3.94	0.85
30/24-31	3195.8	B08	ID	5.00	23.50	18.69	4.07	0.82
Average						**14.82**	**5.63**	**0.73**
30/24-05	2847.6	B04	SF	22.10	34.80	0.00	22.10	0.00
30/24-20z	3157.1	B04	CHB	20.10	34.80	0.00	20.10	0.00
30/24-34	2887.7	B11	CHB	18.00	34.60	0.31	17.94	0.02
30/24-28	2804.8	B10	CHA	18.14	34.44	0.55	18.04	0.03
30/24-34	2895.6	B11	CHC	30.00	33.80	1.51	29.55	0.05
30/24-34	2942.8	B11	CHC	28.00	33.60	1.81	27.49	0.06
30/24-20z	3173.6	B04	CHB	14.10	32.90	2.83	13.70	0.17
30/24-05	2850.0	B04	CHB	25.00	32.20	3.83	24.04	0.14

30/24-34	2949.2	B11	CHB	19.00	32.20	3.83	18.27	0.17
30/24-20z	3156.2	B04	SF	21.00	31.70	4.54	20.05	0.18
30/24-20z	3126.0	B04	SF	19.00	31.60	4.68	18.11	0.21
30/24-28	2809.3	B09	CHB	16.00	31.40	4.96	15.21	0.25
30/24-34	2890.1	B11	CHB	16.00	30.60	6.05	15.03	0.29
30/24-20z	3165.3	B04	CHB	20.00	30.40	6.32	18.74	0.25
30/24-05	2840.7	B04	CHC	10.10	30.10	6.72	9.42	0.42
30/24-20z	3176.6	B04	CHB	13.20	30.00	6.86	12.29	0.36
30/24-05	2850.9	B04	CHB	18.00	29.80	7.12	16.72	0.30
30/24-28	2806.6	B10	CHB	12.10	29.80	7.12	11.24	0.39
30/24-34	2972.4	B11	CHC	20.00	29.50	7.52	18.50	0.29
30/24-20z	3117.8	B04	CHB	19.00	28.90	8.30	17.42	0.32
30/24-20z	3163.5	B04	SF	18.00	28.90	8.30	16.51	0.33
30/24-34	2962.0	B11	CHA	15.00	28.80	8.43	13.74	0.38
30/24-20z	3123.9	B04	CHB	11.10	28.70	8.56	10.15	0.46
30/24-34	2892.2	B11	CHA	18.00	28.70	8.56	16.46	0.34
30/24-20z	3112.0	B04	CHB	10.00	28.40	8.94	9.11	0.50
30/24-28	2828.8	B09	CHB	9.00	28.30	9.07	8.18	0.53
30/24-28	2817.3	B09	CHB	5.00	28.10	9.32	4.53	0.67
30/24-34	2967.8	B11	CHB	14.00	27.80	9.70	12.64	0.43
30/24-28	2819.1	B09	CHB	6.00	27.70	9.82	5.41	0.64
30/24-05	2841.8	B04	CHC	5.10	27.40	10.19	4.58	0.69
30/24-28	2839.8	B09	CHB	10.10	26.70	11.05	8.98	0.55
30/24-28	2797.8	B10	CHB	8.60	26.50	11.29	7.63	0.60
30/24-20z	3125.4	B04	CHB	14.00	26.10	11.77	12.35	0.49

30/24-28	2795.6	B10	CHC	10.97	25.97	11.93	9.66	0.55
30/24-28	2824.6	B09	SF	12.00	25.80	12.13	10.54	0.53
30/24-20z	3097.7	B04	CHB	8.10	25.40	12.60	7.08	0.64
30/24-05	2851.4	B04	CHB	25.00	25.10	12.95	21.76	0.37
30/24-20z	3104.4	B04	CHA	19.10	24.70	13.41	16.54	0.45
30/24-28	2794.1	B10	CHB	3.00	24.50	13.64	2.59	0.84
30/24-20z	3162.6	B04	SF	19.00	24.20	13.98	16.34	0.46
30/24-34	2960.5	B11	CHC	11.00	23.30	14.99	9.35	0.62
30/24-34	2898.6	B11	CHC	6.00	23.00	15.32	5.08	0.75
30/24-28	2851.7	B09	SF	6.10	22.90	15.43	5.16	0.75
30/24-28	2847.7	B09	CHC	2.20	20.20	18.30	1.80	0.91
30/24-28	2824.0	B09	SF	9.00	20.10	18.40	7.34	0.71
30/24-34	2947.4	B11	CHC	15.00	19.60	18.91	12.16	0.61
30/24-28	2795.0	B10	CHC	9.10	16.30	22.10	7.09	0.76
30/24-34	2955.6	B11	CHC	6.00	14.10	24.10	4.55	0.84
30/24-34	2946.5	B11	CHC	6.00	12.10	25.82	4.45	0.85
30/24-28	2827.0	B09	CHA	0.00	7.70	29.36	0.00	1.00
Average						**10.06**	**12.71**	**0.44**

Facies code: AD – Aeolian dune; ID – Interdune; CHA – Channel abandonment; CHB – Channel bar; CHC – Channel conglomeratic base; SF – Sand flat

COPL: porosity loss by compaction; CEPL: porosity loss by cementation; Ic: compaction index

APPENDIX III: ALGORISMS FOR CALCULATING THEORETICAL AMOUNT OF QUARTZ CEMENTATION

Detailed description of algorisms can be found in:

Walderhaug, O., 1996. Kinetic modelling of quartz cementation and porosity loss in deeply buried sandstone reservoirs. AAPG bulletin, 80(5), pp.731-745.

Principle functions:

1) $A_0 = 6fV/D$

2) $Vq_2 = \phi_0 - (\phi_0 - Vq_1)exp\frac{-MaA_0}{\rho\phi_0 bcln10}(10^{bT_2} - 10^{bT_1})$

A_0 is the initial quartz surface area;

f is the fraction of detrital quartz;

V is the unit volume;

D is the diameter of grains;

Vq_2 is the amount of quartz cement (cm^3) precipitated from time T_1 to T_2 (m.y.);

Vq_1 is the amount of quartz cement present at time T_1;

M is the molar mass of quartz (60.09 g/mole);

ρ is the density of quartz (2.65 g/cm^3);

ϕ_0 is the porosity when quartz cement precipitation starts.

a = 1.98×10^{-22} $moles/cm^2s$;

b = $0.022°C^{-1}$

APPENDIX IV: OTHER COOPERATIVE CONTRIBUTIONS

The role played by carbonate cementation in controlling reservoir quality of the Triassic Skagerrak Formation, Norway

Yufeng Cui[a,b,], Stuart J. Jones[b], Christopher Saville[b], Stephan Stricker[b], Guiwen Wang[a], Longxun Tang[b], Xuqiang Fan[a], Jing Chen[a]*

a: State Key Laboratory of Petroleum Resources and Prospecting, China University of Petroleum, Beijing 102249, China

b: Department of Earth Sciences, Durham University, South Road, Durham, DH1 3LE, UK

Abstract

Anomalously high porosities up to 30% at burial depth of >3000 m along with varying amounts and types of carbonate cements occur in the fluvial channel sandstone facies of the Triassic Skagerrak Formation, Central Graben, Norway. However, porosities of the Skagerrak Formation are lower in the Norwegian sector than in the UK sector. In this study, petrographic analysis, core examination, scanning electron microscopy, elemental mapping, carbon and oxygen isotope, fluid inclusion and microgeometry analysis are performed to determine the diagenesis and direct influence on reservoir quality, with particular focus on the role played by carbonate cementation. The sandstones are mainly fine-grained lithic-arkosic to sub-arkosic arenites and display a wide range of intergranular volumes (2.3%–43.7% with an average of 23.6%). Porosity loss is mainly due to compaction (av. 26.6%) with minor contribution from cementation (av. 12.1%). The carbonate cements are patchy in distribution (from trace to 20.7%) and appear as various types e.g. calcretes (i.e. calcareous concreted gravels), poikilitic sparite and sparry ferroan dolomite, and euhedral or/and aggregated ankerite/ferroan dolomite crystals. This study highlights the association of carbonate precipitation with the remobilisation of carbonate from intra-Skagerrak calcretes during early burial stage

i.e. <500 m. During deeper burial, compaction is inhibited by carbonate cements, resulting high intergranular volume of up to 32% and 29% for fine- and medium-grained sandstones, respectively. Carbonate cement dissolution probably results from both meteoric water flow with CO_2 during shallow burial, and organic CO_2 and carboxylic acid during deep burial. The maximum intergranular volume enhanced by dissolution of early carbonate cements is calculated to 8% and 5% for fine- and medium-grained sandstones, respectively. Compaction continues to exert influence after dissolution of carbonate cements, which results in a loss of ~6% intergranular volume for fine- and medium-grained sandstones. Reservoir quality of the Norwegian sector is poorer than that of the UK sector due to a lower coverage of clay mineral coats e.g. chlorite, later and deeper onset of pore fluid overpressure, lower solubility of carbonate compared to halite, and a higher matrix content.

https://doi.org/10.1016/j.marpetgeo.2017.05.020

Cui, Y., Jones, S.J., Saville, C., Stricker, S., Wang, G., Tang, L., Fan, X. and Chen, J., 2017. The role played by carbonate cementation in controlling reservoir quality of the Triassic Skagerrak Formation, Norway. Marine and Petroleum Geology, 85, pp.316-331.

Argyll Field: the first oilfield to be developed on the UK continental shelf

Jon Gluyas, Longxun Tang & Stuart Jones*

Department of Earth Sciences, Durham University, DH1 3LE, UK

Abstract

In June 1975, oil from the Argyll Field became the first to be produced from the UK North Sea. Hamilton Brothers, a US company had beaten BP and their giant Forties Field into production. Seventeen years later the Argyll Field was abandoned with all production facilities removed. The first chapter of UK offshore oil production closed. Argyll lay forgotten by most and unwanted by all.

A new millennium dawned and with it two new companies Acorn Oil and Gas and Tuscan Energy. Both had identified Argyll as a potential field redevelopment. An alliance formed.

The UK's Department of Industry was approached with a request to relicense the Argyll Field out of round in order to redevelop the field. No company previously had sought to obtain a licence for production rather than exploration. It worked, as did the quest by both companies to obtain equity and debt funding.

In September 2003 the first well was drilled on the newly renamed Ardmore Field since abandonment (Gluyas et al 2005). It flowed unaided at 20,000 barrels of dry oil per day; significantly in excess of expectation. However, after two months of sustained high rate the well cut water. With a second well on stream production peaked at 28,000 barrels of oil for one day before the facilities, designed for 50,000 barrels of fluid per day, tripped-out. All was not well; during the next two years, facilities and well issues limited production. Debt was not adequately serviced and funding withdrawn. In mid-2005 the field was abandoned again. Five million from an expected 25 million barrels was produced. Argyll/Ardmore chapter 2 ended

but the story was not yet done. By 2013 Enquest had acquired the licence and drilled 6 wells. Production restart began in late 2015. Chapter 3 has opened for the newly named Alma Field.

This paper has been accepted by **The Geological Society London Special Publications (Section/Category: **History of the European Oil and Gas Industry**) and is now in press.*

APPENDIX V: ORAL AND POSTER PRESENTATIONS FOR ACADEMIC CONFERENCES

Conference: PETEX 2016

Presentation type: oral presentation

Porosity Controls on Devonian Strata of the North Sea: a case study from Ardmore Field, Block 30/24, UKCS

Longxun Tang, Jon Gluyas, Stuart Jones

Department of Earth Sciences, Durham University, Durham, DH1 3LE, United Kingdom

Abstract: the Devonian strata are widely distributed in the North Sea area but rarely regarded as effective petroleum reservoirs. Several oil fields (UK: Ardmore, Auk, Buchan, Stirling; Norway: Embla) proved that Devonian formations can be porous, permeable and productive. Ardmore Field (previous name ‘Argyll’) was selected as the main research target because it was extensively cored when first discovered and produced. It has both high quality Devonian sandstones with around 1 Darcie permeability interbedded with 'white rock’, sandstones which have near zero porosity and immeasurably low permeability and the origin of this heterogeneity of reservoir quality was not understood. This study aims to reveal the controls on Devonian reservoir quality from perspectives of sedimentology, petrography and diagenesis, using both Ardmore Field cores and comparable Devonian outcrops in Dunnet Head and Orkney Islands and offshore Northern Scotland.

Our research, from macro outcrop to micro pore scale, suggests that the Upper Devonian formation shows an upward fluvial-aeolian-fluvial cycle deposited under a generally hot and semi-arid to arid circumstance, different depositional facies and resulting mineralogy exerted a powerful influence on the subsequent diagenesis. For the fluvial sandstone, the lack of rooted vegetation in Devonian age led the frequent combination and bifurcation of fluvial mor-

phology, thus the complex mineral composition and immature grain texture are responsible for low primary porosity, the later compaction, quartz overgrowth and carbonate cementation worsened the situation and the reservoir was limitedly improved by dissolutions on feldspar and dolomite cement. For the aeolian sandstone, the natural deposition property of aeolian transportation led very good sorting and roundness, and high percentage of rigid grains, these are favourable on preserving primary porosity. Another important discovery in this project is the thick and continuous grain coating clay, which effectively inhibited the quartz overgrowth, was confirmed as detrital smectite (with partial illitization) by thin section, SEM and EDX spectrum. It is only found in aeolian sandstone but believed as fluvial origin. The suspended smectite aggregates, deposited in remote part of fluvial system the distal sandflat, will automatically flow into the dry, porous and permeable aeolian sediments by infiltration mechanism once encountered, and precipitated as grain coating and pore-filled clays. In the short future fluid inclusion and stable isotopes will be added for quantitative description of diagenesis events, and try to draw a whole picture of porosity evolution. The outcomes will be a useful reference for future Devonian explorations in the North Sea.

Conference: AAPG/SEG International Conference & Exhibition (ICE) 2017

Presentation type: poster presentation

The grain-coating illite/smectite (I/S): a new discovery on its positive effect on porosity preservation

Longxun Tang, Jon Gluyas, Stuart Jones

Department of Earth Sciences, Durham University, South Road, Durham, DH1 3LE, UK

Introduction

The deeply buried (2.7 km – 3.2 km) Upper Devonian Buchan Formation in Ardmore Field (Block 30/24, UK Continental Shelf) is a locally important reservoir composed by fluvial-aeolian sandstones. While the fluvial sandstones are extensively quartz cemented with porosity values ranging from 3.2% – 22.4% (avg. 14.4%); the porosity of aeolian sandstones ranges from 15% – 28% (avg. 20.2%) and was preserved by grain-coating clays preventing quartz overgrowth. The aeolian sandstones show higher porosity compared with the general depth-porosity trend of oil-bearing sandstones in the Central North Sea (Selley, 1978).

The petrographic analysis show that the grain coating clays only developed in aeolian sandstones and formed on the aeolian grain surface by mechanical infiltration before compaction. Although it is well known that chlorite and microcrystalline quartz coatings inhibit quartz cementation (Ehrenberg, 1993; Aase et al., 1996), our study does show that illite/smectite (I/S) coatings can also be effective in preventing quartz overgrowth. In the studied field, the grain-coating I/S were transformed from smectite precursor which had been introduced by fluvial clay-bearing water.

Illitization was observed to have occurred within a very limited degree, which could be explained by the Devonian strata were at consistently shallow burial depth (< 1 km) and low temperature (< 80°C) until Palaeocene and rapidly buried into its current depth and temperature of 110°C within a short time thus not giving enough time for illite to develop into hairy/fibrous shape. This phenomenon can be expected to occur only under particular circumstances, in which case it has a profound consequence for exploration.

Geological setting

The Ardmore Field is located on the Argyll Ridge, a large SW-NE trending Palaeozoic age tilted fault block on the south-western flank of the Central Graben in Block 30/24, UK North Sea, about 350 km SE from Aberdeen. The field is a horst feature with the crest in the north and fault closure to the NE. It measures 2.5 km wide and 6 km long (Fig. 1A). A combination of dip and faulting defines the limits of the field on the NW and SE flanks, while dip closure defines the southern limits of the field. The major fault trends are in two main directions, WNW–ESE cut by NW-SE faults. Top seal of the field is provided by Triassic shale to the far west, Jurassic shale in the mid-part of the field and impermeable Chalk at the north-eastern crest. The trap relies heavily on the major NW-SE trending graben edge faults to the NE and SW of the field while dip closure occurs to the NW and west (Fig. 1B).

The Upper Devonian Buchan Formation comprises a thick, generally upward-coarsening succession of fluvial-aeolian sandy sediments formed on an alluvial fan system in an arid/semi-arid setting. The whole Buchan succession lacks clear seismic stratigraphic markers, a combination of log and core data has been used to divide the stratigraphic units for the Upper Devonian group: B01 is the oldest unit overlying the Middle Devonian Limestone, and B11 is the youngest unit (Fig. 1B). In the absence of bio-stratigraphic data, sedimentary structures and lithofacies associations have been applied to help correlation (Gluyas et al., 2005). The

total thickness of the Buchan Formation is about 500 m – 800 m according to the seismic profile (Fig. 1C).

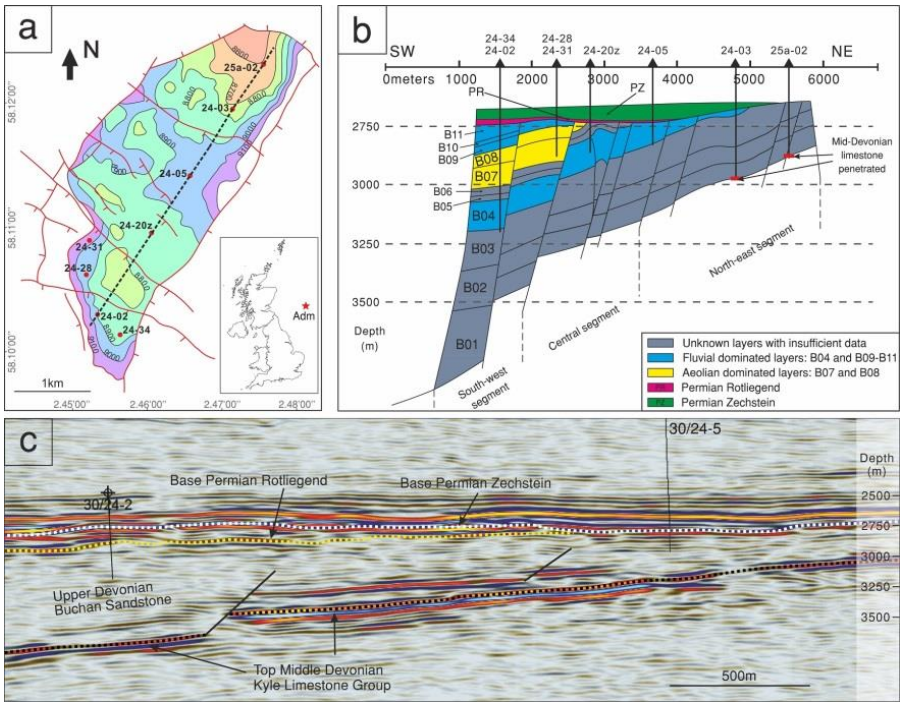

Fig.1: A. the location and structural contour map of Ardmore Field; B. a selected SW-NE vertical profile (line a-b in 1A); C. the seismic profile of selected a-b profile.

Petrography and diagenesis

The studied Buchan sandstones are litharenite to sub-litharenite and minor quartz-arenite, the aeolian sandstones ($Q_{82.1}F_{2.4}R_{15.5}$, upper fine to medium grained, moderate to good sorting, sub-rounded to well-rounded grains) are compositionally and textually more mature than fluvial sandstones ($Q_{76.1}F_{3.3}R_{20.7}$, very fine to medium grained, poor to moderate sorting, sub-angular to sub-rounded grains). The grain contact show point to linear and curved to concavo-convex in aeolian and fluvial sandstones, respectively.

In both sandstone types, quartz is dominantly monocrystalline, showing little undulose extinction; feldspar is commonly presented in trace amount and up to 7%, the main types are microcline, which occur as both fresh and nearly completely dissolved grains; most of the

mica grains are muscovite presenting in all the samples and comprising up to 13% showing distortion due to the compaction; rock fragments are in variable quantities including micaceous and illitic mud clasts.

Authigenic dolomite is prevalent in all Buchan sandstones ranged from 0% – 36% with an average value 6.7%. Quartz overgrowth is absent in aeolian sandstones but shows highly variable in fluvial sandstone (0% – 16%, average value 3.2%). Kaolinite and illite are the two main types of authigenic clays in fluvial sandstones. Kaolinite mainly occurs as euhedral pseudo-hexagonal plates and vermicular or booklet aggregates filling primary pores. Illite occurs as fibrous or hairy crystals mainly based on kaolinite and shows the pore-bridging habit.

The grain-coating I/S is the most important clay type in aeolian sandstones and presents in two forms: a). Grain-coating I/S commonly occurs as cornflake or honeycomb morphology with filamentous terminations (Fig. 2A), and consists of 1 μm – 5 μm thick rim coating all detrital grains in aeolian facies sandstones (Fig. 2B, 2C); it is absent in fluvial facies sandstones. It is also observed that quartz overgrowth are absent in aeolian facies sandstone samples where uniform and robust grain-coating I/S has developed; and b) Pore-filling I/S is commonly presenting as flocculent aggregates existing in the intergranular pore space (Fig. 2A), and is absent in fluvial facies sandstones.

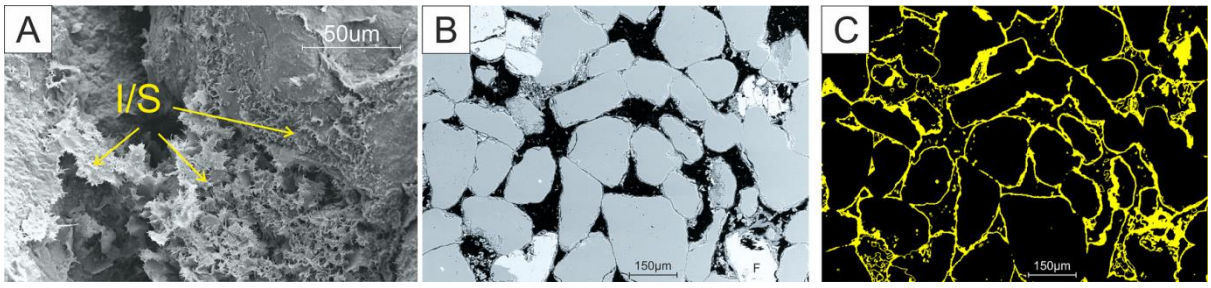

Fig. 2: A. the SEM image of grain coating and pore-filling I/S; B. BSEM image of typical aeolian sandstone; C. the mineral facies map showing good continuity of the grain coating I/S.

The source of grain-coating I/S

Mineralogically, the cornflake or honeycomb morphology observed under SEM supports that the I/S have formed from smectite precursor (Pollastro, 1985), and the smectite crystals would form an effective coat because they nucleate flatly attached to the detrital grain surface and curl away from that surface, this crystal morphology leads to a dense and effective coat (Pittman, 1992).

In terms of facies, the vertical fluvial-aeolian-fluvial variation generally represents a progradation-retreat-progradation cycle of the alluvial fan-based braided system with aeolian deposits occurred mainly between two main progradation periods. The distribution of grain-coating I/S is highly facies-controlled which is only found in aeolian sandstones, however, it is not considered as aeolian in origin. During aeolian dominated period, the studied area was only affected by distal sectors of fluvial distributary system. Thus a very possible source of these smectite precursors is from fluvial clay-bearing water, within such an environment, the lower water table allowed muddy water to infiltrate through the coarser, porous and permeable aeolian sands; and the petrographic features do meet the criteria set by Wilson (1992) for identifying mechanical infiltrated clays.

The effect of grain-coating I/S on reservoir quality

The grain-coating I/S in the aeolian sandstones show an excellent continuity around the grains (Fig. 2C) and has effectively inhibited possible subsequent quartz overgrowth. By using 1D thermo-burial history and the theoretical model proposed by Walderhaug (1996), we calculated that quartz overgrowth would theoretically occupy 6% – 7% of porosity in the fine to medium grained aeolian sandstones if the grain-coating I/S is absent (Fig. 3).

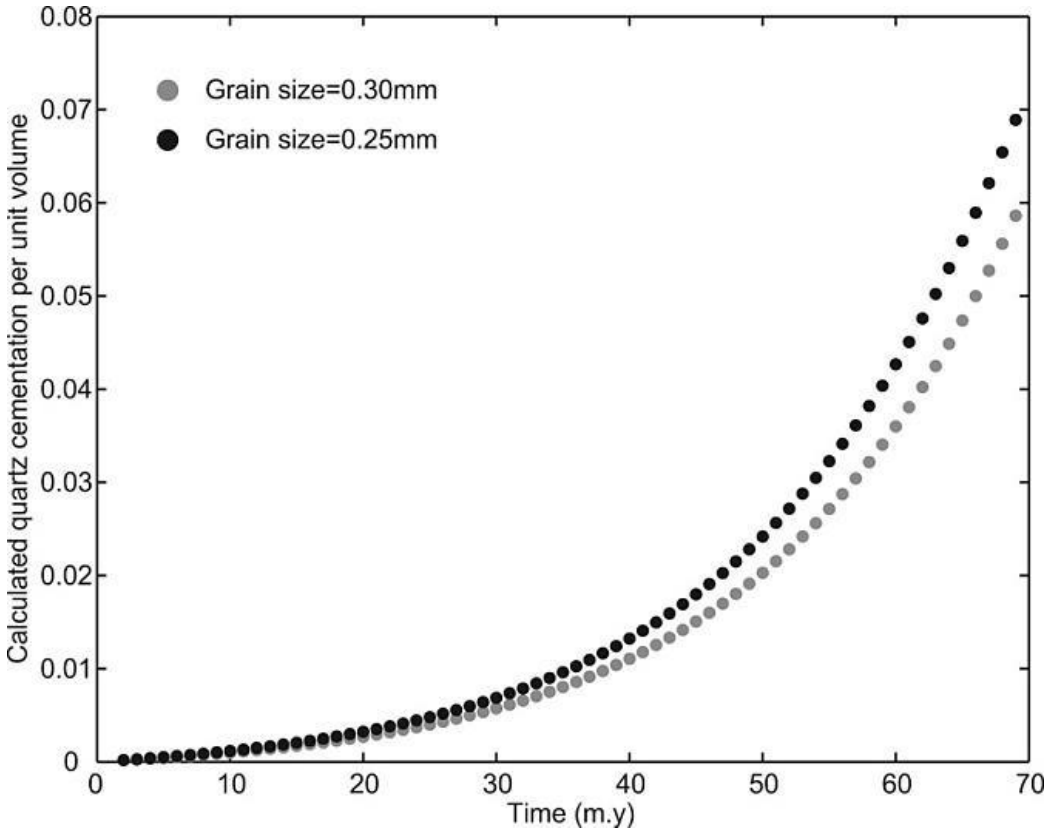

Fig.3: Theoretical quantity of quartz overgrowth in fine to medium grained aeolian sandstones if the grain coatings are absent, the algorithm is after Walderhaug (1996).

Despite this positive effects, the smectite-based clays are commonly known to be harmful to the reservoir quality due to its swelling property (Gray and Rex, 1965) and illitization (Le Gallo et al., 1998). However, the reservoir quality of the aeolian sandstones is not obviously affected by these two shortcomings due to: 1). the pore-filling I/S is only possessed in a minor amount (< 5%) thus would not significantly decrease permeability, and 2). the Devonian strata were consistently at shallow burial depth (< 1.5 km) and low temperature (< 80°C) until Palaeogene and rapidly buried into the current depth within a short time (Fig. 4) which does not allow authigenic illite to develop into elongated hairy/fibrous crystals.

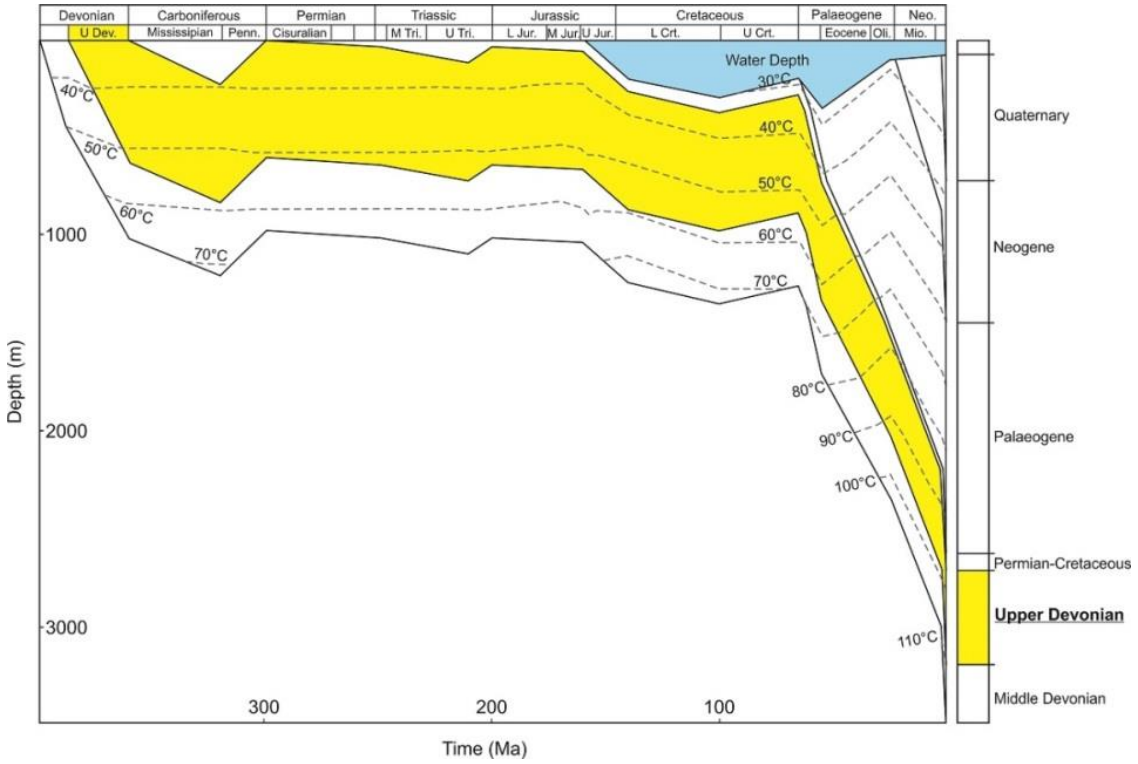

Fig.4: 1D burial and temperature history of the Ardmore Field.

Conclusions

The grain-coatings observed in the studied field have been identified as illite/smectite. This study shows that I/S coatings can be very effective in preventing quartz cementation and thereby help preserve primary porosity. The I/S coatings in the Ardmore field were generated from a smectite precursor, which had originated from fluvial clay-bearing water that represents the deposits of distal sectors of fluvial distributary system, and were formed as grain-coatings in aeolian sandstones by mechanical infiltration. The understanding of the positive effect on porosity preservation from grain-coating I/S may aid the predictions of high quality Devonian-associated reservoirs in the Central North Sea and other places with similar provenance.

Poster for ICE 2017

The Grain-Coating Illite/Smectite (I/S): A New Discovery On Its Positive Effect On Porosity Preservation

***Longxun Tang*[1*], *Jon Gluyas*[1], *Stuart Jones*[1], *Leon Bowen*[2], *Bernard Besly*[3]**

1. Department of Earth Sciences, Durham University, Durham, DH1 3LE, UK
2. Department of Physics, Durham University, Durham, DH1 3LE, UK
3. School of Geography, Geology and the Environment, Keele University, Keele, Staffordshire, ST5 5BG, UK

This research is financially supported by:

EnQuest

1. Introduction

The deeply buried (2.7–3.2km) Upper Devonian Buchan Formation in Ardmore Field (Block 30/24, UKCS) is a locally important reservoir composed by fluvial-aeolian sandstones. Except dolomite cements have similar amount in both types sandstones; the presence of quartz overgrowth shows contrasting differences: the fluvial sandstones are extensively quartz cemented with porosity values ranging from 3.2 – 22.4% (avg. 14.4%); while the porosity of aeolian sandstones ranges from 15 – 28% (avg. 20.2%) and was effectively preserved by grain-coating illite/smectite (I/S) preventing quartz overgrowth.

The petrographic analysis show that the grain coating I/S only developed in the aeolian sandstones; it was formed from smectite precursor which was introduced by mechanical infiltration of fluvial clay-bearing water. Chlorite and micro-crystalline quartz coatings are well known for inhibiting quartz cementation; however, our study has proved that the thick I/S coatings with good continuity can also be effective in preventing quartz overgrowth.

By using Walderhaug's algorithm, we quantitatively calculated that the grain coating I/S have preserved about 6-7% porosity in the aeolian sandstones by preventing quartz overgrowth. Furthermore, illitization has minor negative effect due to have occurred within a very limited degree, which could be explained by the unique burial history: the Devonian strata were at consistently shallow burial depth (<1 km) and low temperature (< 80°C) until Palaeocene and rapidly buried into its current maximum depth and temperature of 120°C within a short time, thus not giving enough time for illite to develop into a completely hairy/fibrous shape. This phenomenon can be expected to occur only under particular circumstances, in which case it has a profound consequence for exploration.

2. Geological setting

The Ardmore Field is located on the Argyll Ridge, a large SW-NE trending Palaeozoic age tilted fault block on the south-western flank of the Central Graben in Block 30/24, UK North Sea. The field is a horst feature with the crest in the north and fault closure to the NE. It measures 2.5 km wide and 6 km long (Fig. 1A). A combination of dip and faulting defines the limits of the field on the NW and SE flanks, while dip closure defines the southern limits of the field. The major fault trends are in two main directions, WNW–ESE cut by NW-SE faults. Top seal of the field is provided by Triassic shale to the far west, Jurassic shale in the mid-part of the field and impermeable Chalk at the north-eastern crest. The trap relies heavily on the major NW-SE trending graben edge faults to the NE and SW of the field while dip closure occurs to the NW and west (Fig. 1B).

The Upper Devonian Buchan Formation comprises a thick, generally upward-coarsening succession of fluvial-aeolian sandy sediments formed on an alluvial fan system in an arid/semi-arid setting. 11 sub-units have been divided by well log and core data: B01 is the oldest unit and B11 is the youngest unit (Fig. 1B). The total thickness of the Buchan Formation is about 300 – 800 m according to the seismic profile (Fig. 1C). Overall, the known units comprise a vertically fluvial (B04)-aeolian (B07 and B08)-fluvial (B09, B10 and B11) variation, which generally represents a progradation-retreat-progradation cycle of the alluvial fan-based braided system with aeolian deposits occurred mainly between two main progradation periods.

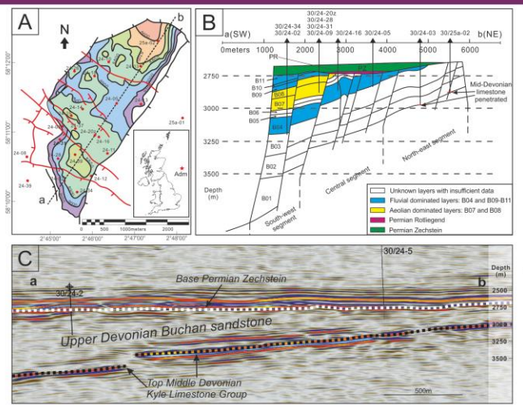

Fig.1: A. the location and structural contour map of Ardmore Field; B. a selected SW-NE vertical profile (line a-b in 1A); C. the seismic profile of selected a-b profile.

3.General Petrography and Diagenesis Information

		Fluvial facies	Aeolian facies
Grain properties	Size	Mud to conglomerate, fine to medium are predominant	Predominantly upper fine to medium
	Roundness	Sub-angular to sub-rounded	Sub-rounded to rounded
	Sorting	Moderate	Good
QFR		$Q_{76.1}F_{3.3}R_{20.7}$	$Q_{82.1}F_{2.4}R_{15.6}$
Compaction		Linear-curve contact	Point-linear contact
Pressure dissolution		Yes	No
Authigenic minerals		Dolomite	
		Quartz overgrowth	**Grain coating & pore filling Illite/smectite**
		Kaolinite	
		Illite	
Reservoir quality		$\bar{\phi}$=12.7% $\bar{K}_{arithmetic}$=147.7mD $\bar{K}_{geometric}$=5.41mD	**$\bar{\phi}$=20.2%** **$\bar{K}_{arithmetic}$=740.6mD** **$\bar{K}_{geometric}$=64.9mD**
Other features		Dissoltuion of feldspars	-

4. Typical Fluvial and Aeolian Sandstone Thin Section Photos

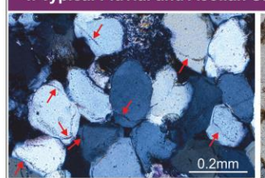

Thin section photo of a typical fluvial sandstone sample, note the extensive quartz overgrowth (red arrows) on the detrital quartz grains. Well 30/24-20z, depth 3126m.

ϕ= 5.2%; K=0.72mD

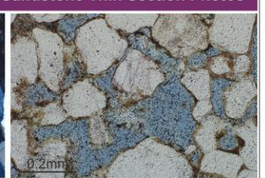

Thin section photo of a typical aeolian sandstone sample, note the extensive distribution of grain coating I/S on the detrital quartz grains. Well 30/24-28, depth 2891.6m.

ϕ= 23.4%; K= 200mD

5. The presence of I/S

The I/S presents in two types and are **only occurred in aeolian sandstones**: grain coating (left) and pore-filling I/S (right). The cornflake or honeycomb morphology may indicate they were altered from smectite precursor. Both types are absent in fluvial channel deposits.

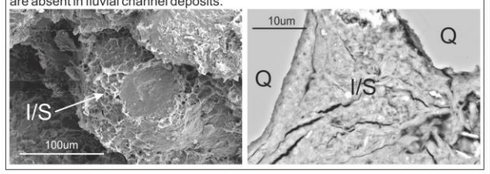

6. Distribution/development of I/S in aeolian sandstones

The grain-coating I/S in the aeolian sandstones show an excellent continuity around grains, which provides no nucleation points for the quartz overgrowths.

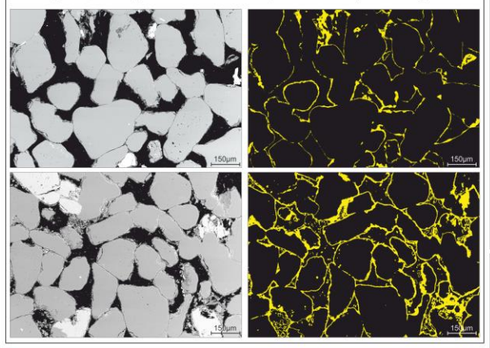

7. Source of I/S Clay: Where Did It Come From?

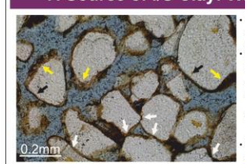

- Although the grain-coating I/S are only found in the aeolian sandstones, however, it is **not** considered as aeolian in origin;
- The presence of grain coating I/S meets criteria for recognizing **mechanically infiltrated clays**:

1). presence at grain contact areas;
2). increased thickness in depressions on framework-grain surface;
3). more extensive development in finer grained laminae or beds.

- QEMSCAN analysis on an overlying sheet flood silty sample show abundant pore-filling smectite (15.5%).

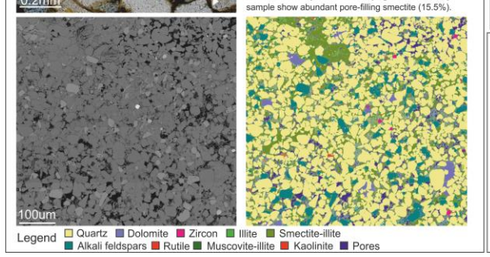

8. The Clay Infiltration Model

In such fluvial-aeolin mixed facies, during the aeolian-dominated period, the studied area was only influenced by distal sectors of fluvial distributary system. Thus **a very possible source of these smectite precursors is from fluvial clay-bearing water**, such as sheet flood deposits; within such an environment, the lower water table allowed muddy water (usually with rich suspened clay) to infiltrate through the coarser, porous and permeable aeolian sands.

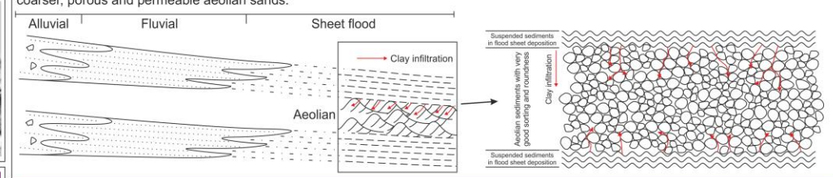

9. Why Did Illitization Only Exert Minor Negative Effect?

The smectite-based clays are commonly known to be harmful to the reservoir quality due to swelling property and illitization.

However, the reservoir quality of aeolian sandstones is not obviously affected by these two shortcomings due to: 1). the pore-filling I/S is only possessed in a minor amount (< 5%) thus would not significantly decrease permeability, and 2). the Devonian strata were consistently at shallow burial depth (<1.5 km) and low temperature (< 80°C) until Palaeogene and rapidly buried into the current depth within a short time, which does not allow authigenic illite to develop into elongated hairy/fibrous crystals.

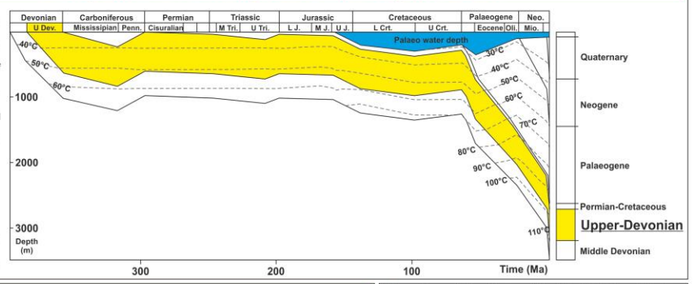

10. The Quantified Positive Effect of Grain Coating I/S

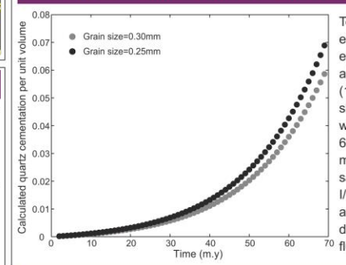

To quantitatively evaluate the effect of grain coating I/S, we employed the theoretical algorithm from Walderhaug (1996), the calculated results show that quartz overgrowth would theoretically occupy 6–7% of porosity in the fine to medium grained aeolian sandstones if the grain-coating I/S is absent. This is approximately the porosity difference between aeolian and fluvial sandstones.

11. Conclusions

- The grain-coatings observed in the studied field have been identified as illite/smectite. This study shows that I/S coatings can be very effective in preventing quartz cementation and thereby help preserve primary porosity.
- The I/S coatings in the Ardmore field were generated from a smectite precursor, which had originated from fluvial clay-bearing water that represents the deposits of distal sectors of fluvial distributary system, and were formed as grain-coatings in aeolian sandstones by mechanical infiltration.
- The understanding of the positive effect on porosity preservation from grain-coating I/S may aid the predictions of high quality Devonian-associated reservoirs in the Central North Sea and other places with similar provenance.

Acknowledgement: the authors would like to thank CGG for providing the seismic data; Enquest PLC for supporting this research through access to core and financial support of analytical work; BGS (British Geological Survey) for its assistance in facilitating the examination of Devonian cores; We are all grateful for the expertise and general assistance offered by Mr Ian Chaplin (Department of Earth Sciences, Durham University).

Key references

- Aase, N. E., Bjorkum, P. A., and Nadeau, P. H., 1996, The effect of grain-coating microquartz on preservation of reservoir porosity: AAPG bulletin, v. 80, no. 10, p. 1654-1673.
- Ehrenberg, S., 1993, Preservation of anomalously high porosity in deeply buried sandstones by grain-coating chlorite: examples from the Norwegian continental shelf: AAPG Bulletin, v. 77, no. 7, p. 1260-1286.
- Gluyas, J., Mair, B., Schofield, P., Arkley, P., and McRae, D., Ardmore Field: rebirth of the first offshore oil field, UKCS, in Proceedings Geological Society, London, Petroleum Geology Conference series2005, Volume 6, Geological Society of London, p. 367-388.
- Gray, D., and Rex, R., Formation damage in sandstones caused by clay dispersion and migration, in Proceedings Proc1965, p. 355-365.
- Le Gallo, Y., Bildstein, O., and Brosse, E., 1998, Coupled reaction-flow modeling of diagenetic changes in reservoir permeability, porosity and mineral compositions: Journal of Hydrology, v. 209, no. 1, p. 366-388.
- Pittman, E. D., 1992, Clay coats: Occurrence and relevance to preservation of porosity in sandstones.
- Pollastro, R. M., 1985, Mineralogical and morphological evidence for the formation of illite at the expense of illite/smectite: Clays and Clay Minerals, v. 33, p. 265-274.
- Selley, R., 1978, Porosity gradients in North Sea oil-bearing sandstones: Journal of the Geological Society, v. 135, no. 1, p. 119-132.
- Walderhaug, O., 1996, Kinetic modeling of quartz cementation and porosity loss in deeply buried sandstone reservoirs: AAPG bulletin, v. 80, no. 5, p. 731-745.
- Wilson, M. D., 1992, Inherited grain-rimming clays in sandstones from eolian and shelf environments: their origin and control on reservoir properties.

Want know more about Devonian reservoir architecure?

Just visit http://dro.dur.ac.uk/22529/ for author's published paper:

Facies architecture of the Fluvial-Aeolian Buchan formation (Upper Devonian) and its implications on field exploration : a case study from Ardmore Field, Central North Sea, UK.

Or simply scan this QR code:

The numerical modelling by using core study, analogue outcrops measurement and well log data which will provide you a bigger picture about Devonian fluvial-aeolian facies.